Carbon Dioxide Utilisation in Block Polymers: Catalysis and Functional Materials

Gregory Scott Sulley



Somerville College

Department of Inorganic Chemistry

University of Oxford

September 2021

A thesis submitted in partial fulfilment of the requirements for the degree of Doctor of Philosophy in Chemistry

For my family

"All we have to decide is what to do with the time that is given us."

- J. R. R. Tolkien

Declaration

The work described in this thesis was conducted between October 2017 and July 2021 at the University of Oxford. This is the work of the author unless otherwise stated.

The copyright of this thesis rests with the author and is made available under a Creative Commons Attribution Non-Commercial No Derivatives licence. Researchers are free to copy, distribute or transmit the thesis on the condition that they attribute it, that they do not use it for commercial purposes, and that they do not alter, transform or build-upon it. For any reuse or distribution, researchers must make clear to others the licence terms of this work.



Gregory Sulley

Abstract

The following thesis describes the synthesis of block polymers comprising polycarbonates (derived from carbon dioxide) and polyesters, and their evaluation as functional materials and possible renewable alternatives to current petrochemical-based plastics. The preparation of the polymers utilises efficient and sequence-controlled polymerisation catalysis, combining lactone ring-opening polymerisation (ROP) and epoxide/CO_2 ring-opening copolymerisation (ROCOP) cycles through a single catalyst.

Chapter 2 evaluates heterodinuclear zinc(II)/magnesium(II) catalysts for the switchable polymerisation catalysis of lactone and epoxide/CO_2. The heterodinuclear catalyst, [LZnMg(OBz^{NMe_2})$_2$] where L = macrocyclic ancillary ligand, OBz^{NMe_2} = *para*-substituted benzoate, is initially assessed for the preparation of ABA-type triblock polymers, but because of poor end-group fidelity the development of a new organometallic catalyst, [LZnMg(C_6F_5)$_2$] is undertaken. The organometallic catalyst shows strong performance with equivalent high activity for epoxide/CO_2 ROCOP and enhanced activity for lactone ROP compared with the benzoate variant. Importantly, it delivers higher molar mass ABA triblock polymers (M_n > 20 kg mol^{-1}) with block sequence-selectivity and with excellent end-group fidelity.

Chapter 3 further explores the application of the organometallic Zn(II)/Mg(II) catalyst in switchable polymerisation catalysis. High molar mass ABA triblock polymers (38 < M_n < 71 kg mol^{-1}) with varying degrees of CO_2 utilisation (6 – 23 wt %) are prepared by controlling the starting monomer stoichiometry, with the final materials comprising hard polycarbonate "A" blocks and a soft polyester "B" block. The effects of varying the relative block ratio on the thermal and mechanical characteristics of the polymers are analysed, and

their performance as toughened plastics, elastomers, and pressure-sensitive adhesives is evaluated.

Chapter 4 investigates the synthesis and thermal/mechanical effects of changing the polymer architecture by varying the initiating alcohol groups, from linear to stars. A range of tri-, tetra-, and hexafunctional star block polymers are synthesised from vinyl-cyclohexene oxide (vCHO), CO_2, and ε-decalactone (ε-DL). It also investigates the selective post-polymerisation modification of the polycarbonate block at fixed relative block composition. Multi-arm star-like polymers are fashioned using a "core-first" approach by employing chain-transfer agents with varying numbers of hydroxyl groups. Trends in thermomechanical and morphological characteristics for both the non-modified and modified polymers are analysed in relation to molar mass (overall and individual arm) and number of star 'arms', and a preliminary assessment of particular advantages/disadvantages for star *vs.* linear architectures in these polymers is presented.

Acknowledgements

Firstly, I would like to thank my supervisor, Professor Charlotte Williams, for allowing me the opportunity to carry out my DPhil in her research group. I am deeply grateful for your motivation, insight, and unwavering support. Thank you for believing in me.

I have had the pleasure and fortune of working alongside a team of incredible researchers who have taught me so much. To Dr Georgina Gregory, Dr Leticia Peña Carrodeguas, and Dr Thomas Chen – thank you for your guidance and friendship. A special mention also to Arron, Tom, Ryan, George, and Alice for the coffee breaks and generally awful chat – you've made these a very memorable 4 years.

To the Williams group, you are a fantastic bunch and you've made my time at Oxford thoroughly enjoyable. To all the post-docs (George, Leti, Ryan, Arron, Tom, Andy, Fer, Patrick, Sumesh, Brad, Thom, Shannon, Andrés, Alex, Caroline, Chris, Frank, Duncan, Giulia), DPhils (Gemma, Alice, Wilf, Saïd, Arnaud, Charlie, Ni, Tim, Peck, Natalia, Gloria, Lisa, Holly, Wouter, Kam, Sandy, Fran, Lukas), and Part IIs (Matylda, Dan, Joost, Emma, Nathan, Clare, Seb) I've met throughout my time here, thank you.

I would also like to take this opportunity to acknowledge the researchers and teams who have lent their expertise in data collection including: Dr Koon-Yang Lee & team (Imperial College London), Prof. Clive Siviour & team (University of Oxford), and Prof. Nick Terrill & team (Diamond Light Source).

Finally, I would like to wholeheartedly thank my family for their immense support and enduring belief in me. To my parents and sister, I am indebted to you and cannot thank you enough for all that you do. And to Gabs, I am forever grateful for your unfaltering love, kindness, and support – I know I wouldn't be where I am now without you. This is for you all.

List of publications

Easy access to oxygenated block polymers via switchable catalysis

T. Stößer, G. S. Sulley, G. L. Gregory, C. K. Williams, *Nat. Commun.* **2019**, 10, 2668.

Switchable Catalysis Improves the Properties of CO_2-Derived Polymers: Poly(cyclohexene carbonate-b-ε-decalactone-b-cyclohexene carbonate) Adhesives, Elastomers, and Toughened Plastics

G. S. Sulley, G. L. Gregory, T. T. D. Chen, L. P. Carrodeguas, G. Trott, A. Santmarti, K-Y. Lee, N. J. Terrill, C. K. Williams, *J. Am. Chem. Soc.* **2020**, 142, 9, 4367-4378.

Triblock polyester thermoplastic elastomers with semi-aromatic polymer end block by ring-opening copolymerization

G. L. Gregory, G. S. Sulley, L. P. Carrodeguas, T. T. D. Chen, A. Santmarti, N. J. Terrill, K-Y. Lee, C. K. Williams, *Chem. Sci.* **2020**, 11, 6567-6581.

Bio-based and Degradable Block Polyester Pressure-Sensitive Adhesives

T. T. D. Chen, L. P. Carrodeguas, G. S. Sulley, G. L. Gregory, C. K. Williams, *Angew. Chem. Int. Ed.* **2020**, 59, 23450.

High elasticity, chemically recyclable, thermoplastics from bio-based monomers: carbon dioxide, limonene oxide and ε-decalactone

L. P. Carrodeguas, T. T. D. Chen, G. L. Gregory, G. S. Sulley, C. K. Williams, *Green Chem.* **2020**, 22, 8298-8307.

Sequence Control from Mixtures: Switchable Polymerization Catalysis and Future Materials Applications

A. C. Deacy, G. L. Gregory, G. S. Sulley, T. T. D. Chen, C. K. Williams, *J. Am. Chem. Soc.* **2021**, DOI: 10.1021/jacs.1c03250

List of abbreviations

1D	One-dimensional
2D	Two-dimensional
AFM	Atomic force microscopy
Ar	Aryl
ATR-IR	Attenuated total reflectance infrared
BDI	β-Diiminate
Bn	Benzyl
BPA-PC	Bisphenol A polycarbonate
Cat	Catalyst
CHD	Cyclohexene-1,2-diol
CHO	Cyclohexene oxide
COSY	Correlated spectroscopy
Conv.	Conversion
CTA	Chain transfer agent
$Đ_M$	Dispersity
DCM	Dichloromethane
DM(T)A	Dynamic mechanical (thermal) analysis
DP	Degree of polymerisation
DPE	Dipentaerythritol
DSC	Differential scanning calorimetry
ε-DL	ε-Decalactone
Equiv.	Equivalents

HMBC	Heteronuclear multiple-bond coherence
HSQC	Heteronuclear single quantum coherence
IR	Infrared
k	Rate constant
L	Ligand
LHS	Left-hand side
LO	Limonene oxide
M	Metal centre
MALDI	Matrix-assisted laser desorption ionisation
ME (2-ME)	2-Mercaptoethanol/β-Mercaptoethanol
MeOH	Methanol
M_n	Number average molar mass
M_w	Weight average molar mass
MS	Mass spectrometry
NMR	Nuclear magnetic resonance
OAc	Acetate
OBz	Benzoate
OTW	Operating temperature window
PC	Polycarbonate
PCHC	Poly(cyclohexene carbonate)
PCHPE	Poly(cyclohexene phthalate)
PCL	Poly(ε-caprolactone)
PDL	Poly(ε-decalactone)
PDMS	Poly(dimethylsiloxane)

PE	Polyester
PER	Pentaerythritol
Ph	Phenyl
PLA	Poly(lactide)
PLimC	Poly(limonene carbonate)
PO	Propylene oxide
PPC	Poly(propylene carbonate)
PPM	Post-polymerisation modification
PSA	Pressure-sensitive adhesive
PTMC	Poly(trimethylene carbonate)
PU	Polyurethane
PvCHC	Poly(vinylcyclohexene carbonate)
R	Alkyl group/Coligand (non-halogen)
RHS	Right-hand side
ROCOP	Ring-opening copolymerisation
ROP	Ring-opening polymerisation
SAXS	Small angle X-ray scattering
SCFT	Self-consistent mean field theory
SEC	Size-exclusion chromatography
t	Time
T	Temperature
$T_{d,5\%}$	Degradation temperature (5% mass loss)
TEM	Transmission electron microscopy
T_g	Glass-transition temperature

TGA	Thermogravimetric analysis
THF	Tetrahydrofuran
TMC	Trimethylene carbonate
TMP	1,1,1-Tris(hydroxymethyl)propane
ToF	Time of flight
TOF	Turnover frequency
TON	Turnover number
Tol.	Toluene
TPE	Thermoplastic elastomer
vCHO	4-Vinyl-1-cyclohexene 1,2-epoxide
X	Coligand (halogen)
χ	Flory-Huggins interaction parameter
λ	Wavelength

List of figures, schemes and tables

Chapter 1: Introduction

Figure 1.1	The linear plastic system highlighting the predominant "*take-make-waste*" pathway for the majority of synthetic polymers.
Figure 1.2	A circular plastic economy.
Figure 1.3	Utilisation of renewable resources and bio-derived monomers for the preparation of oxygenated polymers like polycarbonates and polyesters.
Figure 1.4	Carbon dioxide utilisation pathway into aliphatic polycarbonates and potential end-of-life degradation products. Illustration of the various pathways of carbon dioxide utilisation and removal.
Figure 1.5	Routes to CO_2-derived polycarbonates illustrating the ring-opening copolymerisation (ROCOP) of epoxides and CO_2, and the synthesis and subsequent ring-opening polymerisation (ROP) of cyclic carbonates.
Figure 1.6	Commonly studied aliphatic polycarbonates derived from CO_2 with their corresponding epoxide comonomers.
Table 1.1	Thermal and Mechanical Characteristics of Common Polycarbonates.
Figure 1.7	Formation of polyurethanes by chain-extension of CO_2-polyols with a diisocyanate: one method to obtain higher molar mass CO_2-derived polymer materials.
Figure 1.8	Strategies for block polymer synthesis (clockwise from top: sequential monomer addition; reactivity ratios; orthogonal initiation; switch catalysis).
Figure 1.9	Switch catalysis eliciting sequence control and selective monomer enchainment, and the variety of species accessible by applying this technique to monomer mixtures.
Figure 1.10	Examples of catalysts employed in switchable polymerisation catalysis.

Figure 1.11	Switch catalysis of a three-cycle process illustrating ROCOP of CO_2/epoxide (red/blue), ROCOP of anhydride/epoxide (blue/magenta), and ROP of lactone (green).
Figure 1.12	Range of glass-transition temperatures accessible using polymers obtained from ROP and ROCOP.
Figure 1.13	Phase diagrams and microstructures for linear AB diblock polymer.
Figure 1.14	Stress-strain relationships illustrating ductile plastic (red) and elastomeric (blue) tensile mechanical behaviour.
Figure 1.15	Thermoplastic elastomer (TPE) characteristics: block polymer structure, typical morphologies, elastic recovery.
Figure 1.16	Stylised depiction of domain bridging in relaxed and stretched states for microphase separated samples of linear and branched block polymer architectures.

Chapter 2: Switch Catalysis Using Zinc(II)/Magnesium(II) Heterodinuclear Catalysts

Figure 2.1	Switch catalysis and chain-end control with heterodinuclear Zn(II)/Mg(II) catalysts.
Table 2.1	Data for ε-Decalactone ROP Catalysed by [LZnMg(OBz^{NMe2})$_2$].
Figure 2.2	Analysis of PDL from ROP of ε-DL catalysed by **1** with 8 equivalents of CHD; (a) SEC chromatogram and (b) MALDI-ToF mass spectrum with distributions corresponding to benzoate capped (■) and hydroxyl-telechelic (●) chains.
Figure 2.3	Analysis of PDL from ROP of ε-DL catalysed by **1** with 20 equivalents of CHD; (a) SEC chromatogram and (b) MALDI-ToF mass spectrum with distributions corresponding to benzoate capped (■) and hydroxyl-telechelic (●) chains.
Figure 2.4	SEC trace of PCHC from CHO/CO_2 ROCOP using catalyst **1** at 80 °C.
Scheme 2.1	Switch Catalysis: Combining ROP and ROCOP Cycles Using a Single Catalyst.

Figure 2.5	*In-situ* ATR IR spectroscopy reaction monitoring of a switch polymerisation of ε-DL/CHO/CO_2 at 80 °C. Relative intensity data for bands monitored fitted to monomer conversion values determined by ^{1}H NMR spectroscopy.
Figure 2.6	SEC trace of a crude sample taken from the switch polymerisation of ε-DL/CHO/CO_2 at the end of the reaction.
Figure 2.7	*In-situ* ATR IR spectroscopy reaction monitoring of a switch polymerisation of ε-DL/CHO/CO_2 at 100 °C diluted in toluene ($[CHO]_0$ = 5 M). Relative intensity data for bands monitored fitted to monomer conversion values determined by ^{1}H NMR spectroscopy.
Figure 2.8	SEC traces of final polymer samples from switch polymerisations of ε-DL/CHO/CO_2 conducted at 100 °C under 1 bar (dashed) and 20 bar (solid) CO_2 pressures.
Scheme 2.2	Proposed Synthetic Routes to Heterodinuclear Zn(II)/Mg(II) Catalysts Bearing Organometallic Co-ligands.
Scheme 2.3	Synthesis of the Heterodinuclear [LZnMg$(C_6F_5)_2$] Complex, **2**.
Figure 2.9	^{1}H NMR spectrum of heterodinuclear [LZnMg$(C_6F_5)_2$] complex, **2**.
Figure 2.10	^{13}C{^{1}H} NMR spectrum of heterodinuclear [LZnMg$(C_6F_5)_2$] complex, **2**. Inset spectra highlight splitting of signals for phenyl (d/d'), methine (i/i'), and methyl (j/j' & k/k') carbons.
Table 2.2	ROP and ROCOP Polymerisations Catalysed by Dinuclear Catalysts.
Figure 2.11	SEC trace of PCHC from CHO/CO_2 ROCOP using catalyst **2** at 80 °C.
Figure 2.12	SEC trace of PDL from ε-DL ROP using catalyst **2** at 80 °C.
Figure 2.13	(a) MALDI-ToF mass spectrum of PDL from ROP of ε-DL catalysed by **2**; (b) enlarged region of 8000-9000 m/z (blue section in (a)) highlighting peak separation and DP range, where 'n' corresponds to number of PDL repeat units in $[C_6H_{11}O_2 + (PDL)_n] + K^+$.
Figure 2.14	*In-situ* ATR IR spectroscopy reaction monitoring of switch polymerisation of ε-DL and CHO/CO_2, catalysed by **2**.

Figure 2.15 SEC traces for aliquots of switch polymerisation of ε-DL and CHO/CO_2 taken prior to and a period after switching the reaction atmosphere from N_2 to CO_2.

Chapter 3: High Performance ABA-type Triblock Polymers Derived from CO_2: Adhesives, Elastomers and Toughened Plastics

Figure 3.1 ABA triblock polymer synthesis utilising CO_2 for the preparation of a range of materials displaying plastic, elastomeric, and adhesive behaviours.

Scheme 3.1 Synthesis of High Molar Mass ABA Triblock Polymers Based on Poly(ε-decalactone) and Poly(cyclohexene carbonate).

Table 3.1 PCHC-*b*-PDL-*b*-PCHC (ABA Triblock) Synthetic Characterisation Data.

Figure 3.2 ^{1}H NMR spectrum of a crude sample of ABA-50 highlighting characteristics signals for PDL (4.85 ppm) and PCHC (4.66 ppm) used in determining conversion and relative block composition.

Figure 3.3 $^{13}C\{^{1}H\}$ NMR spectrum of ABA-50. Inset shows zoom in on carbonyl region (177 – 151 ppm).

Figure 3.4 SEC chromatograph for sample ABA-50.

Figure 3.5 $^{31}P\{^{1}H\}$ NMR spectra of ABA-50 triblock polymer and blend of PCHC and PDL homopolymers.

Table 3.2 PCHC-*b*-PDL-*b*-PCHC (ABA Triblock) Thermal Characterisation Data.

Figure 3.6 DSC thermogram of ABA-50 highlighting separate T_gs for PCHC and PDL.

Figure 3.7 DMTA temperature sweep profile for ABA-50. Overlay of storage modulus (*E'*), loss modulus (*E''*), and tan(*δ*).

Figure 3.8 TGA profile for ABA-50 highlighting temperature at 5% mass loss ($T_{d,5}$) and step profile corresponding to two decompositions, each of roughly 50% mass loss.

Figure 3.9 Operating and processing temperature ranges for sample ABA-50, commercial bisphenol-A polycarbonate (BPA-PC), and amorphous poly(lactide) (PLA).

Table 3.3 PCHC-*b*-PDL-*b*-PCHC (ABA Triblock) Mechanical Characterisation Data (Uniaxial).

Figure 3.10 Stress-strain curves for uniaxial extension measurements of ABA triblock polymers. Failure points marked with an "X". Inset: enlargement of the 0 – 200% strain region highlighting region of proportionality for ABA-50 and ABA-40.

Table 3.4 PCHC-*b*-PDL-*b*-PCHC (ABA Triblock) Mechanical Characterisation Data (Cyclical).

Figure 3.11 Cyclical tensile analysis. (a) Plot of normalised maximum stress ($\sigma_{200\%}$) *vs.* cycle number. (b) Measurement profiles for ABA-26. Only cycles 1, 5, and 10 shown and offset horizontally for clarity.

Figure 3.12 Cyclical tensile measurement of ABA-50 illustrating a strain induced plastic-to-rubber transition. Parameters: 0 - 200% strain, 10 cycles. Only cycles 1, 2, 5, and 10 shown for clarity.

Table 3.5 Rheological and Adhesive Performance Data for ABA-20 Triblock Polymer.

Figure 3.13 Frequency sweep (25 °C) for ABA-20. Grey region represents area below Dahlquist's criterion ($G' \leq 3 \times 10^5$ Pa).

Figure 3.14 Rheological characterisation of ABA-20 showing (a) the relationship of shear stress to shear strain rate highlighting shear-thinning behaviour and (b) a double log plot of viscosity against shear strain rate from which the zero shear viscosity (η_0) is estimated.

Figure 3.15 Viscoelastic window constructed for ABA-20. Limits determined using values for *G'* and *G"* at bonding (10^{-1} rad s^{-1}) and debonding (10^{2} rad s^{-1}) frequencies from the frequency sweep. Quadrant titles indicate PSA classification.

Figure 3.16 Schematic representations of 180° Peel and Loop Tack adhesive testing methods.

Figure 3.17 Adhesive performance in 180° peel and loop tack testing methods for ABA-20 (green highlight) and examples of commercial (purple highlight) and literature (yellow highlight) PSAs.

Figure 3.18 Ashby-style plots of tensile toughness (U_T) *vs.* (a) tensile strength (σ) and (b) elongation at break (ε_b) for comparison of ABA-50 with examples of commercial and literature materials.

Chapter 4: $(AB)_n$ Star Polymers Derived from CO_2: Influence of Architecture and Post-Modification

Figure 4.1	Synthesis and post-polymerisation modification of $(AB)_n$ star block polymers utilising CO_2.
Scheme 4.1	Synthesis of $(PDL)_n$ star polymers.
Table 4.1	Multiarm star $(PDL)_n$ Characterisation Data
Figure 4.2	^1H NMR spectra of purified 3- and 4-arm star poly(ε-decalactone) highlighting signals for backbone, core, and end-group proton.
Figure 4.3	SEC chromatographs of 3-arm (red) and 4-arm (blue) star poly(ε-decalactone) samples.
Scheme 4.2	Synthesis of $(AB)_n$ Star Block Polymers Comprising PDL-*b*-PvCHC Diblock Arms.
Table 4.2	(PvCHC-*b*-PDL)$_n$ [$(AB)_n$] Star Block Polymer Characterisation Data
Figure 4.4	Representative ^1H NMR spectrum of a purified $(AB)_n$ star block polymer highlighting signals used for determination of relative block ratio.
Figure 4.5	SEC chromatograph for star block polymer sample $(AB)_3$-88. Highlighted values for M_n and $Đ_M$ corresponding to the majority distribution (central peak) and the overall chromatogram.
Figure 4.6	$^{31}P\{^1H\}$ NMR spectra comparing $(PDL)_3$ and $(AB)_3$ (A = PvCHC, B=PDL) end-group titrations.
Table 4.3	$(AB)_n$ Star Block Polymer Mechanical Characterisation Data.
Figure 4.7	Representative stress-strain curves for linear triblock samples.
Figure 4.8	Digital photographs of sample $(AB)_2$-63 during uniaxial extension: (a) Full view of specimen with areas of interest marked; (b) Enlarged view of yellow highlighted area showing whitening of the central specimen area; (c) Enlarged view of red highlighted area showing lower extent of whitening nearer the specimen shoulder (clamped) area; (d) Full view of specimen with background light darkened to highlight contrast of stress-whitening.
Figure 4.9	Representative stress-strain curves for 3-arm star block polymers of low (52 kg mol^{-1}) and high (88 kg mol^{-1}) molar mass.

Figure 4.10	Representative stress-strain curves for high molar mass star block polymers with 2, 3, and 4 arms.
Figure 4.11	Digital photographs of sample $(AB)_3$-88: (a) Pristine and fractured test specimens before and after uniaxial extension, respectively; (b) Central region of a sample during uniaxial extension with absence of stress-whitening.
Figure 4.12	Trends in yield stress (σ_y), Young's modulus (E_y), tensile stress (σ), and elongation at break (ε_b) with respect to arm molar mass ($M_{n,arm}$) across the range of $(AB)_n$ star block polymers. Lines are used to help guide the eye.
Scheme 4.3	Post-Polymerisation Modification of $(AB)_n$ Star Block Polymers.
Table 4.4	$(A^{ME}B)_n$ Modified Star Block Polymer Thermal Characterisation Data.
Figure 4.13	DMA thermal sweeps for high molar mass, non-modified ($(AB)_3$) and modified ($(A^{ME}B)_3$) 3-arm star block polymers. T_g values highlighted as the peak maxima on the tan(δ) curve.
Figure 4.14	Tan(δ) versus temperature for 3-arm, modified star block polymers at high and low molar mass.
Figure 4.15	Plot of the peak maxima in tan(δ) from DMA against number of arms for non-modified and modified star block polymers.
Table 4.5	$(A^{ME}B)_n$ Modified Star Block Polymer Mechanical Characterisation Data
Figure 4.16	Stress-strain profiles for non-modified ($(AB)_3$-#) 3-arm star block polymers and their modified analogues ($(A^{ME}B)_3$-#) at high and low molar mass.
Figure 4.17	Stress-strain curves for modified star block polymer samples, $(A^{ME}B)_n$, with n = 3, 4, and 6 arms. Failure points marked with an "X".
Table 4.6	Small-Angle X-ray Scattering (SAXS) Data of $(A^{[ME]}B)_n$ Star Block Polymers.
Figure 4.18	1D SAXS profiles for non-modified ($(AB)_3$-52) and modified ($(A^{ME}B)_3$-52) star block polymers. $(A^{ME}B)_3$-52 indexed for lamellar morphology, d^* represents domain periodicity.

Figure 4.19 Plot of domain spacing (d^*) against arm molar mass ($M_{n,arm}$) for the series of non-modified ($(AB)_n$) and modified ($(A^{ME}B)_n$) star block polymers.

Chapter 5: Outlook

Figure 5.1 Future challenges and opportunities for switchable polymerisation catalysis and CO_2-derived polymers.

Figure 5.2 Heterodinuclear catalyst development to optimise polymerisation rates and end-group control.

Figure 5.3 Multiple sequential switches to build $[A\text{-}b\text{-}B]_n$ multiblock polymers from a single starting monomer mixture.

Figure 5.4 Formation of ionomers to promote dynamic cross-linking in block polymer domains and target enhanced properties or responsive behaviour.

Figure 5.5 Additional non-linear architectures, possibly achievable by utilising switchable polymerisation catalysis.

Table of Contents

	Declaration	3
	Abstract	4
	Acknowledgements	6
	List of publications	7
	List of abbreviations	8
	List of figures, schemes and tables	12

Chapter 1: Introduction

1.1	Polymer sustainability	24
1.2	CO_2-derived polymers	27
1.3	Block polymers and switch catalysis	36
1.3.1	Synthetic strategies to prepare block polymers	36
1.3.2	Switchable catalysis: Principles and developments	39
1.3.3	Functional materials	43
1.3.4	Architectural control	52
1.4	Aims and objectives	55
1.5	References	56

Chapter 2: Switch Catalysis Using Zinc(II)/Magnesium(II) Heterodinuclear Catalysts

2.1	Introduction	66
2.2	Aims	67
2.3	Catalysis using a Zn(II)/Mg(II) heterodinuclear catalyst: Benzoate coligands	69
2.3.1	Ring-opening polymerisation of ε-decalactone	69

2.3.2 Ring-opening copolymerisation of cyclohexene oxide and CO_2 74
2.3.3 Combing ROP and ROCOP: Switch catalysis of ε-DL, CHO, and CO_2 76
2.4 Applying an organometallic Zn(II)/Mg(II) heterodinuclear catalyst: Addressing the coligand problem 82
2.4.1 Synthesis and characterisation 82
2.4.2 Polymerisation studies 87
2.5 Summary and future work 93
2.6 References 95

Chapter 3: High Performance ABA-type Triblock Polymers Derived from CO_2: Adhesives, Elastomers and Toughened Plastics

3.1 Introduction 98
3.2 Aims 101
3.3 CO_2-derived ABA triblock polymers: Synthesis and characterisation 103
3.3.1 Material preparation 103
3.3.2 Thermal properties 109
3.4 Mechanical testing 116
3.4.1 Uniaxial tensile experiments 116
3.4.2 Cyclical tensile experiments 119
3.4.3 Adhesion testing 123
3.5 Discussion 131
3.6 Summary and future work 137
3.7 References 141

Chapter 4: $(AB)_n$ Star Polymers Derived from CO_2: Influence of Architecture and Post-Modification

4.1 Introduction 146
4.2 Aims 147

4.3 $(AB)_n$ star polymers: Synthesis and characterisation 148

4.4 Influence of molar mass and arm number 158

4.5 Post-polymerisation modification of the polycarbonate block 168

4.6 Summary and future work 180

4.7 References 183

Chapter 5: Outlook

5.1 Challenges and opportunities 185

5.2 Switchable polymerisation catalysis 186

5.3 High performance materials 189

5.4 Architectural control 191

5.5 References 193

Chapter 6: Experimental Section

6.1 General 196

6.2 Analytical techniques 197

6.3 Experimental procedures 201

6.4 References 209

Chapter 7: Appendices

7.1 Chapter 2 211

7.2 Chapter 3 217

7.3 Chapter 4 234

7.4 Permissions 250

7.5 References 254

CHAPTER 1

Introduction

1.1. Polymer sustainability

Plastics, or more specifically synthetic polymers, have revolutionised materials science and engineering since their discovery just over a century ago. The growth of synthetic polymers has provided unprecedented material versatility and allowed for their use in numerous applications. However, the majority of plastics currently in large-scale production (e.g. polyethylene, polypropylene) are derived from fossil-fuel resources and have therefore been subject to sustained environmental scrutiny, given they appear to pollute a range of ecosystems from soils to oceans. Additional concerns are rightly raised regarding the end-of-life fate of these materials, particularly as they are typically not biodegradable and one of their key advantages is durability.[1] This, alongside issues with recyclability and/or recycling processes, as well as poor waste stream management, has resulted in the increased pervasiveness and accumulation of plastics in the environment (**Figure 1.1**).[2-5]

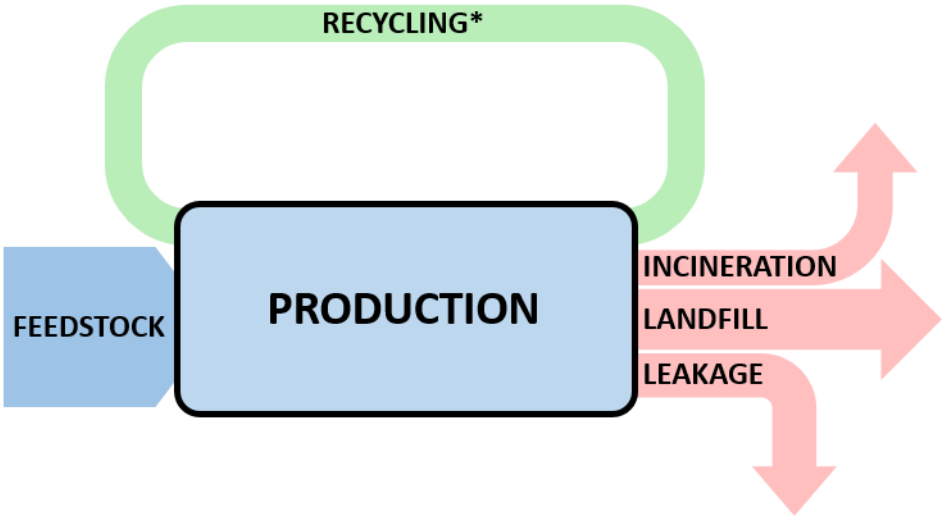


Figure 1.1. The linear plastic system highlighting the predominant "*take-make-waste*" pathway for the majority of synthetic polymers. *Recycling comprises cascade, closed-loop, and process losses. Modified from Ellen MacArthur Foundation.[6]

The issues of plastics and their environmental impacts are complex and no single "silver bullet" strategy exists to solve them.[6] Instead, they must be addressed with various targeted strategies including: utilisation of renewable feedstocks, careful material design and

sustainable synthesis and processing, recyclability, reduction, and waste management, to name a select few. Realisation of these approaches as a whole would ultimately bring about a shift from the current linear system to a circular economy for plastics (**Figure 1.2**).[7-8]

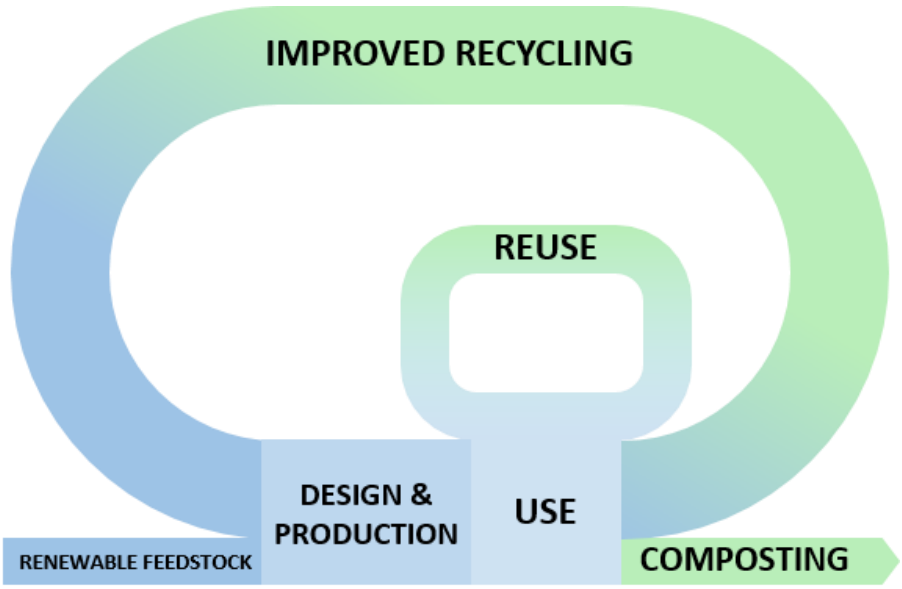


Figure 1.2. A circular plastic economy. Modified from Ellen MacArthur Foundation.[6]

Polymer chemistry will continue to play an important role in the realisation of a circular plastic economy, particularly where research into renewable synthetic polymers is concerned. The goals of this thesis are to investigate oxygenated polymers (polyesters and polycarbonates) and appreciate how they might align with certain aspects of a future circular plastic economy, as outlined below (**Figure 1.3**).

(1) Key to reducing the high use of fossil-fuel resources as raw materials, with the associated carbon emissions, is to develop polymerisation catalysis using renewable resources, such as CO_2 and bio-derived monomers. Working out how to use these feedstocks could allow for reduced carbon dioxide emissions and may help diversify the raw materials used in polymer synthesis.

(2) Considered design of new materials and improvement to their property profiles is important to them being able to compete with or even replace current

petrochemicals. Design and function will, naturally, also factor in to material use, reuse, and end-of-life scenarios; emphasis should be on avoiding pathways leading to accumulation of waste and leakage.

(3) Development of methods and protocols to design and make polymers that are aligned with the principles of sustainability and green chemistry. It is important to attempt a wider consideration of environmental, economic, and social factors to applying methods more generally in the future and at scale.

(4) Decreasing the prevalence of waste and accumulation in end-of-life scenarios is important. It should be addressed with proof-of-concept studies to understand the stability and potential degradability of new materials.

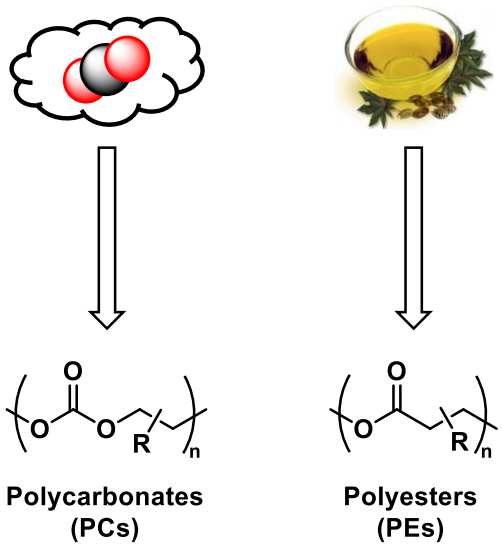


Figure 1.3. Utilisation of renewable resources and bio-derived monomers for the preparation of oxygenated polymers like polycarbonates and polyesters.

1.2. CO_2-derived polymers

The changing sentiment around plastic production and waste has directed research towards the synthesis of new polymers made from annually renewable resources. One resource which has seen particular interest is carbon dioxide; abundant, non-toxic, and renewable, this waste gas is being harnessed as a C1 synthon for the production of aliphatic polycarbonates which, owing to their backbone chemistry, also have the potential to be (bio)degradable (**Figure 1.4**).

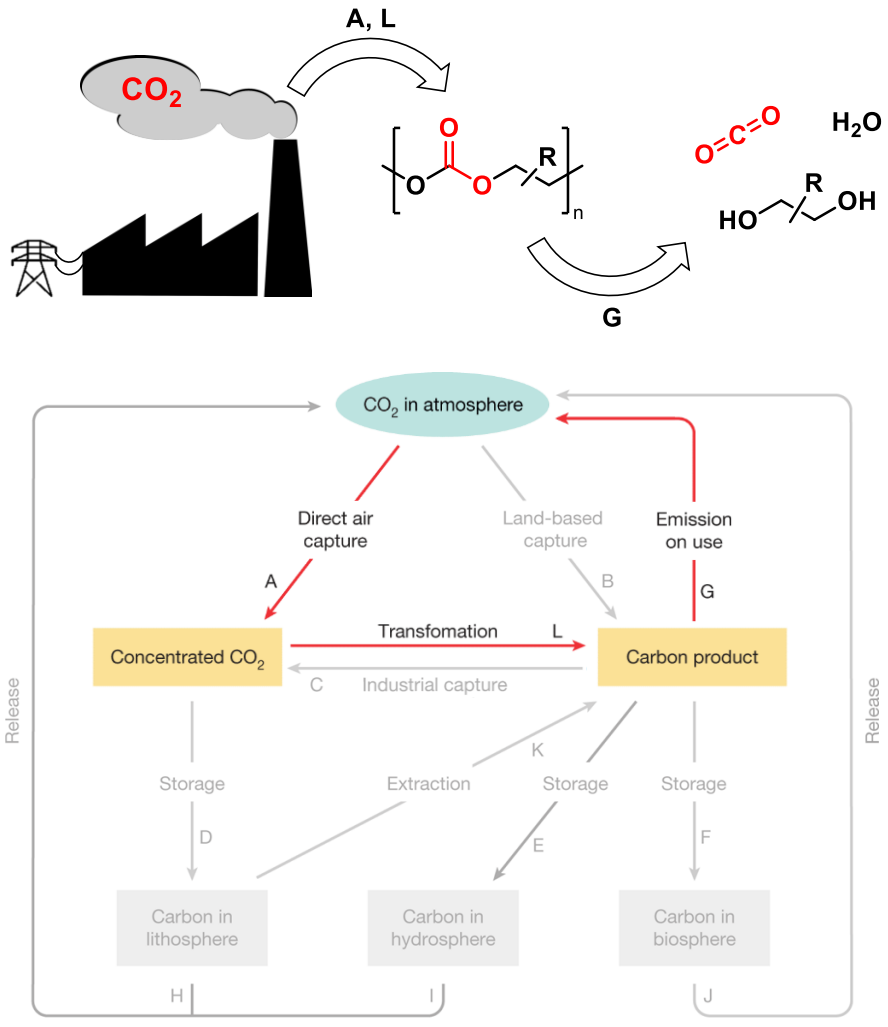


Figure 1.4. Carbon dioxide utilisation pathway into aliphatic polycarbonates and potential end-of-life degradation products. Illustration of the various pathways of carbon dioxide utilisation and removal: Pathway ALG (red arrows, highlighted) represents the cycling pathway for CO_2 → polymer utilisation. Emission on use (G) constitutes hydrolysis or decomposition of CO_2-polymers. Modified from Hepburn *et al.* (see Appendix 7.4 for reuse license).[9]

Life-cycle analysis (LCA) which compared CO_2-derived polyols (up to 20 wt % derived from CO_2) with industrially used polyether polyols (synthesised from 100% epoxide) was conducted by von der Assen and Bardow in 2014.[10] The report highlighted a reduction in both greenhouse gas (GHG) emissions (11 – 19%) and fossil fuel resource usage (13 – 16%) by virtue of reducing the epoxide usage, but the authors note that production of CO_2-polyols alone is not sufficient to act as a GHG sink.

Integration of this utilisation technology with current industrial infrastructure has been described in other reports with discussion points around, for example, its viability when using impure CO_2 sources like flue gas.[11-12] In 2019, a multidisciplinary team reported a detailed techno-economic assessment on carbon dioxide utilisation and removal at scale, identifying 10 key utilisation pathways of which the transformation of CO_2 into chemical products including polymers featured as one of these promising and scalable pathways.[9]

Projections for 2050 estimate the CO_2 utilisation from the polyol sub-pathway could reach 10 – 50 Mt yr^{-1}; the current largest-scale chemical utilisation pathway is urea production, already at 140 Mt CO_2 yr^{-1}. Nonetheless, compared with other sub-pathways the CO_2-polyol technology has already seen commercialisation and the market is currently profitable owing to the higher selling price of product (US$2040 per tonne of product) *vs.* cost of manufacturing with CO_2 utilisation (US$1440 per tonne of product), the latter of which is anticipated to be cheaper in 2050 and continue trending downwards.

The process at the heart of the assessments is the ring-opening copolymerisation (ROCOP) of epoxides and carbon dioxide, which presents an attractive method to preparing CO_2-derived polycarbonates and directly incorporates a CO_2 unit into the repeat unit of the polymer backbone (**Figure 1.5**). This reaction has gained traction since its discovery in the 1960s by Inoue and co-workers, and now attracts significant attention given the drive towards

more sustainable polymer synthesis.[13] Research output has focussed heavily on the development of faster, more selective, catalysts while at the same time exploring the scope of epoxides that can undergo polymerisation with CO_2 as a co-monomer.[14-16]

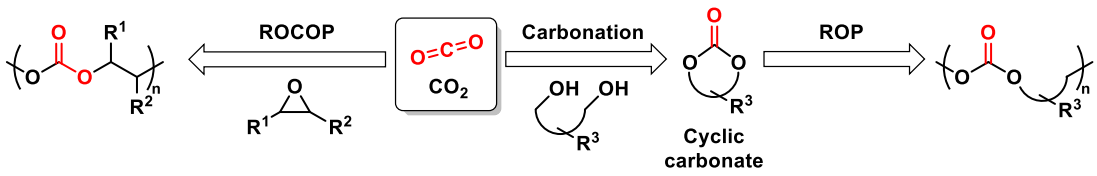


Figure 1.5. Routes to CO_2-derived polycarbonates illustrating the ring-opening copolymerisation (ROCOP) of epoxides and CO_2, and the synthesis and subsequent ring-opening polymerisation (ROP) of cyclic carbonates.

The types of catalysts that have been identified for CO_2-epoxide ROCOP are extensive, covering both homogeneous and heterogeneous as well as both organometallic and, more recently, metal-free examples.[17-19] Some of the most widely studied homogeneous catalysts include metal(III) salen and co-catalyst systems (termed binary systems), zinc β-diiminates (Zn-BDI), and bimetallic complexes, with a macrocyclic ancillary ligand.[20-21] Advanced studies of metal salen based systems, which usually require a co-catalyst to function, found increased efficacy by covalently tethering an organic salt co-catalyst to create a single bifunctional species.[22-23] The development of various bimetallic zinc complexes in a tethered β-diiminate system resulted in exceptional activities for copolymerisation of CO_2 with cyclohexene oxide (CHO), but this came at the expense of selectivity for polycarbonate formation (i.e., formation instead of cyclic carbonate and polyether).[24]

One important advance in the bimetallic class of catalysts was the development of heterodinuclear analogues which generally exhibited enhanced catalytic activity compared to homodinuclear counterparts.[25-26] Further studies from Williams and co-workers on the bimetallic family discussed the role of each metal, probing cooperativity and the synergic effect observed in the copolymerisation of CO_2 with various epoxides.[21, 27-30] Presently, the

fastest catalyst showing quantitative selectivity for perfectly alternating polycarbonate (PCHC) formation is a Co(II)/Mg(II) bimetallic complex.[30]

It is worth mentioning that an alternative route to aliphatic polycarbonates is through the ring-opening polymerisation of cyclic carbonates – typically 6- and 7-membered species but examples of strained 5-membered monomers are also known (**Figure 1.5**).[31-36] Synthesis of the monomers often still involves toxic reagents such as phosgene or its derivatives which, although providing a slightly safer alternative, can remain synthetically challenging or give unwanted side reactions. However, in 2015 the synthesis of 6-membered cyclic carbonate monomers was achieved under mild conditions *via* the carbonation of 1,3-diols with low pressure CO_2 (1 atm) and common reagents (DBU, NEt_2, TsCl).[37] Modifications to the procedure later allowed for the preparation of cyclic carbonate monomers (and subsequently polycarbonates) derived from both CO_2 and the sugar 2-deoxy-D-ribose, thus providing increasingly sustainable polycarbonate syntheses.[38]

Some of the most commonly studied aliphatic polycarbonates derived from CO_2 are poly(propylene carbonate) (PPC), poly(cyclohexene carbonate) (PCHC), and increasingly poly(limonene carbonate) (PLimC); all three can be prepared *via* epoxide/CO_2 ROCOP with their corresponding epoxide comonomers (**Figure 1.6**). A number of factors account for the heightened interest in these three particular polymers including, but not limited to: (1) propylene oxide (PO), used to prepare PPC, is a commodity chemical and resulting PPC polyols, which can contain up to 43 wt% CO_2, are extensively investigated in the manufacturing of polyurethane (PU)[10, 39-43]; (2) PO-CO_2 and CHO-CO_2 ROCOP are used most often as benchmark polymerisations to evaluate new ROCOP catalysts for acyclic and alicyclic epoxide monomer classes, respectively[20-21]; (3) CHO is an inexpensive, commercially available epoxide that offers an option to make rigid aliphatic polycarbonates with high glass transition temperatures[44]; (4) PLimC is prepared from limonene oxide (LO), a commercially

available, renewable epoxide derived from limonene which can be sourced from waste citrus peel.[45-46]

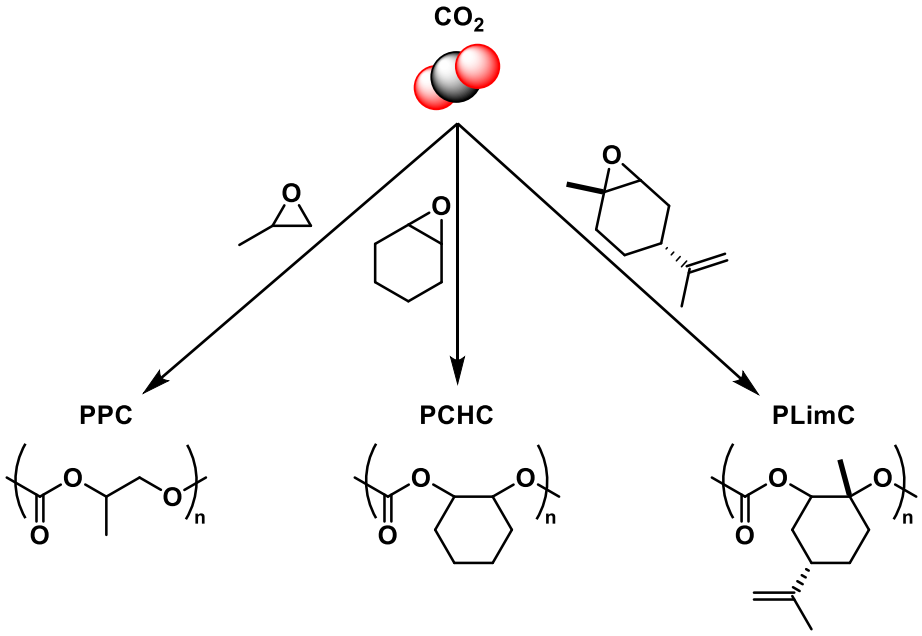


Figure 1.6. Commonly studied aliphatic polycarbonates derived from CO_2 with their corresponding epoxide comonomers. PPC = poly(propylene carbonate); PCHC = poly(cyclohexene carbonate); PLimC = poly(limonene carbonate).

Poly(propylene carbonate) is well established amongst the CO_2-derived aliphatic polycarbonates, not least because the monomer propylene oxide is a commodity chemical (global production: 9 Mt yr^{-1}).[47] Some of the earliest reports of CO_2-epoxide copolymerisation concern the formation of PPC, and a number of the major catalyst families are now well-optimised for the ROCOP of PO and CO_2.[21] The material property profile exhibits a large range in tensile properties which are heavily dependent on the molar mass of PPC (**Table 1.1**). Moreover, without modification or blending, even higher molar mass specimens are limited in their applications at high temperatures given the moderate T_g of around 42 °C. Nevertheless, the increased ductility of PPC and scale of its production account for its prevalence in the synthesis of higher polymers to enhance its property profile, for example in the synthesis of block copolymers and in the manufacturing of polyurethanes.[10, 39-42]

The more rigid poly(cyclohexene carbonate) possesses a high T_g of up to 115 °C, as well as high tensile strength (40-44 MPa) (**Table 1.1**). It is, however, greatly limited by its elongation at break of only 1 – 2%, and accordingly is classified as a brittle polymer. Comparisons to the properties of the classical bisphenol A polycarbonate (BPA-PC) were made by Koning *et al.* and revealed PCHC to be inferior for high temperature applications.[44] They also noted that a low entanglement density for PCHC is a large contributing factor to its brittleness, even given the relatively high molecular weight of the sample. Nevertheless, owing at least in part to the commercial availability of cyclohexene oxide (CHO), catalysis to prepare PCHC still garners significant attention and development while research into methods for the valorisation and enabling of PCHC as a functional material begin to also gain traction.

Poly(limonene carbonate) is an attractive polymer given its high renewability compared with other aliphatic polycarbonates. The derivation of the limonene oxide (LO) monomer from waste citrus peel may offer a more sustainable option for polycarbonate synthesis, and investigations into the ROCOP of limonene oxide and CO_2 have unearthed interesting features of the catalysis. In 2004, Coates and co-workers employed a β-diiminate zinc acetate catalyst in the copolymerisation of LO and CO_2, and observed selective incorporation of the *trans* diastereomer of (*R*)-limonene oxide (*cis* : *trans* = 1.2 : 1), affording low molar mass (3.7 – 10.8 kg mol^{-1}), regioregular poly(*R*-limonene carbonate) under mild conditions (25 – 50 °C, 0.4 mol% catalyst loading).[48] A decade later, Kleij and colleagues were able to incorporate both *cis* and *trans* diastereomers in the copolymerisation with CO_2 by using an amino-trisphenolate Al(III) complex, leading to higher overall conversion of the monomer pool (i.e., *cis*/*trans* mixture) but reduced stereoregularity.[49]

Building from the reports on aspects of catalysis, investigation into the thermomechanical properties of PLimC, as well as higher molar mass samples has also

garnered attention. Greiner and colleagues were able to prepare, on kilogram scale, samples of PLimC with molar mass of over 100 kg mol^{-1}.[50] The polymer possessed a high T_g of around 130 °C and was found to exhibit high stress at break (55 MPa) and Young's modulus (0.95 GPa), but was hindered by its brittleness which restricted much of its use as a standalone material in film form (**Table 1.1**). In subsequent studies, they exploited the pendent –ene moiety present in the repeat unit and applied straightforward methods of post-polymerisation modification (PPM) to valorise the virgin polymer and access materials with tailored properties, from antibacterial coatings to thermoplastic elastomers (TPEs).[51]

Table 1.1. Thermal and Mechanical Characteristics of Common Polycarbonates

Polymer[a]	T_g[b] (°C)	Young's Modulus (GPa)	Tensile Strength (MPa)	Elongation at break (%)	Ref.
PPC	42	0.7-1.4	7-30	600-1200	43
PCHC	115	3.5-3.7	40-44	1.1-2.3	44
PLimC	130	0.95	55	15	50

[a]Polycarbonates from coupling of CO_2 and epoxides: PPC = poly(propylene carbonate); PCHC = poly(cyclohexene carbonate); PLimC = poly(limonene carbonate). [b]Glass transition temperature determined from DSC.

To date, the predominant focus of academic research relating to CO_2-derived polymers has been on understanding and developing the catalysis. Aside from a few exceptions, there is less detailed investigation into the material properties of these polycarbonates, especially as often only low molar mass species are produced. As mentioned, these low molar mass polyols, particularly PPC, are important as feedstock for coupling with diisocyanate reagents to prepare polyurethanes (**Figure 1.7**). This represents one method to achieve higher weight materials which are able to perform in an engineering capacity, for example in rigid or flexible foams, TPEs, and sealants.[52-53]

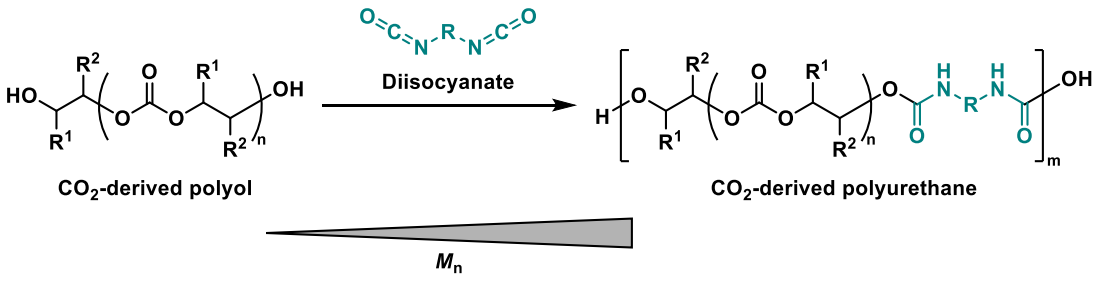


Figure 1.7. Formation of polyurethanes by chain-extension of CO_2-polyols with a diisocyanate: one method to obtain higher molar mass CO_2-derived polymer materials.

The direct synthesis of higher molar mass polycarbonates, without the need for chain-extension, has been the subject of a limited number of reports.[44, 54] Moreover, the general focus of these is placed on the feasibility of synthesis; barriers to achieving high molar mass typically arise from issues with monomer purity, catalyst sensitivity and/or efficiency at low

loadings, or multiple initiating species and so the reports initially have addressed these points. An example of this is a recent report from Feng and colleagues, where high molar mass PCHC (1030 kg mol^{-1}) and PPC (402 kg mol^{-1}) were synthesised through careful drying of the CO_2 using a specialised setup employing triisobutylaluminium (TiBA).[54] Through this method they were able to obtain monomodal molar mass distributions of pure PCHC and PPC, as well as exploiting the chain-end fidelity to prepare exclusively PPC-*b*-PCHC diblock copolymers.

Naturally, higher molar mass aliphatic polycarbonates from ROCOP means increased CO_2 utilisation. However, unlike PPC for example (which at sufficient M_n can exhibit more ductility and increased elongation), the mechanical integrity of desirable higher T_g materials, particularly PCHC, does not always inherently benefit from significantly increased molar mass, and the materials remain brittle and difficult to process or apply in an engineering capacity. It is important to emphasise that established polymers like high-density polyethylene (HDPE) and bisphenol A polycarbonate (BPA-PC) would show equivalent brittleness, but is typically overcome by using plasticisers. However, uncertainty surrounding leaching of these additives motivates investigation into alternative strategies. One interesting option to address this issue, and valorise high molar mass, high T_g, polycarbonates, is to incorporate them into block copolymers, allowing them to function as rigid segments but with the brittleness tempered by the other constituent block(s).

1.3. Block polymers and switch catalysis

The linking of homopolymers into block polymers expands the range of functional materials and enables the physico-chemical properties to be optimised through the selection of constituent blocks and their relative volume fraction. Accordingly, block polymers provide great versatility for applications and are now key components in areas such as biomedical and mechanical engineering, electronics, and lithography.[55-58]

1.3.1. Synthetic strategies to prepare block polymers

A variety of strategies exist to prepare block polymers, applicable to both traditional and more modern polymerisation techniques, with selected examples illustrated below (**Figure 1.8**). While fundamentally all the strategies achieve the same outcome of block polymer synthesis, each have their own benefits and drawbacks, making it important to consider the specifics of the desired polymer as well as any limits on the overall synthetic procedure, for example when utilising renewable sources and targeting oxygenated polymers.

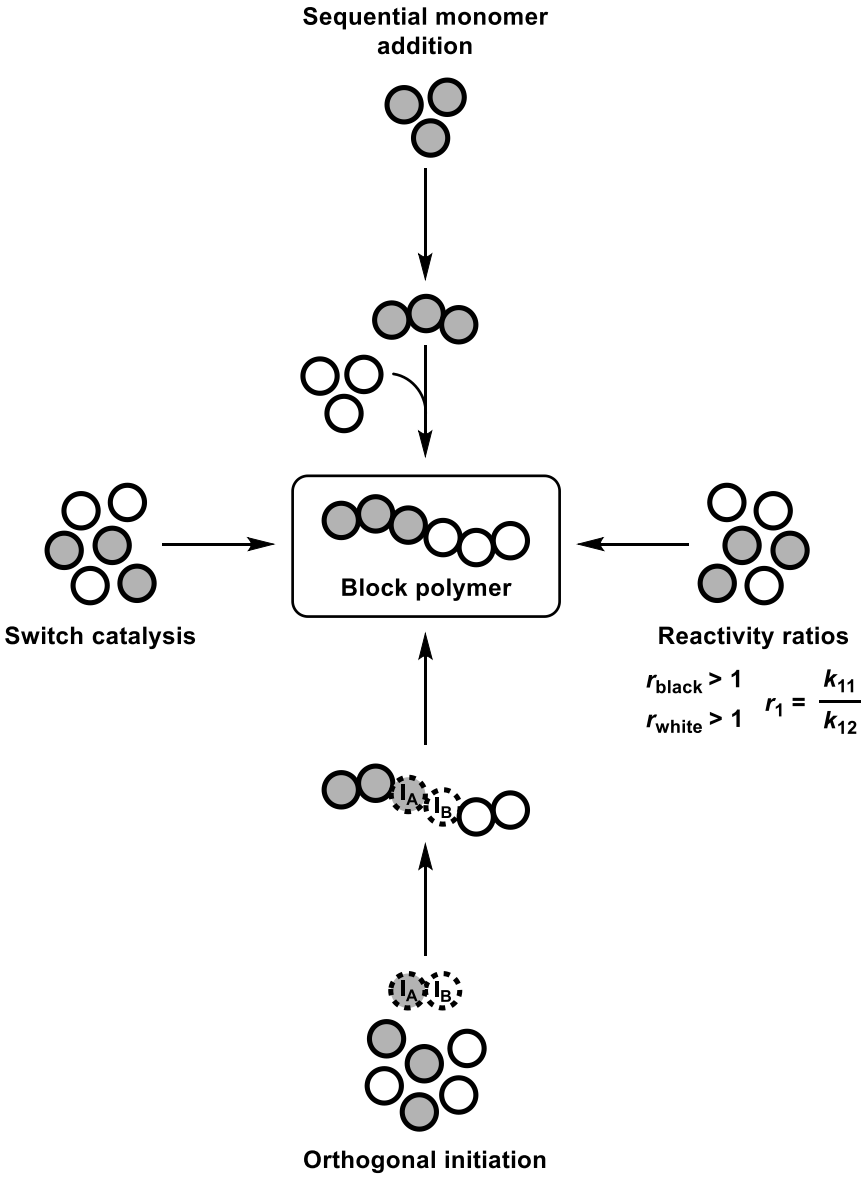


Figure 1.8. Strategies for block polymer synthesis (clockwise from top: sequential monomer addition; reactivity ratios; orthogonal initiation; switch catalysis).

One of the most well-known, and perhaps most widely applied, strategies is *sequential monomer addition*. Regularly employed in ionic and controlled radical polymerisation techniques due to its conceptual simplicity, this method relies on timed additions of different monomers to build up the resulting block sequence. Quantitative depletion of the first monomer (and each thereafter if targeting a multiblock polymer) is necessary to avoid tapering between blocks or larger segments of statistical copolymer within the overall backbone.

Alternatively, by exploiting the specific reactivity of certain monomer combinations, block copolymer formation can be achieved without requiring the timed addition(s) of a secondary monomer(s).[59-60] So called *reactivity ratios* provide a measure of the preference for a particular monomer to homopolymerise or copolymerise in the presence of a secondary monomer. Where the ratios for individual monomers in a pairing exceed unity (i.e. $r_{black} > 1$, $r_{white} > 1$), the propensity for each is to homopolymerise. In the absence of simultaneous homopolymerisation of both monomers (forming discrete homopolymers), the secondary monomer will eventually insert and begin to polymerise on near quantitative conversion of the primary monomer, hence forming the block polymer. This method relies on being able to identify monomer pairings with optimal reactivity ratios, and can therefore be restricted to particular combinations. If the ratios for a certain monomer pair are not optimised for block polymer formation, undesired tapering or statistical copolymers may be observed.

Orthogonal initiation is a strategy which utilises a bifunctional initiating species/catalyst capable of performing distinct polymerization mechanisms, e.g. controlled radical and RO(CO)P, that would otherwise be difficult to link together without intermediary purification or modification.[61-64] The constituent blocks can be formed either simultaneously or sequentially, depending on the reaction conditions required for each polymerisation mechanism. Regardless, given that the block junction is established at the outset, this technique obviates the need for timed monomer additions and/or careful monomer selection to ensure lack of tapering. However, the strategy is instead limited by the selection and/or availability of compounds with the specific functionality required to initiate the desired polymerisation mechanisms.

Switch catalysis, also referred to as *switchable polymerisation catalysis*, has been recently developed as a powerful tool for the preparation of sequence-controlled block polymers from a mixture of monomers.[65-66] This technique applies a single catalyst able to

switch between different polymerisation mechanisms/cycles (e.g. heterocycle/heteroallene ROCOP and heterocycle ROP) while exercising monomer selectivity. The addition or removal of monomers, either passively or actively, directs the catalysis through a mechanistic switch which has both thermodynamic and kinetic driving forces.[66] Passively, block polymer sequences can be built up through monomer consumption of a pre-determined feedstock stoichiometry, whereas an active switch can be achieved by introducing monomers like CO_2 and anhydrides.

1.3.2. Switchable catalysis: Principles and developments

In block polymer synthesis, switch catalysis differentiates itself from techniques like sequential addition and reactivity ratios given that the shift from one polymerisation pathway to another is usually immediate and prompts quantitative selectivity for block sequences. As a result, tapering between blocks is rarely observed even though monomer mixtures are employed and monomer additions over the course of the polymerisation can still feature. At the same time, it's efficacy is not dependent on external factors, such as thermal,[67] electrical,[68-70] or photochemical[71-73] triggers, featuring in other examples of catalysis in which a polymerisation is turned on and off.[74-75] Still in its early stages of development and optimisation, switchable polymerisation catalysis has already demonstrated the ability to deliver varied copolymers with control over the block sequence as well as monomer placement, owing to the nature of the polymerisation cycles accessed (**Figure 1.9**).[66]

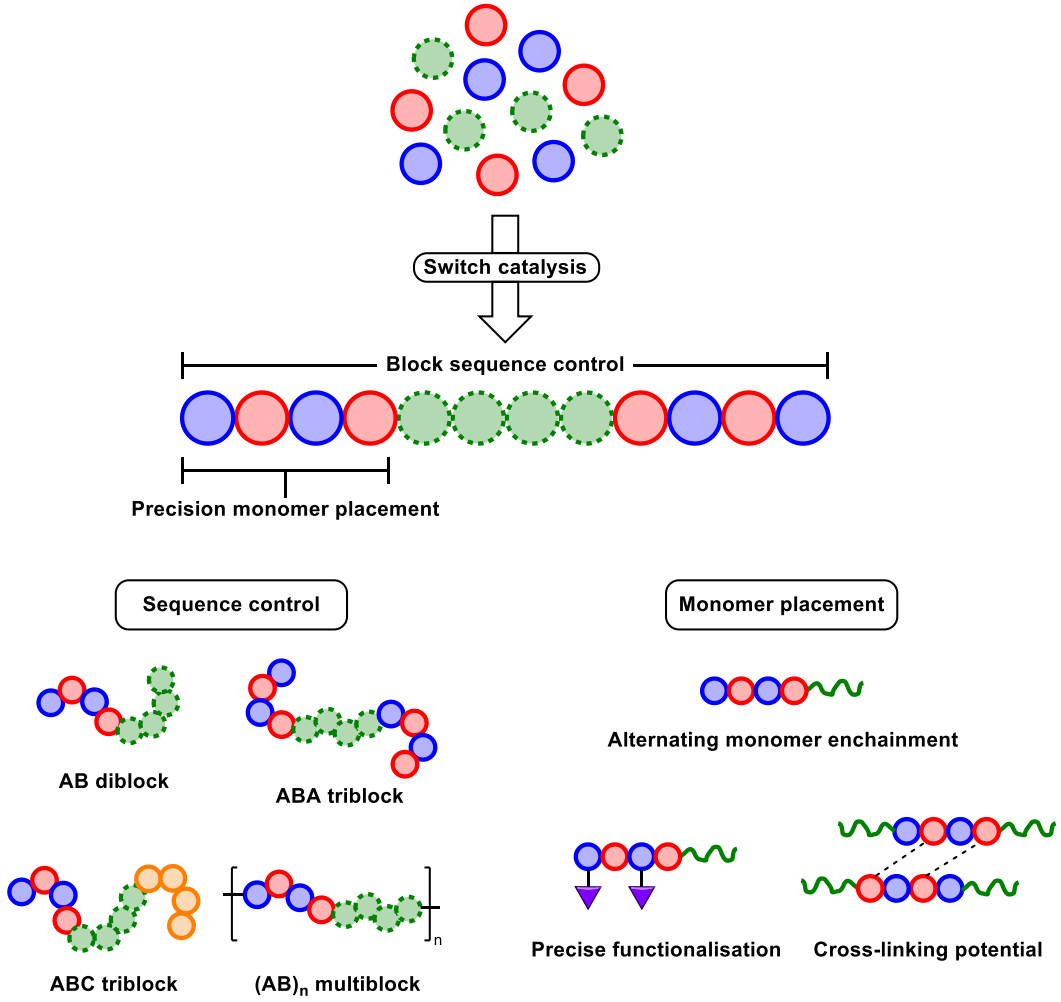


Figure 1.9. Switch catalysis eliciting sequence control and selective monomer enchainment, and the variety of species accessible by applying this technique to monomer mixtures.[66]

Although not designated as switch catalysis at the time, one of the first examples of a catalyst linking heterocycle ROCOP and lactone ROP cycles was an aluminium-porphyrin system reported in 1985 by Inoue and co-workers.[76] The catalyst was able to prepare short chain block polymers (oligomers) from the copolymerisation of phthalic anhydride and propylene oxide followed by the ring-opening polymerisation of β-butyrolactone in a sequential fashion. Two decades later, reports of ROCOP terpolymerisations began to emerge, but scarcely reported were polymerisations involving both ROP and ROCOP of mixtures of lactones, heterocycles, and heteroallenes, with those that did feature suffering

from poorly controlled catalysis and insufficient evidence for a switch between mechanisms.[77-81]

The landscape then changed in 2014 with the development of a dizinc catalyst (**I**) by Williams and co-workers.[82] When exposed to mixtures of epoxide, CO_2, and lactone, this homogeneous catalyst was able to prepare block polymers comprised of polycarbonate and polyester blocks via the ROCOP of cyclohexene oxide/CO_2 and the ROP of ε-caprolactone, respectively. The selectivity for either the ROP or ROCOP cycle was governed by both kinetic and thermodynamic factors, being dictated by the relative rates and stability of monomer insertion and, consequently, the chemistry at the zinc-polymer propagating chain-end; an alkoxide could react with CO_2 or the lactone but would not ring-open the epoxide, whereas a carbonate could facilitate the ring-opening of an epoxide but not of the lactone.[83] Later, the same orthogonal reactivity was observed where CO_2 was replaced with a cyclic anhydride, maintaining a mechanistic switch between ROP and ROCOP but in this case fashioning block polyesters.[84]

Subsequent advances to **I** produced catalysts with trifluoroacetate (TFA) (**II**) and phenyl (Ph) (**III**) coligands which exerted greater control over initiation pathways, suppressing undesired coligand initiation and assisting the preparation of well-defined block polymers.[84-85] Elsewhere, the principles of switchable catalysis were being demonstrated by various established catalyst systems, such as metal salen (**IV**),[47, 60, 86-88] Zn-BDI (**V**),[89-90] and organocatalysts (**VI**),[62, 91-94] showcasing the general applicability of the technique (**Figure 1.10**).

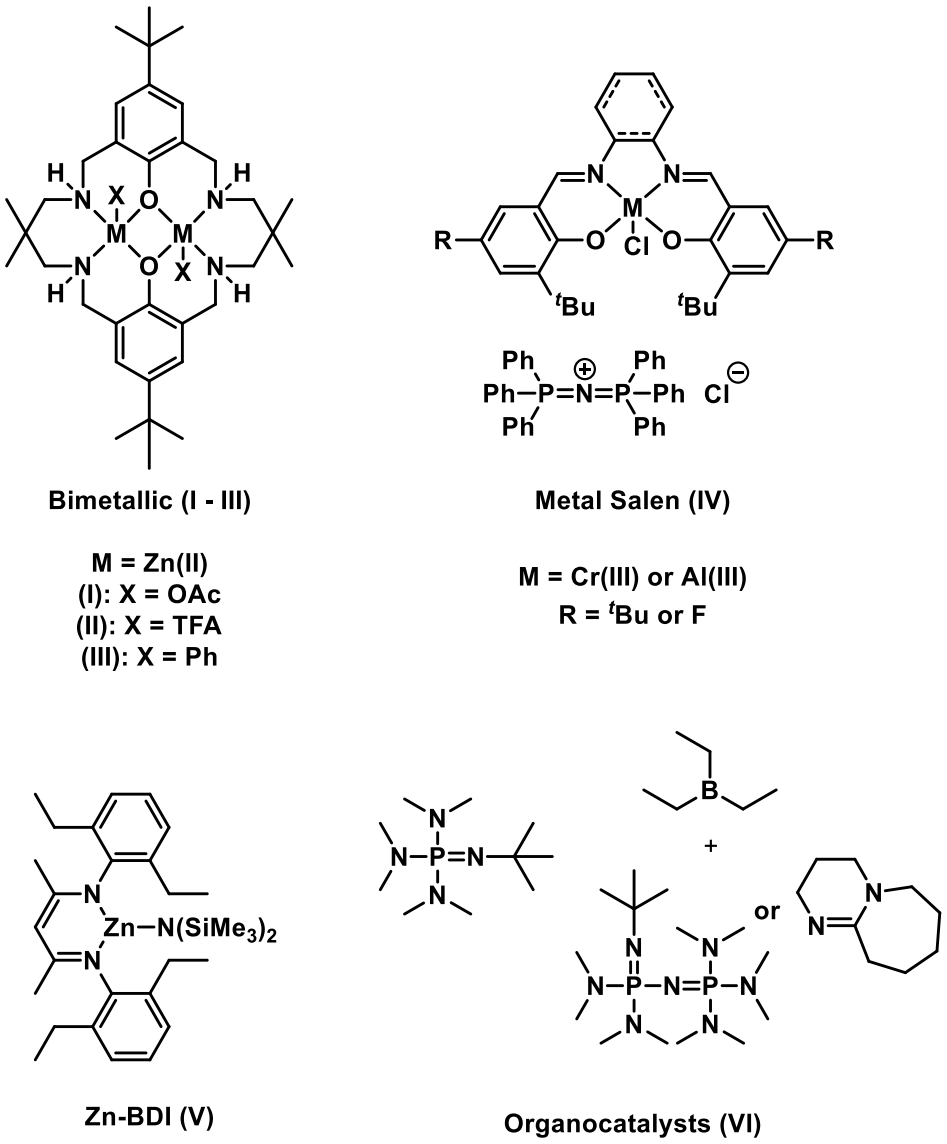


Figure 1.10. Examples of catalysts employed in switchable polymerisation catalysis.[66]

The ability for these catalysts to link together polymerisation cycles operating under different mechanisms is one of the key principles of switchable polymerisation catalysis. The majority of examples demonstrate a switch between two polymerisation cycles, but there are reports of catalysts linking three cycles to prepare more complex multiblock polymers (**Figure 1.11**).[95] Using bimetallic catalyst **III**, a switch from anhydride/epoxide ROCOP (k_3 and k_2) to lactone ROP (k_4) and then back to ROCOP, this time of epoxide/CO_2 (k_2 & k_1), could be achieved by taking advantage of the thermodynamic and kinetic factors which

dictate selectivity and introducing CO_2 at a later stage to ultimately form an ABCBA pentablock polymer.

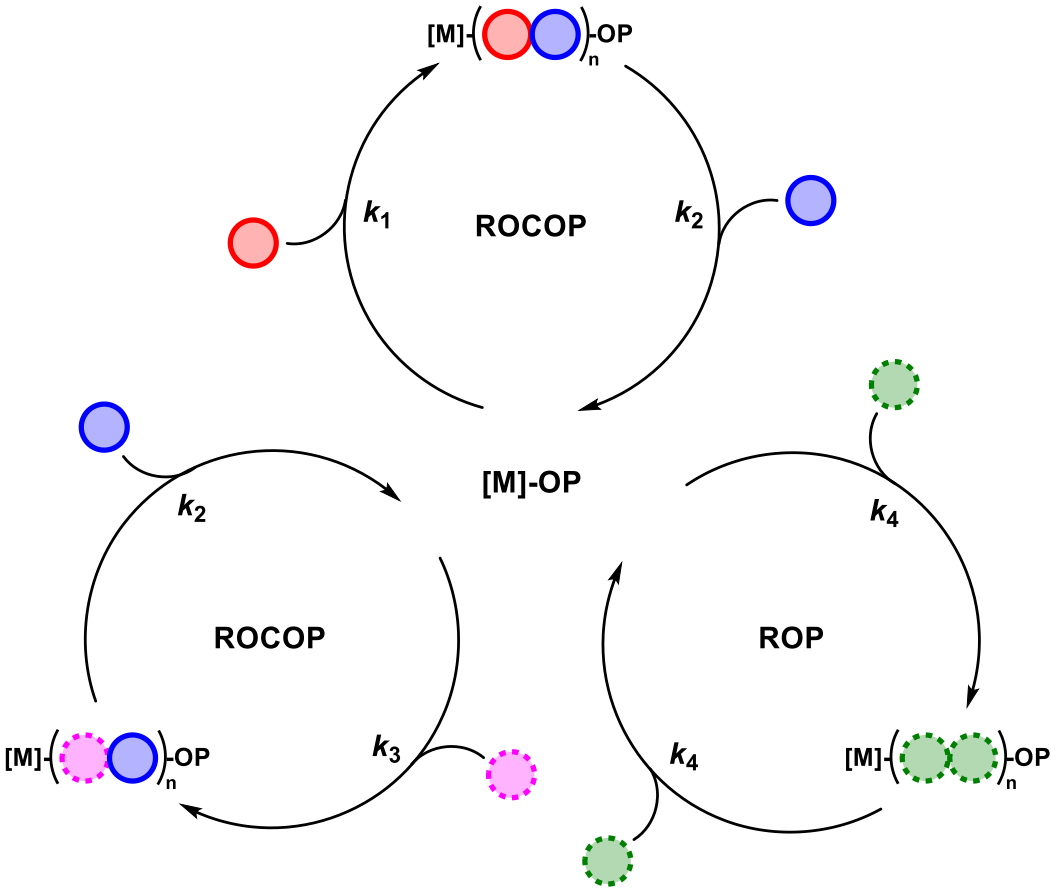


Figure 1.11. Switch catalysis of a three-cycle process illustrating ROCOP of CO_2/epoxide (red/blue), ROCOP of anhydride/epoxide (blue/magenta), and ROP of lactone (green).[66, 95]

1.3.3. Functional materials

The monomer pool accessible to switchable polymerisation catalysts allows not only for the utilisation of renewable feedstocks but also the opportunity to modify the thermal property profile of a given polymer material.[14, 96] The wide variety of polyesters and polycarbonates, already proven in their ability to be incorporated into block polymers through combined heterocycle/heteroallene ROCOP and lactone/cyclic carbonate ROP,

allows access to polymer backbones with glass-transition temperatures spanning almost 200 °C, from as low as -60 °C to highs of 130 °C (**Figure 1.12**).

Accessibility, through the use of switch catalysis, to a range of oxygenated polymer backbones with varying T_g values widens the potential thermal application window for these materials and the preparation of block polymers facilitates fine-tuning. Applying the principles of the Fox equation, lower molar mass block polymers may exhibit a single, mixed T_g, tuneable by selection of constituent blocks and by altering their weight fraction.[97] Alternatively, higher molar mass block polymers may exhibit microphase separation of the constituent blocks and show two separated glass-transition temperatures giving the material an adjustable operating temperature window (OTW).

There is also the potential for the range of accessible T_gs to be expanded beyond the current established bounds. Poly(dimethylsiloxane) (PDMS) for example exhibits a T_g of -120 °C and can be prepared *via* the ROP of a cyclosiloxane. Currently there are no examples of switch catalysis combining siloxane ROP with heterocycle/heteroallene ROCOP, however a block polymer of PCHC-*b*-PDMS-*b*-PCHC, prepared through macroinitiation of CHO/CO_2 ROCOP from hydroxymethyl modified PDMS, was reported in 2016 by Reiter *et al.* and demonstrated tuneable thermal properties by varying the DP of the polycarbonate blocks.[98] Others have reported CO_2-based polycarbonates with T_gs as high as 150 °C by exploiting enantioselective ROCOP catalysis of *meso*-epoxides to prepare isotactic backbones, but similarly this is yet to feature in a switchable catalysis procedure.[99]

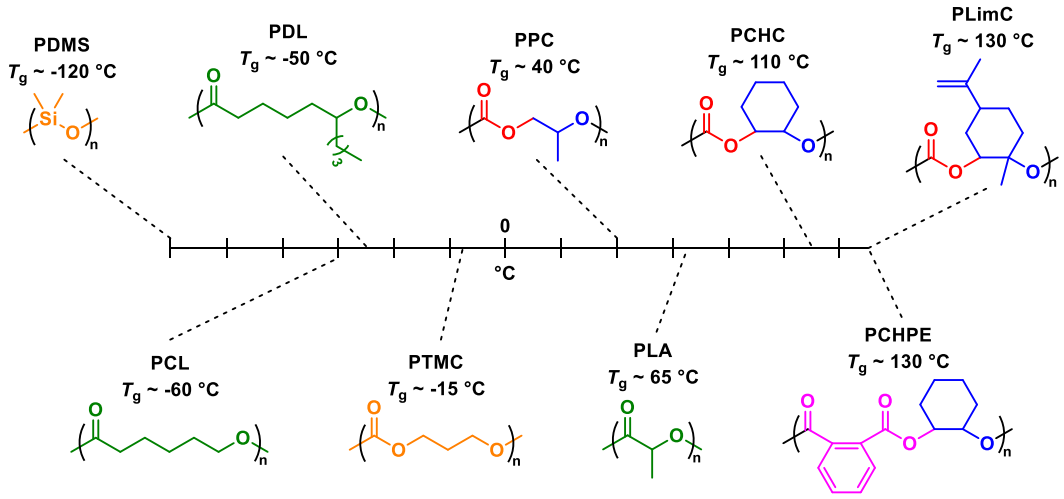


Figure 1.12. Range of glass-transition temperatures accessible using polymers obtained from ROP and ROCOP.

In addition to having optimised OTWs, block polymers showing microphase separation can, in some cases, exhibit enhanced properties compared to analogous materials with disordered structures.[100-101] Microphase separation in a particular block polymer is subject to a combination of factors including the interaction parameter between the constituent blocks (χ_{AB}), the overall degree of polymerisation (N), and the block composition or volume fraction (f).[102] Self-Consistent Mean Field Theory (SCFT) calculations have enabled the construction of phase-diagrams ($\chi_{AB}N$ *vs* f) which illustrated the various morphologies potentially accessible across the range of block compositions for a given block polymer (**Figure 1.13**).[102-108] Empirical data have since shown the similarities with SCFT calculations, but at the same time revealed morphologies which theory could not predict, likely due to the influences of polymer dispersity (i.e. $Đ_M > 1$) and processing history; features inherent to polymers yet difficult to model in theoretical calculations.[109]

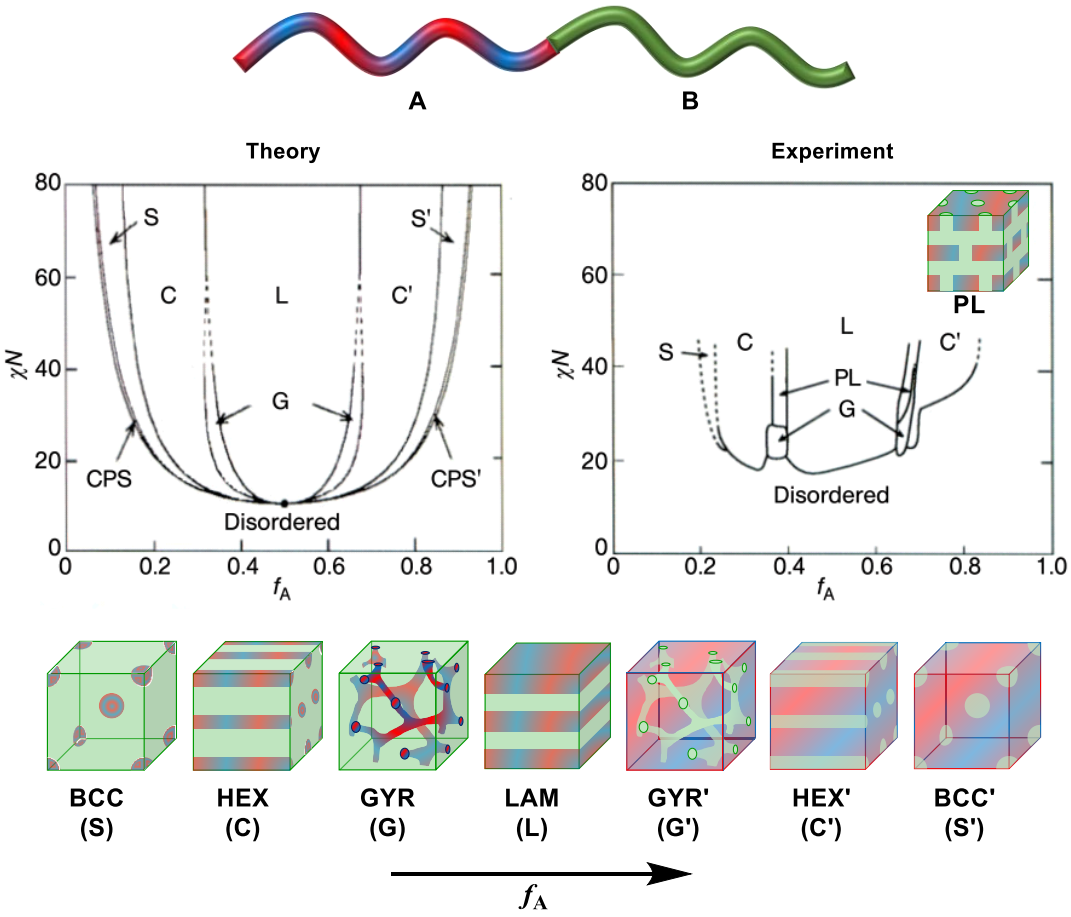


Figure 1.13. Phase diagrams and microstructures for linear AB diblock polymer. Theory (SCFT) predicts four equilibrium morphologies: spherical (BCC/S), cylindrical (HEX/C), bicontinuous gyroid (GYR/G) and lamellar (LAM/L) dependent on block composition (f) and the product of Flory-Huggins interaction parameter (χ) and degree of polymerisation (N). Empirical data for poly(isoprene-*b*-styrene) diblock polymers revealed a metastable perforated lamellae (PL) morphology.[100, 107]

The diverse portfolio of polyesters and polycarbonates that could be incorporated into multiblock polymer architectures has the potential to deliver more renewable materials with these phase separated microstructures. A recent example concerning CO_2-based polycarbonate block polymers was reported by Greiner and co-workers.[110] PLimC-*b*-PCHC diblock polymers showed various morphologies according to M_n and f, highlighting the potential to exploit block incompatibility in such backbone chemistries and precisely control their nanostructures.

Of particular interest is how polymer materials with robust and tailored mechanical/rheological properties can be accessed using more renewable resources and

sustainable synthesis methods. These materials should target properties that are at least competitive with current, petrochemical-derived, polymers; although long-term they should aim to outperform and ideally replace existing non-renewables. Some of the most attractive targets for emerging renewable polymers are as engineering thermoplastics, thermoplastic elastomers (TPEs), and pressure-sensitive adhesives (PSAs).

Presently, there are several accounts of oxygenated block polymers exhibiting desirable property profiles, such as those characteristic of thermoplastics,[89, 111] TPEs,[112-118] or PSAs.[119-125] However, these reports seldom applied switchable polymerisation catalysis as the synthetic protocol, albeit in some cases having used catalysts proven elsewhere, or since, to be capable of performing mechanistic switches. Instead, other methods like sequential addition or terpolymerisation (e.g. one-pot sequential ROCOP) are employed to furnish the block polymers.[116-117] Equally, it should be noted that the majority of examples of block polymers prepared using switchable polymerisation catalysis are a result of proving the catalysis and synthesis are feasible and consequently lack further analysis or investigation into their mechanical properties.[47, 92]

Thermoplastics are defined by their ability to be thermally re-processed, unlike thermosets in which covalent cross-links cure the material and prevent future re-moulding. Oxygenated block polymers with moderate-high strength and ductility are attractive for applications requiring high-performance thermoplastics. Materials suitable for this class often combine soft and rigid polymer chains into block structures at roughly equal volume fractions to afford a desirable balance of rigidity and elasticity, tempering brittleness and improving ductility. Microphase separation of the blocks into a lamellar morphology is typically observed. Several characteristics of plastic behaviour can be identified from the stress-strain relationship (**Figure 1.14**).

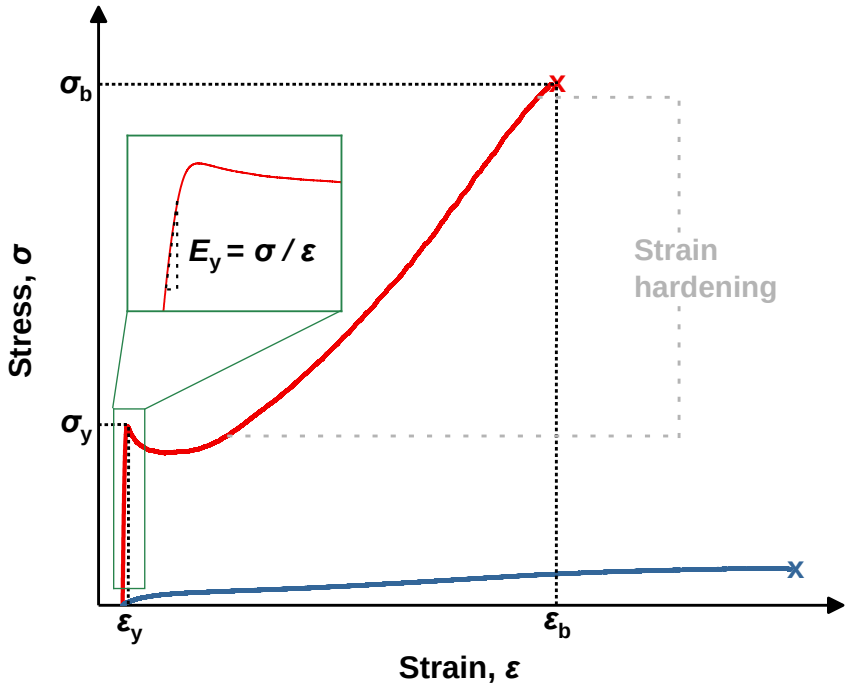


Figure 1.14. Stress-strain relationships illustrating ductile plastic (red) and elastomeric (blue) tensile mechanical behaviour.

A typical stress-strain curves for a ductile plastic (**Figure 1.14**, red curve) features an initial segment of linear elastic behaviour, the differential of which is used to calculate the Young's modulus (E_y) and provide a measure of the material's stiffness in this regime. The yield point (σ_y, ε_y) is the limit of the linear elastic regime, beyond which the polymer material deforms plastically and will sustain some degree of permanent deformation after the load is removed. A consequence of plastic deformation can be strain-hardening, caused by the orientation and alignment of chain molecules with the direction of tensile load and results in strengthening of the material. In comparison, an elastomer will show no yield point and exhibit a linear stress-strain relationship until rupture (**Figure 1.14**, blue curve).

Examples of ductile thermoplastics prepared using switchable catalyses are limited. Recently, Rieger and co-workers used a Zn-BDI class catalyst (**V**) to switch between the ROP

of β-butyrolactone and ROCOP of CHO or LO with CO_2.[89] The resulting poly(ester-*b*-carbonate)s, comprised of PCHC or PLimC hard blocks and poly(hydroxy butyrate) (PHB) soft blocks, showed improved elongation at break compared to the polycarbonate homopolymers (13 – 18% *vs* 1 – 6%) and retained moderate tensile strength (26 – 45 MPa). Williams and co-workers prepared ABA type block polymers also incorporating PLimC as the hard blocks, with PDL as the soft block.[111] Although not synthesised using switchable catalysis, the lead sample highlighted the potential for the renewable materials based on oxygenated polymers to function as robust thermoplastics, exhibiting good tensile strength (σ_b = 21.2 MPa, E_y = 321 MPa) and enhanced elongation (ε_b = 400%).

Thermoplastic elastomers are an important class of functional materials employed in both high end (e.g. automotive/aerospace) and high volume (e.g. consumer goods/appliances) applications. TPEs are usually ABA triblock polymers comprised of a soft (low T_g) "B" block anchored either side by hard (high T_g) "A" blocks. As a result, they combine the rubbery properties of the soft block with the rigidity of the hard blocks, and retain the capability to be thermally re-processed. Microphase separation of the A and B blocks generally confers improved material properties; domains of the hard blocks are distributed within the soft matrix delivering creep resistance and elasticity, respectively. Typically, spherical and hexagonally close-packed cylinder morphologies with low hard block fractions (i.e. $f_A < 0.5$) are associated with elastomeric behaviour, characterised by a linear stress-strain relationship and good elastic recovery (**Figure 1.15**).[55-56, 126]

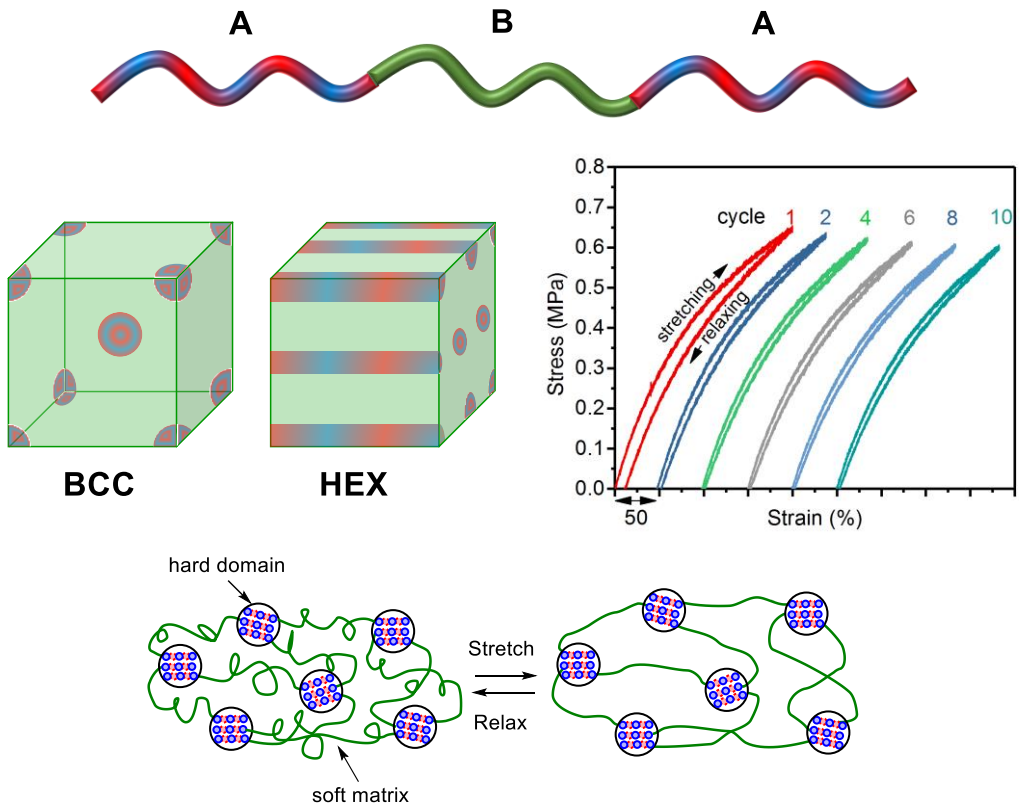


Figure 1.15. Thermoplastic elastomer (TPE) characteristics: block polymer structure, typical morphologies, elastic recovery.[66]

Some of the most well-established and commercially successful TPEs are those based on a polystyrene hard block, specifically poly(styrene-*b*-butadiene-*b*-styrene) (SBS) and poly(styrene-*b*-isoprene-*b*-styrene) (SIS), however these materials lack high temperature stability, synthesis methods are sub-optimal, and their derivation from non-renewable petrochemical resources has raised questions over sustainability and environmental impact. Alternative block polymers that feature polyester and polycarbonate blocks are the subject of current research efforts to address the concerns surrounding sustainability and prepare competitive TPEs with a higher renewable content.

Hillymer and co-workers developed competitive block polyester TPEs from the sequential ROP of various biobased monomers and PLA to form the soft and hard blocks, respectively.[113-114] Other polyester based TPEs were prepared by Williams and co-workers and featured an atypical BAB block structure with the hard block, formed from

anhydride/epoxide ROCOP, as the middle segment.[115] In this case, further chain-extension to form multiblocks was required to afford competitive mechanical properties, with tensile strength values of up to 12 MPa. Several examples of block polycarbonates have been reported, utilising the sequential ROCOP of selected epoxides with CO_2. Yang *et al.* prepared several ABA triblock polymers with varying weight fractions of PCHC as the hard block (19 – 31 wt %).[116] The TPEs displayed tensile strengths between 2 and 7 MPa, reached strains from 250 to 940%, and exhibited self-healing capabilities after post-modification with a telechelic diboronic ester. Similarly, Feng and co-workers fashioned ABA block polycarbonates with PCHC as the rigid block (19 – 25 wt %) but with poly(1-octene carbonate) as the soft block.[117] Microphase separation into the expected spherical and cylindrical morphologies was observed, but the materials produced were relatively soft, reaching a maximum tensile strength of 3.24 MPa at the highest PCHC weight fraction.

In addition to plastics and TPEs, research into the use of oxygenated polymers in pressure-sensitive adhesives (PSAs) has seen an increasing amount of attention. Historically, most PSA formulations have featured petroleum-derived polymers, such as polystyrenics and polyacrylates, but the high oxygen content of newer renewable alternatives could provide better substrate adhesion, as well as presenting better options for degradation.[127-128] Long and co-workers identified strong potential for aliphatic polyester-based PSAs in 2010, highlighting comparable performance to common acrylic-based PSAs.[119] In the following years, Hillmyer and co-workers developed several polyester PSA formulations incorporating renewable ABA triblock polymers but with the addition of tackifiers to tune adhesive performance.[120-121] Similarly, Shin and co-workers prepared a renewable PSA system based on an ABA triblock of ε-decalactone and L-lactide alongside renewable additives, achieving competitive adhesive properties.[122] More recently, Grinstaff and co-workers established CO_2-

derived polycarbonates as strong PSA candidates with robust, and in some cases thermoresponsive, adhesive performance in dry and aqueous environments.[123-124]

1.3.4. Architectural control

Control of polymer architecture is an important factor in polymer synthesis. Aforementioned examples of functional materials have generally featured linear block polymers; while it is vital to be able to prepare well-defined linear species, polymer with non-linear architectures are also attractive for the design of functional materials for specific applications.[129-130] Star polymers are some of the more commonly studied non-linear species and are defined by three of more linear arms emanating from a core point. Compared to a linear analogue, the star architecture provides an increased concentration of functionality at the terminal polymer chain ends and can benefit from variations to thermal properties, morphology, hydrodynamic volume, and melt viscosity.[131-134]

In applications as thermoplastic elastomers, star polymers with linear diblock arms (referred to as star block polymers) have the potential for improved elastomeric properties owing to a greater fraction of chains bridging between minority domains in, for example, the spherical morphology (**Figure 1.16**).[135-136] With a higher tendency for multiple neighbouring hard domains to be linked by a single molecule (the core of which resides in the surrounding soft matrix), properties such as tensile strength and elastic recovery could be improved by reducing the fraction of hard block domain dislocations and loss of bridging when under extension.[136-140]

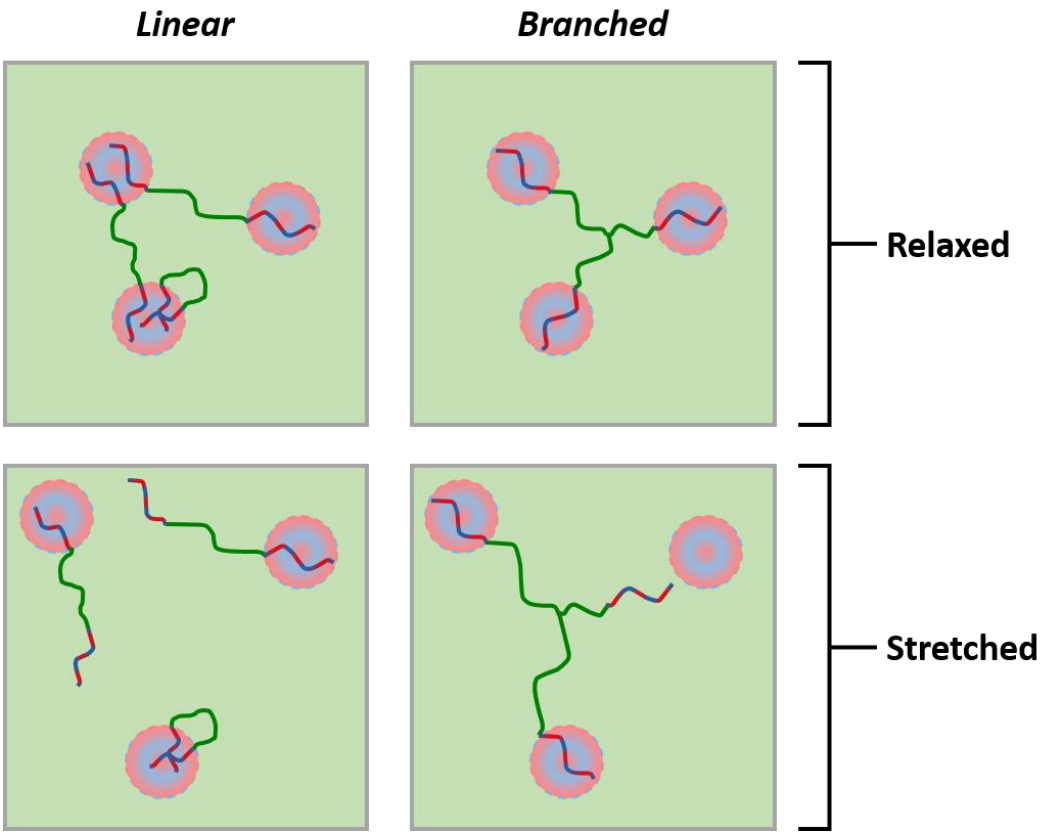


Figure 1.16. Stylised depiction of domain bridging in relaxed and stretched states for microphase separated samples of linear and branched block polymer architectures.[135-136]

Examples of oxygenated polymers with non-linear architectures are found for both polyesters and polycarbonates. Star architectures in particular have been successfully prepared using either divergent (core-first) or convergent (arm-first) techniques, with arms and/or hyperbranched cores comprising block polyesters,[141] poly(ether-*b*-carbonate-*b*-ester)s,[142] or polycarbonates.[143-144] Further non-linear architectures like brush,[145] graft,[146-148] and hyperbranched polymer networks[149] have featured similar variation in the oxygenated polymers comprising the main- or side-chain, but commonly still also incorporate a non-renewable or non-degradable block as either segment. A small number of examples have employed unconventional synthesis techniques such as dual-role catalysis to afford the graft architectures or, in the case of star polymers, an "in-out" approach to fashion more complex arm arrangements.[144, 148] However, the majority still rely on sequential addition, intermediary

purification, or the use of multiple catalysts, highlighting the potential for switchable polymerisation catalysis to be applied here.

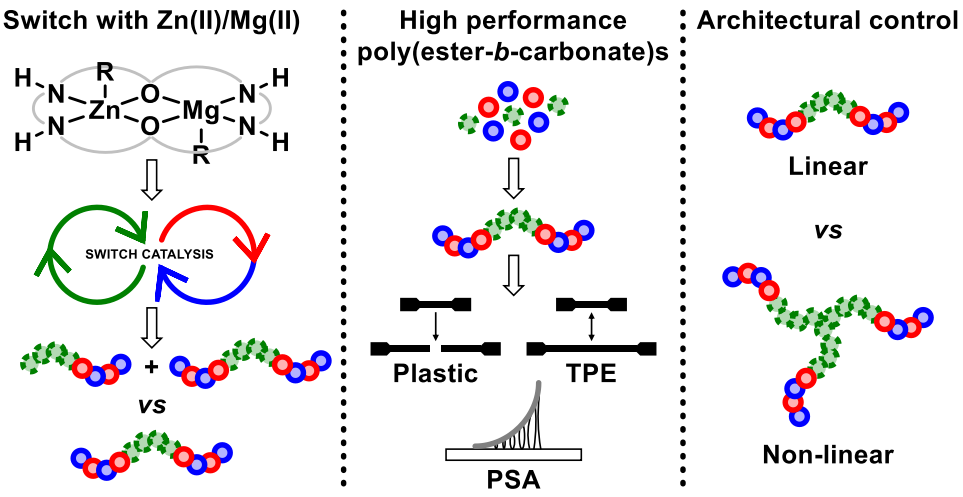
1.4. Aims and objectives

This thesis aims to investigate the activity of Zn(II)/Mg(II) heterodinuclear complexes in switchable polymerisation catalysis to prepare sequence selective block polymers. It intends to expand the current potential of the technique to achieve higher molar mass poly(ester-*b*-carbonate) materials which incorporate CO_2 in their polymer backbone and target high value applications beyond polyols. Chapters 2-4 present research inspired by both a Zn(II)/Mg(II) catalyst developed for epoxide/CO_2 ROCOP as well as developments in switch catalysis using Zn(II)/Zn(II) homodinuclear complexes, and examine the following questions:

1. Are Zn(II)/Mg(II) complexes active for the switchable polymerisation catalysis of lactone/epoxide/CO_2, and can the chain-end be controlled to prepare desired block sequences?

2. Can switch catalysis be applied to prepare linear ABA triblock polymers with high molar mass and controlled CO_2 utilisation? Do the material properties enable applications beyond that of polyols, and can performance be modified by varying CO_2 utilisation?

3. Is the catalyst system tolerant to alternative chain-transfer agents in order to expand the capabilities of technique and target star poly(ester-*b*-carbonate)s? What is the structure-property relationship for these types of polymers?



1.5. References

1. Geyer, R.; Jambeck, J. R.; Law, K. L., Production, use, and fate of all plastics ever made. *Sci. Adv.* **2017,** *3* (7), e1700782.
2. Thompson, R. C.; Moore, C. J.; vom Saal, F. S.; Swan, S. H., Plastics, the environment and human health: current consensus and future trends. *Phil. Trans. R. Soc. B* **2009,** *364* (1526), 2153.
3. Barnes, D. K. A.; Galgani, F.; Thompson, R. C.; Barlaz, M., Accumulation and fragmentation of plastic debris in global environments. *Phil. Trans. R. Soc. B* **2009,** *364* (1526), 1985-1998.
4. Hopewell, J.; Dvorak, R.; Kosior, E., Plastics recycling: challenges and opportunities. *Phil. Trans. R. Soc. B* **2009,** *364* (1526), 2115-2126.
5. PlasticsEurope Plastics - the Facts 2017. https://www.plasticseurope.org/application/files/5715/1717/4180/Plastics_the_facts_2017_FINAL_for_website_one_page.pdf (accessed 01/10/2018).
6. *The new plastics economy: rethinking the future of plastics & catalysing action.*; Ellen MacArthur Foundation: 2017.
7. Coates, G. W.; Getzler, Y. D. Y. L., Chemical recycling to monomer for an ideal, circular polymer economy. *Nat. Rev. Mater.* **2020,** *5* (7), 501-516.
8. *A European Strategy for Plastics in a Circular Economy*; European Union: 2018.
9. Hepburn, C.; Adlen, E.; Beddington, J.; Carter, E. A.; Fuss, S.; Mac Dowell, N.; Minx, J. C.; Smith, P.; Williams, C. K., The technological and economic prospects for CO2 utilization and removal. *Nature* **2019,** *575* (7781), 87-97.
10. von der Assen, N.; Bardow, A., Life cycle assessment of polyols for polyurethane production using CO2 as feedstock: insights from an industrial case study. *Green Chem.* **2014,** *16* (6), 3272-3280.
11. Chapman, A. M.; Keyworth, C.; Kember, M. R.; Lennox, A. J. J.; Williams, C. K., Adding Value to Power Station Captured CO2: Tolerant Zn and Mg Homogeneous Catalysts for Polycarbonate Polyol Production. *ACS Catal.* **2015,** *5* (3), 1581-1588.
12. Burkart, M. D.; Hazari, N.; Tway, C. L.; Zeitler, E. L., Opportunities and Challenges for Catalysis in Carbon Dioxide Utilization. *ACS Catal.* **2019,** *9* (9), 7937-7956.
13. Inoue, S.; Koinuma, H.; Tsuruta, T., Copolymerization of carbon dioxide and epoxide. *J. Polym. Sci. B Polym. Lett.* **1969,** *7*, 287-292.
14. Poland, S. J.; Darensbourg, D. J., A quest for polycarbonates provided via sustainable epoxide/CO2 copolymerization processes. *Green Chem.* **2017,** *19* (21), 4990-5011.
15. Scharfenberg, M.; Hilf, J.; Frey, H., Functional Polycarbonates from Carbon Dioxide and Tailored Epoxide Monomers: Degradable Materials and Their Application Potential. *Adv. Funct. Mater.* **2018,** *28* (10), 1704302.
16. Paul, S.; Zhu, Y.; Romain, C.; Brooks, R.; Saini, P. K.; Williams, C. K., Ring-opening copolymerization (ROCOP): synthesis and properties of polyesters and polycarbonates. *Chem. Commun.* **2015,** *51* (30), 6459-79.
17. Patil, N. G.; Boopathi, S. K.; Alagi, P.; Hadjichristidis, N.; Gnanou, Y.; Feng, X., Carboxylate Salts as Ideal Initiators for the Metal-Free Copolymerization of CO2 with Epoxides: Synthesis of Well-Defined Polycarbonates Diols and Polyols. *Macromolecules* **2019,** *52* (6), 2431-2438.
18. Zhang, D.; Boopathi, S. K.; Hadjichristidis, N.; Gnanou, Y.; Feng, X., Metal-Free Alternating Copolymerization of CO2 with Epoxides: Fulfilling "Green" Synthesis and Activity. *J. Am. Chem. Soc.* **2016,** *138* (35), 11117-11120.
19. Ree, M.; Hwang, Y.; Kim, J.-S.; Kim, H.; Kim, G.; Kim, H., New findings in the catalytic activity of zinc glutarate and its application in the chemical fixation of CO2 into polycarbonates and their derivatives. *Catal. Today* **2006,** *115* (1), 134-145.

20. Kember, M. R.; Buchard, A.; Williams, C. K., Catalysts for CO2/epoxide copolymerisation. *Chem. Commun.* **2011,** *47* (1), 141-163.
21. Trott, G.; Saini, P. K.; Williams, C. K., Catalysts for CO2/epoxide ring-opening copolymerization. *Phil. Trans. R. Soc. A* **2016,** *374* (2061).
22. Ren, W.-M.; Zhang, X.; Liu, Y.; Li, J.-F.; Wang, H.; Lu, X.-B., Highly Active, Bifunctional Co(III)-Salen Catalyst for Alternating Copolymerization of CO2 with Cyclohexene Oxide and Terpolymerization with Aliphatic Epoxides. *Macromolecules* **2010,** *43* (3), 1396-1402.
23. Noh, E. K.; Na, S. J.; S, S.; Kim, S.-W.; Lee, B. Y., Two Components in a Molecule: Highly Efficient and Thermally Robust Catalytic System for CO2/Epoxide Copolymerization. *J. Am. Chem. Soc.* **2007,** *129* (26), 8082-8083.
24. Kissling, S.; Lehenmeier, M. W.; Altenbuchner, P. T.; Kronast, A.; Reiter, M.; Deglmann, P.; Seemann, U. B.; Rieger, B., Dinuclear zinc catalysts with unprecedented activities for the copolymerization of cyclohexene oxide and CO2. *Chem. Commun.* **2015,** *51* (22), 4579-4582.
25. Saini, P. K.; Romain, C.; Williams, C. K., Dinuclear metal catalysts: improved performance of heterodinuclear mixed catalysts for CO2–epoxide copolymerization. *Chem. Commun.* **2014,** *50* (32), 4164-4167.
26. Garden, J. A.; Saini, P. K.; Williams, C. K., Greater than the Sum of Its Parts: A Heterodinuclear Polymerization Catalyst. *J. Am. Chem. Soc.* **2015,** *137* (48), 15078-81.
27. Garden, J. A.; White, A. J. P.; Williams, C. K., Heterodinuclear titanium/zinc catalysis: synthesis, characterization and activity for CO2/epoxide copolymerization and cyclic ester polymerization. *Dalton Trans.* **2017,** *46* (8), 2532-2541.
28. Deacy, A. C.; Durr, C. B.; Garden, J. A.; White, A. J. P.; Williams, C. K., Groups 1, 2 and Zn(II) Heterodinuclear Catalysts for Epoxide/CO2 Ring-Opening Copolymerization. *Inorg. Chem.* **2018**.
29. Trott, G.; Garden, J. A.; Williams, C. K., Heterodinuclear zinc and magnesium catalysts for epoxide/CO2 ring opening copolymerizations. *Chem. Sci.* **2019,** *10* (17), 4618-4627.
30. Deacy, A. C.; Kilpatrick, A. F. R.; Regoutz, A.; Williams, C. K., Understanding metal synergy in heterodinuclear catalysts for the copolymerization of CO2 and epoxides. *Nat. Chem.* **2020,** *12* (4), 372-380.
31. Diallo, A. K.; Kirillov, E.; Slawinski, M.; Brusson, J.-M.; Guillaume, S. M.; Carpentier, J.-F., Syndioselective ring-opening polymerization and copolymerization of trans-1,4-cyclohexadiene carbonate mediated by achiral metal- and organo-catalysts. *Polym. Chem.* **2015,** *6* (11), 1961-1971.
32. Tezuka, K.; Komatsu, K.; Haba, O., The anionic ring-opening polymerization of five-membered cyclic carbonates fused to the cyclohexane ring. *Polym. J.* **2013,** *45* (12), 1183-1187.
33. Guillaume, S. M.; Carpentier, J.-F., Recent advances in metallo/organo-catalyzed immortal ring-opening polymerization of cyclic carbonates. *Catal. Sci. Technol.* **2012,** *2* (5), 898-906.
34. Suriano, F.; Coulembier, O.; Hedrick, J. L.; Dubois, P., Functionalized cyclic carbonates: from synthesis and metal-free catalyzed ring-opening polymerization to applications. *Polym. Chem.* **2011,** *2* (3), 528-533.
35. Brignou, P.; Priebe Gil, M.; Casagrande, O.; Carpentier, J.-F.; Guillaume, S. M., Polycarbonates Derived from Green Acids: Ring-Opening Polymerization of Seven-Membered Cyclic Carbonates. *Macromolecules* **2010,** *43* (19), 8007-8017.
36. Ajellal, N.; Carpentier, J.-F.; Guillaume, C.; Guillaume, S. M.; Helou, M.; Poirier, V.; Sarazin, Y.; Trifonov, A., Metal-catalyzed immortal ring-opening polymerization of lactones, lactides and cyclic carbonates. *Dalton Trans.* **2010,** *39* (36), 8363-8376.

37. Gregory, G. L.; Ulmann, M.; Buchard, A., Synthesis of 6-membered cyclic carbonates from 1,3-diols and low CO_2 pressure: a novel mild strategy to replace phosgene reagents. *RSC Adv.* **2015,** *5* (49), 39404-39408.
38. Gregory, G. L.; Kociok-Köhn, G.; Buchard, A., Polymers from sugars and CO_2: ring-opening polymerisation and copolymerisation of cyclic carbonates derived from 2-deoxy-d-ribose. *Polym. Chem.* **2017,** *8* (13), 2093-2104.
39. Lee, S. H.; Cyriac, A.; Jeon, J. Y.; Lee, B. Y., Preparation of thermoplastic polyurethanes using in situ generated poly(propylene carbonate)-diols. *Polym. Chem.* **2012,** *3* (5), 1215-1220.
40. Langanke, J.; Wolf, A.; Hofmann, J.; Böhm, K.; Subhani, M. A.; Müller, T. E.; Leitner, W.; Gürtler, C., Carbon dioxide (CO_2) as sustainable feedstock for polyurethane production. *Green Chem.* **2014,** *16* (4), 1865-1870.
41. Alagi, P.; Ghorpade, R.; Choi, Y. J.; Patil, U.; Kim, I.; Baik, J. H.; Hong, S. C., Carbon Dioxide-Based Polyols as Sustainable Feedstock of Thermoplastic Polyurethane for Corrosion-Resistant Metal Coating. *ACS Sustainable Chem. Eng.* **2017,** *5* (5), 3871-3881.
42. Xian, W. Q.; Song, L. N.; Liu, B. H.; Ding, H. L.; Li, Z.; Cheng, M. P.; Ma, L., Rheological and mechanical properties of thermoplastic polyurethane elastomer derived from CO_2 copolymer diol. *J. Appl. Polym. Sci.* **2018,** *135* (11).
43. Luinstra, G. A., Poly(Propylene Carbonate), Old Copolymers of Propylene Oxide and Carbon Dioxide with New Interests: Catalysis and Material Properties. *Polym. Rev.* **2008,** *48* (1), 192-219.
44. Koning, C.; Wildeson, J.; Parton, R.; Plum, B.; Steeman, P.; Darensbourg, D. J., Synthesis and physical characterization of poly(cyclohexane carbonate), synthesized from CO_2 and cyclohexene oxide. *Polymer* **2001,** *42* (9), 3995-4004.
45. Ciriminna, R.; Lomeli-Rodriguez, M.; Demma Carà, P.; Lopez-Sanchez, J. A.; Pagliaro, M., Limonene: a versatile chemical of the bioeconomy. *Chem. Commun.* **2014,** *50* (97), 15288-15296.
46. Blanch, G. P.; Nicholson, G. J., Determination of the Enantiomeric Composition of Limonene and Limonene-1,2-epoxide in Lemon Peel by Multidimensional Gas Chromatography with Flame-Ionization Detection and Selected Ion Monitoring Mass Spectrometry. *J. Chromatogr. Sci.* **1998,** *36* (1), 37-43.
47. Stößer, T.; Mulryan, D.; Williams, C. K., Switch Catalysis To Deliver Multi-Block Polyesters from Mixtures of Propene Oxide, Lactide, and Phthalic Anhydride. *Angew. Chem. Int. Ed.* **2018,** *57* (51), 16893-16897.
48. Byrne, C. M.; Allen, S. D.; Lobkovsky, E. B.; Coates, G. W., Alternating copolymerization of limonene oxide and carbon dioxide. *J. Am. Chem. Soc.* **2004,** *126*, 11404-11405.
49. Peña Carrodeguas, L.; González-Fabra, J.; Castro-Gómez, F.; Bo, C.; Kleij, A. W., AlIII-Catalysed Formation of Poly(limonene)carbonate: DFT Analysis of the Origin of Stereoregularity. *Chem. Eur. J.* **2015,** *21* (16), 6115-6122.
50. Hauenstein, O.; Reiter, M.; Agarwal, S.; Rieger, B.; Greiner, A., Bio-based polycarbonate from limonene oxide and CO_2 with high molecular weight, excellent thermal resistance, hardness and transparency. *Green Chem.* **2016,** *18* (3), 760-770.
51. Hauenstein, O.; Agarwal, S.; Greiner, A., Bio-based polycarbonate as synthetic toolbox. *Nat. Commun.* **2016,** *7*, 11862.
52. Product Potential. http://econic-technologies.com/product-potential/ (accessed 01/04/2019).
53. CO_2 Technology. https://www.covestro.com/en/cardyon/co2-technology (accessed 01/04/2019).
54. Jia, M.; Hadjichristidis, N.; Gnanou, Y.; Feng, X., Monomodal Ultrahigh-Molar-Mass Polycarbonate Homopolymers and Diblock Copolymers by Anionic Copolymerization of Epoxides with CO_2. *ACS Macro Lett.* **2019**, 1594-1598.

55. Bates, C. M.; Bates, F. S., 50th Anniversary Perspective: Block Polymers—Pure Potential. *Macromolecules* **2017,** *50* (1), 3-22.
56. Bates, F. S.; Hillmyer, M. A.; Lodge, T. P.; Bates, C. M.; Delaney, K. T.; Fredrickson, G. H., Multiblock Polymers: Panacea or Pandora's Box? *Science* **2012,** *336* (6080), 434.
57. Ruzette, A.-V.; Leibler, L., Block copolymers in tomorrow's plastics. *Nat. Mater.* **2005,** *4* (1), 19-31.
58. Bates, C. M.; Maher, M. J.; Janes, D. W.; Ellison, C. J.; Willson, C. G., Block Copolymer Lithography. *Macromolecules* **2014,** *47* (1), 2-12.
59. Fineman, M.; Ross, S. D., Linear method for determining monomer reactivity ratios in copolymerization. *J. Polym. Sci.* **1950,** *5* (2), 259-262.
60. Stößer, T.; Sulley, G. S.; Gregory, G. L.; Williams, C. K., Easy access to oxygenated block polymers via switchable catalysis. *Nat. Commun.* **2019,** *10* (1), 2668.
61. Wang, Y.; Zhao, Y.; Ye, Y.; Peng, H.; Zhou, X.; Xie, X.; Wang, X.; Wang, F., A One-Step Route to CO2-Based Block Copolymers by Simultaneous ROCOP of CO2/Epoxides and RAFT Polymerization of Vinyl Monomers. *Angew. Chem. Int. Ed.* **2018,** *57* (14), 3593-3597.
62. Zhu, S.; Zhao, Y.; Ni, M.; Xu, J.; Zhou, X.; Liao, Y.; Wang, Y.; Xie, X., One-Step and Metal-Free Synthesis of Triblock Quaterpolymers by Concurrent and Switchable Polymerization. *ACS Macro Lett.* **2020,** *9* (2), 204-209.
63. Fu, C.; Xu, J.; Kokotovic, M.; Boyer, C., One-Pot Synthesis of Block Copolymers by Orthogonal Ring-Opening Polymerization and PET-RAFT Polymerization at Ambient Temperature. *ACS Macro Lett.* **2016,** *5* (4), 444-449.
64. Zhang, Y.-Y.; Yang, G.-W.; Wu, G.-P., A Bifunctional β-Diiminate Zinc Catalyst with CO2/Epoxides Copolymerization and RAFT Polymerization Capacities for Versatile Block Copolymers Construction. *Macromolecules* **2018,** *51* (10), 3640-3646.
65. Stößer, T.; Chen, T. T. D.; Zhu, Y.; Williams, C. K., 'Switch' catalysis: from monomer mixtures to sequence-controlled block copolymers. *Phil. Trans. R. Soc. A* **2018,** *376* (2110), 20170066.
66. Deacy, A. C.; Gregory, G. L.; Sulley, G. S.; Chen, T. T. D.; Williams, C. K., Sequence Control from Mixtures: Switchable Polymerization Catalysis and Future Materials Applications. *J. Am. Chem. Soc.* **2021,** *143* (27), 10021-10040.
67. Olsén, P.; Odelius, K.; Keul, H.; Albertsson, A.-C., Macromolecular Design via an Organocatalytic, Monomer-Specific and Temperature-Dependent "On/Off Switch". High Precision Synthesis of Polyester/Polycarbonate Multiblock Copolymers. *Macromolecules* **2015,** *48* (6), 1703-1710.
68. Magenau, A. J. D.; Strandwitz, N. C.; Gennaro, A.; Matyjaszewski, K., Electrochemically Mediated Atom Transfer Radical Polymerization. *Science* **2011,** *332* (6025), 81.
69. Qi, M.; Dong, Q.; Wang, D.; Byers, J. A., Electrochemically Switchable Ring-Opening Polymerization of Lactide and Cyclohexene Oxide. *J. Am. Chem. Soc.* **2018,** *140* (17), 5686-5690.
70. Peterson, B. M.; Lin, S.; Fors, B. P., Electrochemically Controlled Cationic Polymerization of Vinyl Ethers. *J. Am. Chem. Soc.* **2018,** *140* (6), 2076-2079.
71. Xu, J.; Jung, K.; Atme, A.; Shanmugam, S.; Boyer, C., A Robust and Versatile Photoinduced Living Polymerization of Conjugated and Unconjugated Monomers and Its Oxygen Tolerance. *J. Am. Chem. Soc.* **2014,** *136* (14), 5508-5519.
72. Kottisch, V.; Michaudel, Q.; Fors, B. P., Cationic Polymerization of Vinyl Ethers Controlled by Visible Light. *J. Am. Chem. Soc.* **2016,** *138* (48), 15535-15538.
73. Kottisch, V.; Michaudel, Q.; Fors, B. P., Photocontrolled Interconversion of Cationic and Radical Polymerizations. *J. Am. Chem. Soc.* **2017,** *139* (31), 10665-10668.
74. Teator, A. J.; Lastovickova, D. N.; Bielawski, C. W., Switchable Polymerization Catalysts. *Chem. Rev.* **2016,** *116* (4), 1969-1992.

75. Doerr, A. M.; Burroughs, J. M.; Gitter, S. R.; Yang, X.; Boydston, A. J.; Long, B. K., Advances in Polymerizations Modulated by External Stimuli. *ACS Catal.* **2020,** *10* (24), 14457-14515.
76. Asano, S.; Aida, T.; Inoue, S., Polymerization of epoxide and .beta.-lactone catalyzed by aluminum porphyrin. Exchange of alkoxide or carboxylate group as growing species on aluminum porphyrin. *Macromolecules* **1985,** *18* (10), 2057-2061.
77. Kröger, M.; Folli, C.; Walter, O.; Döring, M., Alternating Copolymerization of Carbon Dioxide and Cyclohexene Oxide and Their Terpolymerization with Lactide Catalyzed by Zinc Complexes of N,N Ligands. *Adv. Synth. Catal.* **2006,** *348* (14), 1908-1918.
78. Jeske, R. C.; Rowley, J. M.; Coates, G. W., Pre-Rate-Determining Selectivity in the Terpolymerization of Epoxides, Cyclic Anhydrides, and CO2: A One-Step Route to Diblock Copolymers. *Angew. Chem. Int. Ed.* **2008,** *47* (32), 6041-6044.
79. Huijser, S.; HosseiniNejad, E.; Sablong, R.; de Jong, C.; Koning, C. E.; Duchateau, R., Ring-Opening Co- and Terpolymerization of an Alicyclic Oxirane with Carboxylic Acid Anhydrides and CO2 in the Presence of Chromium Porphyrinato and Salen Catalysts. *Macromolecules* **2011,** *44* (5), 1132-1139.
80. Wu, G.-P.; Darensbourg, D. J.; Lu, X.-B., Tandem Metal-Coordination Copolymerization and Organocatalytic Ring-Opening Polymerization via Water To Synthesize Diblock Copolymers of Styrene Oxide/CO2 and Lactide. *J. Am. Chem. Soc.* **2012,** *134* (42), 17739-17745.
81. Darensbourg, D. J.; Wu, G.-P., A One-Pot Synthesis of a Triblock Copolymer from Propylene Oxide/Carbon Dioxide and Lactide: Intermediacy of Polyol Initiators. *Angew. Chem. Int. Ed.* **2013,** *52* (40), 10602-10606.
82. Romain, C.; Williams, C. K., Chemoselective Polymerization Control: From Mixed-Monomer Feedstock to Copolymers. *Angew. Chem. Int. Ed.* **2014,** *53* (6), 1607-1610.
83. Romain, C.; Zhu, Y.; Dingwall, P.; Paul, S.; Rzepa, H. S.; Buchard, A.; Williams, C. K., Chemoselective Polymerizations from Mixtures of Epoxide, Lactone, Anhydride, and Carbon Dioxide. *J. Am. Chem. Soc.* **2016,** *138* (12), 4120-4131.
84. Zhu, Y.; Romain, C.; Williams, C. K., Selective Polymerization Catalysis: Controlling the Metal Chain End Group to Prepare Block Copolyesters. *J. Am. Chem. Soc.* **2015,** *137* (38), 12179-12182.
85. Paul, S.; Romain, C.; Shaw, J.; Williams, C. K., Sequence Selective Polymerization Catalysis: A New Route to ABA Block Copoly(ester-b-carbonate-b-ester). *Macromolecules* **2015,** *48* (17), 6047-6056.
86. Stößer, T.; Williams, C. K., Selective Polymerization Catalysis from Monomer Mixtures: Using a Commercial Cr-Salen Catalyst To Access ABA Block Polyesters. *Angew. Chem. Int. Ed.* **2018,** *57* (21), 6337-6341.
87. Diment, W. T.; Stößer, T.; Kerr, R. W. F.; Phanopoulos, A.; Durr, C. B.; Williams, C. K., Ortho-vanillin derived Al(iii) and Co(iii) catalyst systems for switchable catalysis using ε-decalactone, phthalic anhydride and cyclohexene oxide. *Catal. Sci. Technol.* **2021,** *11* (5), 1737-1745.
88. Isnard, F.; Carratù, M.; Lamberti, M.; Venditto, V.; Mazzeo, M., Copolymerization of cyclic esters, epoxides and anhydrides: evidence of the dual role of the monomers in the reaction mixture. *Catal. Sci. Technol.* **2018,** *8* (19), 5034-5043.
89. Kernbichl, S.; Reiter, M.; Mock, J.; Rieger, B., Terpolymerization of β-Butyrolactone, Epoxides, and CO2: Chemoselective CO2-Switch and Its Impact on Kinetics and Material Properties. *Macromolecules* **2019,** *52* (21), 8476-8483.
90. Kernbichl, S.; Reiter, M.; Adams, F.; Vagin, S.; Rieger, B., CO2-Controlled One-Pot Synthesis of AB, ABA Block, and Statistical Terpolymers from β-Butyrolactone, Epoxides, and CO2. *J. Am. Chem. Soc.* **2017,** *139* (20), 6787-6790.

91. Ji, H.-Y.; Wang, B.; Pan, L.; Li, Y.-S., One-Step Access to Sequence-Controlled Block Copolymers by Self-Switchable Organocatalytic Multicomponent Polymerization. *Angew. Chem. Int. Ed.* **2018,** *57* (51), 16888-16892.
92. Li, H.; Luo, H.; Zhao, J.; Zhang, G., Sequence-Selective Terpolymerization from Monomer Mixtures Using a Simple Organocatalyst. *ACS Macro Lett.* **2018,** *7* (12), 1420-1425.
93. Ji, H.-Y.; Song, D.-P.; Wang, B.; Pan, L.; Li, Y.-S., Organic Lewis pairs for selective copolymerization of epoxides with anhydrides to access sequence-controlled block copolymers. *Green Chem.* **2019,** *21* (22), 6123-6132.
94. Zhu, S.; Wang, Y.; Ding, W.; Zhou, X.; Liao, Y.; Xie, X., Lewis pair catalyzed highly selective polymerization for the one-step synthesis of AzCy(AB)xCyAz pentablock terpolymers. *Polym. Chem.* **2020,** *11* (10), 1691-1695.
95. Chen, T. T. D.; Zhu, Y.; Williams, C. K., Pentablock Copolymer from Tetracomponent Monomer Mixture Using a Switchable Dizinc Catalyst. *Macromolecules* **2018,** *51* (14), 5346-5351.
96. Zhang, Y.-Y.; Zhang, X.-H.; Wei, R.-J.; Du, B.-Y.; Fan, Z.-Q.; Qi, G.-R., Synthesis of fully alternating polycarbonate with low Tg from carbon dioxide and bio-based fatty acid. *RSC Adv.* **2014,** *4* (68), 36183-36188.
97. Fox, T. G., Influence of diluent and of copolymer composition on the glass temperature of a polymer system. *Bull. Am. Phys. Soc.* **1956,** *1*, 123.
98. Reiter, M.; Kronast, A.; Kissling, S.; Rieger, B., In Situ Generated ABA Block Copolymers from CO2, Cyclohexene Oxide, and Poly(dimethylsiloxane)s. *ACS Macro Lett.* **2016,** *5* (3), 419-423.
99. Liu, Y.; Wang, M.; Ren, W.-M.; Xu, Y.-C.; Lu, X.-B., Crystalline Hetero-Stereocomplexed Polycarbonates Produced from Amorphous Opposite Enantiomers Having Different Chemical Structures. *Angew. Chem. Int. Ed.* **2015,** *54* (24), 7042-7046.
100. Bates, F. S.; Fredrickson, G. H., Block Copolymers—Designer Soft Materials. *Phys. Today* **1999,** *52* (2), 32-38.
101. Odell, J. A.; Keller, A., Deformation behavior of an S-B-S copolymer. *Polym. Eng. Sci.* **1977,** *17* (8), 544-559.
102. Leibler, L., Theory of Microphase Separation in Block Copolymers. *Macromolecules* **1980,** *13* (6), 1602-1617.
103. Fredrickson, G. H.; Helfand, E., Fluctuation effects in the theory of microphase separation in block copolymers. *J. Chem. Phys.* **1987,** *87* (1), 697-705.
104. Matsen, M. W.; Schick, M., Stable and unstable phases of a diblock copolymer melt. *Phys. Rev. Lett.* **1994,** *72* (16), 2660-2663.
105. Matsen, M. W.; Schick, M., Stable and Unstable Phases of a Linear Multiblock Copolymer Melt. *Macromolecules* **1994,** *27* (24), 7157-7163.
106. Matsen, M. W.; Bates, F. S., Unifying Weak- and Strong-Segregation Block Copolymer Theories. *Macromolecules* **1996,** *29* (4), 1091-1098.
107. Schwartz, E. L.; Ober, C. K., Phase-Selective Chemistry in Block Copolymer Systems. In *Advanced Nanomaterials*, Geckeler, K. E.; Nishide, H., Eds. 2009; pp 1-66.
108. Matsen, M. W., Field theoretic approach for block polymer melts: SCFT and FTS. *J. Chem. Phys.* **2020,** *152* (11), 110901.
109. Khandpur, A. K.; Foerster, S.; Bates, F. S.; Hamley, I. W.; Ryan, A. J.; Bras, W.; Almdal, K.; Mortensen, K., Polyisoprene-Polystyrene Diblock Copolymer Phase Diagram near the Order-Disorder Transition. *Macromolecules* **1995,** *28* (26), 8796-8806.
110. Bailer, J.; Feth, S.; Bretschneider, F.; Rosenfeldt, S.; Drechsler, M.; Abetz, V.; Schmalz, H.; Greiner, A., Synthesis and self-assembly of biobased poly(limonene carbonate)-block-poly(cyclohexene carbonate) diblock copolymers prepared by sequential ring-opening copolymerization. *Green Chem.* **2019,** *21* (9), 2266-2272.

111. Carrodeguas, L. P.; Chen, T. T. D.; Gregory, G. L.; Sulley, G. S.; Williams, C. K., High elasticity, chemically recyclable, thermoplastics from bio-based monomers: carbon dioxide, limonene oxide and ε-decalactone. *Green Chem.* **2020,** *22* (23), 8298-8307.
112. Hillmyer, M. A.; Tolman, W. B., Aliphatic Polyester Block Polymers: Renewable, Degradable, and Sustainable. *Acc. Chem. Res.* **2014,** *47* (8), 2390-2396.
113. Martello, M. T.; Schneiderman, D. K.; Hillmyer, M. A., Synthesis and Melt Processing of Sustainable Poly(ε-decalactone)-block-Poly(lactide) Multiblock Thermoplastic Elastomers. *ACS Sustainable Chem. Eng.* **2014,** *2* (11), 2519-2526.
114. Schneiderman, D. K.; Hill, E. M.; Martello, M. T.; Hillmyer, M. A., Poly(lactide)-block-poly(ε-caprolactone-co-ε-decalactone)-block-poly(lactide) copolymer elastomers. *Polym. Chem.* **2015,** *6* (19), 3641-3651.
115. Zhu, Y.; Radlauer, M. R.; Schneiderman, D. K.; Shaffer, M. S. P.; Hillmyer, M. A.; Williams, C. K., Multiblock Polyesters Demonstrating High Elasticity and Shape Memory Effects. *Macromolecules* **2018,** *51* (7), 2466-2475.
116. Yang, G.-W.; Wu, G.-P., High-Efficiency Construction of CO2-Based Healable Thermoplastic Elastomers via a Tandem Synthetic Strategy. *ACS Sustainable Chem. Eng.* **2019,** *7* (1), 1372-1380.
117. Jia, M.; Zhang, D.; de Kort, G. W.; Wilsens, C. H. R. M.; Rastogi, S.; Hadjichristidis, N.; Gnanou, Y.; Feng, X., All-Polycarbonate Thermoplastic Elastomers Based on Triblock Copolymers Derived from Triethylborane-Mediated Sequential Copolymerization of CO2 with Various Epoxides. *Macromolecules* **2020,** *53* (13), 5297-5307.
118. Gregory, G. L.; Sulley, G. S.; Carrodeguas, L. P.; Chen, T. T. D.; Santmarti, A.; Terrill, N. J.; Lee, K.-Y.; Williams, C. K., Triblock polyester thermoplastic elastomers with semi-aromatic polymer end blocks by ring-opening copolymerization. *Chem. Sci.* **2020,** *11* (25), 6567-6581.
119. Ozturk, G. I.; Pasquale, A. J.; Long, T. E., Melt Synthesis and Characterization of Aliphatic Low-Tg Polyesters as Pressure Sensitive Adhesives. *J. Adhes.* **2010,** *86* (4), 395-408.
120. Shin, J.; Martello, M. T.; Shrestha, M.; Wissinger, J. E.; Tolman, W. B.; Hillmyer, M. A., Pressure-Sensitive Adhesives from Renewable Triblock Copolymers. *Macromolecules* **2011,** *44* (1), 87-94.
121. Ding, K.; John, A.; Shin, J.; Lee, Y.; Quinn, T.; Tolman, W. B.; Hillmyer, M. A., High-Performance Pressure-Sensitive Adhesives from Renewable Triblock Copolymers. *Biomacromolecules* **2015,** *16* (8), 2537-2539.
122. Lee, S.; Lee, K.; Kim, Y.-W.; Shin, J., Preparation and Characterization of a Renewable Pressure-Sensitive Adhesive System Derived from ε-Decalactone, l-Lactide, Epoxidized Soybean Oil, and Rosin Ester. *ACS Sustainable Chem. Eng.* **2015,** *3* (9), 2309-2320.
123. Beharaj, A.; Ekladious, I.; Grinstaff, M. W., Poly(Alkyl Glycidate Carbonate)s as Degradable Pressure-Sensitive Adhesives. *Angew. Chem. Int. Ed.* **2019,** *58* (5), 1407-1411.
124. Beharaj, A.; McCaslin, E. Z.; Blessing, W. A.; Grinstaff, M. W., Sustainable polycarbonate adhesives for dry and aqueous conditions with thermoresponsive properties. *Nat. Commun.* **2019,** *10* (1), 5478.
125. Chen, T. T. D.; Carrodeguas, L. P.; Sulley, G. S.; Gregory, G. L.; Williams, C. K., Bio-based and Degradable Block Polyester Pressure-Sensitive Adhesives. *Angew. Chem. Int. Ed.* **2020,** *59* (52), 23450-23455.
126. Wang, W.; Lu, W.; Goodwin, A.; Wang, H.; Yin, P.; Kang, N.-G.; Hong, K.; Mays, J. W., Recent advances in thermoplastic elastomers from living polymerizations: Macromolecular architectures and supramolecular chemistry. *Prog. Polym. Sci.* **2019,** *95*, 1-31.
127. Foster, J. C.; Reilly, R. K., How to better control polymer chemistry. *Science* **2019,** *363* (6434), 1394.
128. Awaja, F.; Gilbert, M.; Kelly, G.; Fox, B.; Pigram, P. J., Adhesion of polymers. *Prog. Polym. Sci.* **2009,** *34* (9), 948-968.

129. Bi, L.-K.; Fetters, L. J., Synthesis and Properties of Block Copolymers. 3. Polystyrene-Polydiene Star Block Copolymers. *Macromolecules* **1976,** *9* (5), 732-742.
130. Lynd, N. A.; Oyerokun, F. T.; O'Donoghue, D. L.; Handlin, D. L.; Fredrickson, G. H., Design of Soft and Strong Thermoplastic Elastomers Based on Nonlinear Block Copolymer Architectures Using Self-Consistent-Field Theory. *Macromolecules* **2010,** *43* (7), 3479-3486.
131. Matsen, M. W.; Schick, M., Microphase Separation in Starblock Copolymer Melts. *Macromolecules* **1994,** *27* (23), 6761-6767.
132. Barbon, S. M.; Song, J.-A.; Chen, D.; Zhang, C.; Lequieu, J.; Delaney, K. T.; Anastasaki, A.; Rolland, M.; Fredrickson, G. H.; Bates, M. W.; Hawker, C. J.; Bates, C. M., Architecture Effects in Complex Spherical Assemblies of (AB)n-Type Block Copolymers. *ACS Macro Lett.* **2020,** *9* (12), 1745-1752.
133. Hawker, C. J., Architectural Control in "Living" Free Radical Polymerizations: Preparation of Star and Graft Polymers. *Angew. Chem. Int. Ed.* **1995,** *34* (13-14), 1456-1459.
134. Hadjichristidis, N.; Pitsikalis, M.; Pispas, S.; Iatrou, H., Polymers with Complex Architecture by Living Anionic Polymerization. *Chem. Rev.* **2001,** *101* (12), 3747-3792.
135. Spencer, R. K. W.; Matsen, M. W., Domain Bridging in Thermoplastic Elastomers of Star Block Copolymer. *Macromolecules* **2017,** *50* (4), 1681-1687.
136. Burns, A. B.; Register, R. A., Mechanical Properties of Star Block Polymer Thermoplastic Elastomers with Glassy and Crystalline End Blocks. *Macromolecules* **2016,** *49* (24), 9521-9530.
137. Juhari, A.; Mosnáček, J.; Yoon, J. A.; Nese, A.; Koynov, K.; Kowalewski, T.; Matyjaszewski, K., Star-like poly (n-butyl acrylate)-b-poly (α-methylene-γ-butyrolactone) block copolymers for high temperature thermoplastic elastomers applications. *Polymer* **2010,** *51* (21), 4806-4813.
138. Nese, A.; Mosnáček, J.; Juhari, A.; Yoon, J. A.; Koynov, K.; Kowalewski, T.; Matyjaszewski, K., Synthesis, Characterization, and Properties of Starlike Poly(n-butyl acrylate)-b-poly(methyl methacrylate) Block Copolymers. *Macromolecules* **2010,** *43* (3), 1227-1235.
139. Kwee, T.; Taylor, S. J.; Mauritz, K. A.; Storey, R. F., Morphology and mechanical and dynamic mechanical properties of linear and star poly(styrene-b-isobutylene-b-styrene) block copolymers. *Polymer* **2005,** *46* (12), 4480-4491.
140. Pakula, T.; Koynov, K.; Boerner, H.; Huang, J.; Lee, H.-i.; Pietrasik, J.; Sumerlin, B.; Matyjaszewski, K., Effect of chain topology on the self-organization and the mechanical properties of poly(n-butyl acrylate)-b-polystyrene block copolymers. *Polymer* **2011,** *52* (12), 2576-2583.
141. Lee, S.; Lee, K.; Jang, J.; Choung, J. S.; Choi, W. J.; Kim, G.-J.; Kim, Y.-W.; Shin, J., Sustainable poly(ε-decalactone)–poly(l-lactide) multiarm star copolymer architectures for thermoplastic elastomers with fixed molar mass and block ratio. *Polymer* **2017,** *112*, 306-317.
142. Zhao, J.; Pahovnik, D.; Gnanou, Y.; Hadjichristidis, N., One-pot synthesis of linear- and three-arm star-tetrablock quarterpolymers via sequential metal-free ring-opening polymerization using a "catalyst switch" strategy. *J. Polym. Sci., Part A: Polym. Chem.* **2015,** *53* (2), 304-312.
143. Hilf, J.; Schulze, P.; Seiwert, J.; Frey, H., Controlled Synthesis of Multi-Arm Star Polyether–Polycarbonate Polyols Based on Propylene Oxide and CO2. *Macromol. Rapid Commun.* **2014,** *35* (2), 198-203.
144. Augustine, D.; Hadjichristidis, N.; Gnanou, Y.; Feng, X., Hydrophilic Stars, Amphiphilic Star Block Copolymers, and Miktoarm Stars with Degradable Polycarbonate Cores. *Macromolecules* **2020,** *53* (3), 895-904.
145. Zhang, J.-F.; Ren, W.-M.; Sun, X.-K.; Meng, Y.; Du, B.-Y.; Zhang, X.-H., Fully Degradable and Well-Defined Brush Copolymers from Combination of Living CO2/Epoxide

Copolymerization, Thiol–Ene Click Reaction and ROP of ε-caprolactone. *Macromolecules* **2011,** *44* (24), 9882-9886.
146. Alagi, P.; Zapsas, G.; Hadjichristidis, N.; Hong, S. C.; Gnanou, Y.; Feng, X., All-Polycarbonate Graft Copolymers with Tunable Morphologies by Metal-Free Copolymerization of CO_2 with Epoxides. *Macromolecules* **2021,** *54* (13), 6144-6152.
147. Zhang, J.; Li, T.; Mannion, A. M.; Schneiderman, D. K.; Hillmyer, M. A.; Bates, F. S., Tough and Sustainable Graft Block Copolymer Thermoplastics. *ACS Macro Lett.* **2016,** *5* (3), 407-412.
148. Higuchi, M.; Kanazawa, A.; Aoshima, S., Design of Graft Architectures via Simultaneous Kinetic Control of Cationic Vinyl-Addition Polymerization of Vinyl Ethers, Coordination Ring-Opening Polymerization of Cyclic Esters, and Merging at the Propagating Chain End. *Macromolecules* **2020,** *53* (10), 3822-3831.
149. De Hoe, G. X.; Zumstein, M. T.; Tiegs, B. J.; Brutman, J. P.; McNeill, K.; Sander, M.; Coates, G. W.; Hillmyer, M. A., Sustainable Polyester Elastomers from Lactones: Synthesis, Properties, and Enzymatic Hydrolyzability. *J. Am. Chem. Soc.* **2018,** *140* (3), 963-973.

CHAPTER 2

Switch Catalysis Using Zinc(II)/Magnesium(II) Heterodinuclear Catalysts

2.1. Introduction

Multi-nuclear catalysts show particular promise, as well as being early pioneers, in performing both the ring-opening polymerisation (ROP) and ring-opening copolymerisation (ROCOP) to produce oxygenated polymers (polyesters and polycarbonates).[1-10] Particularly successful and important for this work are dinuclear catalysts coordinated by a diphenol tetraamine macrocyclic ancillary ligand; a number of prior studies have examined the choice and role of the metal centres.[1, 4, 9-15] Crucially, heterodinuclear complexes featuring Zn(II)/Mg(II) metal centres showed a marked enhancement to the rate of polymerisation in the ROCOP of epoxides and CO_2 when compared to individual homodinuclear analogues or to 50:50 mixtures of them.[12]

Most recently, Mg(II)/Co(II) heterodinuclear catalysts coordinated by the same ancillary ligand showed excellent activity and selectivity for the copolymerisation of epoxides and CO_2 to produce polycarbonate polyols.[10] Detailed analysis of the kinetics for this catalyst revealed the synergic effect between the two metal centres, supporting and rationalising heterodinuclear cooperativity and catalytic synergy.

Recent demonstrations of switchable catalysis using the homodinuclear [LZn_2Ph_2] catalyst have enabled the preparation of both well-defined pentablock copolymers[16], as well as triblock polymers of poly(ε-decalactone)-*b*-poly(cyclohexene oxide-*alt*-phthalic anhydride)-*b*-poly(ε-decalactone) which showed promising elastomeric behaviour after chain-extension with a diisocyanate.[17] Given the rate enhancement reported in CO_2/epoxide ROCOP for heterodinuclear catalysts over homodinuclear analogues, the next logical step would be to evaluate these heterodinuclear catalysts for switch polymerisation.[18] Should they be effective in switch catalysis, it is anticipated they should show superior activity, high selectivity, and efficiency at low catalyst loading.

2.2. Aims

This chapter aims to investigate switch catalysis using heterodinuclear catalysts and tests the hypothesis that Zn(II)/Mg(II) catalysts should show higher rates compared to homodinuclear analogues. Additionally, it will explore the preparation of organometallic Zn(II)/Mg(II) complexes, proposed to elicit superior end-group control given results with an analogous dizinc catalyst. Used with diols, the catalyst is expected to produce hydroxyl telechelic polymers, crucial to obtaining desired ABA triblock structures without contamination. Further to this, the aim is to also develop a fast and selective catalyst system for lactone/epoxide/CO_2 switch catalysis and use it to obtain ABA-type polymers with high end-group fidelity, molar masses greater than the polyol regime (M_n > 20 kg mol^{-1}), and with the "correct" block sequence to deliver materials like thermoplastic elastomers.

The approach to deliver on these aims will involve: (1) testing a known Zn(II)/Mg(II) catalyst for individual epoxide/CO_2 ROCOP and lactone ROP, and establishing its potential in combining these cycles to achieve switch catalysis; (2) investigation into the synthesis of [LZnMgR_2], where R is a coligand susceptible to reaction with alcohols to generate an alkoxide *in-situ* and an unreactive RH species which does not interfere with polymerisations; (3) testing the new [LZnMgR_2] complex in ROP, ROCOP, and switch catalysis in order to understand rates, end-group control, and optimised conversion conditions (**Figure 2.1**).

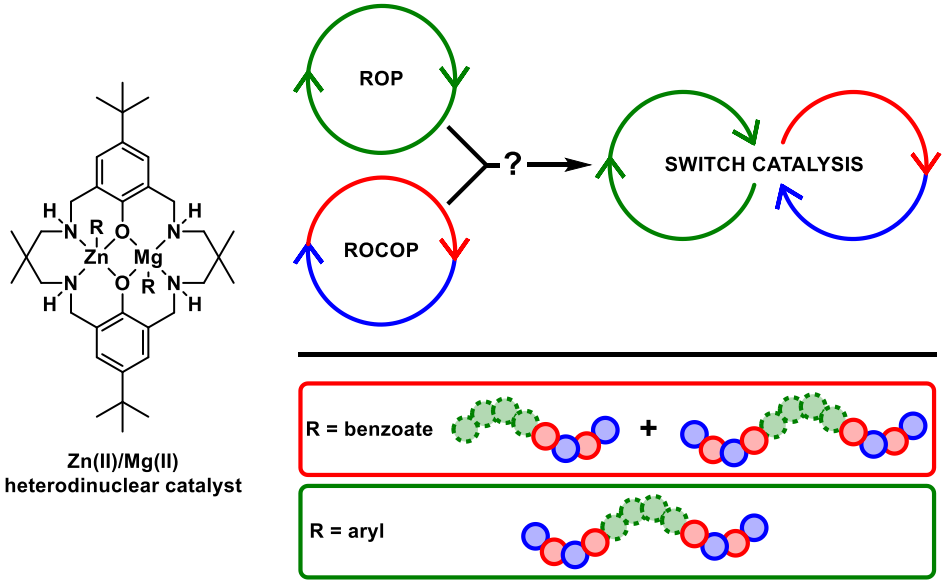


Figure 2.1. Switch catalysis and chain-end control with heterodinuclear Zn(II)/Mg(II) catalysts.

2.3. Catalysis using a Zn(II)/Mg(II) heterodinuclear catalyst: Benzoate coligands

A recently developed heterodinuclear Zn(II)/Mg(II) catalyst with *para*-dimethylamino benzoate co-ligands, **1**, was reported as active in the ring-opening copolymerisation of epoxides and CO_2.[19] This particular catalyst was chosen as a starting point for switch catalysis investigations due to its high yielding synthesis, acceptable rate in ROCOP of epoxides and CO_2 as well as its stability under polymerisation conditions and low cyclic carbonate formation.

The heterodinuclear catalyst [LZnMg(OBz^{NMe2})$_2$], **1**, was synthesised according to the previously reported procedure.[19] First, the macrocyclic pro-ligand was reacted with [$ZnEt_2$] to form a monozinc complex *in-situ*, which was then reacted with [$MgBr_2$] and isolated to yield the precursor complex [$LZnMgBr_2$]. The final step of the synthesis involved a salt metathesis reaction of the [$LZnMgBr_2$] with [$KOBz^{NMe2}$] which placed a benzoate co-ligand on each metal centre. The characterisation data for this new complex was in agreement with that reported previously (Appendix Figure S7.1).

2.3.1. Ring-opening polymerisation of *ε*-decalactone

The heterodinuclear Zn(II)/Mg(II) catalyst (**1**) was employed in the ROP of ε-decalactone (ε-DL) in the presence of cyclohexene oxide (CHO) as solvent. This particular lactone monomer was chosen due to its propagating chain end being a 2° alkoxide which has been noted to offer greater control during polymerisation and reduce the prevalence of transesterification compared to analogues featuring primary alkoxide propagating chain ends, e.g. ε-caprolactone.[16-17, 20]

Table 2.1. Data for ε-Decalactone ROP Catalysed by [LZnMg(OBz^{NMe2})$_2$].

Entry	[CHD]:[1][a]	Time (h)	Conv. (%)[b]	TON[c]	TOF (h^{-1})[d]	M_n (kg mol^{-1}) [$Đ_M$][e,f]
1	8	0.5	95	379	757	15.4 [1.08] 6.1 [1.10]
2	20	1	97	388	388	5.3 [1.18]

[a]Additional conditions: [1]:[ε-DL]:[CHO] = 1:400:1000, 80 °C. [b]Determined by ^{1}H NMR spectroscopy of a crude sample of polymerisation solution. [c]Number of moles of monomer consumed per mole of catalyst. [d]TON per unit time. [e]Determined by SEC, in THF, using narrow dispersity polystyrene standards. [f]$Đ_M = M_w/M_n$.

The polymerisation, at 80 °C, was relatively fast (TOF = 757 h^{-1}) at low catalyst loading (0.25 mol %), with 95% conversion observed after 30 minutes (**Table 2.1**, entry 1). An excess of cyclohexane diol (CHD) chain-transfer agent was used ([CHD]:[**1**] = 8:1) to preferentially yield hydroxyl telechelic polymer chains. However, it was immediately evident from the SEC analysis that two polymer distributions remained: a major distribution at higher molar mass, and a shoulder at lower molar mass (**Figure 2.2(a)**). The difference between the two distributions was identified using MALDI-ToF mass spectrometry using a sample of overall lower molar mass to enable successful ionisation (**Figure 2.2(b)**). It showed that the higher molar mass distribution corresponded to the desired hydroxyl telechelic polymer chains, and the lower molar mass shoulder arose from polymer chains initiated from the benzoate coligand.

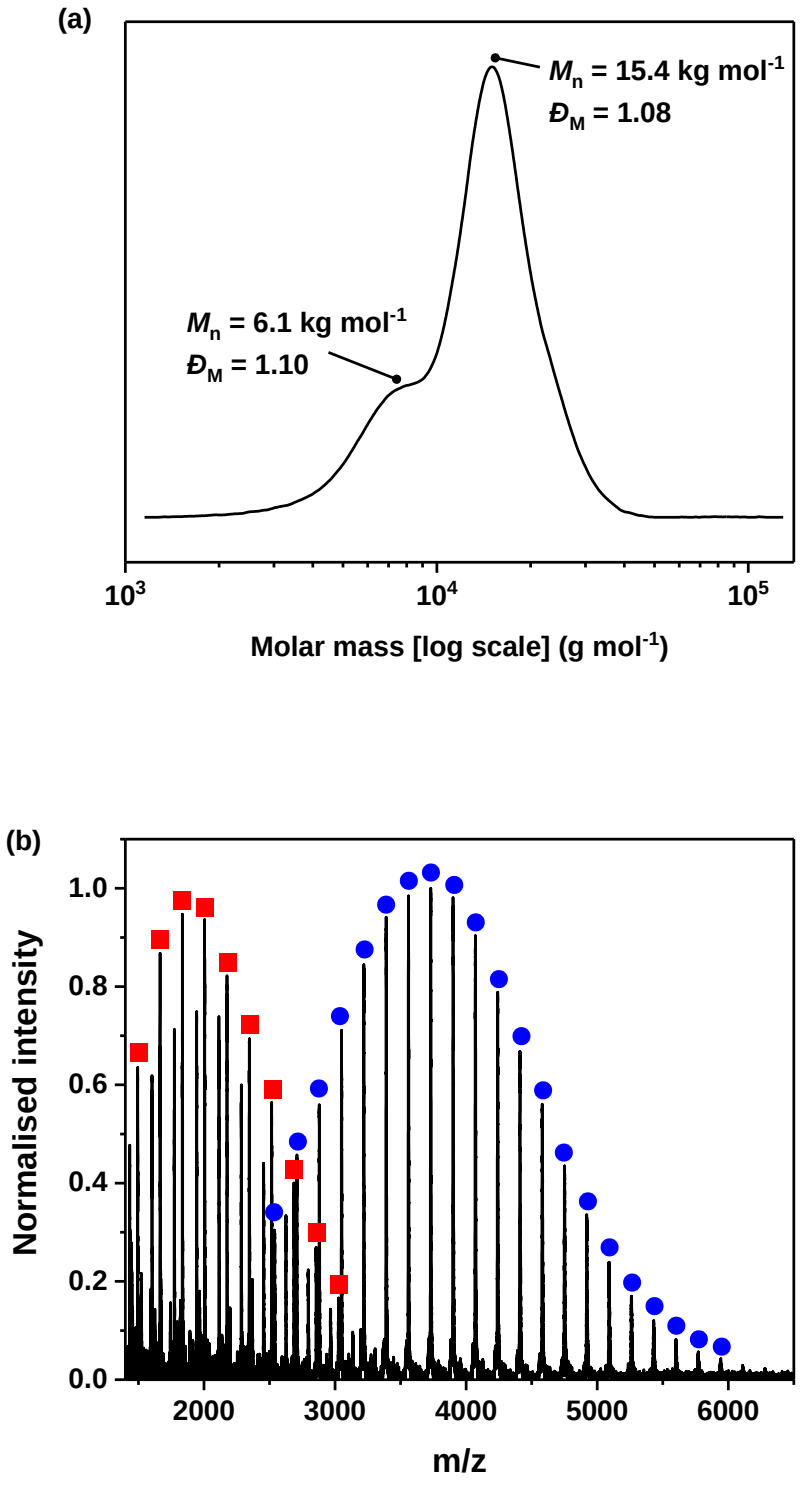


Figure 2.2. Analysis of PDL from ROP of ε-DL catalysed by **1** with 8 equivalents of CHD; (a) SEC chromatogram and (b) MALDI-ToF mass spectrum with distributions corresponding to benzoate capped (■) and hydroxyl-telechelic (●) chains.

An even greater excess of chain-transfer agent ([CHD]:[**1**] = 20:1) was then employed to suppress the benzoate coligand initiation pathway (**Table 2.1**, entry 2). Under these conditions only a single distribution was observed in the SEC analysis, but the molar mass of the polymer was significantly lower at around 5.3 kg mol^{-1} (**Figure 2.3(a)**). While the chain end group could be selected to be hydroxyl telechelic, the reduced polymer molar mass presented a new limitation in terms of delivering polymers showing mechanical strength without using chain end coupling/resin cross-linking strategies.

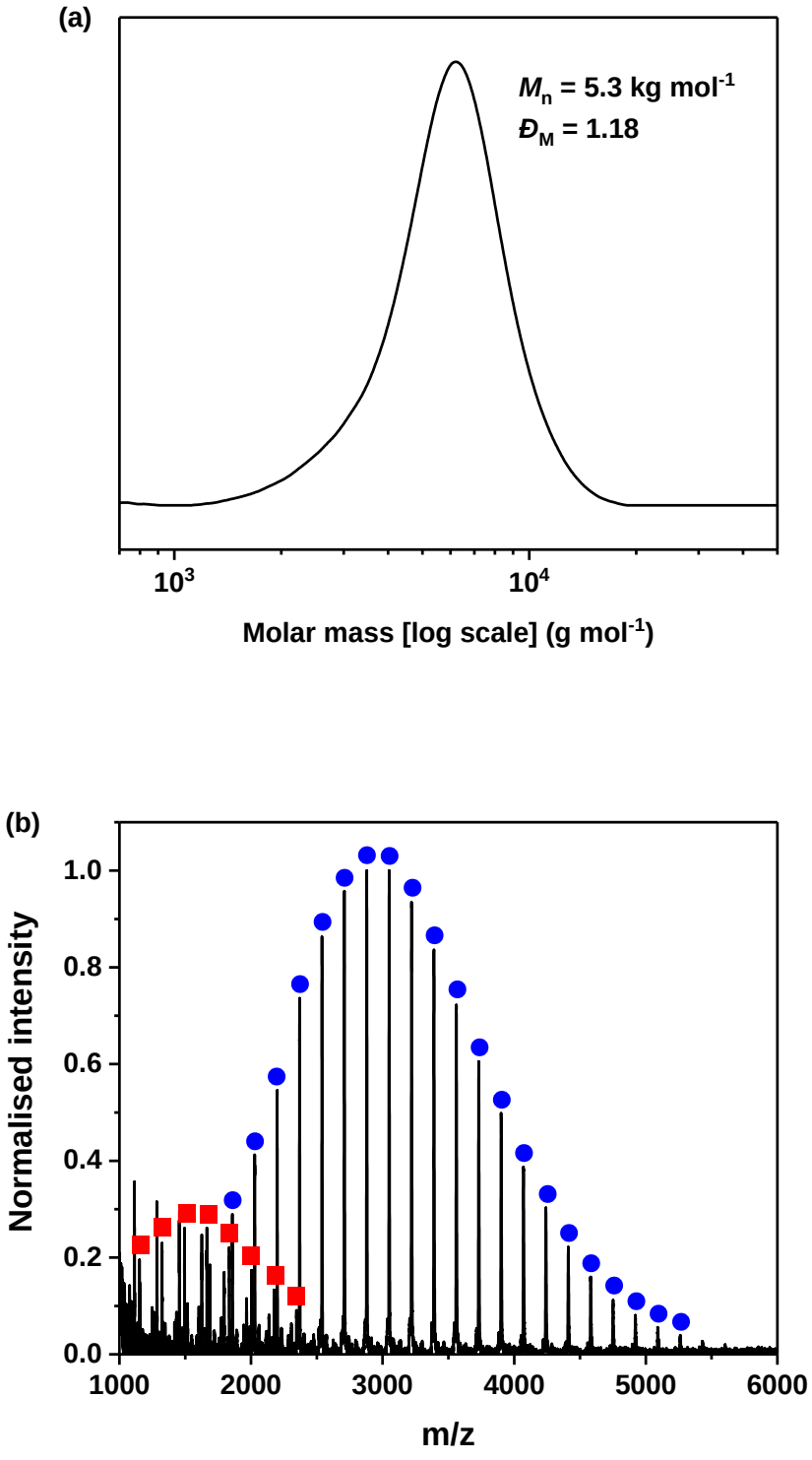


Figure 2.3. Analysis of PDL from ROP of ε-DL catalysed by **1** with 20 equivalents of CHD; (a) SEC chromatogram and (b) MALDI-ToF mass spectrum with distributions corresponding to benzoate capped (■) and hydroxyl-telechelic (●) chains.

Analysis of the MALDI-ToF spectra revealed a minor distribution of benzoate capped chains still remained, with lower intensity (concentration) compared to the previous example (**Figure 2.3(b)**). This observation signalled the need for a new catalyst, comparable or better in rate to **1** but bearing coligands with no propensity to initiate polymer chains themselves.

2.3.2. Ring-opening copolymerisation of cyclohexene oxide and CO_2

In the targeted switch polymerisation, ROCOP of CHO and CO_2 would comprise the second stage and grow polycarbonate blocks from both ends of the poly(ε-decalactone) formed in the first stage. It was therefore important to (re)evaluate **1** in terms of its rate and selectivity for this constituent polymerisation cycle.

Polymerisations conducted at 80 °C displayed moderate rates (TOF = 87 h^{-1}) and quantitative selectivity for the desired polycarbonate (> 99%) in line with previous reports.[19] It was also observed that 8 equivalents of CHD was sufficient in forming a polymer with a monomodal molar mass distribution in the SEC (**Figure 2.4**).

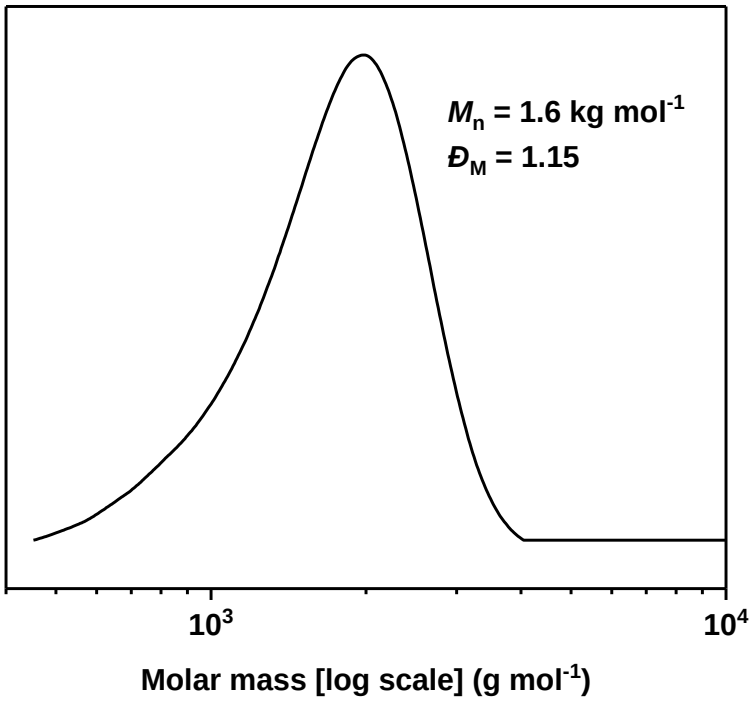
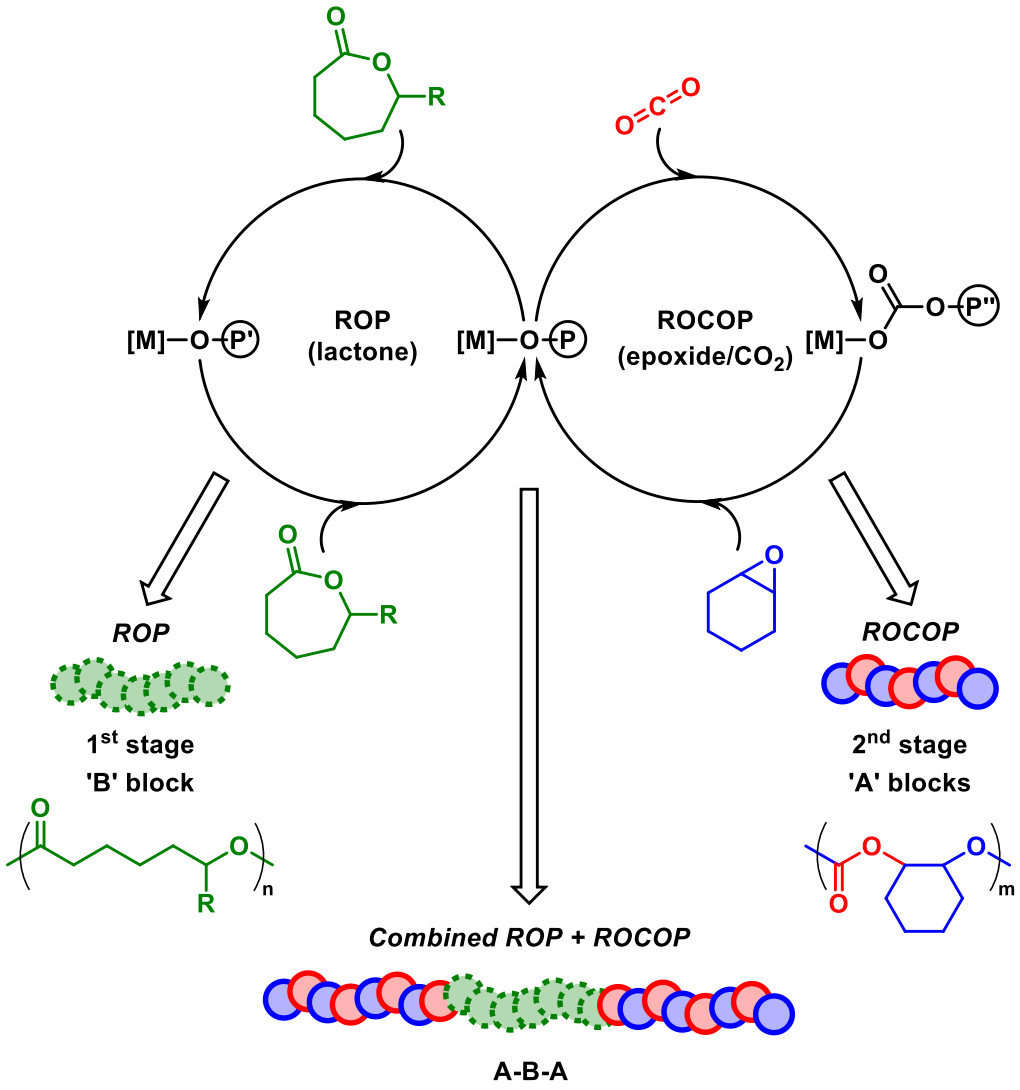


Figure 2.4. SEC trace of PCHC from CHO/CO_2 ROCOP using catalyst **1** at 80 °C.

Given the catalysis rate law shows a first order dependence in cyclohexene oxide concentration, it is generally preferable to conduct these polymerizations in neat epoxide to maximise rate, yet such polymerisations typically encounter viscosity limitations at 40-50% conversion. Combined with the large excess of chain-transfer agent employed, only low molar mass polymers were obtained (M_n = 1.6 kg mol^{-1}), which are in the polyol regime.

2.3.3. Combining ROP and ROCOP: Switch catalysis of ε-DL, CHO, and CO_2

Scheme 2.1. Switch Catalysis: Combining ROP and ROCOP Cycles Using a Single Catalyst.



Catalyst **1** was evaluated in switch polymerisation which combined the ROP of ε-DL with the ROCOP of CHO and CO_2 (**Scheme 2.1**). The latter cycle is accessible through the introduction of the CO_2 as the switch reagent. The rate of CO_2 insertion into the metal-alkoxide bond (central intermediate, [M]-O-P in **Scheme 2.1**) is proposed to be much faster compared with ε-DL (or CHO) binding and ring-opening, and the resulting metal-carbonate species ([M]-O-C(O)-O-P") is expected to be unable to ring-open ε-DL monomer, thus enabling the ring-opening copolymerisation to proceed selectively.[21]

The results of the individual polymerisation tests indicated that 20 equivalents of CHD should be used in the switch polymerisation to obtain monomodal polymer distributions and end-group control, especially given the ROP stage was conducted first. The polymerisation was carried out at 80 °C in excess CHO (as a solvent in the first stage and reagent in the second stage of the reaction) with a starting [ε-DL]:[CHO] monomer feed ratio of 400:1000. Starting under an atmosphere of N_2, the mixture was reacted for approximately 1 hour at which point the vessel was pressurised with CO_2 gas (P = 1 bar) through several vacuum/CO_2 cycles to fully replace the nitrogen atmosphere and allowed to continue for approximately another 4.5 hours. The entire reaction was monitored using *in-situ* ATR-IR spectroscopy, by changes to absorptions for the PDL ester linkages (1190 cm^{-1}) and PCHC carbonate linkages (1237 cm^{-1}) (**Figure 2.5**).

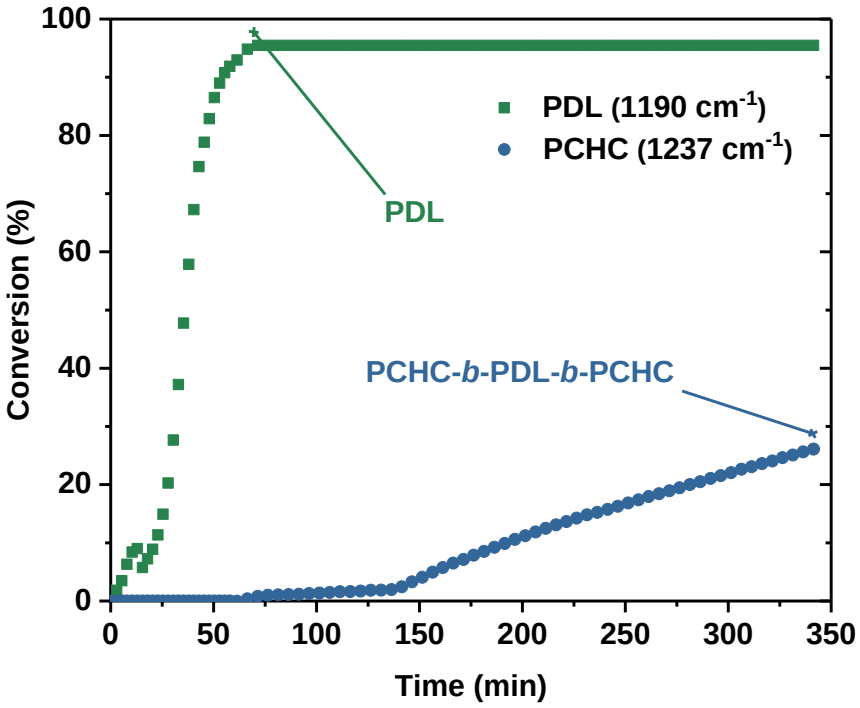


Figure 2.5. *In-situ* ATR IR spectroscopy reaction monitoring of a switch polymerisation of ε-DL/CHO/CO_2 at 80 °C. Relative intensity data for bands monitored fitted to monomer conversion values determined by ^{1}H NMR spectroscopy.

The data illustrate the high catalyst selectivity: in the first stage, under N_2, there was only conversion of ε-DL to form PDL; when the atmosphere is replaced with CO_2, the ROCOP of CHO and CO_2 proceeds and there was no further conversion of ε-DL. While the data gave important information regarding selectivity, it could not provide evidence for block connectivity in the resulting polymer(s). To assess whether the desired ABA type triblock polymer or a mixture of separate PDL and PCHC polymers had formed, a sample of the crude polymerisation mixture at the end of the reaction was analysed by SEC (**Figure 2.6**).

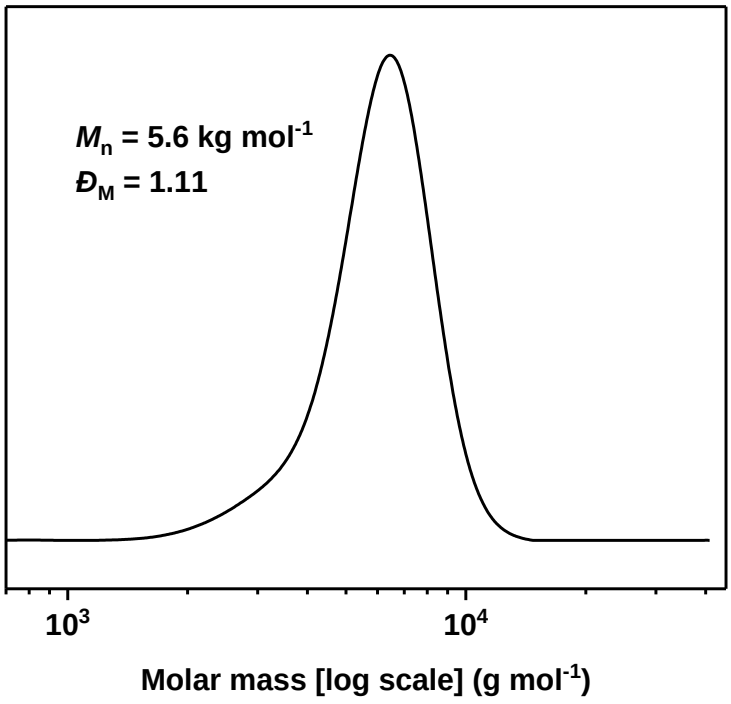


Figure 2.6. SEC trace of a crude sample taken from the switch polymerisation of ε-DL/CHO/CO_2 at the end of the reaction.

The SEC analysis showed the polymer had a monomodal molar mass distribution which is indicative of triblock formation. There were, however, a couple of limitations to this catalyst: (1) the large excess of CTA required and (2) the low (viscosity-limited) conversion of PCHC (< 30%) resulted in a very low molar mass triblock (M_n = 5.6 kg mol^{-1}). To address these limitations, two modifications were tested: (1) the reaction was diluted with toluene ($[CHO]_0$

= 5 M) to alleviate viscosity limitations and allow for higher PCHC conversion; (2) reaction temperature was increased to 100 °C to accelerate rates and hence increase conversion/molar mass. *In-situ* reaction monitoring showed successful progress of this modified switch polymerisation (**Figure 2.7**).

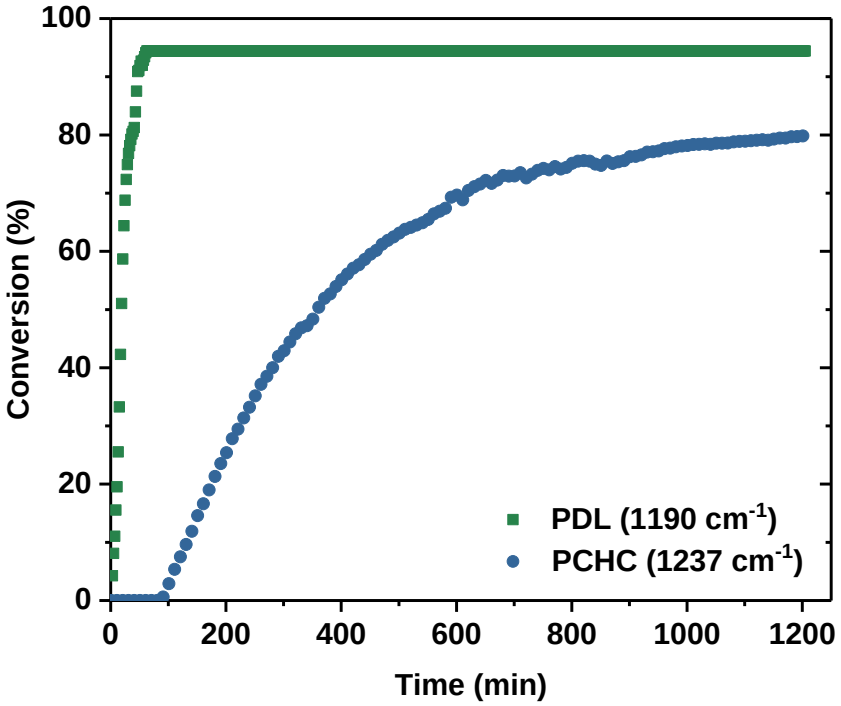


Figure 2.7. *In-situ* ATR IR spectroscopy reaction monitoring of a switch polymerisation of ε-DL/CHO/CO_2 at 100 °C diluted in toluene ($[CHO]_0$ = 5 M). Relative intensity data for bands monitored fitted to monomer conversion values determined by ^{1}H NMR spectroscopy.

The ring-opening polymerisation of ε-DL was conducted for approx. 1 hour before cycling the atmosphere to CO_2 and, then, the ROCOP of CHO and CO_2 was conducted for a further 19 hours. The high selectivity in switch catalysis was maintained under these increased dilution and elevated temperature conditions. There was a small decrease in the overall selectivity for PCHC with trace *trans*-1,2-cyclohexene carbonate being observed in the ^{1}H NMR of the final crude polymer, its formation attributed to the elevated temperature and it being the thermodynamic product of carbon dioxide/epoxide coupling (Appendix, Figure

S7.2). These conditions resulted in the desired high polycarbonate conversions (~ 80%) and slightly increased the overall molar mass of the final triblock polymer (8.7 kg mol^{-1}) albeit with the SEC trace suggesting some minor low molar mass species remained present (**Figure 2.8**, dashed line).

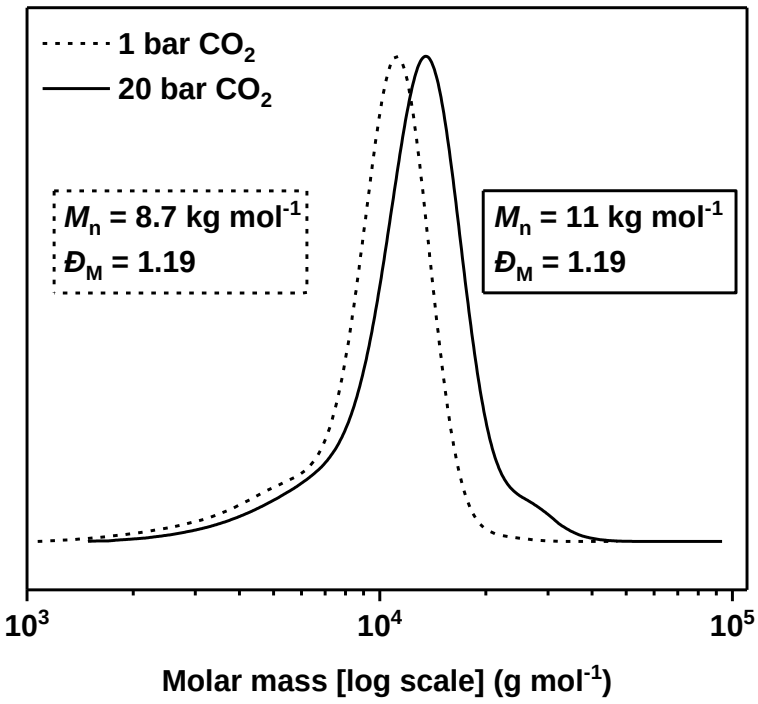


Figure 2.8. SEC traces of final polymer samples from switch polymerisations of ε-DL/CHO/CO_2 conducted at 100 °C under 1 bar (dashed) and 20 bar (solid) CO_2 pressures.

Thus far, all the ROCOP stages of switch polymerisations using **1** were conducted under 1 bar of CO_2 pressure, but the heterodinuclear catalyst performed equivalently successfully under higher CO_2 pressures of 20 bar (**Figure 2.8**, solid line). It was important to evaluate the switch polymerisation under these conditions because the high pressure autoclave is equipped with mechanical stirring which was expected to overcome the viscosity limitation to polymer conversions observed under magnetic stirring, even under dilute conditions. Nonetheless, it remained clear that the use of such a large excess of CTA, because of the

presence of the benzoate co-ligands, was severely limiting the catalysis and preventing access to high molar mass polymers.

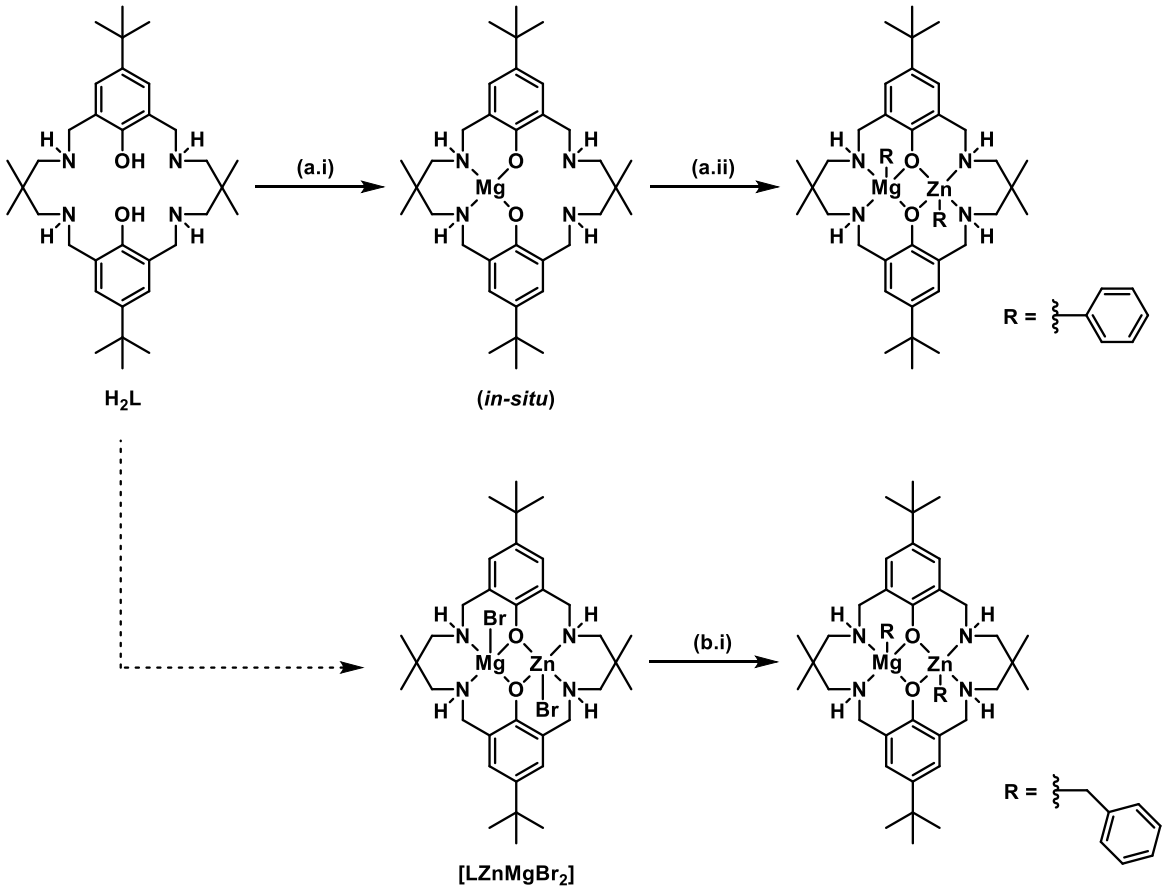
2.4. Applying an organometallic Zn(II)/Mg(II) heterodinuclear catalyst: Addressing the coligand problem

2.4.1. Synthesis and characterisation

While the success of heterodinuclear Zn(II)/Mg(II) catalyst, **1**, in showing selective switch catalysis is important in improving rates *vs.* homodinuclear Zn(II)/Zn(II) analogues, the co-ligand initiation issue ultimately limits access to high molar mass polymers. To solve this problem, the syntheses of heterodinuclear Zn(II)/Mg(II) catalysts with non-initiating co-ligands were targeted.

These catalysts should have labile, organometallic co-ligands that react *in-situ* with the diol to form the desired metal-alkoxide initiator and with an arene as the by-product. Phenyl and benzyl co-ligands were investigated first because suitable reagents are accessible and syntheses could be proposed which were similar to those already shown to be successful for these heterodinuclear catalysts. Specifically, a two-step synthetic procedure involving reacting the pro-ligand with $[Mg(N(SiMe_3)_2)_2]$ and then $[ZnPh_2]$ was attempted to introduce two phenyl co-ligands, while a salt metathesis involving the $[LZnMgBr_2]$ precursor complex and potassium benzyl was also attempted to introduce benzyl co-ligands (**Scheme 2.2**).

Scheme 2.2. Proposed Synthetic Routes to Heterodinuclear Zn(II)/Mg(II) Catalysts Bearing Organometallic Co-ligands.



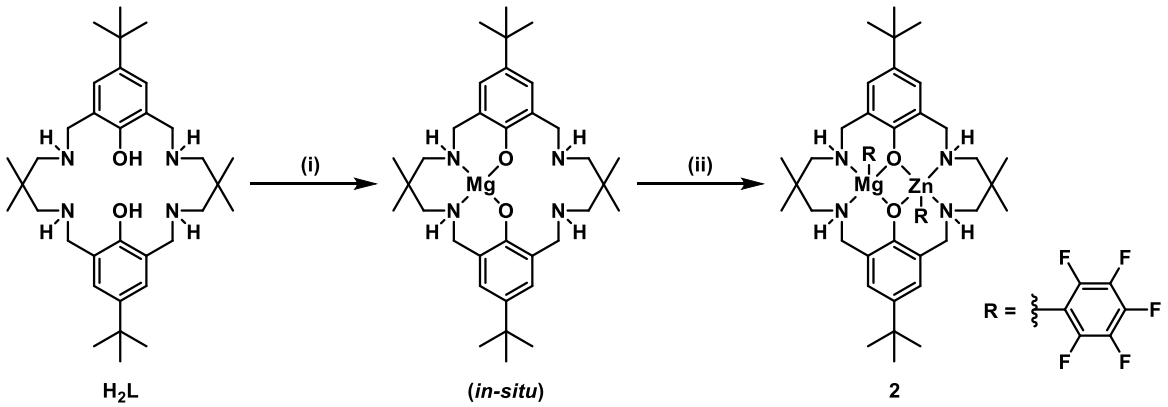
Reaction conditions: Phenyl co-ligand - (a.i) $[Mg(N(SiMe_3)_2)_2]$ (1 equiv.), THF, 25 °C, 1 h; (a.ii) $[ZnPh_2]$ (1 equiv.), THF, 25 °C, 16 h. Benzyl co-ligand – (b.i) KBn (2 equiv.), THF, 25 °C, 1 h; dotted arrow indicates $[LZnMgBr_2]$ is initially synthesised from pro-ligand H_2L as previously reported.[12, 19]

The ^{1}H NMR spectra revealed both reactions were unsuccessful (Appendix Figure S7.3). Characteristic signals with high intensity corresponding to aromatic protons on benzene and methyl protons on toluene were identifiable at 7.30 ppm and 2.31 ppm, respectively, indicating protonolysis of either the complexes or precursors had occurred. The absence of a diagnostic splitting pattern for the methylene/benzylic protons on the macrocyclic ligand, characteristic for heterodinuclear complex formation, was another indicator of an unsuccessful reaction and could also indicate decomposition of complexes. Since the formation of the homodinuclear $[LZnZnPh_2]$ complex is known, and utilises the $[ZnPh_2]$ reagent in its synthesis, the presence of magnesium in this case is hypothesised as the cause of failure. Moreover, the basicity of both the phenyl and benzyl protons is relatively high (pK_a

~ 43), and so these groups could perhaps deprotonate the macrocyclic N-H groups adjacent to the magnesium centre. As such, it was proposed that a co-ligand target with lower basicity might prevent the deprotonation of the macrocycle and decomposition reactions.

Bis(pentafluorophenyl) zinc(II), $[Zn(C_6F_5)_2]$, was identified as a promising reagent given that the fluorine substituents should render it far less basic. The first step involved deprotonation of the macrocyclic pro-ligand with $[Mg(N(SiMe_3)_2)_2]$ forming, *in-situ*, a putative monomagnesium complex. This was then reacted with $[Zn(C_6F_5)_2]$ to isolate the desired catalyst **2** in good yield (70%) (**Scheme 2.3**).

Scheme 2.3. Synthesis of the Heterodinuclear $[LZnMg(C_6F_5)_2]$ Complex, 2.



Reaction conditions: (i) $[Mg(N(SiMe_3)_2)_2]$ (1 equiv.), THF, 25 °C, 1 h. (ii) $[Zn(C_6F_5)_2]$ (1 equiv.), THF, 25 °C, 16 h, 70% isolated yield.

The ^{1}H NMR spectrum of complex **2** is sharp at room temperature and shows multiple pieces of evidence supporting the formation of a heterodinuclear complex (**Figure 2.9**). Eight signals corresponding to benzylic (c, c', d, d') and methylene (f, f', g, g') protons were visible and assigned as being on either the zinc or magnesium side of the macrocycle through use of 2D NMR spectroscopy, as well as with reference to a previously synthesised homodinuclear $[LZnZn(C_6F_5)_2]$ complex.[13] Splitting of aromatic signals (b & b') into two which are mutually coupled to one another was also highly diagnostic of a pure heterodinuclear compound. The macrocycle N-H proton was clearly visible in the spectrum for the magnesium side (e') but in the case of the zinc side (e) it overlapped with methylene proton signals and was identified

through relative integrals. The clear signals for the N-H protons also confirmed that no deprotonation of the macrocycle had taken place and instead the desired complex had been formed.

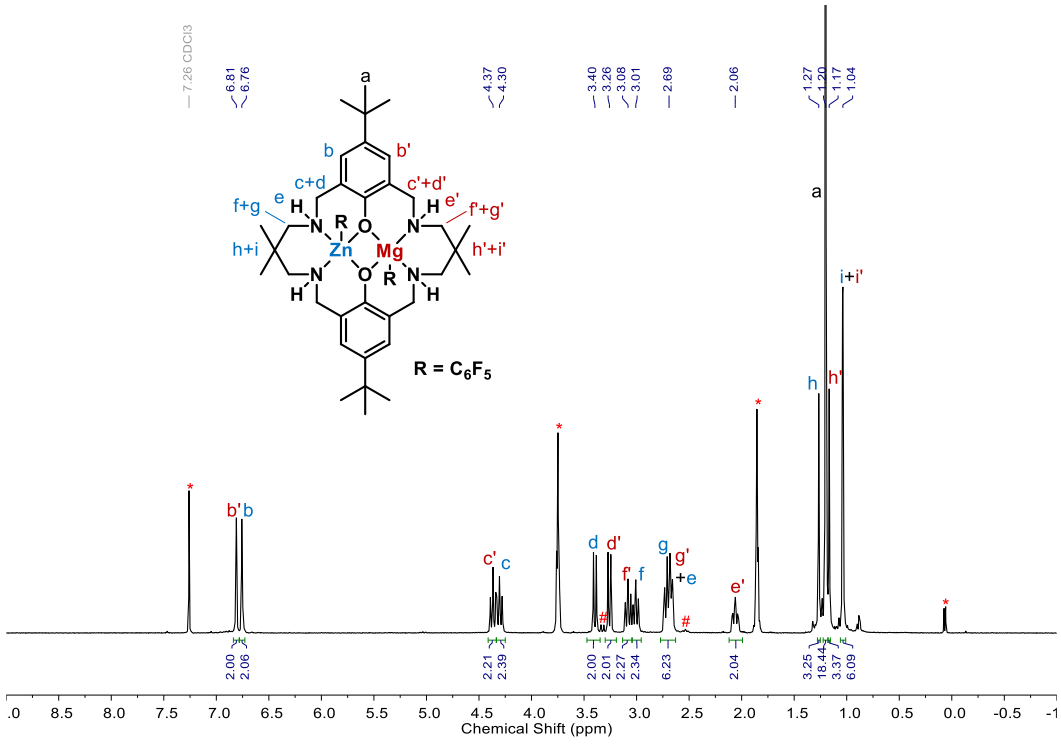


Figure 2.9. ^{1}H NMR spectrum of heterodinuclear [LZnMg$(C_6F_5)_2$] complex, **2**. Where possible, assignment of signals as either on the Zn or Mg side of the macrocycle was made using 2D NMR spectroscopy (see Appendix Figures S7.5 – 7.7 for relevant spectra). # assigns impurity signals from [$LZn_2(C6F5)_2$]; heterodinuclear content calculated as 97% (see Appendix Figure S7.4 for comparison spectra). [500 MHz, $CDCl_3$].

Likewise, the ^{13}C{^{1}H} NMR spectrum of complex **2** is consistent with the formation of a low-symmetry heterodinuclear complex (**Figure 2.10**). In particular, the splitting of aromatic (d/d' & e/e') and methylene (g/g' & h/h') carbons into separate signals was visible, and these were similarly assigned to either the zinc or magnesium side of the complex where possible using 2D NMR spectroscopy. It was also noted that there was an absence of signals corresponding to the aromatic carbons of the pentafluorophenyl co-ligands. Lack of these signals was attributed to the multiple carbon-fluorine couplings these carbons would experience, and has been seen before in the spectrum of the aforementioned [LZnZn$(C_6F_5)_2$]

complex. Nonetheless, a $^{19}F\{^{1}H\}$ spectrum of **2** showed six fluorine environments corresponding to *ortho*, *meta*, and *para* positions on either the zinc- or magnesium-centred co-ligand (Appendix Figures S7.8 – 7.9). This was also consistent with a low-symmetry complex, and hence with one pentafluorophenyl co-ligand residing on zinc and one on magnesium.

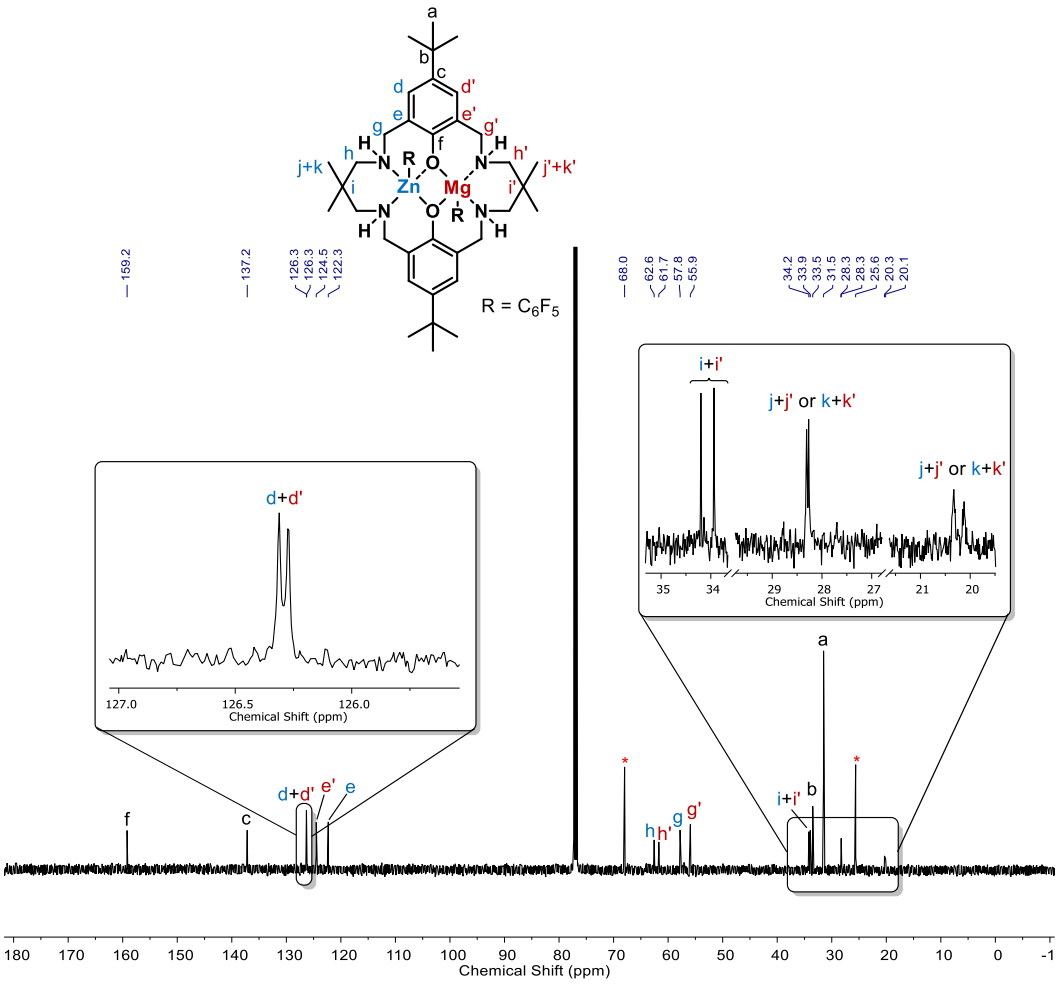


Figure 2.10. $^{13}C\{^{1}H\}$ NMR spectrum of heterodinuclear $[LZnMg(C_6F_5)_2]$ complex, **2**. Inset spectra highlight splitting of signals for phenyl (d/d'), methine (i/i'), and methyl (j/j' & k/k') carbons. Where possible, assignment of signals being either on the Zn or Mg side of the macrocycle was made using 2D NMR spectroscopy (see Appendix Figures S7.5 – 7.7 for relevant spectra). [125 MHz, $CDCl_3$].

2.4.2. Polymerisation studies

The new heterodinuclear catalyst, **2**, was employed in both the ROCOP and ROP of CHO/CO_2 and ε-DL, respectively (**Table 2.2**). As with the testing of complex **1**, these were an important initial tests of the catalyst's ability to facilitate the individual polymerisation cycles, and allowed for its evaluation as a suitable replacement for [LZnMg(OBz^{NMe2})$_2$] (**1**) and [LZnZnPh$_2$] (Zn_2) in the pursuit of higher molar mass polymers (**Table 2.2**, entries 2-3 & 5-6). Subsequently, complex **2** could then be evaluated in the combined ROP/ROCOP (switch polymerisation) of a mixed monomer feedstock.

Table 2.2. ROP and ROCOP Polymerisations Catalysed by Dinuclear Catalysts

Entry	Cat[a]	Mon.	[Cat] (mol %)	T (°C)	Conv. (%)[b]	PC (%)[c]	TON[d]	TOF (h^{-1})[e]	M_n (kg mol^{-1}) [$Đ_M$][f,g]
1	2	CHO/CO_2	0.1	80	50	>99	503	101	12.8 [1.24]
2	1	CHO/CO_2	0.1	80	44	>99	435	87	1.6 [1.15]
3[13]	Zn_2	CHO/CO_2	0.1	80	40	>99	400	20	4.8 [1.06]
4	2	ε-DL	0.25	80	99	n.a.	394	4730	33.1 [1.10]
5	1	ε-DL	0.25	80	97	n.a.	389	389	5.3 [1.18]
6[22]	Zn_2	ε-DL	0.5	100	>95	n.a.	200	160	14.0 [1.16]

[a](Hetero/Homo)dinuclear catalysts: 1 = [LZnMg(OBz^{NMe2})$_2$]; 2 = [LZnMg(C_6F_5)$_2$]; Zn_2 = [LZnZn(Ph)$_2$]. [b]Determined by ^{1}H NMR spectroscopy of a crude sample of polymerisation solution. [c]Selectivity for polycarbonate linkages, calculated by ^{1}H NMR spectroscopy using integrals of signals corresponding to PCHC (4.66 ppm), cyclic carbonate (4.00 ppm), and polyether (3.50 ppm). [d]Number of moles of monomer consumed per mole of catalyst. [e]TON per unit time. [f]Determined by SEC, in THF, using narrow dispersity polystyrene standards. [g]$Đ_M = M_w/M_n$.

In the ROCOP of CHO and CO_2 at 1 bar CO_2 pressure and 80 °C, catalyst **2** performed well showing good activity (TOF = 101 h^{-1}) and excellent selectivity for carbonate linkages (99%) (**Table 2.2**, entry 1). The activity was comparable to that of catalyst **1** indicating that the aryl co-ligands had a minimal effect on the polymerisation kinetics, and encouragingly did not negatively impact the ring-opening copolymerisation. The resulting PCHC homopolymer was dihydroxyl telechelic (as 4 equivalents of CHD was used as chain-transfer

agent) and exhibited a monomodal molar mass distribution with M_n = 12.8 kg mol^{-1} and $Đ_M$ = 1.24 (**Figure 2.11**).

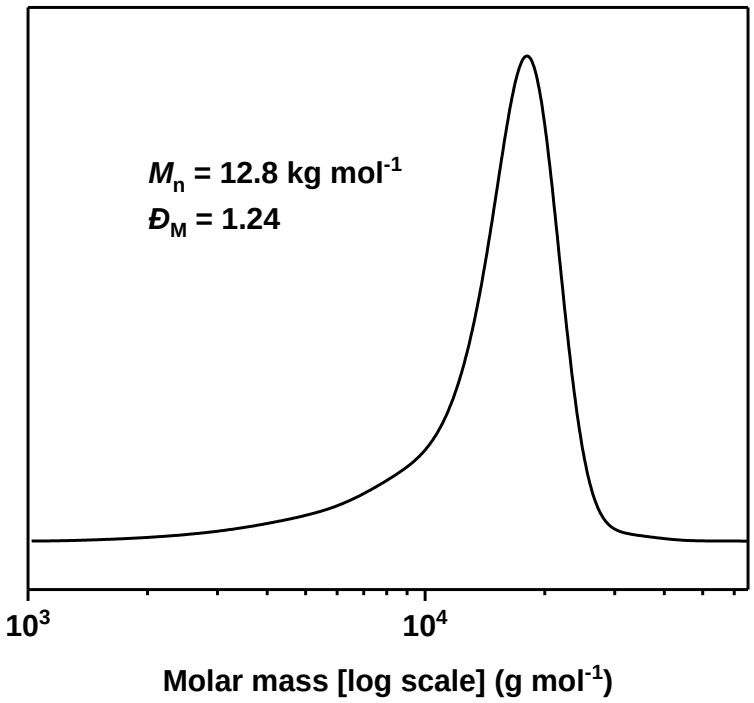


Figure 2.11. SEC trace of PCHC from CHO/CO_2 ROCOP using catalyst **2** at 80 °C.

Similarly, catalyst **2** showed excellent performance in the ROP of ε-DL exhibiting a TOF of >4500 h^{-1} (**Table 2.2**, entry 2). Again, only 4 equivalents of chain-transfer agent were used, which afforded high molar mass PDL (M_n = 33.1 kg mol^{-1}) with a monomodal, narrow distribution ($Đ_M$ = 1.10) (**Figure 2.12**).

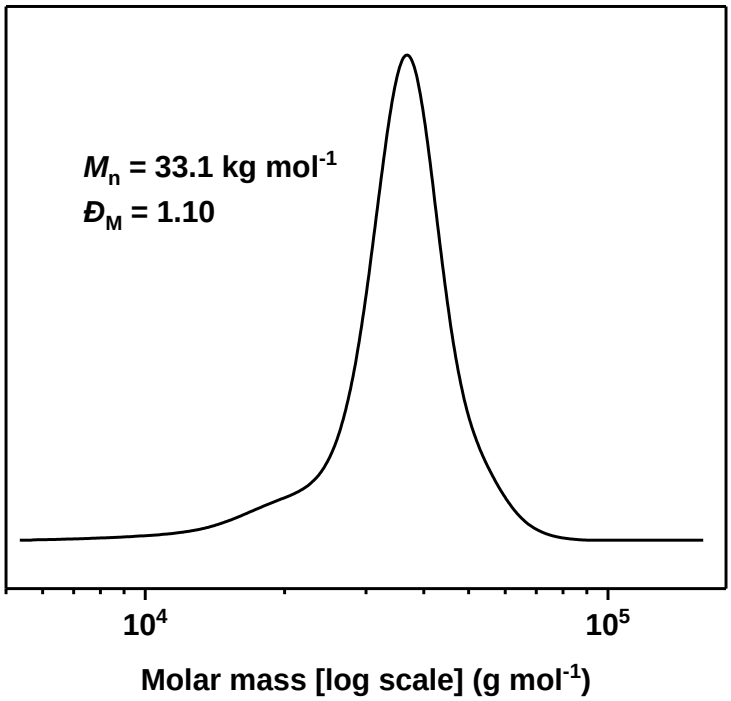


Figure 2.12. SEC trace of PDL from ε-DL ROP using catalyst **2** at 80 °C.

Given that the ROP of ε-DL forms the first stage (i.e. the B block) in ultimately preparing the desired ABA triblock polymers, it is vitally important that only dihydroxyl telechelic chains are produced, from which the subsequent PCHC chains (A blocks) are able to grow on both ends. The presence of only these chains was confirmed by MALDI-ToF mass spectrometry, which highlighted the clear advantage of using catalyst **2** over catalyst **1** (**Figure 2.13**). As illustrated previously, **1** required the addition of 20 equivalents of CHD to significantly suppress the distribution of undesired benzoate-capped chains, which in turn greatly reduced the molar mass of the resulting dihydroxyl telechelic PDL. Here however, **2** was successful in generating dihydroxyl telechelic chains with the addition of only 4 equivalents of CHD, and showed no evidence of a distribution arising from co-ligand initiated chains.

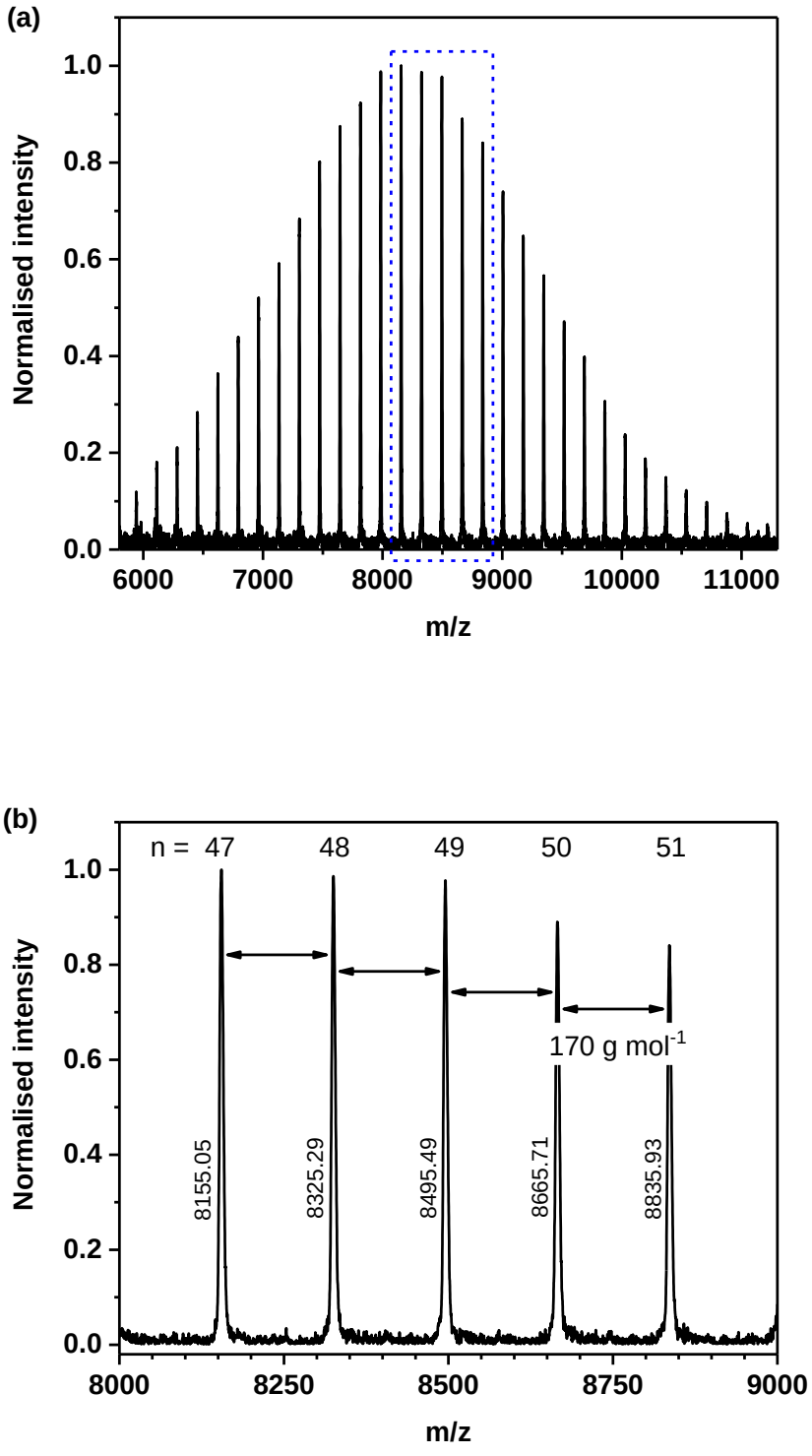


Figure 2.13. (a) MALDI-ToF mass spectrum of PDL from ROP of ε-DL catalysed by **2**; (b) enlarged region of 8000-9000 m/z (blue section in (a)) highlighting peak separation and DP range, where 'n' corresponds to number of PDL repeat units in $[C_6H_{11}O_2 + (PDL)_n] + K^+$.

Building from a strong foundation in both individual polymerisations, catalyst **2** was employed in a "switch" polymerisation of ε-DL, CHO, and CO_2 in order to target high molar mass ABA triblock polymers and succeed where catalyst **1** fell short. *In-situ* ATR-IR spectroscopy was used to monitor the polymerisation at 1 bar CO_2 pressure and determine monomer selectivity, while SEC aliquot analysis was used to assess block formation and molar mass (**Figure 2.14**). The IR bands selected for monitoring the polymerisation showed an exponential growth of PDL (ν = 1190 cm^{-1}) in the first stage of the reaction (under N_2 atmosphere). This was consistent with the expected first order rate dependence with respect to ε-DL concentration, and in line with previous work on lactone ROP.[23] The second stage of polymerisation, initiated by replacing the N_2 atmosphere with one of CO_2 at 1 bar pressure, saw the conversion of ε-DL cease and PCHC (ν = 1237 cm^{-1}) begin to form which illustrated the high monomer selectivity of catalyst **2**.

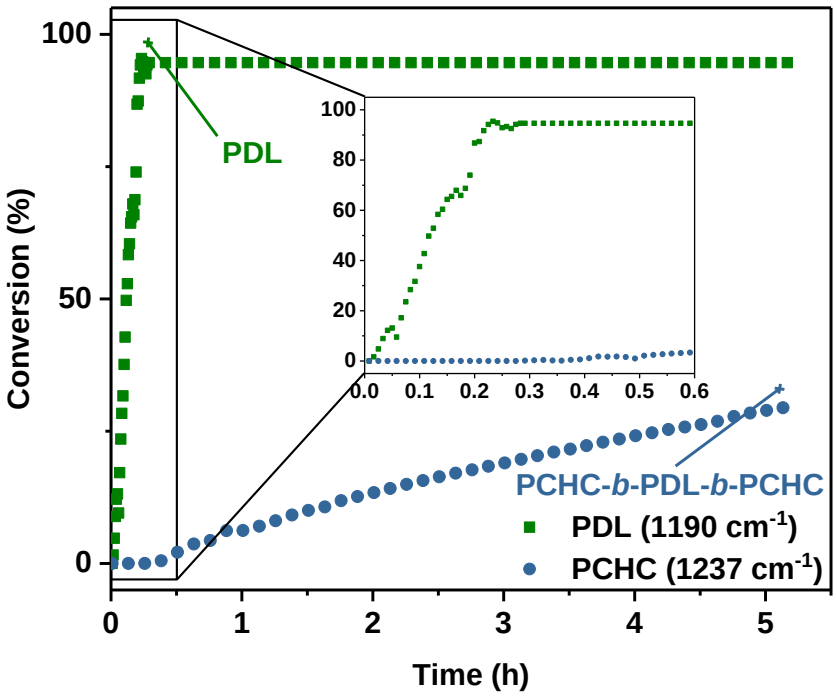


Figure 2.14. *In-situ* ATR IR spectroscopy reaction monitoring of switch polymerisation of ε-DL and CHO/CO_2, catalysed by **2**.

Aliquots removed for SEC analysis during the course of the polymerisation, specifically at time points before and after switching the gas atmosphere in the vessel, revealed a clear increase in molar mass of the polymer, also with retention of a narrow, monomodal distribution (**Figure 2.15**). This was indicative of block connectivity and the formation of the desired ABA triblock polymer. As an exemplary study to investigate the selectivity of **2** in switch polymerisation, this reaction did not target particularly high molar mass or the full conversion of monomers. Nonetheless, it was demonstrated that a total triblock molar mass of around 20 kg mol^{-1} is achievable on a very reasonable timescale (~5 h); a promising result for future, more engineered triblock syntheses applying tailored feed ratios and maximising conversion.

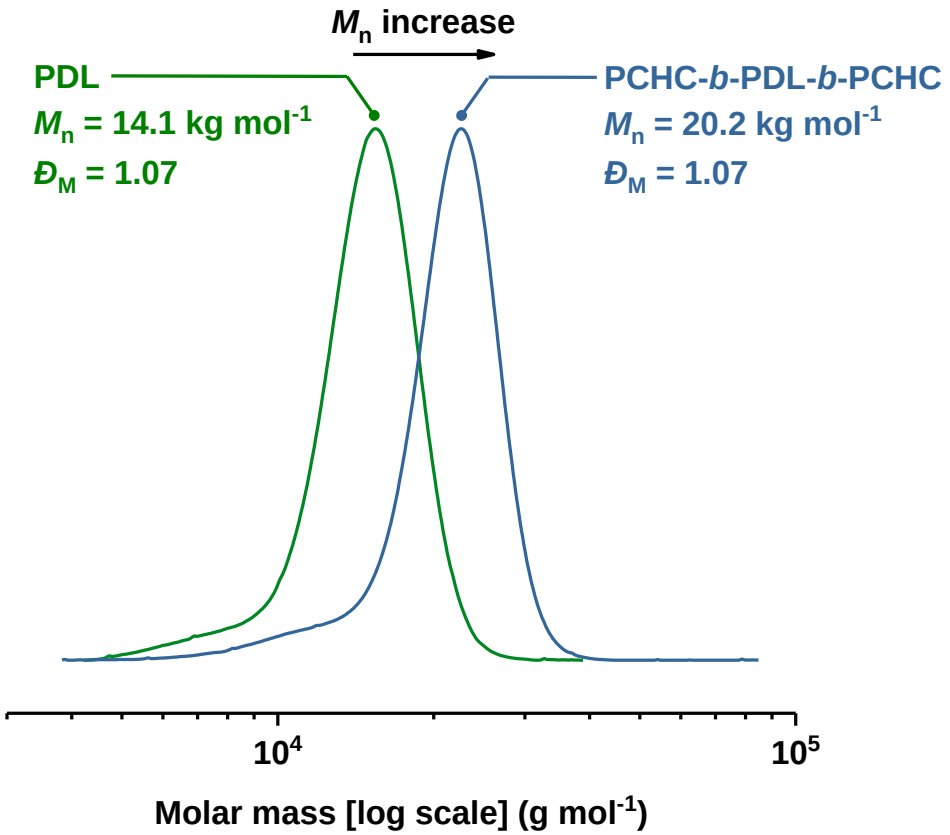


Figure 2.15. SEC traces for aliquots of switch polymerisation of ε-DL and CHO/CO_2 taken prior to and a period after switching the reaction atmosphere from N_2 to CO_2.

2.5. Summary and future work

Heterodinuclear Zn(II)/Mg(II) catalysts bearing *para*-dimethylamino benzoate and pentafluorophenyl co-ligands were evaluated for the switchable polymerisation catalysis of ε-DL, CHO, and CO_2, linking ROP and ROCOP polymerisation cycles to selectively prepare ABA triblock polymers. Both variants were active for switch, and showed excellent selectivity between ROP and ROCOP mechanisms which afforded the desired ABA polymers. Contamination with AB diblock polymers, formed from the initiation of chains by the benzoate co-ligands, was addressed by first optimising the equivalents of diol chain-transfer agent in use, but later by developing the non-initiating aryl co-ligand (C_6F_5) analogue. This variant was successful in producing ABA triblock polymers with considerably fewer equivalents of diol CTA and compared favourably with both the benzoate and homodinuclear zinc(II) analogues in terms of polymerisation rates, ultimately giving higher molar mass polymers on an acceptable timescale.

There are a number of avenues down which this research could be pursued, utilised or expanded upon, the following being those most attractive in the shorter term: (1) preparation of higher molar mass triblock polymers, facilitated by the new catalyst, which incorporate high CO_2 utilisation; (2) synthesis of non-linear polymer architectures by exploiting the co-ligand's labile nature and chain-transfer processes; (3) investigation into faster heterodinuclear catalysts that bear similar aryl, non-initiating, co-ligands; (4) exploration of the reversibility of polymerisation cycle switching to prepare $(A\text{-}b\text{-}B)_n$ multiblock polymers.

The first and second points present a natural progression to the findings of this chapter. The new catalyst, **2**, lends itself to the preparation of higher molar mass ABA triblock polymers due to the aryl coligand lability and use of far fewer equivalents of chain-transfer agent while avoiding contamination by other polymer species. The nature of the catalyst (i.e. coligand reactivity to free hydroxyls) and the chain-transfer process should also provide a

facile means to moderate initiation.[24] Through this, accessing non-linear architectures such as star block polymers should be possible by employing a triol or tetrol chain-transfer agent, rather than the diol species, to yield tri- or tetra-arm star block polymers with the switch catalysis functioning as before. Thus, the first and second points are explored in chapters 3 and 4 of this thesis, respectively.

Recent advances in other aspects of catalyst design such as metal centre combination/synergy and ancillary ligand structure have resulted in considerably faster and optimised catalysis, but owing to synthetic routes many catalysts still possess acetate coligands.[10, 25] Developing these complexes further by targeting variants with non-initiating coligands should enable even quicker access to a wide range of higher molar mass block polymers and accelerate the progress of switchable catalysis and the preparation of functional polyesters and polycarbonates derived from renewables and/or CO_2.

Finally, reversible switching between polymerisation cycles could be a useful technique to prepare linear multiblock polymers and achieve higher molar mass samples with interesting properties and functionality. While this thesis explores a single switch from an N_2 to a CO_2 atmosphere, future work could investigate the tolerance of these catalysts to multiple sequential atmosphere changes or monomer additions (e.g. anhydrides). Retention of monomer selectivity between multiple switches, efficacy at low catalyst loadings, and excellent block connectivity would be critical to ensure the preparation of the desired multiblock polymers from ROP and ROCOP cycles, but the possibility to exploit particular selectivity/reactivity of various monomer combinations would allow for the synthesis of both alternating "A-*b*-B" multiblock polymers and more complex "A-*b*-B-*b*-C-*b*-…" repeating sequences.

2.6. References

1. Kember, M. R.; Knight, P. D.; Reung, P. T.; Williams, C. K., Highly active dizinc catalyst for the copolymerization of carbon dioxide and cyclohexene oxide at one atmosphere pressure. *Angew. Chem. Int. Ed.* **2009,** *48* (5), 931-3.
2. Kember, M. R.; Buchard, A.; Williams, C. K., Catalysts for CO2/epoxide copolymerisation. *Chem. Commun.* **2011,** *47* (1), 141-163.
3. Anderson, C. E.; Vagin, S. I.; Hammann, M.; Zimmermann, L.; Rieger, B., Copolymerisation of Propylene Oxide and Carbon Dioxide by Dinuclear Cobalt Porphyrins. *ChemCatChem* **2013,** *5* (11), 3269-3280.
4. Saini, P. K.; Romain, C.; Williams, C. K., Dinuclear metal catalysts: improved performance of heterodinuclear mixed catalysts for CO2–epoxide copolymerization. *Chem. Commun.* **2014,** *50* (32), 4164-4167.
5. Kissling, S.; Lehenmeier, M. W.; Altenbuchner, P. T.; Kronast, A.; Reiter, M.; Deglmann, P.; Seemann, U. B.; Rieger, B., Dinuclear zinc catalysts with unprecedented activities for the copolymerization of cyclohexene oxide and CO2. *Chem. Commun.* **2015,** *51* (22), 4579-4582.
6. Yi, N.; Unruangsri, J.; Shaw, J.; Williams, C. K., Carbon dioxide capture and utilization: using dinuclear catalysts to prepare polycarbonates. *Faraday Discuss.* **2015,** *183* (0), 67-82.
7. Zhou, Y.; Duan, R.; Li, X.; Pang, X.; Wang, X.; Chen, X., Preparation and Thermal Properties of Polycarbonates/esters Catalyzed by Using Dinuclear Salph-Al from Ring-Opening Polymerization of Epoxide Monomers. *Chem. Asian. J.* **2017,** *12* (24), 3135-3140.
8. Nagae, H.; Aoki, R.; Akutagawa, S.-n.; Kleemann, J.; Tagawa, R.; Schindler, T.; Choi, G.; Spaniol, T. P.; Tsurugi, H.; Okuda, J.; Mashima, K., Lanthanide Complexes Supported by a Trizinc Crown Ether as Catalysts for Alternating Copolymerization of Epoxide and CO2: Telomerization Controlled by Carboxylate Anions. *Angew. Chem. Int. Ed.* **2018,** *57* (9), 2492-2496.
9. Deacy, A. C.; Durr, C. B.; Garden, J. A.; White, A. J. P.; Williams, C. K., Groups 1, 2 and Zn(II) Heterodinuclear Catalysts for Epoxide/CO2 Ring-Opening Copolymerization. *Inorg. Chem.* **2018**.
10. Deacy, A. C.; Kilpatrick, A. F. R.; Regoutz, A.; Williams, C. K., Understanding metal synergy in heterodinuclear catalysts for the copolymerization of CO2 and epoxides. *Nat. Chem.* **2020,** *12* (4), 372-380.
11. Buchard, A.; Jutz, F.; Kember, M. R.; White, A. J. P.; Rzepa, H. S.; Williams, C. K., Experimental and Computational Investigation of the Mechanism of Carbon Dioxide/Cyclohexene Oxide Copolymerization Using a Dizinc Catalyst. *Macromolecules* **2012,** *45* (17), 6781-6795.
12. Garden, J. A.; Saini, P. K.; Williams, C. K., Greater than the Sum of Its Parts: A Heterodinuclear Polymerization Catalyst. *J. Am. Chem. Soc.* **2015,** *137* (48), 15078-81.
13. Romain, C.; Garden, J. A.; Trott, G.; Buchard, A.; White, A. J. P.; Williams, C. K., Di-Zinc-Aryl Complexes: CO2 Insertions and Applications in Polymerisation Catalysis. *Chem. Eur. J.* **2017,** *23*, 7367-7376.
14. Garden, J. A.; White, A. J. P.; Williams, C. K., Heterodinuclear titanium/zinc catalysis: synthesis, characterization and activity for CO2/epoxide copolymerization and cyclic ester polymerization. *Dalton Trans.* **2017,** *46* (8), 2532-2541.
15. Jutz, F.; Buchard, A.; Kember, M. R.; Fredriksen, S. B.; Williams, C. K., Mechanistic Investigation and Reaction Kinetics of the Low-Pressure Copolymerization of Cyclohexene Oxide and Carbon Dioxide Catalyzed by a Dizinc Complex. *J. Am. Chem. Soc.* **2011,** *133* (43), 17395-17405.

16. Chen, T. T. D.; Zhu, Y. Q.; Williams, C. K., Pentablock Copolymer from Tetracomponent Monomer Mixture Using a Switchable Dizinc Catalyst. *Macromolecules* **2018,** *51* (14), 5346-5351.
17. Zhu, Y.; Radlauer, M. R.; Schneiderman, D. K.; Shaffer, M. S. P.; Hillmyer, M. A.; Williams, C. K., Multiblock Polyesters Demonstrating High Elasticity and Shape Memory Effects. *Macromolecules* **2018,** *51* (7), 2466-2475.
18. Stößer, T.; Chen, T. T. D.; Zhu, Y.; Williams, C. K., 'Switch' catalysis: from monomer mixtures to sequence-controlled block copolymers. *Phil. Trans. R. Soc. A* **2018,** *376* (2110).
19. Trott, G.; Garden, J. A.; Williams, C. K., Heterodinuclear zinc and magnesium catalysts for epoxide/CO2 ring opening copolymerizations. *Chem. Sci.* **2019,** *10* (17), 4618-4627.
20. Olsén, P.; Borke, T.; Odelius, K.; Albertsson, A.-C., ε-Decalactone: A Thermoresilient and Toughening Comonomer to Poly(l-lactide). *Biomacromolecules* **2013,** *14* (8), 2883-2890.
21. Romain, C.; Zhu, Y.; Dingwall, P.; Paul, S.; Rzepa, H. S.; Buchard, A.; Williams, C. K., Chemoselective Polymerizations from Mixtures of Epoxide, Lactone, Anhydride, and Carbon Dioxide. *J. Am. Chem. Soc.* **2016,** *138* (12), 4120-31.
22. Zhu, Y.; Romain, C.; Williams, C. K., Selective polymerization catalysis: controlling the metal chain end group to prepare block copolyesters. *J. Am. Chem. Soc.* **2015,** *137* (38), 12179-82.
23. van der Meulen, I.; Gubbels, E.; Huijser, S.; Sablong, R.; Koning, C. E.; Heise, A.; Duchateau, R., Catalytic Ring-Opening Polymerization of Renewable Macrolactones to High Molecular Weight Polyethylene-like Polymers. *Macromolecules* **2011,** *44* (11), 4301-4305.
24. Zhu, Y.; Romain, C.; Poirier, V.; Williams, C. K., Influences of a Dizinc Catalyst and Bifunctional Chain Transfer Agents on the Polymer Architecture in the Ring-Opening Polymerization of ε-Caprolactone. *Macromolecules* **2015,** *48* (8), 2407-2416.
25. Deacy, A. C.; Moreby, E.; Phanopoulos, A.; Williams, C. K., Co(III)/Alkali-Metal(I) Heterodinuclear Catalysts for the Ring-Opening Copolymerization of CO2 and Propylene Oxide. *J. Am. Chem. Soc.* **2020,** *142* (45), 19150-19160.

CHAPTER 3

High Performance ABA-type Triblock Polymers Derived from CO_2: Adhesives, Elastomers and Toughened Plastics

3.1. Introduction

The development and innovation in block copolymer synthesis has led to a wealth of potential for the production of high performance polymer materials.[1-2] Consequently, there are various applications which utilise block copolymers, with some key examples being engineering thermoplastics, pressure-sensitive adhesives, and thermoplastic elastomers. Specifically, ABA-type triblock polymers play host to some of the most important, and well-known, examples like SBS/SIS in the area of thermoplastic elastomers. However, the majority of the current lead materials still rely heavily on fossil fuel resources for their production, and cannot be easily degraded after use. Ultimately, a drive towards a circular plastic economy means that there is now greater emphasis on the development of high-performance sustainable materials (e.g. based on polyesters and polycarbonates) derived from renewable sources (e.g. certain cyclic esters and epoxides, and CO_2). Of course, a circular economy also necessitates recycling and, ultimately, biodegradation of the materials within it.

Considering CO_2 utilisation in the synthesis of high-performance materials, a focus of current academic and industrial research is the application of ring-opening copolymerisation (ROCOP) to make low molar mass poly(carbonate/ether carbonate) polyols.[3-4] These shorter chain polymers (M_n = 1–10 kg mol^{-1}) with hydroxyl chain-end groups are then subsequently employed with additives to give high-performance thermosets or polyurethanes which cater to applications spanning coatings, adhesives, elastomers, and sealants (CASE).[5-9]

Developments in ROCOP catalysts have led to the process being able to also deliver higher molar mass polycarbonates (M_n = 10–100 kg/mol^{-1}). Poly(cyclohexene carbonate) (PCHC) is one of the most extensively studied with respect to catalyst development and synthesis, yet reports examining the properties, potential applications, or future directions for improving the material are lacking in comparison.[10-11] Around two decades ago, Koning *et al.* reported the physical properties of PCHC as having a high glass transition temperature

(105–115 °C), reasonable tensile strength (11–42 MPa), and excellent tensile modulus (2400–3600 MPa).[12] However, the standalone polymer is greatly limited by its very low elongation at break (0.5–2%) and brittleness.[12-13] Others have identified that the thermal decomposition temperature for PCHC can be heavily influenced by metal residues (e.g. from catalysts) resulting in a very low onset (<200 °C), which may then pose limitations for processing.[14] Material development for PCHC has unfortunately been limited and in order to overcome brittleness and facilitate current applications, the polymer requires plasticizers and additives.

Incorporating PCHC into a block polymer presents one possible strategy to improve the properties of this material, and the concept could apply more broadly to improve properties of other CO_2-polycarbonates. There are indeed reports of copolymers of PCHC with petrochemical-derived blocks such as poly(acrylates), -ethers, -styrenes, -vinyl ethers, and –siloxanes, but the combination of a CO_2-derived polycarbonate and a non-degradable petrochemical block could be somewhat detrimental from a sustainability standpoint, and raises queries about end-of-life scenarios.[15-16] Moreover, the reports on these block polymers offer little investigation into the resulting materials properties. The lack of property investigation may be attributed partly to the low overall copolymer molar masses (M_n < 20 kg mol^{-1}) which would hinder block phase separation and, by extension, compromise mechanical performances.

Using polyester blocks in place of the aforementioned petrochemical ones, in combination with CO_2-polycarbonates, presents a more positive option in terms of fostering sustainability. In this case, both blocks contain degradable backbone linkages and there are many opportunities to source renewable raw materials.[17-20] Similarly to reports on PCHC though, most research on block polymer synthesis comprising various block polyesters, -carbonates, and -ethers has focused on understanding and improving the catalysis with

investigation of the polymer properties only serving a minor role, if one at all.[21-31] Recently however, Rieger and co-workers synthesised block and statistical copolymers of poly(β-butyrolactone) and PCHC which exhibited phase separation and afforded a small enhancement to the material's elongation at break compared to pure PCHC (5% *vs.* 0.5–2%).[32] This strategy therefore looks promising, and so a better selection of soft-block could improve the properties of PCHC and, by extension, other CO_2-polycarbonates that suffer brittleness.

3.2. Aims

Building on the results of Chapter 2, the following chapter aims to explore the efficacy of the organometallic Zn(II)/Mg(II) catalyst in the switchable polymerisation of lactone/epoxide/CO_2 to synthesise high molar mass ABA triblock polymers (target M_n = 50 kg mol^{-1}) with varying degrees of CO_2 utilisation, and with the intention of tempering the brittleness of the epoxide/CO_2 copolymer. Moreover, it will aim to examine the effects of controlling the CO_2 incorporation and the combination of soft polyester and hard polycarbonate blocks on the materials' thermal and mechanical properties, and evaluate their performance as toughened plastics, elastomers, and pressure-sensitive adhesives.

The approach to deliver on these aims will involve: (1) testing the [LZnMg(C_6F_5)$_2$] catalyst's ability to prepare high molar mass ABA triblock polymers while varying the relative block ratio by controlling the monomer stoichiometry in the switch polymerisation of ε-DL, CHO, and CO_2; (2) investigating the processing viability and thermomechanical properties to understand how changing CO_2 incorporation impacts characteristics such as strength, elasticity, toughness, and adhesion; (3) comparing the polymers' performances to relevant commercial and literature materials to evaluate their potential as more renewable alternatives for applications as ductile plastics, thermoplastic elastomers, and pressure-sensitive adhesives (**Figure 3.1**).

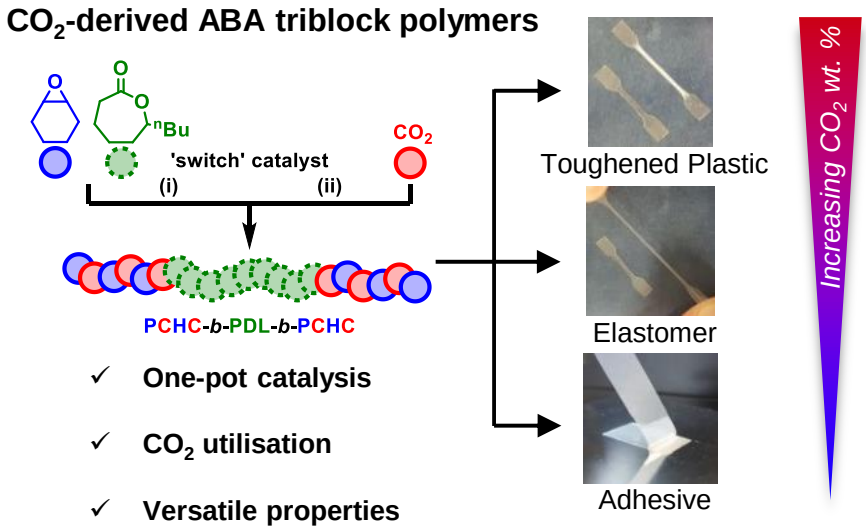


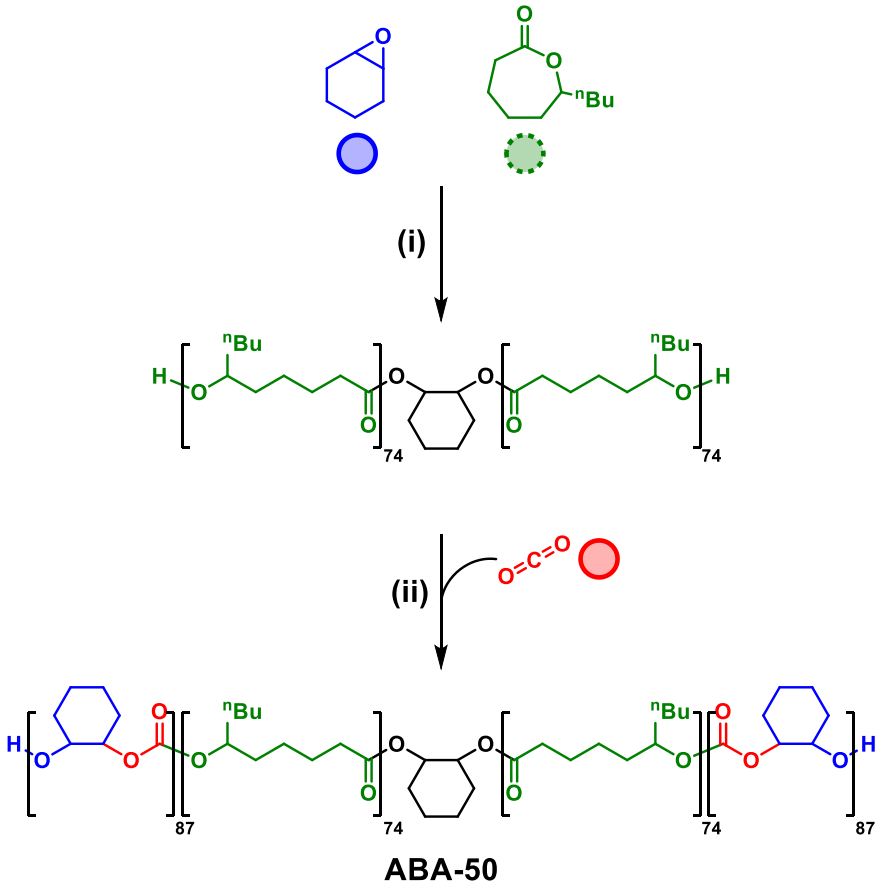
Figure 3.1. ABA triblock polymer synthesis utilising CO_2 for the preparation of a range of materials displaying plastic, elastomeric, and adhesive behaviours.

3.3. CO_2-derived ABA triblock polymers: Synthesis and characterisation

3.3.1. Material preparation

The development of catalyst **2** (detailed in Chapter 2, Section 2.4) was essential for the synthesis of high molar mass ABA triblock polymers. Its employment in the previously described one-pot switchable catalysis procedure with ε-decalactone, cyclohexene oxide, and CO_2 enabled the preparation of a series of PCHC-*b*-PDL-*b*-PCHC triblock polymers with total molar masses ranging from 38 – 72 kg mol^{-1}. For brevity, triblock polymer ABA-50 will serve as an exemplary sample when discussing triblock material preparation and certain aspects of characterisation, as appropriate.

Scheme 3.1. Synthesis of High Molar Mass ABA Triblock Polymers Based on Poly(ε-decalactone) and Poly(cyclohexene carbonate).[a]



[a]Highlighted example for ABA-50. Reaction conditions: (i) [LZnMg(C_6F_5)$_2$]:CHD:ε-DL:CHO = 1:4:587:703, $[CHO]_0$ ~ 3 M in toluene, 80 °C, 20 min. (ii) CO_2 (20 bar), 80 °C, 20 h.

The synthesis of ABA-50 was conducted in two key stages: under an inert atmosphere, catalyst **2** and 4 equivalents of CHD were combined with 600 equivalents of ε-DL and 700 equivalents of CHO and diluted with toluene. Heating the mixture at 80 °C for 20 minutes in a sealed autoclave resulted in the efficient ROP of ε-DL monomer with conversion exceeding 90%, and the selective formation of dihydroxyl telechelic PDL. The second key stage saw the autoclave pressurised to 20 bar with CO_2 and heated at 80 °C for a further 20 hours (**Scheme 3.1**). After this time, the pressure readout had noticeably decreased which indicated consumption of CO_2 and conversion of this along with CHO monomer to PCHC. On cooling and depressurisation of the autoclave, a crude sample of the reaction mixture was removed for analysis and revealed high PCHC conversion (>90%) as well as a high molar mass polymer (59.8 kg mol^{-1}, $Đ_M$ = 1.10) (**Table 3.1**, entry 5). It should be noted that in almost all cases of ABA triblock polymer preparation, the reaction mixture was found, on removing the autoclave headpiece, to have partially solidified in the cylinder. At this point the addition of approximately 5 mL THF was required to facilitate recovery and removal.

Table 3.1. PCHC-*b*-PDL-*b*-PCHC (ABA Triblock) Synthetic Characterisation Data

Entry	Polymer[a,b]	wt % PDL:PCHC[c]	DP PDL:PCHC[d]	M_n[e] (kg mol^{-1})	$Đ_M$[f]	wt % CO_2[g]
1	ABA-20	80:20	232:68	55.9	1.16	6.2
2	ABA-26	74:26	307:131	71.9	1.16	8.0
3	ABA-28	72:28	200:93	46.4	1.07	8.7
4	ABA-40	60:40	168:135	49.4	1.08	12.4
5	ABA-50	50:50	147:173	59.8	1.10	15.5
6	ABA-76	24:76	59:225	38.0	1.12	23.5

[a]ABA refers to PCHC-b-PDL-b-PCHC. [b]ABA-#: where # denotes the weight fraction of PCHC (wt %). [c]Determined by ^{1}H NMR spectroscopy using the integrals for PCHC (4.66 ppm) and PDL (4.85 ppm). [d]DP = degree of polymerisation. Overall DP shown, calculated based on overall monomer conversion determined from ^{1}H NMR spectra. [e]Determined by SEC, in THF, using narrow dispersity polystyrene standards. [f]M_w/M_n. [g]Weight fraction of CO_2 in the entire ABA triblock polymer.

The ^{1}H NMR spectrum of ABA-50 clearly illustrates quantitative selectivity for both carbonate linkages (>99%) and polymer formation (>99%) in the PCHC blocks, as opposed

to ether linkages and cyclic formation, respectively (**Figure 3.2**). Given that both polymerisation stages (ROP followed by ROCOP) proceed to high monomer conversion (>90%), the block composition determined by ^{1}H NMR spectroscopy using the relative ratio of characteristic integrals for PDL (4.85 ppm) and PCHC (4.66 ppm) closely matches that of the starting monomer stoichiometry (Appendix Figures S7.11 – 7.15). Naturally this presents two clear benefits: (a) the desired block composition can be tuned easily and with good precision, and (b) the synthesis of materials results in only a small amount of residual (waste) monomer.

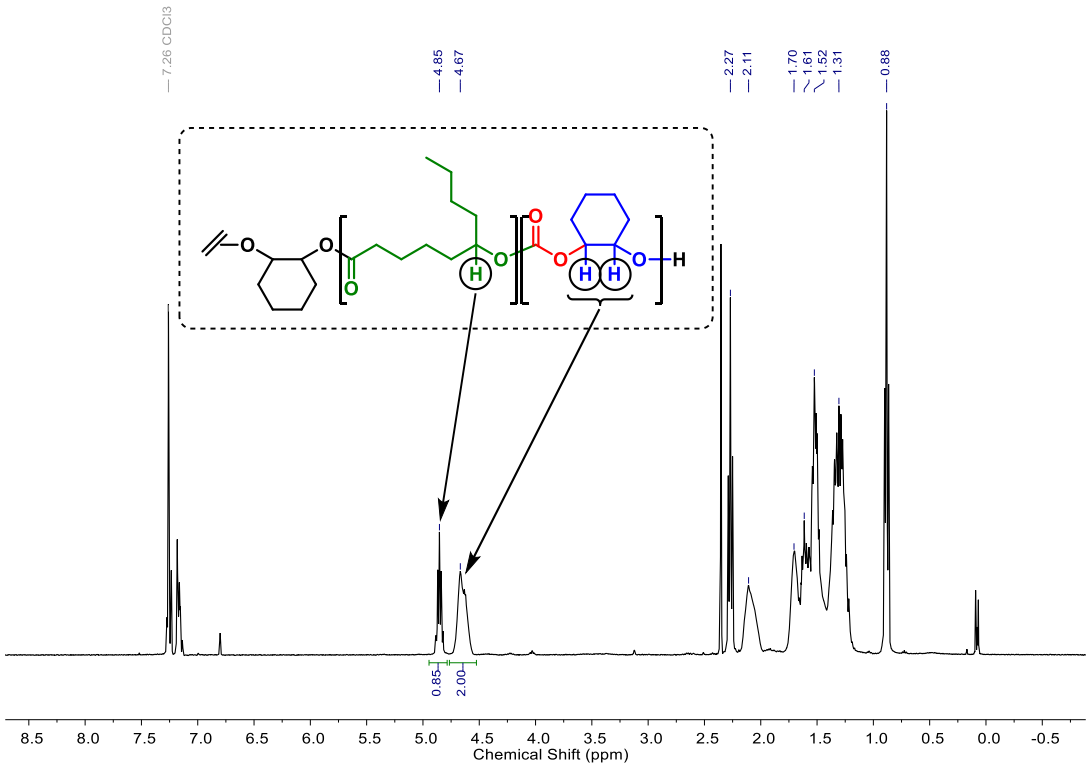


Figure 3.2. ^{1}H NMR spectrum of a crude sample of ABA-50 highlighting characteristics signals for PDL (4.85 ppm) and PCHC (4.66 ppm) used in determining conversion and relative block composition. [400 MHz, $CDCl_3$].

Analysis of the $^{13}C\{^{1}H\}$ spectrum for ABA-50 revealed two distinct signals in the carbonyl region corresponding to the PDL ester and PCHC carbonate blocks, respectively (**Figure 3.3**). There was also no evidence for transesterification or block scrambling owing to the absence of secondary, lower intensity signals clustered around the originals. The splitting

observed for the PCHC carbonyl signal at 154 ppm is attributed to the variation in which epoxide ring-opening occurs and consequently the stereochemistry either side of the carbonyl unit. This different stereochemistry is governed by the epoxide site at which the propagating carbonyl chain-end attacks, which is influenced by the orientation and electronics of epoxide binding. In this system there is, expectedly, little stereochemical preference and the resulting PCHC is atactic, hence the observed splitting.

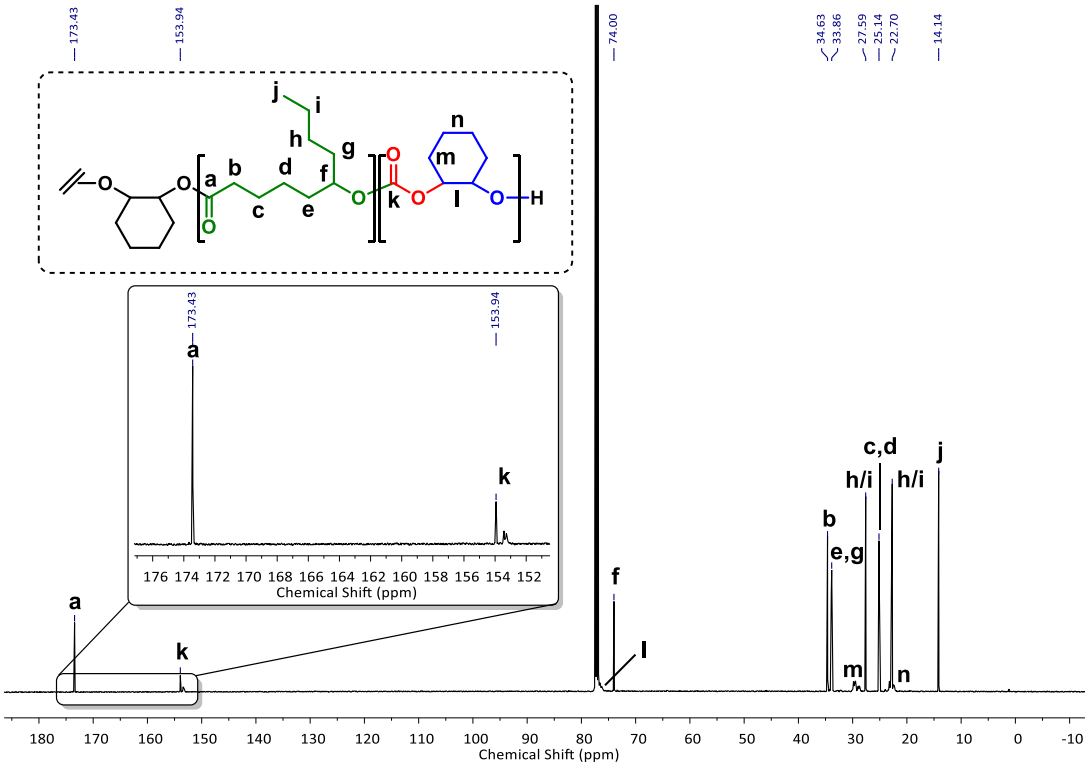


Figure 3.3. $^{13}C\{^{1}H\}$ NMR spectrum of ABA-50. Inset shows enlarged carbonyl region (177 – 151 ppm). [125 MHz, $CDCl_3$].

SEC analyses revealed minor amounts of a low molar mass impurity which is assigned to PCHC homopolymer, and is highlighted here in the chromatogram for ABA-50 (**Figure 3.4**). It is hypothesised that the formation of these separate PCHC chains occurs during the second key synthesis stage; that is to say on the addition of CO_2 in which there are ppm quantities of water present as a contaminant in the gas stream despite the use of drying columns. This issue of water contamination and drying CO_2 is well-known in the field, with

a recent report having gone to great lengths of employing a pressure vessel filled with triisobutylaluminium (TiBA) to see the most success in attempting to remove residual quantities of water.[33] With respect to material preparation and mechanical performance, minor contamination of PCHC homopolymer is not considered a detrimental factor, particularly given the synthesis of these triblock polymers is aimed at improving the properties of PCHC. Considering the entire series of materials synthesised, the major distribution in the SEC chromatograms, corresponding in each case to the pure ABA triblock, is narrow and has a molar mass (M_n) close to that which was targeted (Appendix Figure S7.16).

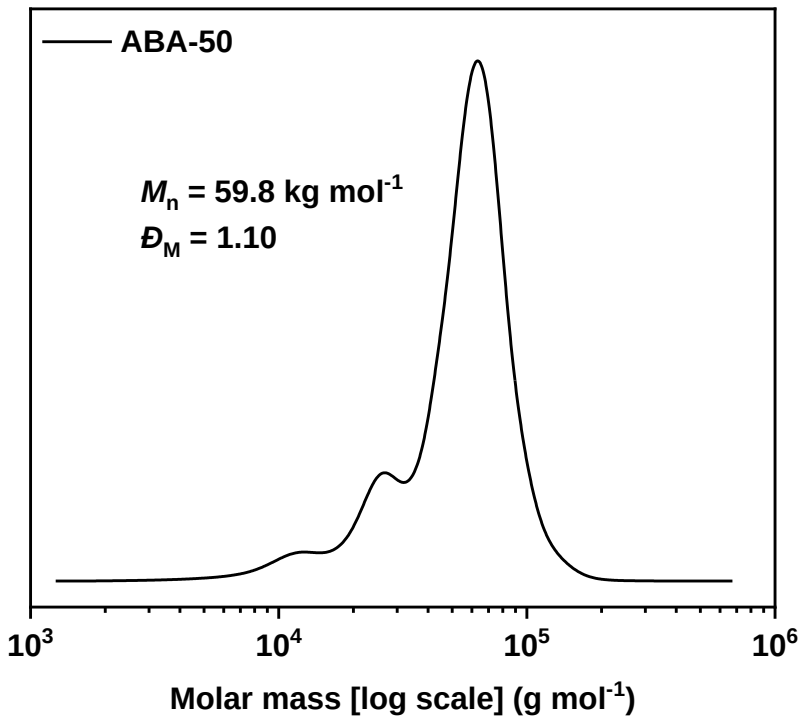


Figure 3.4. SEC chromatograph for sample ABA-50. See Appendix Figure S7.16 for traces of other triblock polymer samples.

To provide further evidence for the formation of ABA triblock polymers, $^{31}P\{^1H\}$ NMR spectroscopy was utilised. The phosphorous end-group titration technique sees the condensation reaction of [2-chloro-4,4,5,5-tetramethyl-1,3,2-dioxaphospholane] with the

terminal hydroxyl end-groups of the polymer chains. This process caps the polymer chain ends with the dioxaphospholane, and signals can then be easily identified using $^{31}P\{^{1}H\}$ NMR spectroscopy. The spectrum corresponding to ABA-50 is shown here, with a comparison to a spectrum obtained using a blend of PDL and PCHC homopolymers (**Figure 3.5**). As illustrated, a signal corresponding to the 2° hydroxyl end-group of PDL is assignable at 147.1 ppm in the spectrum of the homopolymer blend. This signal is clearly absent in the spectrum for ABA-50, where the only end-group corresponds to the 2° PCHC hydroxyl, which by extension indicates the successful growth of PCHC from each end of the telechelic PDL block.

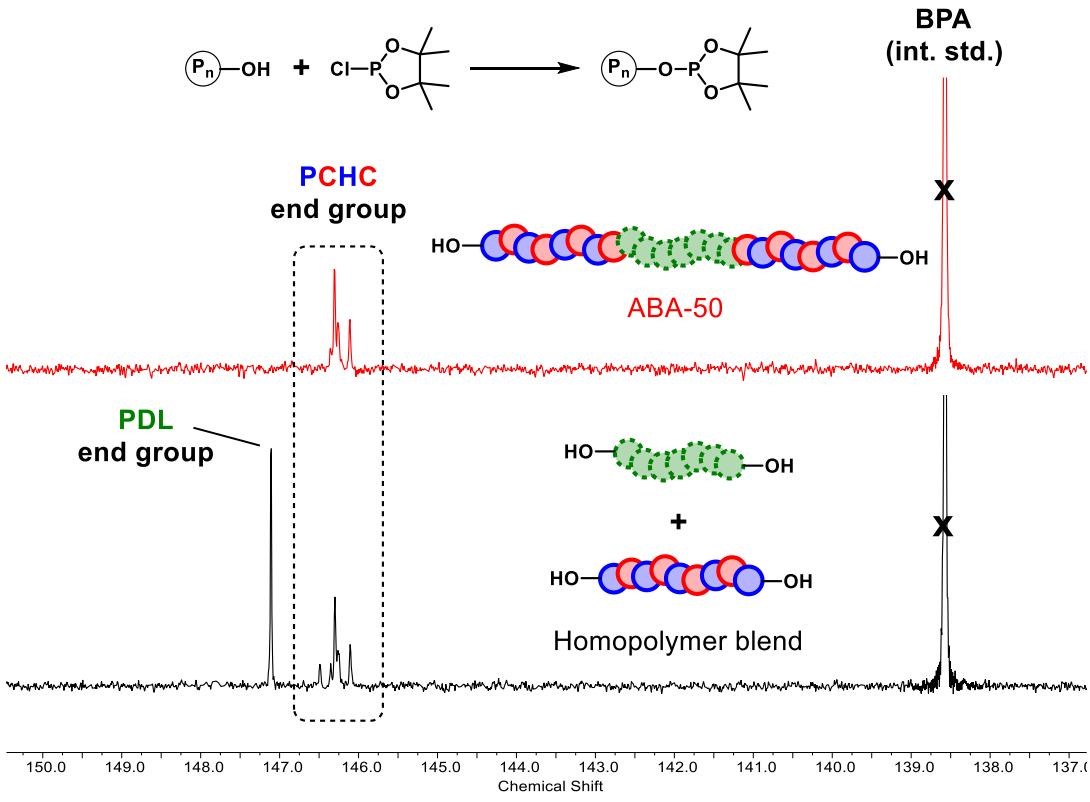


Figure 3.5. $^{31}P\{^{1}H\}$ NMR spectra of ABA-50 triblock polymer and blend of PCHC and PDL homopolymers (see Appendix Figure S7.17 for other spectra).

With the exception of ABA-20, which was too soft, each sample could be processed into a freestanding polymer film using a solvent casting method. A 30 wt % solution of the polymer in methylene chloride was poured into a PTFE mould and the solvent was allowed

to evaporate under ambient conditions for 72 h. The mould was then placed in a vacuum oven at 40 °C for a further 48 h to complete the drying process. The resulting films were transparent and colourless (Appendix Figure S7.18).

3.3.2. Thermal properties

The series of polymers were analysed using a range of complementary techniques to characterise their thermal behaviour (**Table 3.2**). Qualitative insight into the polymer microstructure can be obtained by observing the position of thermal transitions in both DSC and DMTA. Moreover, it is important to ascertain both the operating and processing temperature windows for these types of materials, especially with applications in the areas of elastomers and thermoplastics in mind.

Table 3.2. PCHC-*b*-PDL-*b*-PCHC (ABA Triblock) Thermal Characterisation Data

Entry	Polymer[a,b]	wt % PDL:PCHC[c]	M_n[d] (kg mol^{-1})	$T_{g,DSC}$[e] (°C)	$T_{g,DMTA}$[f] (°C)	$T_{d,5\%}$[g] (°C)
1	ABA-20	80:20	55.9	-48; *n.d.*	*n.d.*	286
2	ABA-26	74:26	71.9	-50; *n.d.*	-40; +69	290
3	ABA-28	72:28	46.4	-48; *n.d.*	*n.d.*	272
4	ABA-40	60:40	49.4	-49; *n.d.*	-41; +102	278
5	ABA-50	50:50	59.8	-50; +110	-41; +118	283
6	ABA-76	24:76	38.0	-44; +81	*n.d.*	254

[a]ABA refers to PCHC-*b*-PDL-*b*-PCHC. [b]ABA-#: where # denotes the weight fraction of PCHC (wt %). [c]Determined by ^{1}H NMR spectroscopy using the integrals for PCHC (4.66 ppm) and PDL (4.85 ppm). [d]Determined by SEC analysis in THF. [e]Determined by DSC analysis from the second heating cycles. T_g values reported as the midpoint of each transition; *n.d.* = upper T_g not determined. [f]Acquired by DMTA thermal sweeps (-70 – 40 °C and 35 – 110 °C). T_g values reported as the maxima in tan(δ); *n.d.* = not determined. [g]Determined by TGA. Reported as temperature at 5% mass loss.

Differential scanning calorimetry showed that the two constituent blocks are amorphous in nature, given that no transitions corresponding to melting endotherms were observed in the thermograms, and instead only glass transitions were visible (Appendix Figures S7.19 – 7.24). In the case of ABA-50, two glass transition temperatures (T_g) were visible: one at -50 °C and another at 110 °C corresponding to the soft PDL block and hard

PCHC blocks, respectively (**Figure 3.6** and **Table 3.2**, entry 5). The temperatures at which these two transitions were observed are close to the values expected for the individual homopolymers of PDL and PCHC, which are reported at -50 – -60 °C and 110-120 °C, respectively.[12, 34-35]

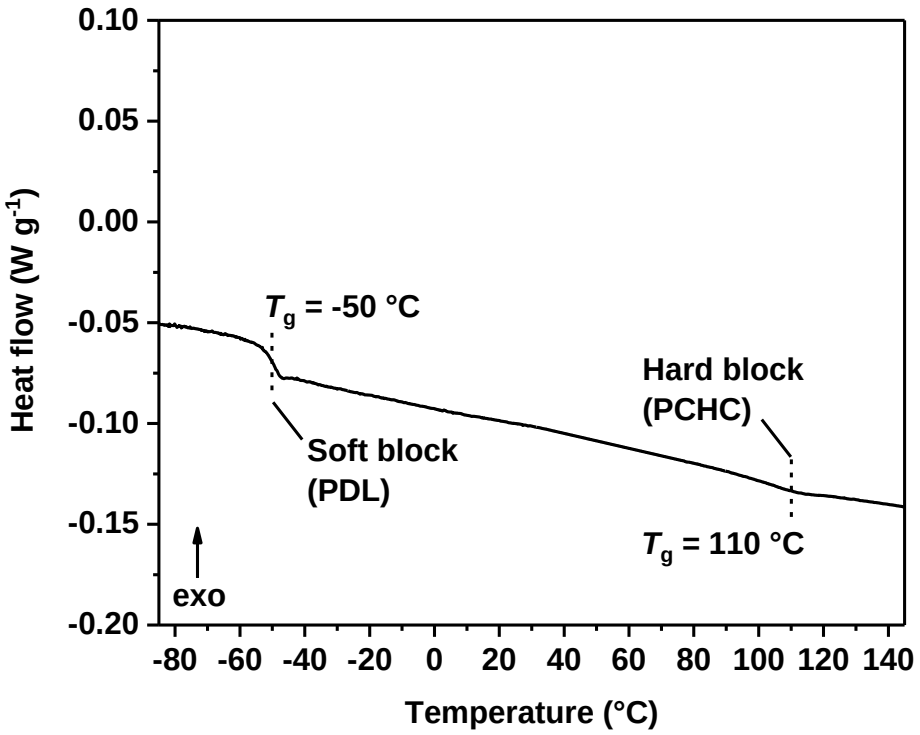


Figure 3.6. DSC thermogram of ABA-50 highlighting separate T_gs for PCHC and PDL.

Samples with a lower wt % of PCHC (ABA-20 to ABA-40 inclusive) showed only the lower T_g in their DSC thermograms, although in all cases this was around -50 °C, i.e. at the value expected for the soft PDL block (**Table 3.2**, entries 1-4). The absence of the upper glass transition in these samples is likely a result of the reduced concentration of the hard block, as well as low signal intensity compared to that of the soft block; and indeed even ABA-50's upper transition (110 °C) is of very low intensity compared to the soft block T_g at -50 °C. An additional factor to consider is block miscibility, which can in some cases explain shifts and/or absences of thermal transitions. However, given the position of the lower T_g for

samples ABA-20, -26, -28, and -40, block miscibility is unlikely to have occurred. More evidence to rule out miscibility can be provided by the Fox equation, which is used for miscible polymer blocks to generate values of $T_{g,mix}$ based on relative block weight fractions.[36] Values for $T_{g,mix}$ calculated for these samples range from -23 – 7.5 °C, and hence it is highly unlikely that block miscibility was a contributing factor to the absence of the hard block T_g. It follows that, given the block connectivity, microphase separation of the PDL and PCHC blocks is present and results in the formation of discrete hard and soft domains.

Certain samples were further analysed using dynamic mechanical thermal analysis (DMTA). This technique provides an additional, complementary measurement of thermal transitions by examining the mechanical response of the material over a given temperature range when subjected to a pre-applied load and sinusoidal oscillating stress. DMTA is generally considered to be a more sensitive technique compared to conventional DSC, given that the responses in elastic (*G'* or *E'*) and viscous (*G''* or *E''*)[*] components of a material are typically very well pronounced when experiencing a thermal transition. Illustrative of this, the DMTA temperature sweep profile for sample ABA-50 showed a decrease in the storage modulus (*E'*) from around 200 MPa and its gradual convergence with an increasing loss modulus (*E''*), as temperature increases from 30 – 100 °C (**Figure 3.7**). Continued heating beyond 100 °C quickly resulted in obtaining a maximum value for loss modulus, followed promptly by a sharp decrease in both dynamic moduli, indicative of a thermal transition – in this case the upper T_g for the material.

[*] *E'* and *E''* correspond to **tensile** storage (elastic) and loss (viscous) moduli, respectively; *G'* and *G''* correspond to **shear** storage and loss moduli, respectively.

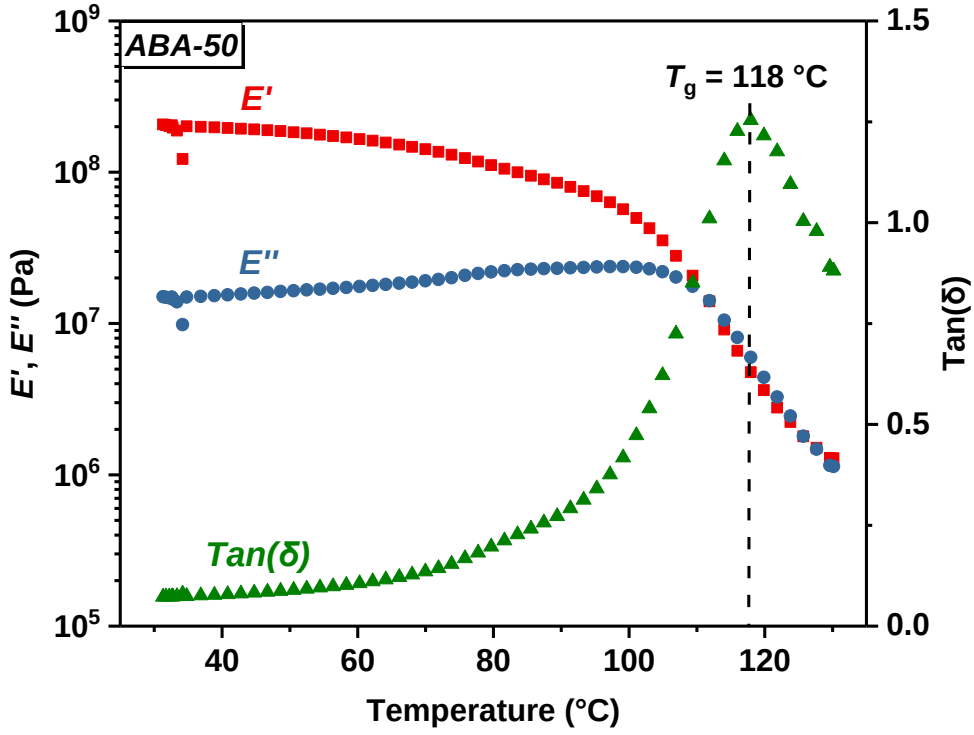


Figure 3.7. DMTA temperature sweep profile for ABA-50. Overlay of storage modulus (*E'*), loss modulus (*E''*), and tan(*δ*). Glass transition temperature (T_g) marked on the maxima of tan(*δ*). Conditions: 30 – 130 °C at 5 °C min^{-1}, ω = 1 Hz, γ = 1%.

The ratio between the loss and storage moduli, tan(δ), is used here as the variable to determine the glass-transition temperature. Tan(δ) provides an indication of damping in the material, with a larger value corresponding to a higher degree of damping, and can be alternatively described as the tangent of the phase angle between the sinusoidal responses of storage and loss moduli. In the case of ABA-50, tan(δ) achieved a maxima at around 118 °C which is in good agreement with the value obtained by DSC and supports the assignment of this low intensity transition. Similarly for other samples, namely ABA-26 and ABA-40, the DMTA data enables the determination of the upper T_g corresponding to PCHC, and therefore reinforces the claim that these materials are microphase separated (Appendix Figures S7.25 – 7.28 and **Table 3.2**).

In terms of processing requirements of these polymers, a further thermal property must be considered; that is the temperature at which thermal decomposition is observed. Thermogravimetric analysis (TGA) was performed to determine this value as the temperature at 5% mass loss ($T_{d,5\%}$), and revealed it to be around 280 °C for the series of ABA-20 to -50 (**Table 3.2**, entries 1-5). In the case of ABA-76, the somewhat lesser value for $T_{d,5\%}$ (254 °C) was attributed to the overall lower triblock molar mass. Additionally, a step profile was observed for all samples, which corresponded roughly with the relative block weight fractions. For example, with ABA-50 the first step corresponds to 50% mass loss, and the second degradation step (at 322 °C) is the remaining 50% thereafter (**Figure 3.8**). A vertical shift in the step position was seen, with sample ABA-20 (lowest wt % of PCHC) showing the highest (w.r.t mass remaining) onset of the step (Appendix Figures S7.29 – 7.34). Hence, it is proposed that chain-end decomposition, beginning with the outer PCHC blocks, is the principal thermal decomposition pathway.

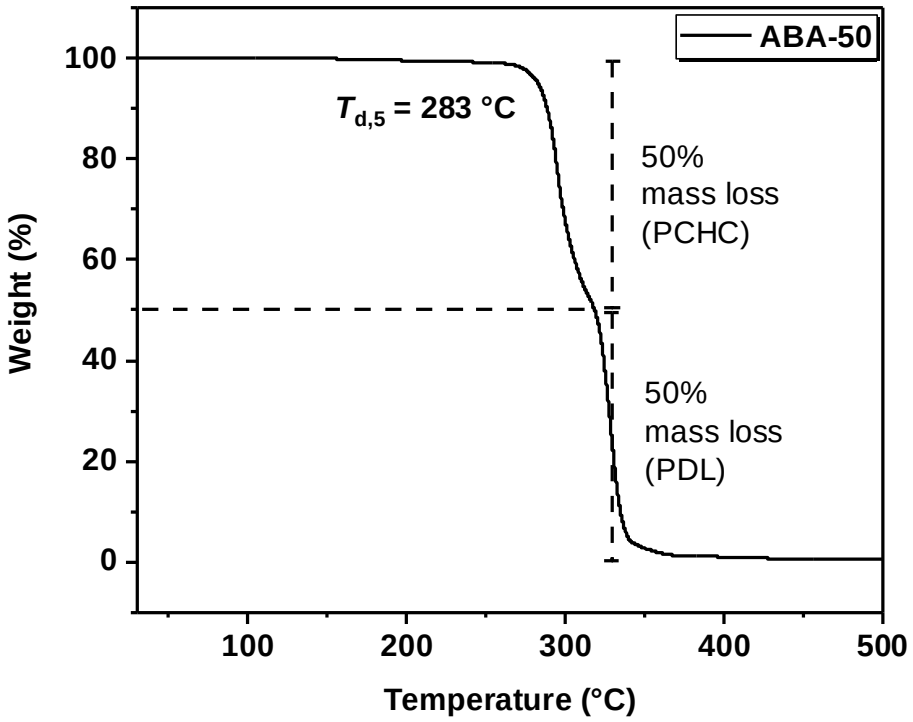


Figure 3.8. TGA profile for ABA-50 highlighting temperature at 5% mass loss ($T_{d,5}$) and step profile corresponding to two decompositions, each of roughly 50% mass loss.

The data obtained from thermal characterisation techniques allow for the construction of anticipated operating and processing temperature windows for these triblock polymers. Taking ABA-50 as the example, an operating temperature window, nominally of 160 °C, exists between -50 °C and 110 °C (**Figure 3.9**). Moreover, a moderately sized processing temperature window exists between 110 °C and 283 °C. Given that this processing window spans around 170 °C, it should allow for conventional thermoplastic processing of these materials. One should be mindful, however, of the anticipated breakdown of material properties and decomposition as these boundary temperatures are closely approached.

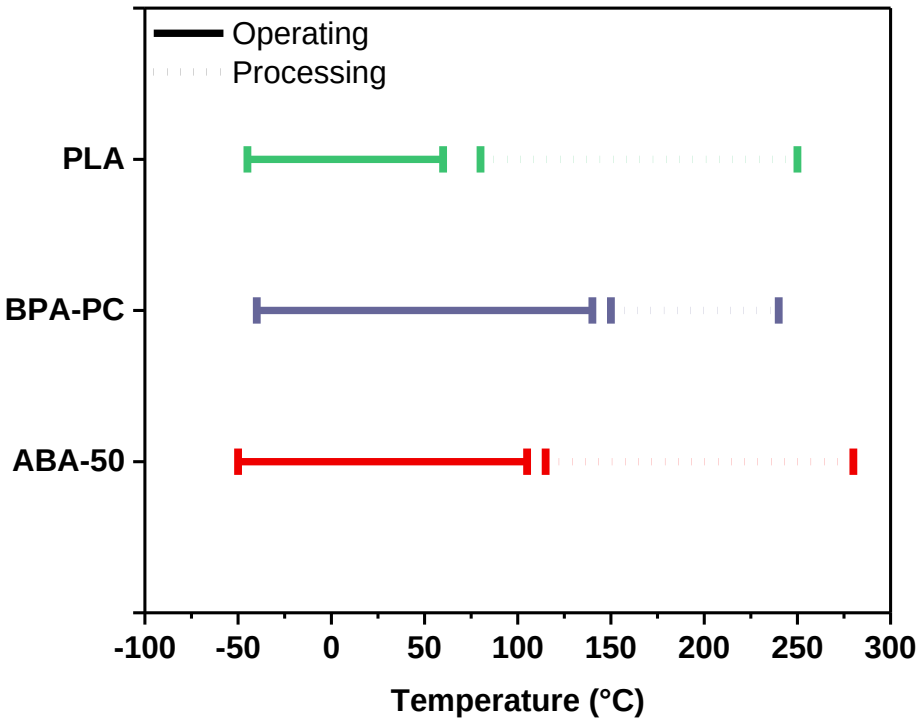


Figure 3.9. Operating and processing temperature ranges for sample ABA-50, commercial bisphenol-A polycarbonate (BPA-PC), and amorphous poly(lactide) (PLA).[37-38]

3.4. Mechanical testing

3.4.1. Uniaxial tensile experiments

Mechanical testing of the four readily processable polymers (ABA-26, -28, -40, -50) was performed on dumbbell-shaped specimens cut from a solvent-cast sheet. Sample thickness was uniform (~ 150 μm) as determined by a digital calliper, and remaining dimensions conformed to ISO 527-2 type 5B. The uniaxial extension measurements were conducted at 10 mm min^{-1} cross-head speed, in accordance with ISO 527, and used to generate stress-strain relationships.

Given the precedent for tuneable properties in block copolymers, a range of mechanical properties were expected in line with the series of materials having varied relative block compositions. Indeed, it can be identified that by controlling the relative content of CO_2 in the polymers (by weight %), characteristics such as Young's modulus (E_y) and tensile strength (σ) vary significantly (**Table 3.3**).

Table 3.3. PCHC-*b*-PDL-*b*-PCHC (ABA Triblock) Mechanical Characterisation Data (Uniaxial)

Entry	Polymer[a]	wt % CO_2[b]	M_n[c] (kg mol^{-1})	E_y[d] (MPa)	σ[e] (MPa)	ε_y[f] (%)	ε_b[g] (%)	U_T[h] (MJ m^{-3})
1	ABA-50	15.5	59.8	238 ± 35	20 ± 2	9.0 ± 1.7	900 ± 104	112
2	ABA-40	12.4	49.4	81 ± 13	5.1 ± 0.2	17 ± 2	1920 ± 235	86.7
3	ABA-28	8.7	46.4	3.0 ± 0.8	0.85 ± 0.04	*n.d.*	1060 ± 54	5.9
4	ABA-26	8.0	71.9	3.9 ± 0.7	1.4 ± 0.1	*n.d.*	1400 ± 69	13.0

[a]ABA refers to PCHC-b-PDL-b-PCHC. ABA-#: where # denotes the weight fraction of PCHC (wt %). [b]Determined from relative block weight fractions and weight percent of CO_2 in the PCHC repeat unit. [c]Determined by SEC analysis in THF. [d]Young's modulus. [e]Tensile strength. [f]Strain at yield point; *n.d.* = not determined as samples are elastomeric. [g]Strain at break. [h]Tensile toughness, calculated by integrating the stress-strain curve.

The two specimens containing the highest weight fractions of CO_2 (ABA-50 and -40) displayed typical plastic characteristics. In each case, the stress-strain profiles show a region of proportionality at low strain (0-9% for ABA-50, 0-17% for ABA-40) in which the materials

behave according to Hooke's law; that is to say they observe a linear stress-strain relationship and should exhibit non-permanent deformation (**Figure 3.10**). The gradient of the line in this region enables calculation of the Young's modulus, which was 238 MPa and 81 MPa for ABA-50 and ABA-40, respectively. The yield points for both materials indicate the limit of proportionality, and these were found at 9% and 17% strain for ABA-50 and ABA-40, respectively.

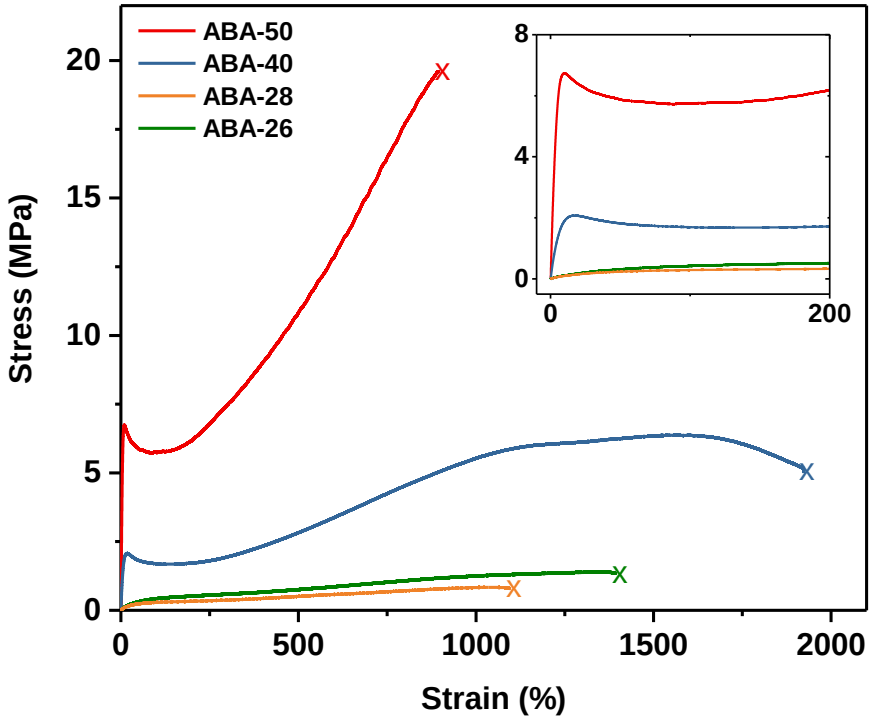


Figure 3.10. Stress-strain curves for uniaxial extension measurements of ABA triblock polymers. Failure points marked with an "X". Inset: enlargement of the 0 – 200% strain region highlighting region of proportionality for ABA-50 and ABA-40.

Extension of the specimens beyond their yield points resulted in permanent plastic deformation. This is observed on the stress-strain curve as a decrease in stress followed by a region of strain hardening. Significant strain hardening was seen for ABA-50, and was coupled with the appearance of stress whitening or "crazing" (Appendix Figure S7.35). Ultimately, ABA-50 achieved the highest tensile strength of around 20 MPa, along with a high

tensile toughness (U_T) of 112 MJ m^{-3} which is estimated from the area under the stress-strain curve. Fracture of the specimen was of a ductile fashion, and observed at a strain of around 900%.

In line with a ductile fracture mode, necking was observed prior to failure. ABA-40 experienced a more sustained necking region as compared to ABA-50. Moreover, although both ABA-50 and ABA-40 showed characteristic ductile plastic behaviour, the stress-strain profile for ABA-40 is noticeably different to that of ABA-50; there is less pronounced strain hardening and far greater extensibility leading overall to a much flatter curve. The cause of this marked difference in stress-strain relationship is currently unaccounted for, but one potential hypothesis relates it to a change in morphology corresponding to the change in relative block weight (and by extension, volume) fractions.

At lower polycarbonate (and CO_2) weight fractions, ABA-28 and ABA-26 displayed behaviour more characteristic of elastomers. Yield points could not be determined from the stress-strain data; as such the specimens exhibit no permanent plastic deformation and quickly recover their original shape, even after the point of fracture (**Figure 3.10 inset** and Appendix Figure S7.36). The first material to be tested, ABA-28 displayed high extensibility (ε_b = 1060%) but a low tensile strength (σ < 1 MPa). ABA-26 was subsequently synthesised in order to explore what effect an increase to the overall triblock polymer molar mass (while retaining similar relative block composition) has on the elastomeric properties of the material.

As demonstrated by ABA-26, an increase in molar mass of the overall triblock to around 70 kg mol^{-1} (*vs.* 50 kg mol^{-1} for ABA-28) resulted in a marked increase in the elongation at break, with the specimen eventually failing at around 1400%. However, the effect on the tensile strength appears minimal as only a slight increase to 1.4 MPa was observed. It is

plausible that the magnitude of molar mass increase here was not sufficient to elicit a significant change in tensile strength of the material; particularly as the block composition is already heavily biased towards a softer material, with bulk properties influenced more so by the majority poly(ε-decalactone) block. Nonetheless, high strain-low strength properties like those displayed by ABA-26 and ABA-28 can be desirable; materials with such traits show promise for future applications as synthetic mimics to soft natural materials such as tissue or elastin.[39]

3.4.2. Cyclical tensile experiments

Cyclical tensile experiments were primarily conducted to evaluate the elasticity of the two elastomeric samples, ABA-28 and ABA-26. Ductile specimens, ABA-40 and ABA-50, were also subjected to testing in order to assess their degree of elasticity following permanent plastic deformation. Specimen bars, with the same dimensions as those used for uniaxial measurements, were subjected to ten, repeated, stress-strain cycles. Specifically, one cycle consisted of extension to 200% strain at a rate of 10 mm min^{-1} followed immediately by relaxation to 0% strain at the same rate. Data obtained from these experiments enabled the calculation of elastic recovery (ER) and hysteresis loss for all samples (**Table 3.4**).

Table 3.4. PCHC-*b*-PDL-*b*-PCHC (ABA Triblock) Mechanical Characterisation Data (Cyclical)

Entry	Polymer[a]	wt % CO_2[b]	M_n[c] (kg mol^{-1})	Elastic recovery (%)	Hysteresis loss (%)
1	ABA-50	15.5	59.8	85 ± 1[d]	56 ± 2[d]
2	ABA-40	12.4	49.4	73 ± 0.3[d]	79 ± 4[d]
3	ABA-28	8.7	46.4	75 ± 2	75 ± 7
4	ABA-26	8.0	71.9	95 ± 6	36 ± 3

[a]ABA refers to PCHC-*b*-PDL-*b*-PCHC. ABA-#: where # denotes the weight fraction of PCHC (wt %). [b]Determined by ^{1}H NMR spectroscopy using the integrals for PCHC (4.66 ppm) and PDL (4.85 ppm). [c]Determined by SEC analysis in THF. [d]Excluding first cycle.

Considering first the two elastomers, both ABA-28 and ABA-26 displayed slight reduction in the maximum stress between the first and subsequent cycles which was indicative of some plastic deformation during the first cycle, and was more pronounced in the case of ABA-28 (**Figure 3.11a**). Subsequent cycles (2-10) show a significantly more gradual loss to the maximum stress achieved, as well as a relatively constant area within the loading and unloading portions of each cycle's curve, which indicated good elastic recovery and consistent hysteresis.

The higher molar mass specimen, ABA-26, predictably outperformed its lower molar mass analogue in all respects (**Figure 3.11b**). ABA-26 exhibited very high elastic recovery of 95% and a moderate hysteresis loss of 36%, whereas ABA-28 showed 75% for both properties equating to low elastic recovery and high energy loss during cycles, respectively.

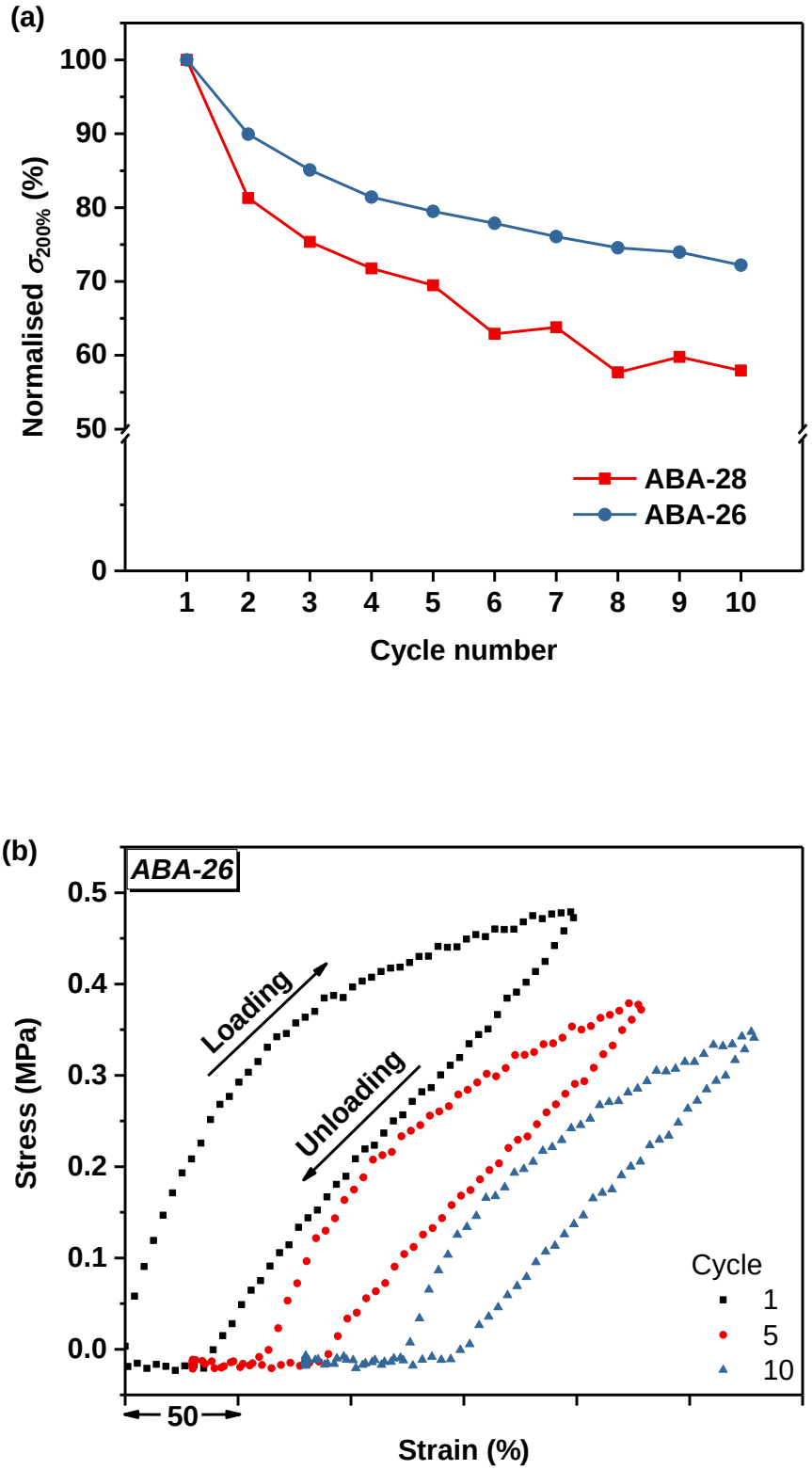


Figure 3.11. Cyclical tensile analysis. (a) Plot of normalised maximum stress ($\sigma_{200\%}$) *vs.* cycle number. (b) Measurement profiles for ABA-26. Only cycles 1, 5, and 10 shown and offset horizontally for clarity.

Analysis of ABA-40 and ABA-50 revealed that both materials exhibit a strain-induced plastic-to-rubber transition. Highlighted for sample ABA-50, the first cycle shows the expected yield point as well as a portion of cold drawing during the loading phase, yet subsequent cycles display apparent elastic profiles (**Figure 3.12**). Indeed, the characteristically sharp yield point is no longer discernible, and the area between the loading and unloading curves is significantly reduced when compared to the first cycle. The maximum stress achieved does, however, continue to decrease between each consecutive cycle which still points to cumulative permanent plastic deformation.

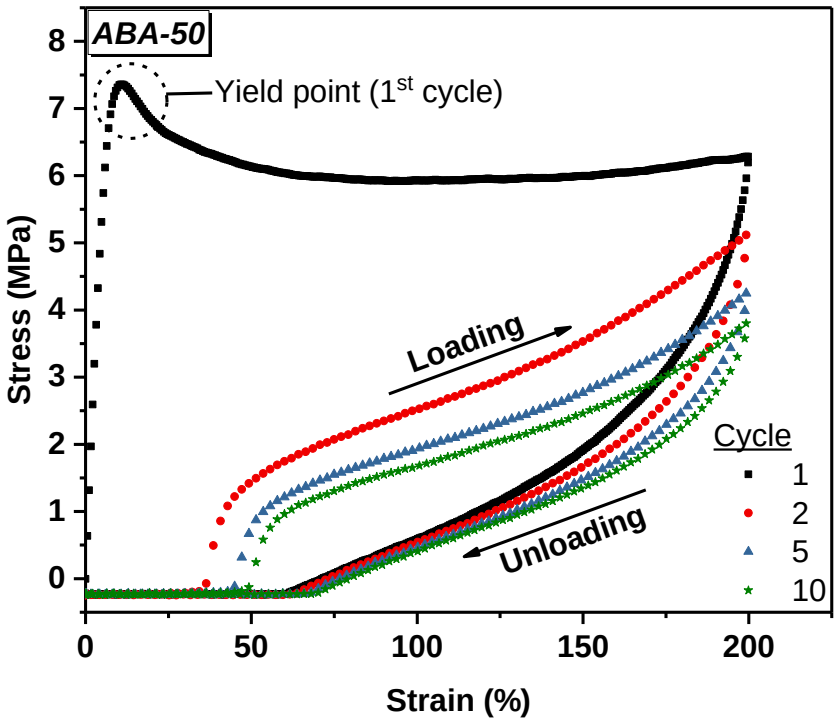


Figure 3.12. Cyclical tensile measurement of ABA-50 illustrating a strain induced plastic-to-rubber transition. Parameters: 0 - 200% strain, 10 cycles. Only cycles 1, 2, 5, and 10 shown for clarity.

Overall, the two ductile plastic samples show good elastic recovery (when excluding the first cycle) of 73% and 85% for ABA-40 and ABA-50, respectively. Similar plastic-to-rubber transition behaviour has been observed in a range of polymers from poly(styrene-

butadiene-styrene) (SBS) to block copolyesters, and the phenomenon is hypothesised to arise according to a change in polymer microstructure.[40-42] Specifically, the application of strain to the point at which chains align such that PCHC (hard) domains are more uniformly distributed within the PDL (soft) matrix.

3.4.3. Adhesion testing

With the lowest weight fraction of hard block, ABA-20 was a substantially soft material unable to retain its shape outside of a mould. The appearance and tangible properties of the material thus dictated its assessment as a potential pressure-sensitive adhesive. Oscillatory rheology was used to characterise the viscoelasticity, while common adhesive test methods were employed to quantify the polymer's peel and tack strength, as well as providing a rudimentary assessment of its bonding affinity to steel when applied directly as a coating (**Table 3.5**).

Table 3.5. Rheological and Adhesive Performance Data for ABA-20 Triblock Polymer

				Rheology		Adhesion		
Entry	**Polymer**	**wt % CO_2**	**M_n (kg mol^{-1})**	**G' [a] (10^5 Pa)**	**η_0 [b] (kPa·s)**	**180° peel[c] (N cm^{-1})**	**Loop tack[c] (N cm^{-1})**	**Cross hatch[d]**
1	ABA-20	6.2	55.9	2.6	8.7	10 ± 0.87	8.7 ± 1.1	1

[a]Shear storage modulus at 1 Hz. [b]Zero-shear viscosity. [c]Performed on PSTC-grade stainless steel using adhesive coated PETE (Mylar) strips. Mean values and standard deviation from a minimum of 4 samples. [d]Performed on PSTC-grade stainless steel coated with ABA-20.

A frequency sweep conducted at ambient temperature (25 °C) captured the transition between terminal and rubbery plateau regions (**Figure 3.13**). The presence of a rubbery plateau region is attributed to networks of polymer chains, and in this case corresponds to chain entanglements. The crossover of dynamic moduli, *G'* and *G"*, was observed at a frequency (ω_τ) of 1.7 rad s^{-1} and the polymer chain's terminal relaxation time can then be calculated (from $2\pi/\omega_\tau$) as 3.6 s. In the terminal region, prior to crossover of dynamic moduli, the shear loss modulus (*G"*) is of greater magnitude than the storage modulus (*G'*) which

demonstrates that the viscous component of the material dominates the elastic component. However, when the material enters the rubbery plateau region *G'* exceeds *G"* and the elastic portion now dominates while also tending towards being independent of frequency. Additional rheological experiments were conducted at a common frequency of 6.28 rad s^{-1} (1 Hz) as this was also determined from the frequency sweep to lie both within the rubbery plateau region and below the Dahlquist criterion[43] (*G'* < 3 x 10^5 Pa), and is corroborated by a fixed oscillation (ω = 1 Hz) over time experiment which showed *G'* consistently higher than *G"* (Appendix Figure S7.37).

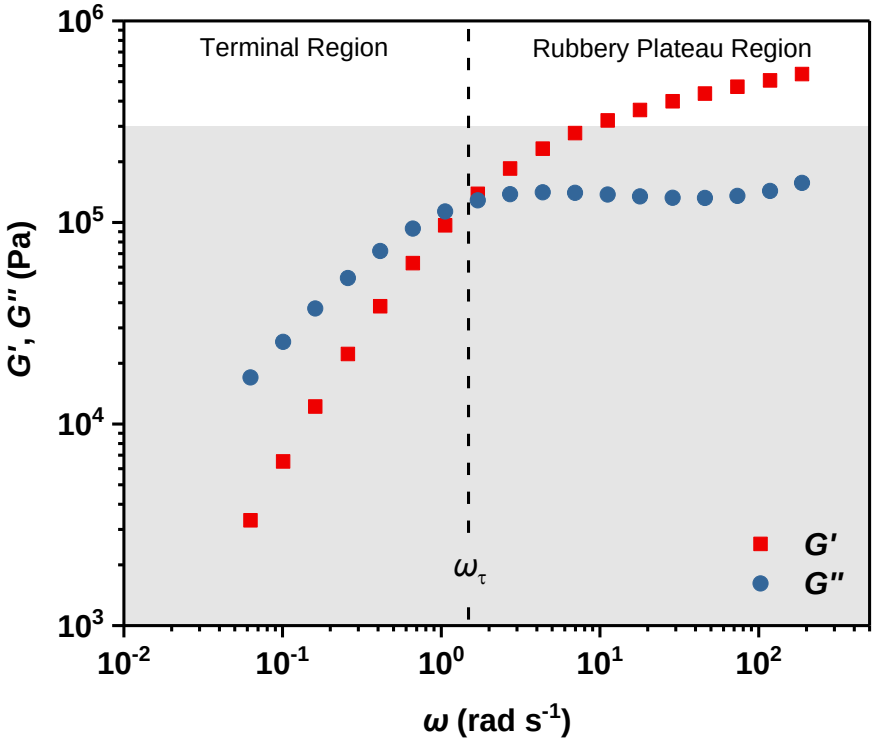


Figure 3.13. Frequency sweep (25 °C) for ABA-20. Grey region represents area below Dahlquist's criterion (*G'* ≤ 3 x 10^5 Pa).

In addition to monitoring the response of dynamic moduli, shear stress was also measured and can be divided by the shear strain rate to calculate viscosity (η). The relationship between shear stress and shear strain rate, as well as between viscosity and shear

strain rate allows for certain material characteristics and behaviours, such as non-Newtonian classification and zero-shear viscosity, to be determined. A plot of shear stress *vs.* shear strain rate revealed typical shear-thinning behaviour for ABA-20, which is most common for polymer melts and solutions (**Figure 3.14a**). In line with this observation, viscosity showed dependence on shear strain rate and exhibited a non-linear relationship, ultimately with it being lowest at the highest strain rate measured (**Figure 3.14b**). Placing a horizontal on the double log viscosity-strain rate curve at the point of shallowest gradient (i.e. lowest strain rate) generates an estimate for zero-shear viscosity (η_0) at the intersection on the y-axis corresponding to 8.7 kPa·s.

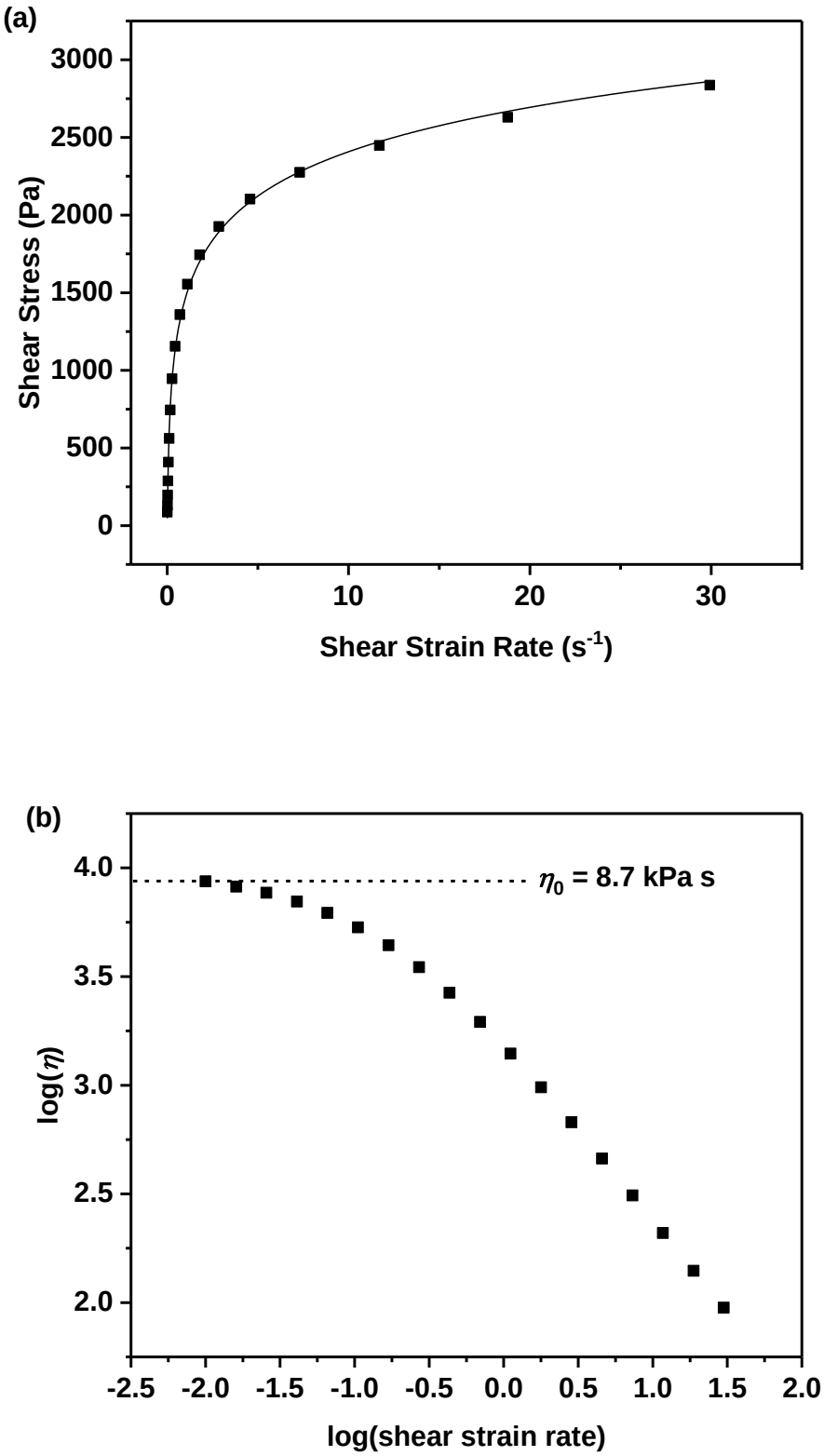


Figure 3.14. Rheological characterisation of ABA-20 showing (a) the relationship of shear stress to shear strain rate highlighting shear-thinning behaviour and (b) a double log plot of viscosity against shear strain rate from which the zero shear viscosity (η_0) is estimated.

A viscoelastic window for ABA-20 was constructed by taking the values of *G'* and *G"* at characteristic frequencies for adhesive bonding (10^{-1} rad s^{-1}) and debonding (10^{2} rad s^{-1}). Plotting the four paired combinations of these values on a chart of *G' vs. G"* generated the window, which was then contextualised by dividing the chart into quadrants corresponding to particular classes of pressure-sensitive adhesives: release (or non-PSA), high shear, removable, and cold-temperature (**Figure 3.15**).[44] The position of the window suggests that ABA-20 should perform most like a high shear, permanent adhesive. The upper boundary of the window, or debonding aspect, is positioned high in the upper right quadrant which predicts ABA-20 to show good resistance to shear. The lower boundary of the window, or bonding aspect, is situated well below the Dahlquist criterion, indicating that ABA-20 should also be contact efficient without requiring tackifying additives. In other words, it can be characterised as a single-component pressure-sensitive adhesive.

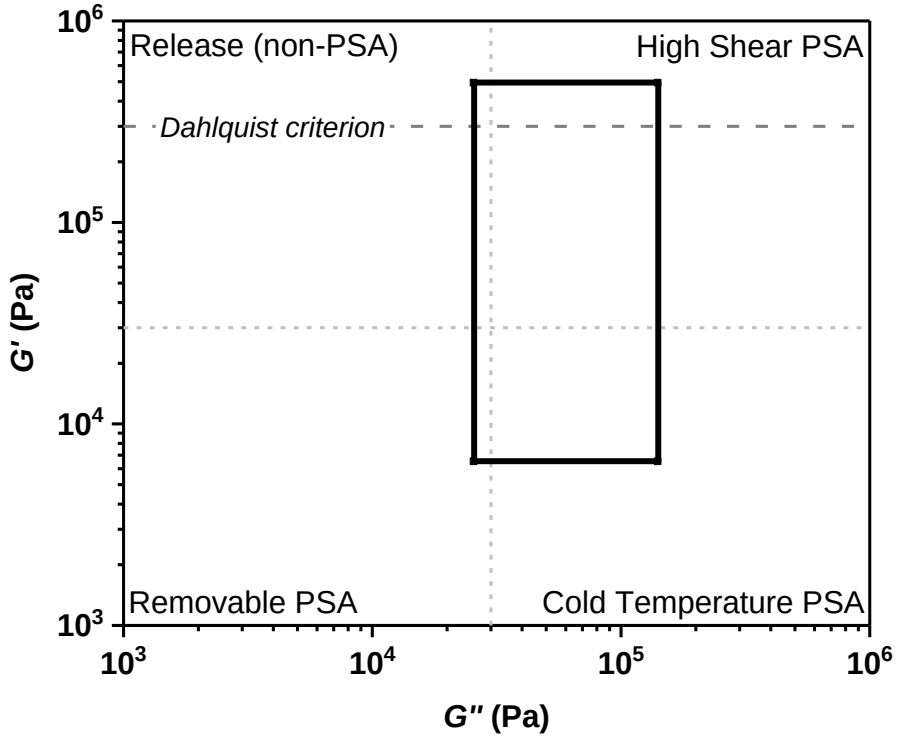


Figure 3.15. Viscoelastic window constructed for ABA-20. Limits determined using values for *G'* and *G''* at bonding (10^{-1} rad s^{-1}) and debonding (10^{2} rad s^{-1}) frequencies from the frequency sweep. Quadrant titles indicate PSA classification.

In preparation for adhesive testing, the polymer was applied to a piece of 5 μm thick PETE (Mylar®) film from a 30 wt % solution in DCM using a wound wire rod (K-bars), with a targeted wet film thickness of approximately 60 μm. The coating was allowed to dry under ambient conditions overnight and then *in vacuo* at 40 °C. Test strips were attached to Pressure-Sensitive Tape Council (PSTC) grade stainless steel substrate either prior to or during testing, depending on the test being performed. In the case of 180° peel measurements, pre-test pressure was applied by rolling a 500 g weight over the applied area.

The adhesive capabilities of ABA-20 were assessed using 180° peel and loop tack test methods (**Figure 3.16**). The polymer performed well in both tests and showed high peel and tack forces of 10 N cm^{-1} and 8.7 N cm^{-1}, respectively. Although good contact efficiency was predicted, and demonstrated by high adhesive forces in the loop tack, wetting was naturally

enhanced by application of pressure as evidenced by the higher peel force in the 180° peel test (**Table 3.5**). The magnitude of the forces exhibited provide good evidence for ABA-20 being a high shear PSA, especially considering its single-component nature and absence of tackifying agents.

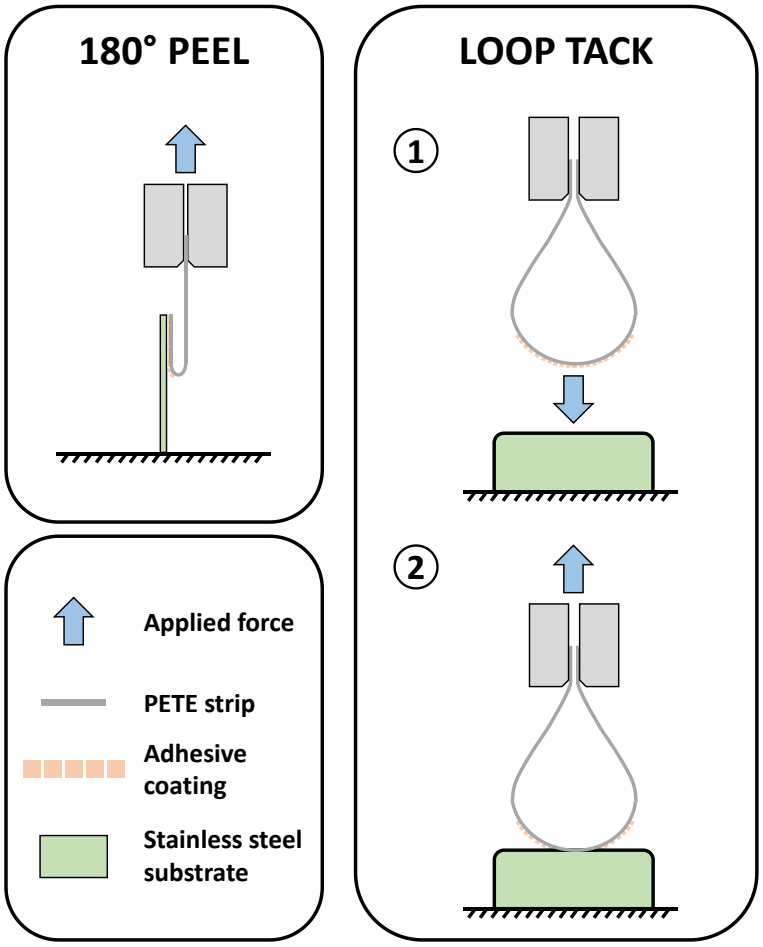


Figure 3.16. Schematic representations of 180° Peel and Loop Tack adhesive testing methods.

Moreover, it should be noted that cohesive failure was observed in all cases, which left residue on the steel substrate (Appendix Figure S7.38). This manner of failure arises due to failure of the bulk material rather than clean separation of the adhesive from the substrate surface. It was therefore indicative of both a weak elastomeric base in ABA-20 (in line with it having the lowest weight fraction of hard block) and strong substrate adhesion. The latter was probed further by performing a cross-hatch test; whereby the polymer was coated

directly onto the stainless steel substrate and allowed to dry, after which a cross-hatch pattern of cuts was laid into the coating, scotch tape applied over the cut area, rapidly removed, and the damage to the coating assessed. This test highlighted the strong adhesion of the polymer to stainless steel, having been classified as a "1" (minimal removal of/damage to coating) on the ISO scale.

3.5. Discussion

The series of ABA triblock polymers were prepared using a straightforward method aided by efficient catalysis, the nature of which allowed for excellent control over CO_2 utilisation and position within the polymer chain. The upshot of this control was clearly visible in the modulation of material properties; a variety of characteristics were realised, from viscoelastic pressure-sensitive adhesives (ABA-20) at low CO_2 utilisation, to thermoplastic elastomers with high elongation (ABA-26 and ABA-28), to toughened plastics at the highest CO_2 utilisation (ABA-40 and ABA-50). Evidently the scope of applications for polymers and materials based on CO_2-derived polycarbonates, in particular PCHC, is more expansive than previously thought.

Considering first adhesive characteristics, ABA-20, with a CO_2 utilisation of 6.2 wt %, performed well as a single-component PSA. The peel and tack strengths displayed in testing exceed those of commercial PSA formulations as are to be found in common tapes such as duct, masking, electrical, and scotch. As alluded to, these commercial examples are formulated products, and as such contain mixtures of polymers, plasticisers, fillers, and tackifiers in order to augment or fine-tune the adhesion. The data for ABA-20, on the other hand, are stand-alone but further analysis should look at the effect on formulations which incorporate these CO_2-derived polymers.

Current polymeric components applied in PSAs are predominantly polyacrylate or styrenic-based, but the promising characteristics of ABA-20 suggest it could be used as an alternative. Moreover, in comparison to leading literature examples of PSAs, of which some incorporate tackifying additives, ABA-20 performs equivalently or better than bio-based block polyester and polyacrylate adhesives (**Figure 3.17**).[45-49] Specifically, a benchmark against an ABA block polyester, comprising PLLA A-blocks and a soft PDL or menthide B-block, showed ABA-20 has much higher peel strength, which highlights the advantages of

the rigid PCHC polycarbonate blocks.[45, 48] An additional benefit of these rigid PCHC blocks compared with the equivalent PLA hard blocks is the allowance for higher operating temperatures, given the marked difference in glass-transition temperatures exhibited by the two different polymers: PCHC = 110 – 120 °C *vs.* PLA = 50 – 60 °C. When then compared to the highest performing polyacrylate pressure-sensitive adhesives, particularly those mimicking muscle adhesive proteins, the peel force and tack results are modest, demonstrating the significant scope to optimise structures in the future.[50-52]

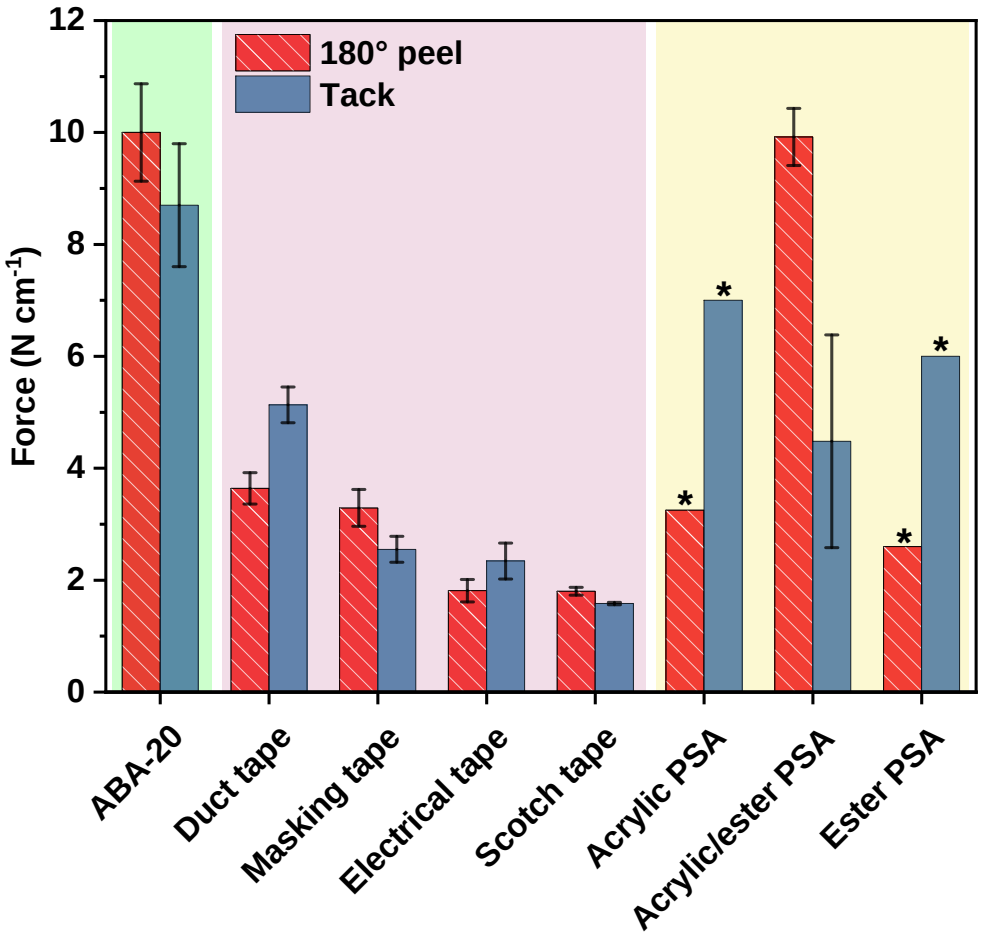


Figure 3.17. Adhesive performance in 180° peel and loop tack testing methods for ABA-20 (green highlight) and examples of commercial (purple highlight) and literature (yellow highlight) PSAs. "Acrylic PSA" = PAAI-PEHA-PAAI[47]; "Acrylic/ester PSA" = PMeMBL-PM-PMeMBL[46]; "Ester PSA" = PLLA-PDL-PLLA[45] (See Appendix Figure S7.39 for polymer structures). *errors not reported.

In the case of higher utilisation ABA-50, with 15.5 wt % CO_2, was a toughened plastic which showed considerably enhanced toughness compared to standalone PCHC. The well-known brittleness of PCHC is therefore moderated by the inclusion of the soft PDL midblock (**Figure 3.18**). Similar brittleness is also a problem in bioderived poly(limonene carbonate), prepared from the ROCOP of limonene oxide and CO_2, but it's clear one strategy to overcome this would be the incorporation of a soft block given ABA-50 showed significantly higher tensile toughness than PLimC (U_T = 112 MJ m^{-3} for ABA-50 *vs.* ~3.15 MJ m^{-3} for PLimC).[53] It is worth noting also a recent report on PBL-PCHC block copolymers; 50 wt % incorporation of PCHC achieved comparable tensile strength (17 MPa) but was still limited to only 1.3% elongation at break.[32]

Benchmarking the performance against other materials, one observes that ABA-50 shows higher tensile toughness than the well-established, commercial polycarbonate prepared from bisphenol-A (U_T ~ 19 MJ m^{-3}), however this comes at a great expense to tensile strength.[38] Likewise, the toughness of ABA-50 greatly exceeds that of a purposefully toughened PLA samples (best U_T = 14 – 18 MJ m^{-3}), yet in this case the tensile strengths of the two materials are largely comparable (PLA = 25.8 MPa).[54-55]

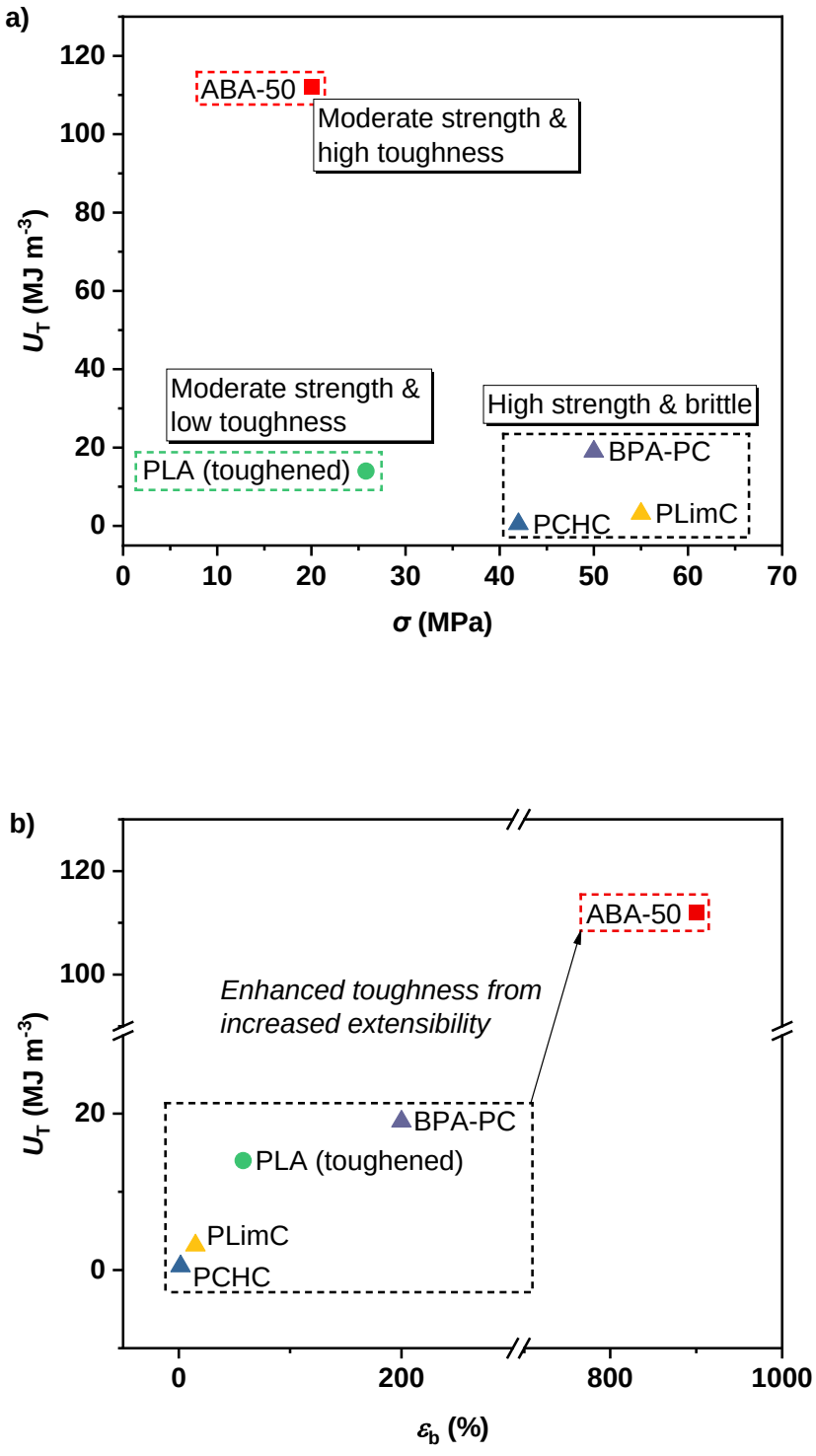


Figure 3.18. Ashby-style plots of tensile toughness (U_T) *vs.* (a) tensile strength (σ) and (b) elongation at break (ε_b) for comparison of ABA-50 with examples of commercial and literature materials. Material classifications: polycarbonate (▲), polyester (●), poly(carbonate-*b*-ester-*b*-carbonate) (■).

It is important to also illustrate the sustainability of these materials and a key feature of these triblock polymers is their high bioderived content. Indeed, the incorporation of CO_2 as a cheap, renewable, feedstock is a major highlight, but this is further compounded by the use of commercially available monomers. As an example, ε-decalactone is prepared from ricinoleic acid, with it being ultimately sourced from castor oil.[56-57] Cyclohexene oxide is currently produced *via* petrochemical pathways, however methods utilising triglyceride coproducts are being explored and could be adopted if completely bio-based analogues are sought.[58] Nonetheless, with CO_2 content easily controllable, the series of polymers presented here offer theoretical renewable contents from 47% (ABA-76) to 86% (ABA-20).

Ultimately, when considering end of life/service scenarios these triblock polymers offer routes to degradation given the presence of ester and carbonate linkages in the backbone. At the same time, the stability of the processed polymer films must also be considered, as any immediate deterioration under common environmental exposure would compromise integrity and limit potential applications. The data for ABA-50 indicate that the films are stable to mass loss when submerged in acidic (2 M HCl) or basic (2 M NaOH) media at ambient temperature for a period of at least 9 months. As and when required, the polymer can be degraded by dissolving in toluene and treating with a weak acid ([*p*-toluenesulfonic acid] = 5 mM) while warming to 60 °C (Appendix Figure S7.40). Rapid loss of polymer molar mass was observed over a period of 96 h under these conditions.

An additional benefit is that the expected degradation products, being hydroxy-acids, diols, and CO_2, are anticipated to be non-toxic. However, the nature of these products means there are fewer opportunities to recycle to monomers, hypothetically with the potential to re-polymerise. Hadjichristidis and co-workers showed it is possible to copolymerise CO_2 with a diol but reports of this are otherwise limited.[59] The possibility of recycling to monomer(s) was identified in a similar triblock material comprised of poly(limonene carbonate) and

poly(ε-decalactone) blocks where degradation of the polycarbonate block recovered the limonene oxide monomer.[60] This therefore presents an attractive target for future research in order to help close the loop on a circular economy with these, and similar, materials.

3.6. Summary and future work

A series of ABA triblock polymers were prepared from mixtures of ε-DL, CHO, and CO_2, utilising a switchable catalysis technique which facilitated selectivity between ROP and ROCOP polymerisation mechanisms. The series of polymers comprised hard poly(cyclohexene carbonate) 'A' blocks with a high T_g, and a soft poly(ε-decalactone) 'B' block with a low T_g. The feed ratio of monomers could be easily altered which afforded good control over CO_2 utilisation; between 6 and 31 wt % of the materials are derived from CO_2.

A variety of techniques were used to analyse triblock polymers and determine characteristics such as block connectivity by SEC and $^{31}P\{^1H\}$ NMR spectroscopy, glass transitions and microphase separation by DSC and DMTA, and mechanical performance by tensile mechanical analysis. The polymers showed promising thermal and mechanical properties, and access to applications covering toughened plastics, thermoplastic elastomers, and pressure-sensitive adhesives was possible by controlling the extent of CO_2 utilisation. The polymer with 15 wt % CO_2 in the backbone produced a toughened plastic with good tensile strength and extensibility, and was the lead sample in terms of moderating the well-known brittleness of PCHC. With progressively lower CO_2 incorporation the samples became softer and more elastomeric, ultimately giving good pressure-sensitive adhesive behaviour in the sample with 6 wt % CO_2. Demonstrably, the application scope of CO_2-containing polymers was expanded beyond that of polyols for the polyurethane industry with the range of new properties exhibited.

This research could easily be further explored down multiple potential routes, though they can be loosely organised into three themes: (1) further investigation into physical characteristics of current polymers; (2) evolution and utilisation of the current materials, with a focus on application potential, while retaining PDL and PCHC as constituent blocks;

(3) development of alternate soft and/or hard blocks, ideally incorporating more renewably sourced monomers.

Considering the first theme, a deeper understanding of the polymer microstructure and morphology would aid in generating a more complete profile for these polymers. In-depth SAXS, AFM, and even TEM analysis on an expanded range of relative block fractions would help with determining the boundaries for various morphologies (e.g. spherical, lamellar, hexagonally packed cylinders) and how these relate to material properties and mechanical performance.[61-64] Ultimately, a phase-diagram for these symmetric ABA triblock polymers could be constructed and would be beneficial in directing the polymer synthesis to tailor properties further.

The second theme focuses on expanding the application potential of these materials. Given the encouraging properties of the toughened plastics and elastomers, there may be potential to incorporate them as secondary components in formulations, with the aim of moderating the brittleness of bulk PCHC or bio-based PLimC. In this regard the polymers would therefore double as impact modifiers, in addition to performing well as standalone materials.

Currently, ultimate tensile strength of the materials is a point where they fall short compared to literature and commercial examples. Maximising the polymers overall molar mass and/or carefully increasing the CO_2 incorporation beyond 50 wt % could then be one strategy to try and improve upon the tensile strength of the lead sample (and also the softer elastomers) while attempting to minimise the impact on its high tensile toughness. Another option worth consideration is assessing the impact of replacing the current PCHC block with an isotactic PCHC block, rendering it semi-crystalline.[19, 65-66] Certainly in the case of PCHC homopolymer and poly(lactide) this has a marked difference on thermal and mechanical

properties but the extent of improvement for the ABA triblock system in this work is unknown and worth investigation.

Lastly, the third theme looks at changing the constituent blocks of the polymer while still retaining the aspect of CO_2 incorporation into one or even both blocks. Alternative lactone monomers could replace the PDL soft block, which would allow for greater versatility in synthesis and operating temperature range of the materials, as well as potentially reducing the cost of raw materials. Trimethylene carbonate (TMC), although expensive, could also be implemented as the soft block by ROP to form poly(trimethylene carbonate) (PTMC) and give an entirely polycarbonate-based ABA triblock. To reduce costs here, TMC could be copolymerised with ε-caprolactone (feed ratio [ε-CL]:[TMC] = 90:10) instead.[67]

Another option for the soft block is to depart from a polyester/polycarbonate backbone and instead look at a polysiloxane. Poly(dimethylsiloxane) (PDMS), for instance, is a ubiquitous polymer with a very low T_g (-120 °C) and is easily formed from the ROP of a cyclic siloxane. Incorporation of this into the triblock polymer would therefore greatly expand the operating temperature range of the material and possibly enable them for use in applications at extreme cold. Initial screening of cyclic siloxane monomers in switch catalysis is currently being conducted. However, preliminary reactions have already highlighted that the insertion of CO_2 into the siloxide propagating chain-end (to switch to epoxide/CO_2 ROCOP) is not as simple as the case with a metal-alkoxide (from the ROP of a lactone) and so more in-depth investigation in required.

Altering the hard block would be a straightforward procedure by simply exchanging CHO for a different epoxide. Limonene oxide is the most attractive target given it is bio-based, but polymerising this monomer with CO_2 has proved difficult and only a select few catalysts have been successful.[68-70] A range of other bio-based epoxides exist which may also

be explored, with many having precedent in ROCOP with CO_2 to form bio-based polycarbonates.[71] Epoxides bearing internal or pendent C=C double bonds, like vinyl-cyclohexene oxide (vCHO), could offer the opportunity to increase tensile strength by providing a cross-linkable or modifiable group within the hard domains. A further benefit of using these commercially available epoxides is the potential to perform post-polymerisation modification and "pattern" the resulting materials with functionalities that control other properties like hydrophilicity or pH responsiveness.[72]

3.7. References

1. Ruzette, A.-V.; Leibler, L., Block copolymers in tomorrow's plastics. *Nat. Mater.* **2005,** *4*, 19.
2. Bates, C. M.; Bates, F. S., 50th Anniversary Perspective: Block Polymers—Pure Potential. *Macromolecules* **2017,** *50* (1), 3-22.
3. Darensbourg, D. J., Chain transfer agents utilized in epoxide and CO2 copolymerization processes. *Green Chem.* **2019,** *21* (9), 2214-2223.
4. Langanke, J.; Wolf, A.; Hofmann, J.; Böhm, K.; Subhani, M. A.; Müller, T. E.; Leitner, W.; Gürtler, C., Carbon dioxide (CO2) as sustainable feedstock for polyurethane production. *Green Chem.* **2014,** *16* (4), 1865-1870.
5. Scharfenberg, M.; Hilf, J.; Frey, H., Functional Polycarbonates from Carbon Dioxide and Tailored Epoxide Monomers: Degradable Materials and Their Application Potential. *Adv. Funct. Mater.* **2018,** *28* (10), 1704302.
6. Stößer, T.; Li, C.; Unruangsri, J.; Saini, P. K.; Sablong, R. J.; Meier, M. A. R.; Williams, C. K.; Koning, C., Bio-derived polymers for coating applications: comparing poly(limonene carbonate) and poly(cyclohexadiene carbonate). *Polym. Chem.* **2017,** *8* (39), 6099-6105.
7. Alagi, P.; Ghorpade, R.; Choi, Y. J.; Patil, U.; Kim, I.; Baik, J. H.; Hong, S. C., Carbon Dioxide-Based Polyols as Sustainable Feedstock of Thermoplastic Polyurethane for Corrosion-Resistant Metal Coating. *ACS Sustainable Chem. Eng.* **2017,** *5* (5), 3871-3881.
8. DeBolt, M.; Kiziltas, A.; Mielewski, D.; Waddington, S.; Nagridge, M. J., Flexible polyurethane foams formulated with polyols derived from waste carbon dioxide. *J. Appl. Polym. Sci.* **2016,** *133* (45).
9. Lee, S. H.; Cyriac, A.; Jeon, J. Y.; Lee, B. Y., Preparation of thermoplastic polyurethanes using in situ generated poly(propylene carbonate)-diols. *Polym. Chem.* **2012,** *3* (5), 1215-1220.
10. Kozak, C. M.; Ambrose, K.; Anderson, T. S., Copolymerization of carbon dioxide and epoxides by metal coordination complexes. *Coord. Chem. Rev.* **2018,** *376*, 565-587.
11. Wang, Y.; Darensbourg, D. J., Carbon dioxide-based functional polycarbonates: Metal catalyzed copolymerization of CO2 and epoxides. *Coord. Chem. Rev.* **2018,** *372*, 85-100.
12. Koning, C.; Wildeson, J.; Parton, R.; Plum, B.; Steeman, P.; Darensbourg, D. J., Synthesis and physical characterization of poly(cyclohexane carbonate), synthesized from CO2 and cyclohexene oxide. *Polymer* **2001,** *42* (9), 3995-4004.
13. Thorat, S. D.; Phillips, P. J.; Semenov, V.; Gakh, A., Physical properties of aliphatic polycarbonates made from CO2 and epoxides. *J. Appl. Polym. Sci.* **2003,** *89* (5), 1163-1176.
14. Li, G.; Qin, Y.; Wang, X.; Zhao, X.; Wang, F., Study on the influence of metal residue on thermal degradation of poly(cyclohexene carbonate). *J. Polym. Res.* **2011,** *18* (5), 1177-1183.
15. Zhang, Y.-Y.; Yang, G.-W.; Wu, G.-P., A Bifunctional β-Diiminate Zinc Catalyst with CO2/Epoxides Copolymerization and RAFT Polymerization Capacities for Versatile Block Copolymers Construction. *Macromolecules* **2018,** *51* (10), 3640-3646.
16. Reiter, M.; Kronast, A.; Kissling, S.; Rieger, B., In Situ Generated ABA Block Copolymers from CO2, Cyclohexene Oxide, and Poly(dimethylsiloxane)s. *ACS Macro Lett.* **2016,** *5* (3), 419-423.
17. Darensbourg, D. J.; Wu, G.-P., A One-Pot Synthesis of a Triblock Copolymer from Propylene Oxide/Carbon Dioxide and Lactide: Intermediacy of Polyol Initiators. *Angew. Chem.* **2013,** *125* (40), 10796-10800.
18. Kember, M. R.; Copley, J.; Buchard, A.; Williams, C. K., Triblock copolymers from lactide and telechelic poly(cyclohexene carbonate). *Polym. Chem.* **2012,** *3* (5), 1196-1201.

19. Kim, J. G.; Cowman, C. D.; LaPointe, A. M.; Wiesner, U.; Coates, G. W., Tailored Living Block Copolymerization: Multiblock Poly(cyclohexene carbonate)s with Sequence Control. *Macromolecules* **2011,** *44* (5), 1110-1113.
20. Zhu, Y. Q.; Romain, C.; Williams, C. K., Sustainable polymers from renewable resources. *Nature* **2016,** *540* (7633), 354-362.
21. Chen, T. T. D.; Zhu, Y. Q.; Williams, C. K., Pentablock Copolymer from Tetracomponent Monomer Mixture Using a Switchable Dizinc Catalyst. *Macromolecules* **2018,** *51* (14), 5346-5351.
22. Kernbichl, S.; Reiter, M.; Adams, F.; Vagin, S.; Rieger, B., CO2-Controlled One-Pot Synthesis of AB, ABA Block, and Statistical Terpolymers from beta-Butyrolactone, Epoxides, and CO2. *J. Am. Chem. Soc.* **2017,** *139* (20), 6787-6790.
23. Paul, S.; Romain, C.; Shaw, J.; Williams, C. K., Sequence Selective Polymerization Catalysis: A New Route to ABA Block Copoly(ester-b-carbonate-b-ester). *Macromolecules* **2015,** *48* (17), 6047-6056.
24. Stößer, T.; Chen, T. T. D.; Zhu, Y.; Williams, C. K., 'Switch' catalysis: from monomer mixtures to sequence-controlled block copolymers. *Phil. Trans. R. Soc. A* **2018,** *376* (2110).
25. Romain, C.; Zhu, Y.; Dingwall, P.; Paul, S.; Rzepa, H. S.; Buchard, A.; Williams, C. K., Chemoselective Polymerizations from Mixtures of Epoxide, Lactone, Anhydride, and Carbon Dioxide. *J. Am. Chem. Soc.* **2016,** *138* (12), 4120-31.
26. Stößer, T.; Sulley, G. S.; Gregory, G. L.; Williams, C. K., Easy access to oxygenated block polymers via switchable catalysis. *Nat. Commun.* **2019,** *10* (1), 2668.
27. Raman, S. K.; Raja, R.; Arnold, P. L.; Davidson, M. G.; Williams, C. K., Waste not, want not: CO2 (re)cycling into block polymers. *Chem. Commun.* **2019,** 55 (51), 7315-7318.
28. Zhu, Y.; Radlauer, M. R.; Schneiderman, D. K.; Shaffer, M. S. P.; Hillmyer, M. A.; Williams, C. K., Multiblock Polyesters Demonstrating High Elasticity and Shape Memory Effects. *Macromolecules* **2018,** *51* (7), 2466-2475.
29. Stößer, T.; Williams, C. K., Selective Polymerization Catalysis from Monomer Mixtures: Using a Commercial Cr-Salen Catalyst To Access ABA Block Polyesters. *Angew. Chem. Int. Ed.* **2018,** *57* (21), 6337-6341.
30. Stößer, T.; Mulryan, D.; Williams, C. K., Switch Catalysis To Deliver Multi-Block Polyesters from Mixtures of Propene Oxide, Lactide, and Phthalic Anhydride. *Angew. Chem. Int. Ed.* **2018,** *57* (51), 16893-16897.
31. Zhu, Y.; Romain, C.; Williams, C. K., Selective polymerization catalysis: controlling the metal chain end group to prepare block copolyesters. *J. Am. Chem. Soc.* **2015,** *137* (38), 12179-82.
32. Kernbichl, S.; Reiter, M.; Mock, J.; Rieger, B., Terpolymerization of β-Butyrolactone, Epoxides, and CO2: Chemoselective CO2-Switch and Its Impact on Kinetics and Material Properties. *Macromolecules* **2019,** *52* (21), 8476-8483.
33. Jia, M.; Hadjichristidis, N.; Gnanou, Y.; Feng, X., Monomodal Ultrahigh-Molar-Mass Polycarbonate Homopolymers and Diblock Copolymers by Anionic Copolymerization of Epoxides with CO2. *ACS Macro Lett.* **2019**, 1594-1598.
34. Lin, J.-O.; Chen, W.; Shen, Z.; Ling, J., Homo- and Block Copolymerizations of ε-Decalactone with l-Lactide Catalyzed by Lanthanum Compounds. *Macromolecules* **2013,** *46* (19), 7769-7776.
35. Zhou, Y.; Duan, R.; Li, X.; Pang, X.; Wang, X.; Chen, X., Preparation and Thermal Properties of Polycarbonates/esters Catalyzed by Using Dinuclear Salph-Al from Ring-Opening Polymerization of Epoxide Monomers. *Chem. Asian J.* **2017,** *12* (24), 3135-3140.
36. Fox, T. G., Influence of diluent and of copolymer composition on the glass temperature of a polymer system. *Bull. Am. Phys. Soc.* **1956,** *1*, 123.
37. Koronis, G.; Silva, A., In *Green Composites for Automotive Applications*, Koronis, G.; Silva, A., Eds. Woodhead Publishing: 2019; pp xv-xvi.

38. Stevens, M. P., *Polymer chemistry: an introduction*. 2nd ed.; Oxford University Press: New York, 1990.
39. Vatankhah-Varnosfaderani, M.; Keith, A. N.; Cong, Y.; Liang, H.; Rosenthal, M.; Sztucki, M.; Clair, C.; Magonov, S.; Ivanov, D. A.; Dobrynin, A. V.; Sheiko, S. S., Chameleon-like elastomers with molecularly encoded strain-adaptive stiffening and coloration. *Science* **2018,** *359* (6383), 1509.
40. Arai, K.; Kotaka, T.; Kitano, Y.; Yoshimura, K., Poly(styrene-b-butadiene-b-4-vinylpyridine) Three-Block Polymers. Synthesis, Characterization, Morphology, and Mechanical Properties. *Macromolecules* **1980,** *13* (6), 1670-1678.
41. Hashimoto, T.; Fujimura, M.; Saijo, K.; Kawai, H.; Diamant, J.; Shen, M., Strain-Induced Plastic-to-Rubber Transition of a SBS Block Copolymer and Its Blend with PS. In *Multiphase Polymers*, AMERICAN CHEMICAL SOCIETY: 1979; Vol. 176, pp 257-275.
42. Fujimura, M.; Hashimoto, T.; Kawai, H., Structural Change Accompanied by Plastic-to-Rubber Transition of SBS Block Copolymers. *Rubber Chem. Technol.* **1978,** *51* (2), 215-224.
43. Dahlquist, C. A., Pressure-Sensitive Adhesive. In *Treatise on Adhesion and Adhesives*, Patrick, R. L., Ed. Dekker: New York, 1969; Vol. 2, p 219.
44. Chang, E. P., Viscoelastic Windows of Pressure-Sensitive Adhesives. *J. Adhes.* **1991,** *34* (1-4), 189-200.
45. Lee, S.; Lee, K.; Kim, Y.-W.; Shin, J., Preparation and Characterization of a Renewable Pressure-Sensitive Adhesive System Derived from ε-Decalactone, l-Lactide, Epoxidized Soybean Oil, and Rosin Ester. *ACS Sustainable Chem. Eng.* **2015,** *3* (9), 2309-2320.
46. Ding, K.; John, A.; Shin, J.; Lee, Y.; Quinn, T.; Tolman, W. B.; Hillmyer, M. A., High-Performance Pressure-Sensitive Adhesives from Renewable Triblock Copolymers. *Biomacromolecules* **2015,** *16* (8), 2537-9.
47. Gallagher, J. J.; Hillmyer, M. A.; Reineke, T. M., Acrylic Triblock Copolymers Incorporating Isosorbide for Pressure Sensitive Adhesives. *ACS Sustainable Chem. Eng.* **2016,** *4* (6), 3379-3387.
48. Shin, J.; Martello, M. T.; Shrestha, M.; Wissinger, J. E.; Tolman, W. B.; Hillmyer, M. A., Pressure-Sensitive Adhesives from Renewable Triblock Copolymers. *Macromolecules* **2011,** *44* (1), 87-94.
49. Nasiri, M.; Saxon, D. J.; Reineke, T. M., Enhanced Mechanical and Adhesion Properties in Sustainable Triblock Copolymers via Non-covalent Interactions. *Macromolecules* **2018,** *51* (7), 2456-2465.
50. Tiu, B. D. B.; Delparastan, P.; Ney, M. R.; Gerst, M.; Messersmith, P. B., Enhanced Adhesion and Cohesion of Bioinspired Dry/Wet Pressure-Sensitive Adhesives. *ACS Appl. Mater. Interfaces* **2019,** *11* (31), 28296-28306.
51. Brubaker, C. E.; Messersmith, P. B., The Present and Future of Biologically Inspired Adhesive Interfaces and Materials. *Langmuir* **2012,** *28* (4), 2200-2205.
52. Jenkins, C. L.; Siebert, H. M.; Wilker, J. J., Integrating Mussel Chemistry into a Bio-Based Polymer to Create Degradable Adhesives. *Macromolecules* **2017,** *50* (2), 561-568.
53. Hauenstein, O.; Agarwal, S.; Greiner, A., Bio-based polycarbonate as synthetic toolbox. *Nat. Commun.* **2016,** *7*, 11862.
54. Yuan, Y.; Ruckenstein, E., Polyurethane toughened polylactide. *Polym. Bull.* **1998,** *40* (4), 485-490.
55. Delgado, P. A.; Hillmyer, M. A., Combining block copolymers and hydrogen bonding for poly(lactide) toughening. *RSC Adv.* **2014,** *4* (26), 13266.
56. Olsén, P.; Borke, T.; Odelius, K.; Albertsson, A.-C., ε-Decalactone: A Thermoresilient and Toughening Comonomer to Poly(l-lactide). *Biomacromolecules* **2013,** *14* (8), 2883-2890.

57. Romero-Guido, C.; Belo, I.; Ta, T. M. N.; Cao-Hoang, L.; Alchihab, M.; Gomes, N.; Thonart, P.; Teixeira, J. A.; Destain, J.; Waché, Y., Biochemistry of lactone formation in yeast and fungi and its utilisation for the production of flavour and fragrance compounds. *Appl. Microbiol. Biotechnol.* **2011,** *89* (3), 535-547.
58. Winkler, M.; Romain, C.; Meier, M. A. R.; Williams, C. K., Renewable polycarbonates and polyesters from 1,4-cyclohexadiene. *Green Chem.* **2015,** *17* (1), 300-306.
59. Chen, Z.; Hadjichristidis, N.; Feng, X.; Gnanou, Y., Cs2CO3-promoted polycondensation of CO2 with diols and dihalides for the synthesis of miscellaneous polycarbonates. *Polym. Chem.* **2016,** *7* (30), 4944-4952.
60. Carrodeguas, L. P.; Chen, T. T. D.; Gregory, G. L.; Sulley, G. S.; Williams, C. K., High elasticity, chemically recyclable, thermoplastics from bio-based monomers: carbon dioxide, limonene oxide and ε-decalactone. *Green Chem.* **2020,** *22* (23), 8298-8307.
61. Gregory, G. L.; Sulley, G. S.; Carrodeguas, L. P.; Chen, T. T. D.; Santmarti, A.; Terrill, N. J.; Lee, K.-Y.; Williams, C. K., Triblock polyester thermoplastic elastomers with semi-aromatic polymer end blocks by ring-opening copolymerization. *Chem. Sci.* **2020,** *11* (25), 6567-6581.
62. Honeker, C. C.; Thomas, E. L., Impact of Morphological Orientation in Determining Mechanical Properties in Triblock Copolymer Systems. *Chem. Mater.* **1996,** *8* (8), 1702-1714.
63. Matsen, M. W.; Thompson, R. B., Equilibrium behavior of symmetric ABA triblock copolymer melts. *J. Chem. Phys.* **1999,** *111* (15), 7139-7146.
64. Bates, F. S.; Fredrickson, G. H., Block Copolymers—Designer Soft Materials. *Phys. Today* **1999,** *52* (2), 32-38.
65. Guerin, W.; Diallo, A. K.; Kirilov, E.; Helou, M.; Slawinski, M.; Brusson, J.-M.; Carpentier, J.-F.; Guillaume, S. M., Enantiopure Isotactic PCHC Synthesized by Ring-Opening Polymerization of Cyclohexene Carbonate. *Macromolecules* **2014,** *47* (13), 4230-4235.
66. Ellis, W. C.; Jung, Y.; Mulzer, M.; Di Girolamo, R.; Lobkovsky, E. B.; Coates, G. W., Copolymerization of CO2 and meso epoxides using enantioselective β-diiminate catalysts: a route to highly isotactic polycarbonates. *Chem. Sci.* **2014,** *5* (10), 4004.
67. Bergfelt, A.; Lacey, M. J.; Hedman, J.; Sångeland, C.; Brandell, D.; Bowden, T., ε-Caprolactone-based solid polymer electrolytes for lithium-ion batteries: synthesis, electrochemical characterization and mechanical stabilization by block copolymerization. *RSC Adv.* **2018,** *8* (30), 16716-16725.
68. Hauenstein, O.; Reiter, M.; Agarwal, S.; Rieger, B.; Greiner, A., Bio-based polycarbonate from limonene oxide and CO2 with high molecular weight, excellent thermal resistance, hardness and transparency. *Green Chem.* **2016,** *18* (3), 760-770.
69. Byrne, C. M.; Allen, S. D.; Lobkovsky, E. B.; Coates, G. W., Alternating copolymerization of limonene oxide and carbon dioxide. *J. Am. Chem. Soc.* **2004,** *126*, 11404-11405.
70. Peña Carrodeguas, L.; González-Fabra, J.; Castro-Gómez, F.; Bo, C.; Kleij, A. W., Al(III) -catalysed formation of poly(limonene)carbonate: DFT analysis of the origin of stereoregularity. *Chemistry* **2015,** *21* (16), 6115-22.
71. Poland, S. J.; Darensbourg, D. J., A quest for polycarbonates provided via sustainable epoxide/CO2 copolymerization processes. *Green Chem.* **2017,** *19* (21), 4990-5011.
72. Yi, N.; Chen, T. T. D.; Unruangsri, J.; Zhu, Y.; Williams, C. K., Orthogonal functionalization of alternating polyesters: selective patterning of (AB)n sequences. *Chem. Sci.* **2019,** *10* (43), 9974-9980.

CHAPTER 4

$(AB)_n$ Star Polymers Derived from CO_2: Influence of Architecture and Post-Modification

4.1. Introduction

Switchable catalysis has generally employed mono- or bi-functional chain-transfer agents to prepare block polymers with linear (e.g. AB or ABA-type) architecture. Yet the controlled polymerisation cycles that are accessed during switch (ROP and ROCOP) have the advantage of being amenable to initiation from multifunctional alcohol chain-transfer agents which could allow access to non-linear polymers, for example those with star architectures, and has the potential to expand the capability of the switch catalysis technique.

Star polymers can be synthesised using either a convergent or divergent approach, with both methods allowing for control over the number of arms and their chemistry.[1-3] The former is also referred to as "arm-fist" and concerns the coupling of pre-synthesised arms to a core structure or molecule, often using click-chemistry techniques or condensation reactions. The latter approach, also called "core-first", involves the direct initiation and growth of the star arms outward from a core molecule or structure. The idea to utilise multifunctional initiators with "switch catalysts" therefore represents a divergent approach to star block polymer synthesis.

Presently there are reports on the synthesis and structure-property relationship of oxygenated star polymers prepared *via* either ROP or ROCOP techniques.[1, 3-4] For instance, multi-arm star poly(ε-DL)-poly(L-lactide) copolymers at fixed molar mass and block ratio showed improved mechanical properties as TPEs with increasing number of arms.[3] Aside from reports involving scope or proof-of-concept, where for example a Cr(III)-salen "switch catalyst" was applied with various multifunctional initiating species but the catalysis was not well-optimised for the preparation of high molar mass and high performance materials, there are limited investigations into the application of multifunctional CTAs in switchable polymerisation catalysis, particularly with the intention of preparing high molar mass, oxygenated star block polymers to examine structure-property relationships.[5-6]

4.2. Aims

This chapter aims to investigate architectural control in the switchable polymerisation catalysis of lactone/epoxide/CO_2 using a Zn(II)/Mg(II) organometallic catalyst and tests the hypothesis that the system should be amenable to the use of alternative chain-transfer agents with multiple hydroxyl groups in order to fashion polymers with non-linear architectures. Moreover, it intends to examine the potential for the catalysis technique to access other functional CO_2-based poly(ester-*b*-carbonate)s, additional to the linear ABA-type materials shown previously. An additional aim is to incorporate a vinyl-functionality in the polycarbonate block and exploit this using post-polymerisation modification to increase hydrogen-bonding capability, expected to promote microphase separation between constituent blocks.

The approach to deliver on these aims will involve: (1) testing the tolerance of the Zn(II)/Mg(II) organometallic catalyst to multifunctional chain-transfer agents, initially in lactone ROP and subsequently in lactone/epoxide/CO_2 switch catalysis; (2) exploring the synthesis of high molar mass, multi-arm star block polymers with equivalent relative hard/soft weight fractions and evaluating their thermal and mechanical properties; (3) modifying the repeat unit of the polycarbonate block using thiol-ene chemistry to install pendent hydroxyl moieties, and probing the effects on the thermal, mechanical, and morphological characteristics of the star block polymers (**Figure 4.1**).

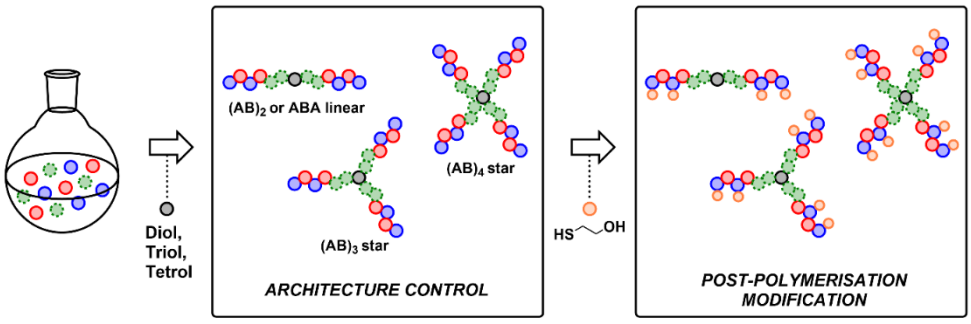
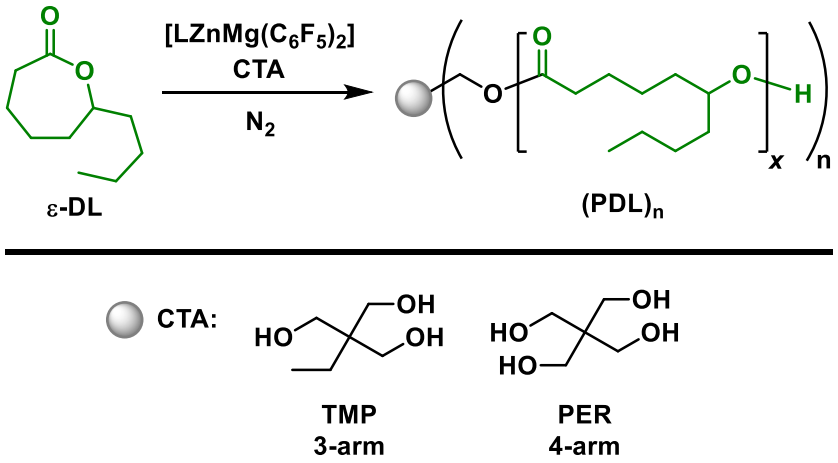


Figure 4.1. Synthesis and post-polymerisation modification of $(AB)_n$ star block polymers utilising CO_2.

4.3. $(AB)_n$ star polymers: Synthesis and characterisation

Scheme 4.1. Synthesis of $(PDL)_n$ star polymers.



Initially, the ROP of ε-decalactone was performed using **2** and multifunctional chain-transfer agents tris(hydroxymethyl)propane (TMP, n_{OH} = 3) and pentaerythritol (PER, n_{OH} = 4) (**Scheme 4.1**). These polymerisation studies served as a benchmark from which to further evaluate the tolerance of the catalyst to CTA and to determine the degree of functionalisation on the various cores (**Table 4.1**).

Table 4.1. Multiarm star $(PDL)_n$ Characterisation Data

CTA[a]	n_{OH}[b]	Conversion (%)[c]	DP_{total}[d]	$M_{n,NMR}$[e] (kg mol^{-1})	$M_{n,SEC}$[f] (kg mol^{-1})	$Đ_M$[g]
TMP	3	44	27	4.6	7.6	1.09
PER	4	95	62	10.6	13.9	1.19

[a]Reaction conditions: [**2**]:[CTA]:[ε-DL] = 1:4:200, 80 °C, toluene ([ε-DL]$_0$ = 1.7 M); TMP = 1,1,1-Tris(hydroxymethyl)propane, PER = Pentaerythritol. [b]Number of hydroxide functional groups on the CTA, i.e. theoretical maximum number of star arms. [c]Determined from ^{1}H NMR spectroscopy of crude polymer samples by comparing relative integrals of ε-DL (4.21 ppm) and PDL (4.85 ppm). [d]Total degree of polymerisation; calculated from ^{1}H NMR spectra of purified polymer samples by comparing integrals for PDL backbone (4.85 ppm) and end-group (3.58 ppm) (See Appendix Figures S7.41 – 7.42). [e]Determined from ^{1}H NMR spectroscopy, (DP_{total} * 170.25). [f]Determined from SEC analysis in THF, calibrated using narrow polystyrene standards. [g]M_w/M_n.

The ^{1}H NMR spectra for the precipitated samples of multi-arm star poly(ε-decalactone) polymers revealed characteristic signals corresponding to methine protons in the main polymer backbone (4.85 ppm) and end-group (3.58 ppm), and methylene protons on the

initiating species (3.95 – 4.20 ppm) (**Figure 4.2**). Observation of these signals after precipitation of the polymer into methanol reassured that initiation from the multifunctional initiator had occurred, given the good solubility of both CTAs in methanol. The relative integrals suggested complete arm functionalisation, i.e. the formation of either 3- or 4-arm star polymers (Appendix Figures S7.41 – 7.42). The total degree of polymerisation (DP_{total}) for each star polymer, calculated from the relative integrals of PDL backbone and end-group signals in a purified sample, was in good agreement with the value expected based on the conversion and initial monomer loading.

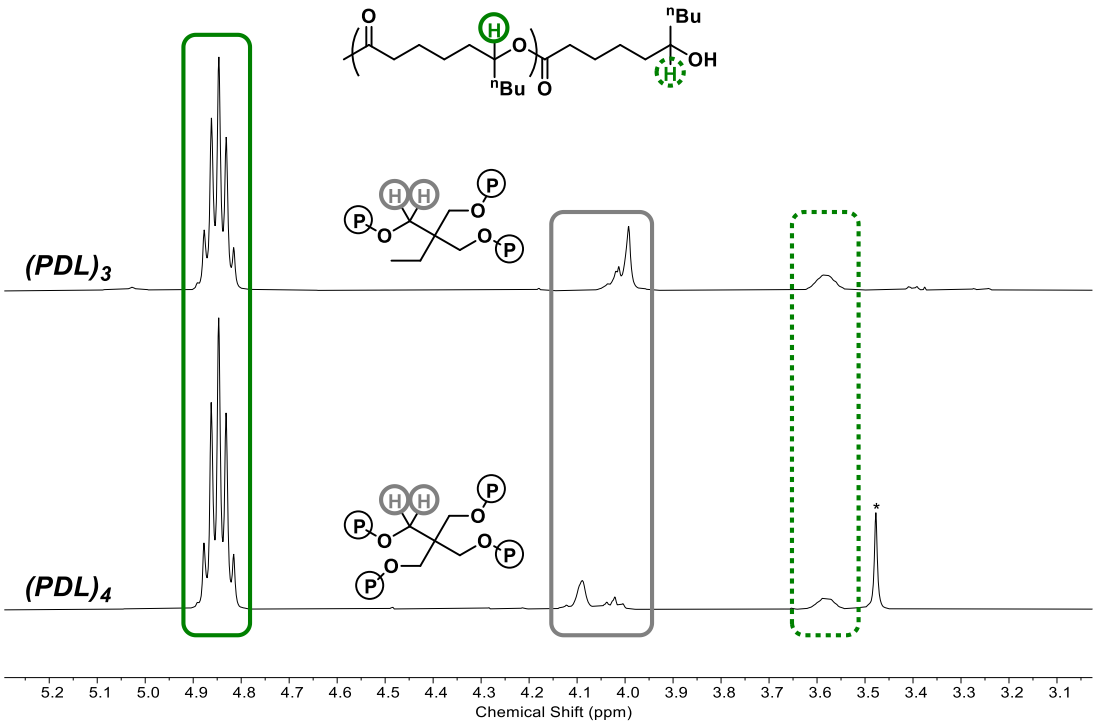


Figure 4.2. ^{1}H NMR spectra of purified 3- and 4-arm star poly(ε-decalactone) highlighting signals for backbone, core, and end-group protons [400 MHz, $CDCl_3$].

The reaction of the polymer hydroxyl end-groups with [2-chloro-4,4,5,5-tetramethyl-1,3,2-dioxaphospholane] was used as a qualitative measure of end-group fidelity and core functionalisation by observing the signals present in the $^{31}P\{^{1}H\}$ NMR spectra. A diagnostic signal for the 2° hydroxyl chain-end in PDL was observed at 147.1 ppm, with no clear evidence

of 1° hydroxyl groups arising from uninitiated arms; in some cases, minor baseline signals were observed downfield of the 2° hydroxyl, however these were not due to unreacted hydroxyl groups on either TMP or PER cores and remain unassigned (Appendix Figure S7.43).

Analysis of the PDL star polymers by SEC revealed monomodal molar mass distributions with narrow dispersity ($Đ_M$ < 1.20) (**Figure 4.3**). Comparison between molar mass by SEC and M_n calculated from the ^{1}H NMR spectrum of the pure samples showed the value from SEC to be slightly higher in each case which could be attributed to the significantly lower T_g value for PDL *vs.* poly(styrene) (calibration standards) which likely causes very different chain conformations in solution.

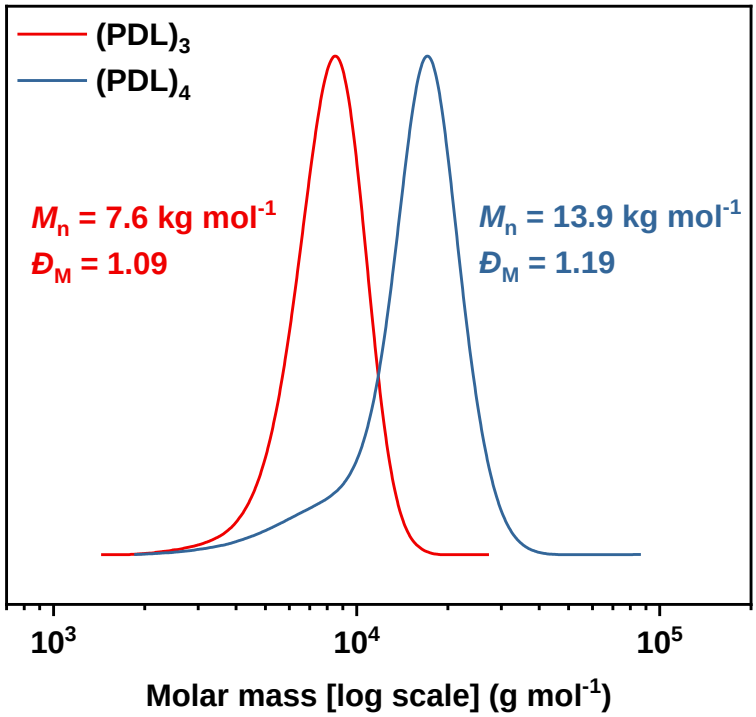
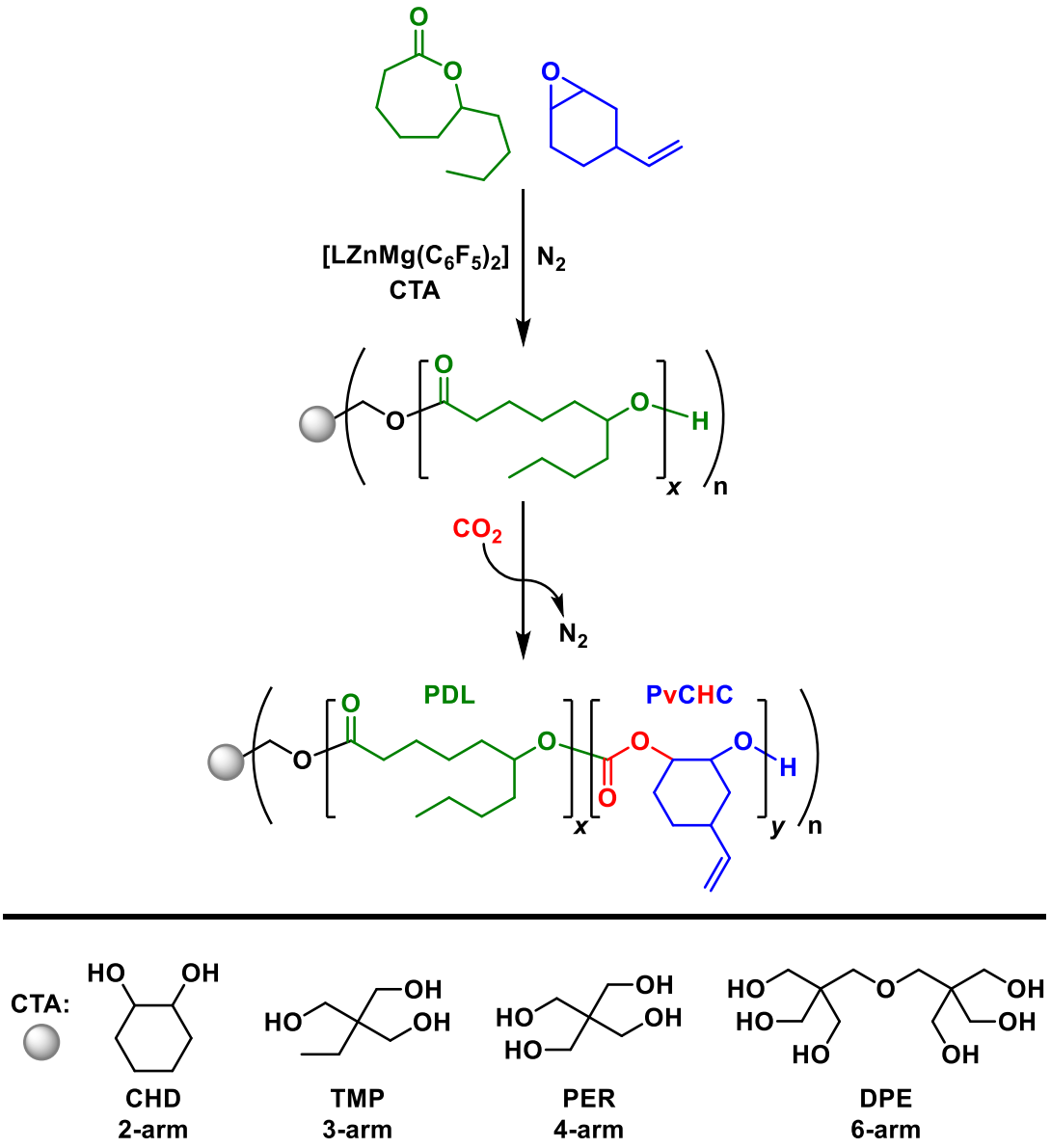


Figure 4.3. SEC chromatographs of 3-arm (red) and 4-arm (blue) star poly(ε-decalactone) samples.

Building from the promising data showing desired arm functionalisation on the multifunctional CTA cores, switch catalysis principles were applied to prepare star block

polymers, with each arm comprised of poly(ε-decalactone)-*b*-poly(vinyl cyclohexene carbonate) (PDL-*b*-PvCHC) (**Scheme 4.2**). In a similar method to how the ABA triblock polymers were prepared (Section 3.3), ROP of ε-DL was followed by the ROCOP of vCHO and CO_2, fashioning a series of multiarm star block polymers with a soft (i.e. low T_g) polyester interior of PDL blocks, hard (i.e. high T_g) polycarbonate exterior of PvCHC blocks, and with a target block ratio of 50 wt % (**Table 4.2**). At this stage, the synthesis of an additional 6-arm star block polymer was targeted by employing dipentaerythritol (DPE) as the CTA.

Scheme 4.2. Synthesis of $(AB)_n$ Star Block Polymers Comprising PDL-*b*-PvCHC Diblock Arms.



The block ratio of 50 wt % was preferred given the promising thermomechanical properties observed in linear ABA triblock polymers of PCHC-*b*-PDL-*b*-PCHC at 50 wt % (Chapter 3), and also allowed for high utilisation of CO_2 in the resulting materials. The pendent vinyl moiety provided by the vCHO monomer and located in the repeat unit of the polycarbonate outer block also offered the opportunity to later apply post-polymerisation modification (PPM) techniques, e.g. thiol-ene transformations. The star block polymers are denoted $(AB)_n$-#, where A = polycarbonate outer block, B = polyester inner block, n = number of arms, and # = molar mass by SEC.

Table 4.2. (PvCHC-*b*-PDL)$_n$ [(AB)$_n$] Star Block Polymer Characterisation Data

Entry	Polymer[a]	n_{arms}[b]	wt % PDL:PvCHC[c]	$M_{n,SEC}$[d] (kg mol^{-1}) [$Đ_M$] Total[e]	Split[f]	$T_{g,DSC}$[g] (°C)	$T_{g,DMTA}$[h] (°C)
1	$(AB)_2$-63	2	49:51	66.3 [1.22]	160 [1.02] **63.3 [1.18]**	-52; *n.d.*	+91
2	$(AB)_3$-52	3	50:50	36.0 [1.40]	**51.9 [1.08]** 12.4 [1.20]	-38; *n.d.*	*n.d.*
3	$(AB)_3$-88	3	52:48	75.1 [1.18]	172 [1.02] **87.9 [1.04]** 43.2 [1.06]	-55; *n.d.*	+71
4	$(AB)_4$-90	4	52:48	79.9 [1.34]	192 [1.06] **90.0 [1.05]** 40.4 [1.05]	-63; *n.d.*	+73
5	$(AB)_6$-72	6	51:49	63.4 [1.34]	156 [1.07] **71.9 [1.04]** 27.2 [1.08]	-32; *n.d.*	*n.d.*

[a]$(AB)_n$-#; where A = PvCHC, B = PDL, n = number of arms, # = molar mass, major distribution (SEC). [b]Number of arms based on full functionalisation from CTA. [c]Relative block weight fraction, determined from ^{1}H NMR spectroscopy (Appendix Figures S7.45 – 7.49). [d]Molar mass determined from SEC, $Đ_M = M_w/M_n$. [e]Molar mass data for entire chromatogram without peak deconvolution. [f]Molar mass data for constituent chromatogram peaks (bold indicates majority distribution), deconvoluted using Shimadzu GPC Postrun software. [g]Glass transition temperature determined from DSC (-90 – 120 °C), taken as the midpoint of transition on the third heating cycle (Appendix Figures S7.52 – 7.56). [h]Upper glass transition temperature determined from DMTA (30 – 110 °C), taken as the peak maxima in tan(δ) (Appendix Figures S7.57 – 7.59). *n.d.* = glass transition temperature not determinable.

Polymerisations to prepare high molar mass star block polymers with varying arm numbers were performed under 20 bar CO_2 pressure using stainless steel pressure vessels. As with the synthesis of linear ABA triblock polymers, the use of these pressure vessels allowed for high CO_2 saturation and powerful mechanical stirring, and enabled the polymerisations to advance to high monomer conversion within a reasonable timeframe (<24 h). However, to determine monomer selectivity an additional polymerisation was run using 1 bar CO_2 pressure and monitored using *in-situ* ATR-IR spectroscopy and SEC aliquots. The data showed the expected catalyst selectivity of ROP followed by a switch to ROCOP after the introduction of a CO_2 atmosphere, and was substantiated by an increase in the molar mass of samples taken from ROP to ROCOP stages with retention of narrow dispersity (Appendix Figure S7.44).

The high monomer conversions reached in each polymerisation resulted in the final block compositions being representative of the starting monomer stoichiometry. As such, the target block ratio of ~50 wt % was achieved in all samples, as determined by comparing the relative integrals for the PDL side chain methyl signal (0.88 ppm) and PvCHC side chain vinyl C*H* signal (5.88 – 5.63 ppm); signal overlap prevented the typical use of backbone polymer signals corresponding to PDL (4.85 ppm) and PvCHC (4.77 ppm) methine signals (**Figure 4.4** and Appendix Figures S7.45 – 7.49).

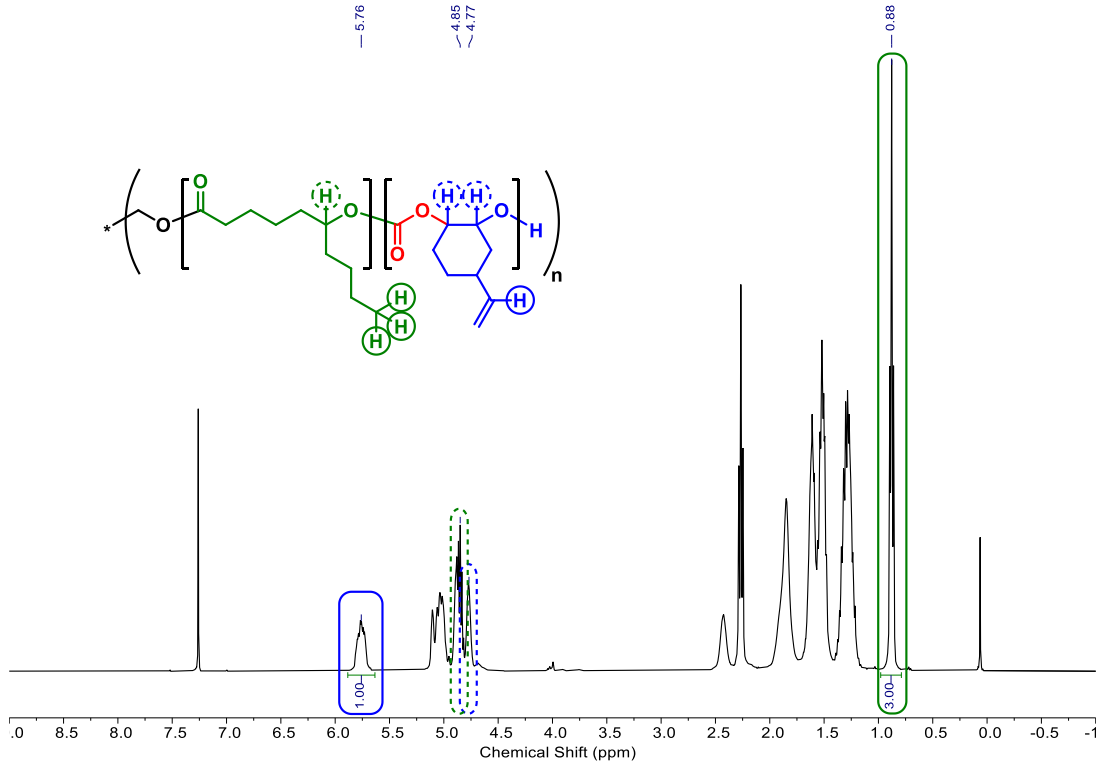


Figure 4.4. Representative ^{1}H NMR spectrum of a purified $(AB)_n$ star block polymer highlighting signals used for determination of relative block ratio [400 MHz, $CDCl_3$].

Analysis of the star block polymers by SEC revealed all samples to have multimodality, in particular a trimodal molar mass distribution (**Figure 4.5** and Appendix Figure S7.50). This observation was puzzling given the monomodality observed for the $(PDL)_n$ star homopolymers, but this difference might be attributed to the higher molar mass of $(AB)_n$ star block polymers more clearly revealing different distributions. However, in each case the major distribution matches closely to the target molar mass for a given polymer, with a smaller secondary distribution at lower molar mass and a shoulder at higher molar mass.

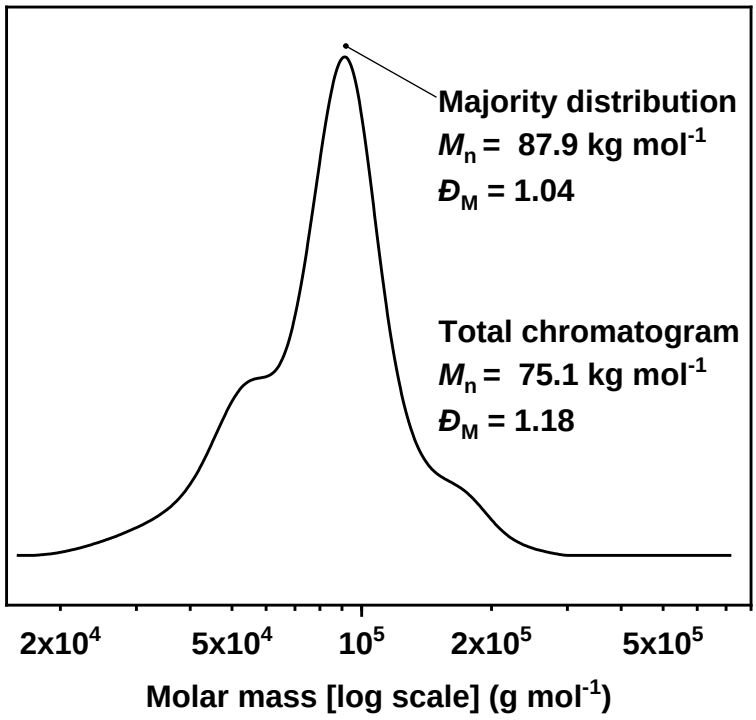


Figure 4.5. SEC chromatograph for star block polymer sample $(AB)_3$-88. Highlighted values for M_n and $Đ_M$ corresponding to the majority distribution (central peak) and the overall chromatogram.

In star polymer synthesis, unanticipated high molar mass shoulders can be attributed to star-star coupling reactions, although these are more common in controlled radical polymerisations where radical recombination at chain-ends is possible.[1] The coupling of star poly(ester-*b*-carbonate)s would require transesterification reactions of the ester/carbonate linkages which, in this case, would likely be indiscriminate of polymer chain-ends. Consequently, effects of general transesterification, like overall broadening of molar mass distributions, would be expected and likewise observed in the $(PDL)_n$ star polymers, which was not the case.

Transesterification of the ester and carbonate backbone linkages would also generate polymer chains with both polycarbonate and polyester hydroxyl end-groups. End-group analysis of the star block polymers by $^{31}P\{^1H\}$ NMR spectroscopy showed only a multiplet

corresponding to PvCHC secondary hydroxyl chain-ends (146.9 – 146.4 ppm) (**Figure 4.6**). Signals corresponding to initiator primary hydroxyls and the sharp singlet corresponding to PDL hydroxyl chain-ends (147.1 ppm) were not observed which indicated full initiator functionalisation and good blocking efficiency (Appendix Figure S7.51).

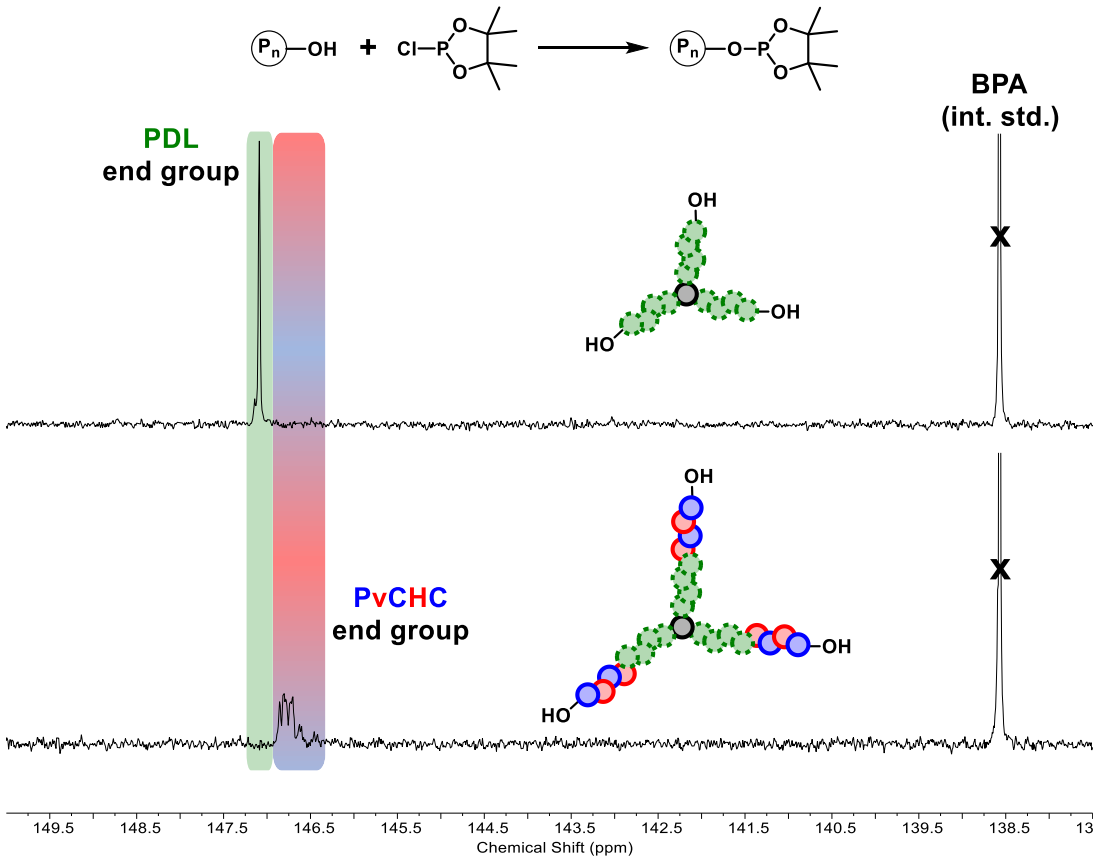


Figure 4.6. $^{31}P\{^{1}H\}$ NMR spectra comparing $(PDL)_3$ and $(AB)_3$ (A = PvCHC, B = PDL) end-group titrations.

Thermal characterisation of the star block polymers identified glass transition temperatures for the constituent blocks (Appendix Figures S7.52 – 7.59). DSC showed the low temperature transition corresponding to the PDL blocks between -52 and -63 °C for linear, 3-arm (88 kg mol^{-1}), and 4-arm samples (**Table 4.2**, entries 1, 3-4). The lower molar mass 3-arm (52 kg mol^{-1}) and 6-arm samples exhibited broad transitions at -38 °C and -32 °C, respectively, indicating partial block miscibility (**Table 4.2**, entries 2, 5). The T_g for PvCHC (expected around 100 °C) was difficult to observe by DSC but instead could be identified clearly, for all

but two samples, using DMA by taking the peak maxima in tan(δ). The 3-arm (52 kg mol^{-1}) and 6-arm samples could not be analysed by DMA due to their softness and difficulty in processing, likely a result of their lower overall molar mass. The linear (2-arm star block) sample showed the highest upper T_g at 91 °C, close to the value expected for pure PvCHC. Star block polymers $(AB)_3$-88 and $(AB)_4$-90 showed upper T_g values of around 70 °C, somewhat lower than the linear analogue and the value expected for PvCHC which may indicate some degree of block miscibility and incomplete microphase separation, though to a lesser extent than samples $(AB)_3$-52 and $(AB)_6$-72.

4.4. Influence of molar mass and arm number

The effect of molar mass and arm number on the mechanical properties of the star block polymers was investigated with tensile mechanical testing. Specimens were prepared, where possible, from solvent cast films and subjected to uniaxial extension experiments to measure their stress-strain profiles and determine important mechanical characteristics (**Table 4.3**).

Table 4.3. $(AB)_n$ Star Block Polymer Mechanical Characterisation Data

Entry	Polymer	$M_{n,arm}$[a] (kg mol^{-1})	E_y[b] (MPa)	σ_y[c] (MPa)	ε_y[d] (%)	σ[e] (MPa)	ε_b[f] (%)
1	ABA-50[g]	29.9	238 ± 35	6.7 ± 0.3	9.0 ± 1.7	20 ± 2	900 ± 104
2	$(AB)_2$-63	31.7	212 ± 12	9.9 ± 0.3	9.9 ± 0.3	19 ± 1.7	1167 ± 147
3	$(AB)_3$-52	17.3	7.2 ± 0.1	*n.d.*	*n.d.*	0.7 ± 0.07	663 ± 186
4	$(AB)_3$-88	29.3	78 ± 9	4.8 ± 0.5	14 ± 0.6	12 ± 0.5	1500 ± 219
5	$(AB)_4$-90	22.5	25 ± 7	1.7 ± 0.3	33 ± 9	6.8 ± 0.4	1678 ± 195
6	$(AB)_6$-72	12.0	*n.d.* (unable to process free-standing film)				

[a]Calculated as $(M_{n,SEC})$/n, where n is number of arms or AB segments, assuming full core functionalisation and equal arm lengths. [b]Young's modulus. [c]Yield stress. [d]Yield strain. [e]Tensile strength. [f]Elongation at break. Average values and standard deviation from a minimum of 5 specimens. *n.d.* = not determined. [g]Linear ABA triblock sample comprised PCHC-*b*-PDL-*b*-PCHC at 50 wt % relative block ratio (Chapter 3).

The linear sample, $(AB)_2$-63, was established as a benchmark from which to compare the higher arm star block polymers. It also facilitated direct comparison to the analogous, linear ABA triblock polymer (ABA-50) previously investigated in Chapter 3, in order to identify any effects of changing the hard block segments from PCHC to PvCHC. Both ABA-50 and $(AB)_2$-63 possessed 50 wt % hard block and similar molar mass at 59.8 and 63.3 kg mol^{-1}, respectively. It was anticipated that the pendent vinyl moieties of PvCHC would slightly soften the materials with these hard blocks compared to those with PCHC, due to an increase in degrees of freedom and reduced ability for polymer chain segments to pack as closely together.

Tensile mechanical analysis conducted on $(AB)_2$-63 showed overall a similar stress-strain profile to ABA-50 (**Figure 4.7**). The Young's modulus was comparable between ABA-50 and $(AB)_2$-63 (238 *vs*. 212 MPa) indicating a similar material stiffness within the elastic regime. The relative hard/soft block ratio of 50 wt % for $(AB)_2$-63 resulted in it displaying properties akin to a ductile plastic, with a well-defined yield point visible on the curve below 10% strain. Beyond this point, the material deformed plastically like ABA-50 but showed variation in certain features.

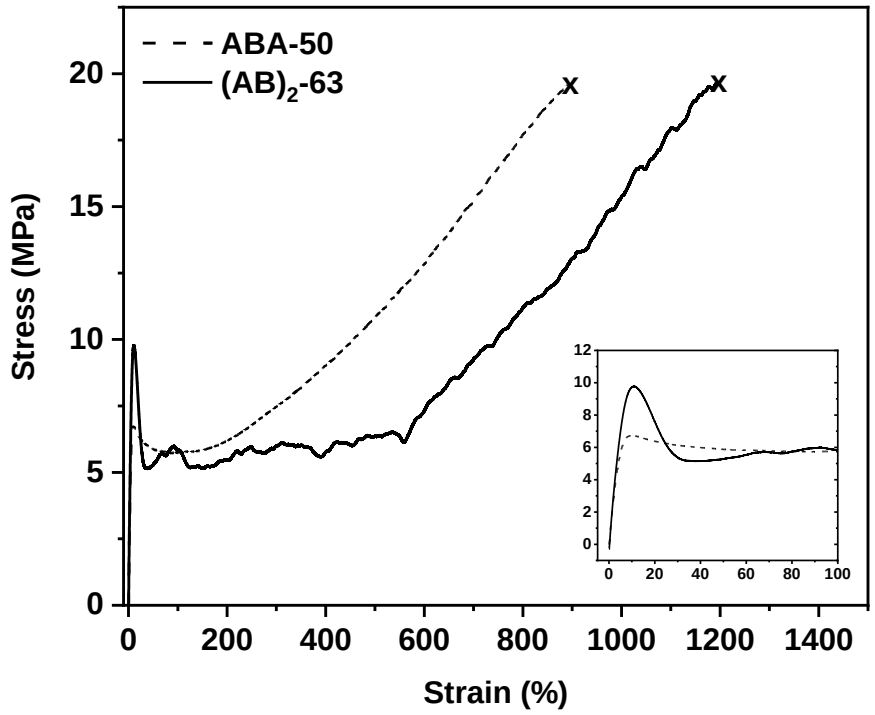


Figure 4.7. Representative stress-strain curves for linear triblock samples. ABA-50 is a linear triblock analogue (50 wt % PCHC hard blocks and $M_{n,total}$ = 59.8 kg mol^{-1}), $(AB)_2$-63 is a linear ABA-type triblock (50 wt % PvCHC hard blocks and $M_{n,total}$ = 63.3 kg mol^{-1}). Failure points marked with an "X". Inset: enlargement of 0-100% region.

Most notable was a lengthened region of drawing or localised stretching (ε: 50 – 550%) in which polymer chains align parallel to the direction of extension and the sample's elongation increases substantially with minimal increase in stress. The result of this chain alignment manifested as the region of strain hardening, with sharply increasing stress until

the point of fracture as was observed for ABA-50 but with an earlier onset. The tensile strengths of the materials were roughly equivalent at around 20 MPa but $(AB)_2$-63 reached higher elongation before failure (1167% *vs*. 900%). It is worth noting that the specimens possessed visual similarities during uniaxial extension; $(AB)_2$-63 exhibited a large degree of stress-whitening over the course of the strain-hardening region, with almost the entire area under load becoming opaque in an identical fashion to ABA-50 (**Figure 4.8**).

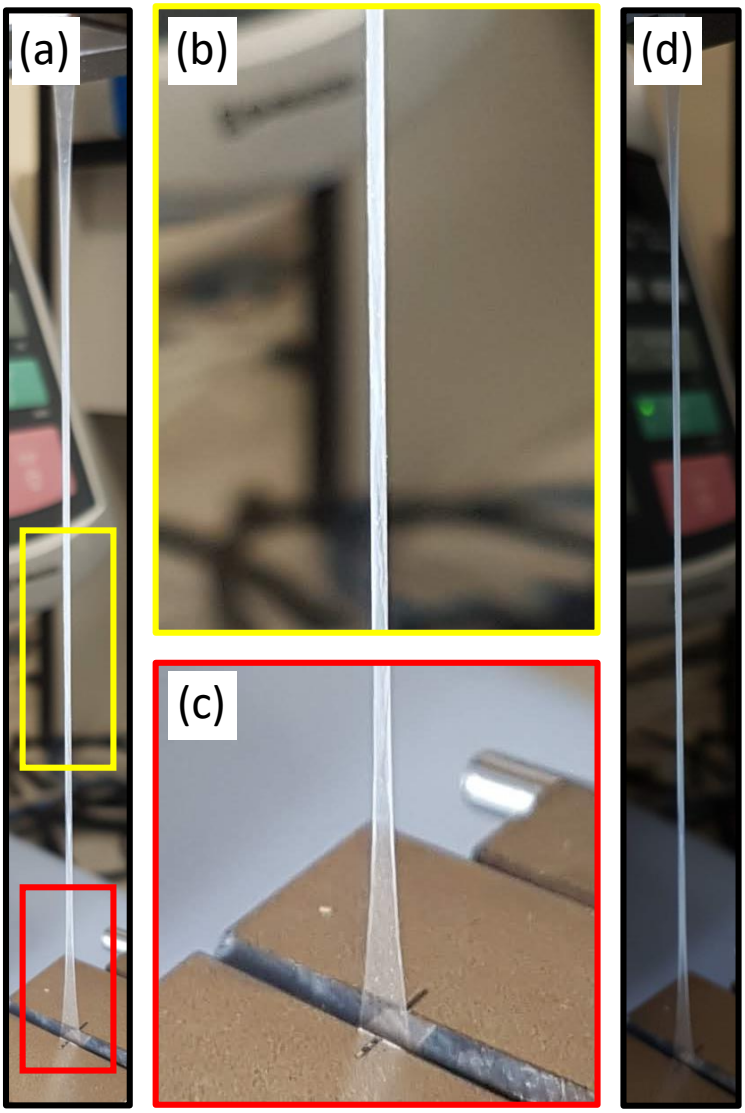


Figure 4.8. Digital photographs of sample $(AB)_2$-63 during uniaxial extension: (a) Full view of specimen with areas of interest marked; (b) Enlarged view of yellow highlighted area showing whitening of the central specimen area; (c) Enlarged view of red highlighted area showing lower extent of whitening nearer the specimen shoulder (clamped) area; (d) Full view of specimen with background light darkened to highlight contrast of stress-whitening.

Given that the relative block ratio in all samples was targeted at 50 wt %, the higher arm (n ≥ 3) star block polymer samples showed broadly similar mechanical behaviour to the linear comparison insofar as the stress-strain profile shapes and defining features were characteristic of a ductile plastic. However, particular samples showed exception and relationships were observed between overall molar mass, arm number, and mechanical characteristics.

The first higher star block polymer to be tested was $(AB)_3$-52 which revealed an immediate deviation from ductile plastic behaviour. The film obtained from solvent casting was soft and highly flexible, almost at the threshold of easy manipulation outside of the mould. Uniaxial extension experiments showed characteristically soft plastic behaviour, with specimens possessing a low Young's modulus (E_y = 7.2 MPa), a diffuse yield point and low resistance to plastic deformation ending with failure at very low tensile stress (σ < 1 MPa) and moderate strain (ε_b = 663%) (**Table 4.3**, entry 3 and **Figure 4.9**).

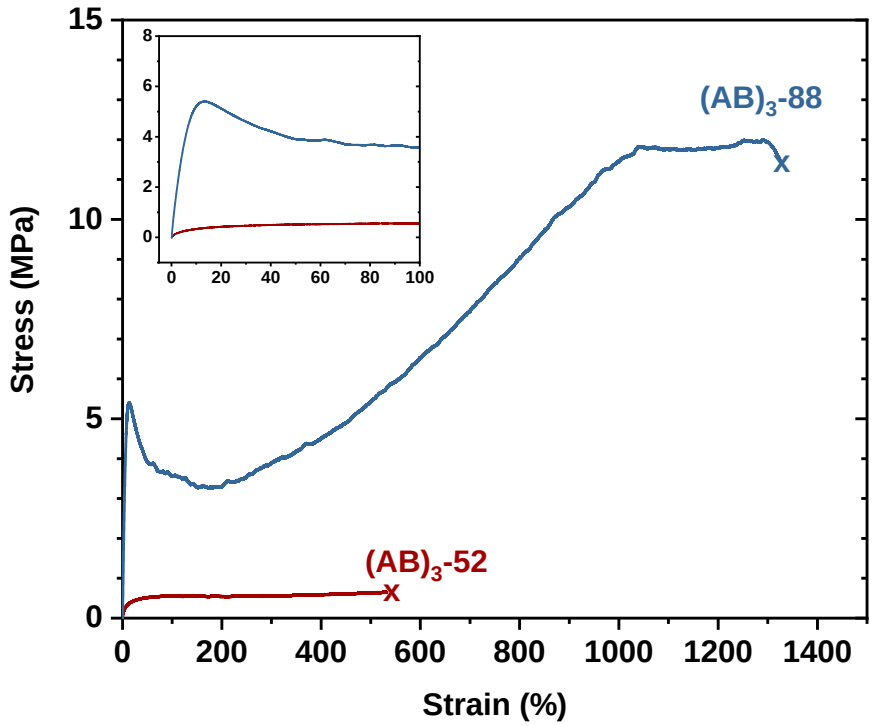


Figure 4.9. Representative stress-strain curves for 3-arm star block polymers of low (52 kg mol^{-1}) and high (88 kg mol^{-1}) molar mass. Failure points marked with an "X". Inset: enlargement of 0-100% strain region.

In contrast, when the molar mass of the 3-arm star polymer was increased to 88 kg mol^{-1} the mechanical properties were greatly improved. This was to be expected, given increased molar mass usually improves mechanical performance, however it can sometimes be at the expense of processing capability. Fortunately, $(AB)_3$-88 was still readily processed *via* solvent-casting methods and produced free-standing films that were easily handled outside of the mould. The specimens were tangibly more ductile and tougher which was reflected in the stress-strain curve (**Figure 4.9**).

The increased molar mass saw a 10-fold increase to the Young's modulus and a more defined yield point (σ_y = 4.8 MPa, ε_y = 14%) which in turn provided a more reliable boundary in which the material should exhibit elastic behaviour. After yielding in the low strain region, $(AB)_3$-88 displayed enhanced ductility with a large period of plastic deformation which

included a region of strain hardening, ultimately reaching a tensile stress of 12 MPa before necking and failing at 1500% elongation. Based on the marked enhancement to both the thermal and mechanical properties, subsequent star block polymers aimed to achieve molar masses exceeding the original 50 kg mol^{-1} target.

The 4-arm star sample, $(AB)_4$-90, had around the same molar mass as $(AB)_3$-88 so provided a useful comparison between 3- and 4-arm architectures at equal overall molar mass. Tensile analysis revealed the 4-arm star block polymer to be mechanically inferior in terms of strength, possessing a tensile strength of around 6.8 MPa (**Table 4.3**, entry 5). The lower Young's modulus also indicated a softer material, and the shape of the stress-strain profile suggested somewhat reduced ductility and toughness (**Figure 4.10**). The sample still exhibited strain hardening but to a lesser degree as identified by a shallower incline in the higher strain region (above 300%). Moreover, the yield point was considerably less prominent, which altogether gave a profile with fewer well-defined features compared to both the 3-arm and linear samples.

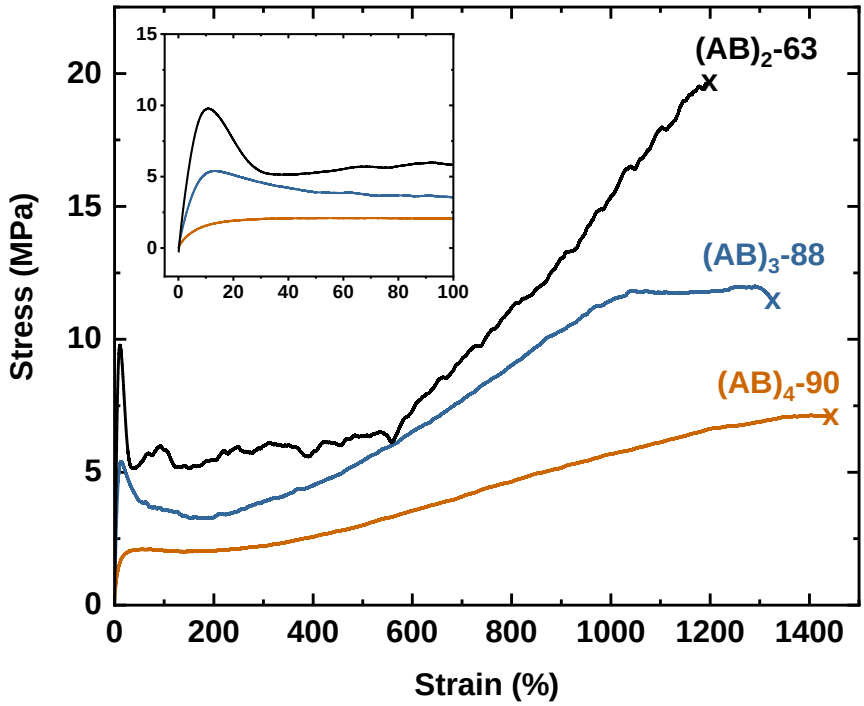


Figure 4.10. Representative stress-strain curves for high molar mass star block polymers with 2, 3, and 4 arms. Inset: enlargement of 0-100% strain region.

Interestingly, neither $(AB)_3$-88 nor $(AB)_4$-90 exhibited any stress-whitening, which set them apart from the linear analogue and suggested a direct effect of the change in architecture, given that specimen size, thickness, and processing conditions were identical between samples (**Figure 4.11**). Whether or not the absence of stress-whitening is a beneficial characteristic is likely to be application-dependent. One clear advantage is the retention of optical clarity and transparency at stresses above the yield point. On the other hand, the presence of stress-whitening is often a good visual indicator for high stress or fatigue in materials, usually preceding failure, and can also provide some improvement to stress dissipation. In any case, the potential to alter the fracture dynamics of these polymers through a change in architecture is an interesting concept.

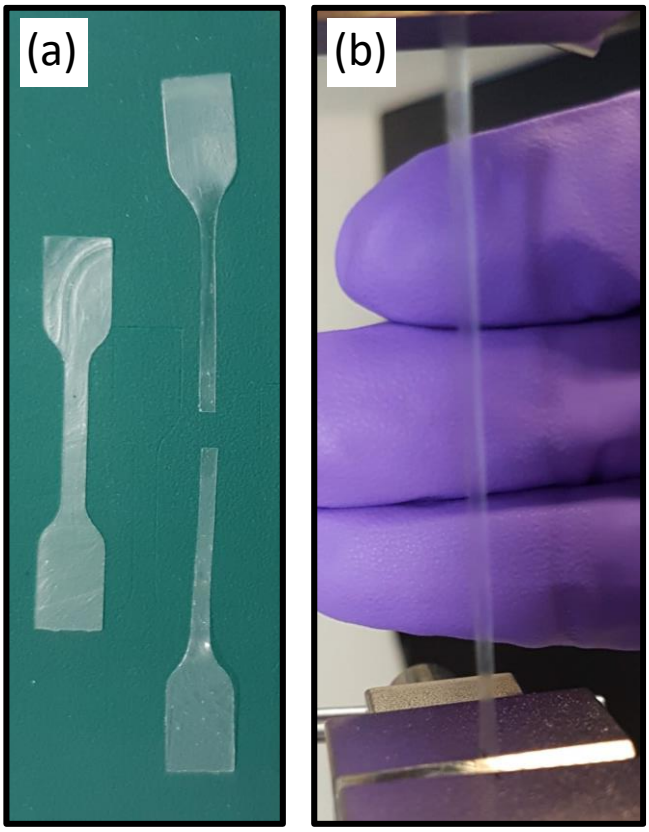


Figure 4.11. Digital photographs of sample $(AB)_3$-88: (a) Pristine and fractured test specimens before and after uniaxial extension, respectively; (b) Central region of a sample during uniaxial extension with absence of stress-whitening.

Overall, $(AB)_2$-63 was mechanically superior to all of the multi-arm star polymers despite it having a lower overall molar mass compared to all but $(AB)_3$-52. Indeed, the 6-arm star sample, $(AB)_6$-72, was unable to form a free-standing film when processed *via* solvent casting even though its overall molar mass (72 kg mol^{-1}), while not quite equal to the 3- and 4-arm counterparts, was still relatively high for these polymers.

Although $(AB)_2$-63 has a slightly lower overall molar mass than the higher molar mass 3- and 4-arm samples, the tensile mechanical data suggest there is feasibly a limiting molar mass for mechanical robustness specific to these particular polyester-polycarbonate block polymers. This can be better illustrated with reference to arm molar mass ($M_{n,arm}$), which allows for comparison and translation between different arm numbers and, therefore, architectural variance (**Figure 4.12**). With increasing $M_{n,arm}$, characteristics relating to

strength and stiffness like tensile stress and Young's modulus increased. Elongation a break decreased somewhat with increasing $M_{n,arm}$ for the higher molar mass samples, although the values remained in excess of 1000% and also had the largest statistical errors; the low ε_b observed for $(AB)_2$-52 could be a result of ineffective stress distribution owing to incomplete microphase separation in the sample.

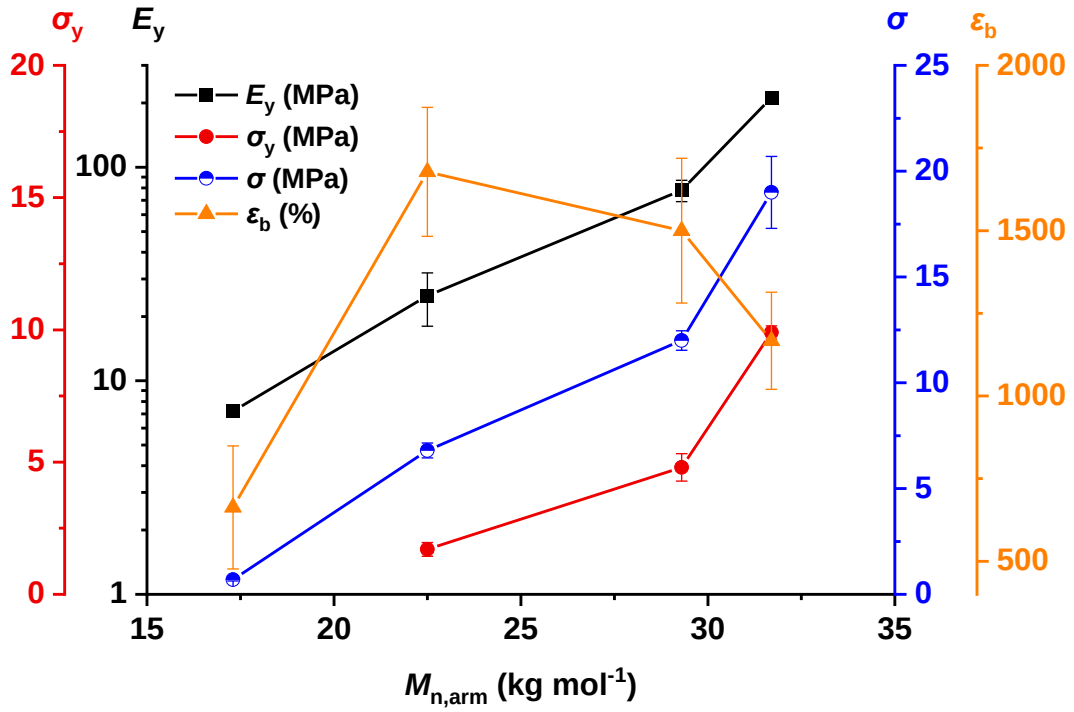


Figure 4.12. Trends in yield stress (σ_y), Young's modulus (E_y), tensile stress (σ), and elongation at break (ε_b) with respect to arm molar mass ($M_{n,arm}$) across the range of $(AB)_n$ star block polymers. Lines are used to help guide the eye.

In the case of these $(AB)_n$ star block polymers, for the mechanical performance of a sample with higher n to equal or surpass that of a lower n sample then it is likely that $M_{n,arm}$ must be equivalent across samples or possibly even higher with increasing values of n, a concept identified for (PSt-*b*-PIB)$_{5\text{-}21}$ star polymers and since observed for other systems, yet some reports suggest it does not apply as a general rule.[3, 7-9] However, for these PvCHC-*b*-PDL star block polymers the system is then subsequently limited by the overall molar mass

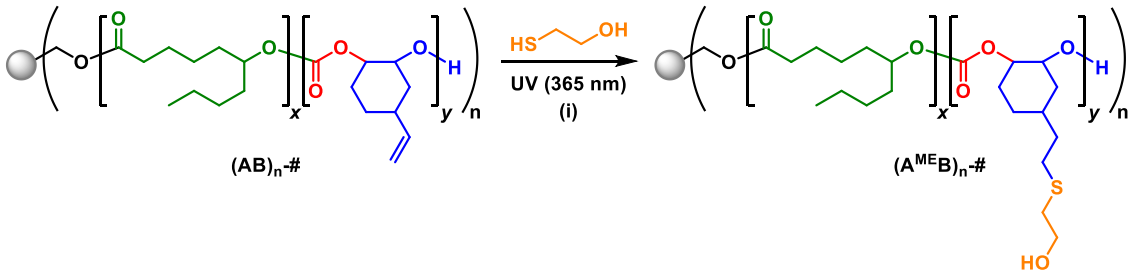
achievable with the current catalyst and/or conditions. Empirically, an overall molar mass of ~63 kg mol^{-1} for a linear sample was sufficient to provide good mechanical performance, although it should be noted this is not the proven lower limit and future research into these polymers should aim to determine this value. Nonetheless, it equates to an $M_{n,arm}$ of 31.5 kg mol^{-1} which gives an estimate for the hypothetical minimum overall M_n for analogous 4- and 6-arm samples of 126 and 189 kg mol^{-1}, respectively. Currently, molar masses as high as this have yet to be achieved for these block polymers, regardless of arm number.

4.5. Post-polymerisation modification of the polycarbonate block

A common strategy to enhance the performance or particular functionality of a polymer is post-polymerisation modification. Here, thiol-ene click chemistry was employed to install pendent hydroxyl moieties along the polycarbonate block of each star arm (**Scheme 4.3**). It was hypothesised that this should increase block immiscibility and improve the strength of intermolecular bonding within the hard domains of microphase separated structures through hydrogen-bonding.

The resulting modified star polymers were denoted $(A^{ME}B)_n$-#, where A^{ME} = PvCHC functionalised with 2-mercaptoethanol, B = PDL, n = number of arms, and # = molar mass, in this case of the precursor star polymer for ease of comparison. It should also be noted that after functionalisation the relative block ratio is increased for each star block polymer to a higher hard block weight fraction, approximately 60 wt %.

Scheme 4.3. Post-Polymerisation Modification of $(AB)_n$ Star Block Polymers.[a]



[a]Reaction conditions (equiv. w.r.t. C=C moiety): (i) 2-mercaptoethanol (4 equiv.), 2,2-dimethoxyphenylacetophenone (DMPA) (0.4 equiv.), THF, UV (365 nm), 2 h.

Thermal characterisation of the modified star polymers by DSC revealed two glass-transition temperatures, one at low temperature (-47 to -49 °C) and one at high temperature (+59 to +76 °C) corresponding to the soft polyester blocks and hard hydroxyl-functionalised polycarbonate blocks, respectively (**Table 4.4**). Compared to the non-modified star samples, the more pronounced upper transitions gave evidence for better microphase separation

across all materials, particularly samples $(A^{ME}B)_3$-52 and $(A^{ME}B)_6$-72 where their precursors indicated more block miscibility.

Table 4.4. $(A^{ME}B)_n$ Modified Star Block Polymer Thermal Characterisation Data

Entry	Polymer[a]	$T_{g,DSC}$[b] (°C)	$T_{g,DMTA}$[c] (°C)
1	$(A^{ME}B)_2$-63	-49; +76	+99
2	$(A^{ME}B)_3$-52	-48; +64	+90
3	$(A^{ME}B)_3$-88	-49; +65	+95
4	$(A^{ME}B)_4$-90	-49; +59	+87
5	$(A^{ME}B)_6$-72	-47; +61	+79

[a]$(A^{ME}B)_n$-#; A^{ME} = OH-functional PvCHC, B = PDL, n = number of arms, # = molar mass (SEC). [b]Glass transition temperatures determined by DSC (-90 – 120 °C) from the midpoint of transition in the third heating cycle (Appendix Figures S7.52 – 7.56). [c]Upper glass transition temperature determined from a DMTA thermal sweep (30 – 110 °C), taken as the peak maxima in tan(δ) (Appendix Figures S7.57 – 7.61).

Studying the mechanical behaviour of the materials as a function of temperature using a DMA temperature sweep from 30 - 110 °C showed further evidence of the upper glass-transition corresponding to the hard polycarbonate block (**Table 4.4**). The peak maxima in tan(δ) was prominent and in each case at a higher value compared to that which was observed for those non-modified star precursors which could be analysed by this technique (Appendix Figures S7.57 – 7.61). This was perhaps most clearly illustrated for the sample pair of $(AB)_3$-88 and $(A^{ME}B)_3$-88 (**Figure 4.13**). Additionally, post-functionalisation resulted in improved thermal stability with respect to mechanical properties as identified by the extended plateau region of *E'* and its later point of decline. This indicated that the mechanical performance of the modified star block polymers should be better maintained at elevated temperatures closer to the upper glass transition temperature compared with the non-modified variants.

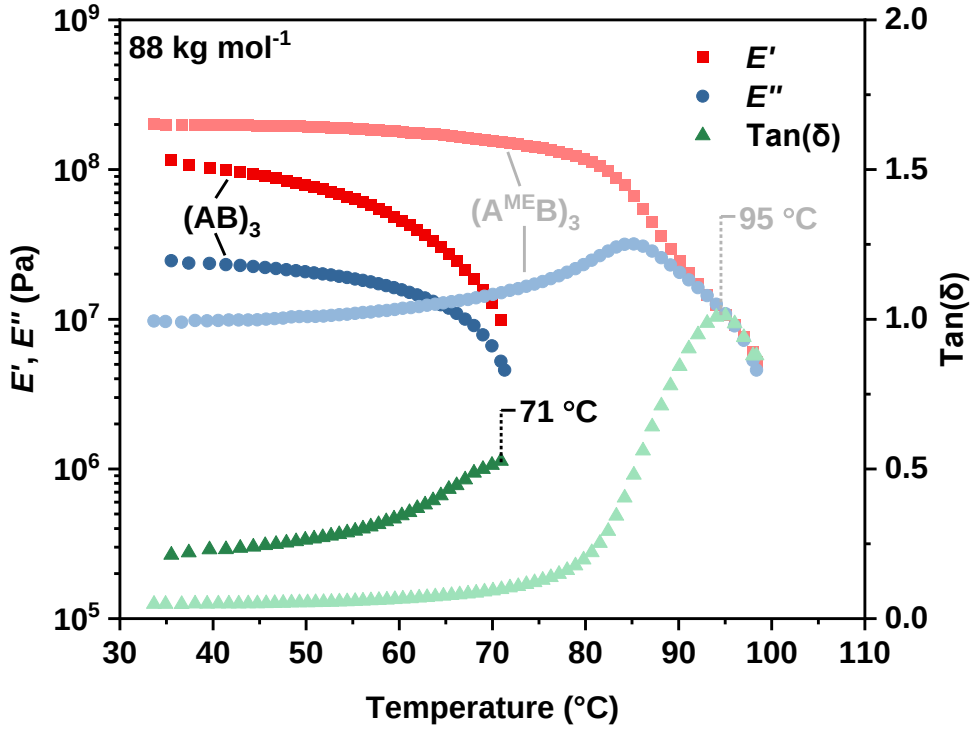


Figure 4.13. DMA thermal sweeps for high molar mass, non-modified ($(AB)_3$) and modified ($(A^{ME}B)_3$) 3-arm star block polymers. T_g values highlighted as the peak maxima on the tan(δ) curve.

The separation between the dynamic moduli was increased for all specimens after functionalisation, in most cases arising as a lower viscous component (decreased *E''*) and higher elastic component (increased *E'*). This should correlate to a stiffer material with a lower degree of damping, as more energy is stored rather than dissipated.

Despite the difference in molar mass between the two 3-arm samples, only a slight increase in the temperature at which tan(δ) peaked was observed for the higher molar mass sample and little difference in the degree of damping (**Figure 4.14**). This was an interesting observation given the stark contrast observed in thermal transitions and mechanical properties of the two precursor samples.

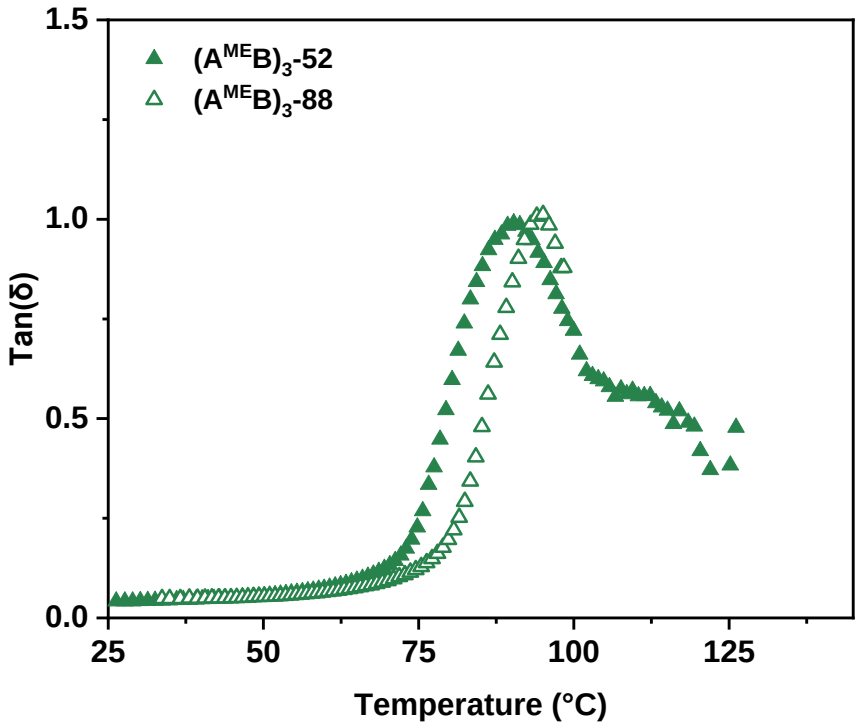


Figure 4.14. Tan(δ) versus temperature for 3-arm, modified star block polymers at high and low molar mass.

The overall trends in tan(δ) maxima across the range of arm numbers for both precursors and modified stars can also be visualised in the graph below (**Figure 4.15**). A downward trend, that is decreasing temperature at tan(δ) maximum with increasing arm number, was observed for the range of modified star polymers. Non-modified samples showed a steep drop of around 20 °C going from 2- to 3-arm samples and then a slight increase from 3- to 4-arm, albeit by only 2 °C. Further illustrated is the greater difference between precursor and modified T_g for 3-arm and higher star samples compared with the linear analogue, the latter only differing by 8 °C. This indicated a greater benefit of functionalisation for the star architectures compared to the linear sample in enhancing the microphase separation.

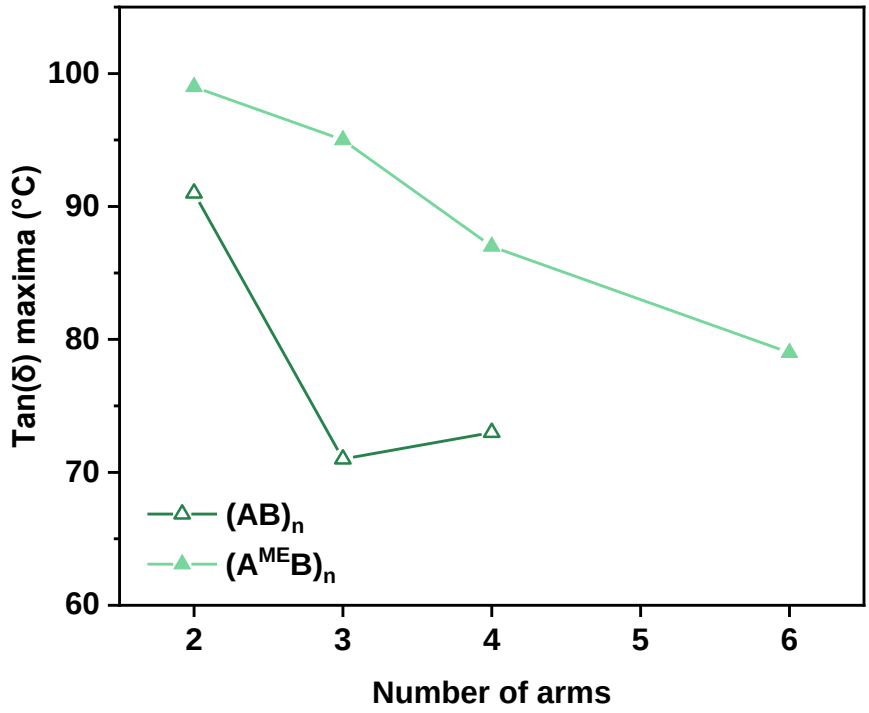


Figure 4.15. Plot of the peak maxima in tan(δ) from DMA against number of arms for non-modified and modified star block polymers.

Tensile testing of the modified star block polymers was performed on specimens cut from solvent cast films, and their mechanical properties determined from the stress-strain profiles produced by uniaxial extension experiments (**Table 4.5**). All samples showed comparable values for Young's modulus which indicated similar stiffness in the elastic deformation region. Moreover, each higher arm star polymer (n = 3, 4, 6) showed an increased E_y compared to its respective precursor material, with the largest quantifiable improvement observed for $(A^{ME}B)_3$-52. Notably, functionalisation of the linear analogue in $(A^{ME}B)_2$-63 appeared to show detrimental effects across all mechanical properties, whereas higher arm samples were, to varying degrees, enhanced in terms of strength and stiffness.

Table 4.5. $(A^{ME}B)_n$ Modified Star Block Polymer Mechanical Characterisation Data

Entry	Polymer	E_y[a] (MPa)	σ_y[b] (MPa)	ε_y[c] (%)	σ[d] (MPa)	ε_b[e] (%)
1	$(A^{ME}B)_2$-63	172 ± 23	5.3 ± 1.1	5.4 ± 0.8	10 ± 1.5	550 ± 205
2	$(A^{ME}B)_3$-52	165 ± 15	7.4 ± 0.6	7.2 ± 1.2	12 ± 1.0	1051 ± 115
3	$(A^{ME}B)_3$-88	186 ± 20	6.2 ± 1.5	5.9 ± 1.1	12 ± 4.0	661 ± 254
4	$(A^{ME}B)_4$-90	169 ± 10	6.9 ± 0.3	6.3 ± 0.3	8.5 ± 0.6	737 ± 67
5	$(A^{ME}B)_6$-72	156 ± 13	6.5 ± 0.5	8.3 ± 1.0	11 ± 1.4	615 ± 161

[a]Young's modulus. [b]Yield stress. [c]Yield strain. [d]Tensile strength. [e]Elongation at break. Average values and standard deviation from a minimum of 5 specimens.

The effect that the difference in molar mass between the two 3-arm samples had on the mechanical performance in the non-modified versions was significantly less pronounced after functionalisation (**Figure 4.16**). The higher molar mass sample may have exhibited a slightly larger degree of strain hardening as illustrated in the representative stress-strain profiles, but average values from a number of specimens gave comparable results for tensile stress. Furthermore, a greater elongation at break was now observed for $(A^{ME}B)_3$-52 resulting in a large increase to the material's ductility compared with its precursor. In contrast, $(A^{ME}B)_3$-88 saw a considerable reduction in its extensibility, suggesting that lower molar mass samples may be more amenable to post-polymerisation modification strategies which target improvements to strength.

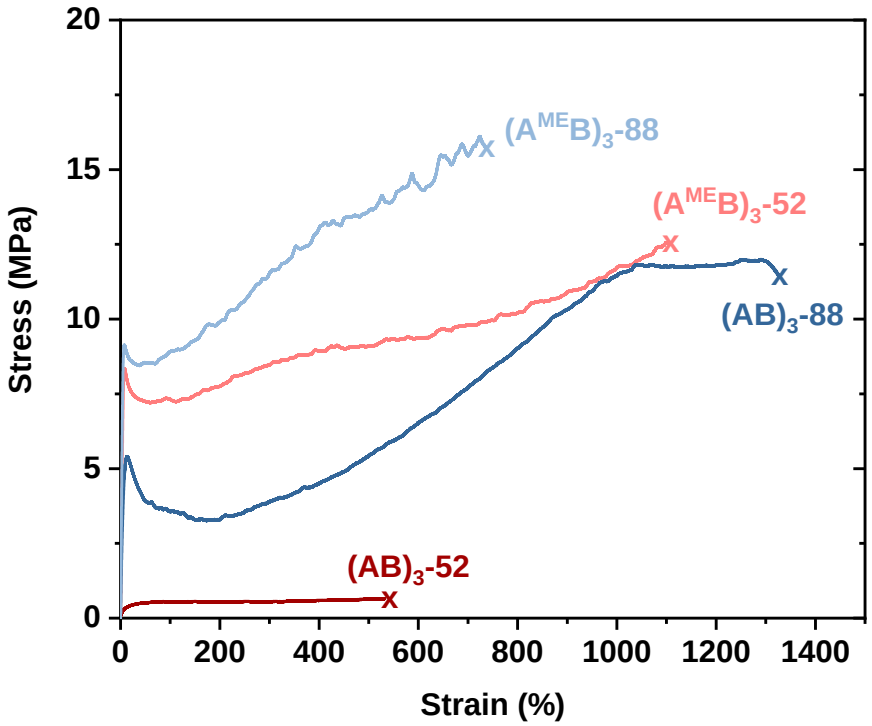


Figure 4.16. Stress-strain profiles for non-modified ($(AB)_3$-#) 3-arm star block polymers and their modified analogues ($(A^{ME}B)_3$-#) at high and low molar mass.

Broadly similar stress-strain profile shapes were observed for the higher molar mass samples with varying arm numbers (**Figure 4.17**). The degrees of strain hardening illustrated in the representative curves and mean values for yield stress and strain were comparable across samples, regardless of arm number. Tensile stress and elongation at break values were also broadly similar across samples but with slightly greater variance. The data suggested that a limit had been reached, possibly due to the greater block immiscibility after modification resulting in all samples sharing a similar phase-separated microstructure and hence similar mechanical performance.

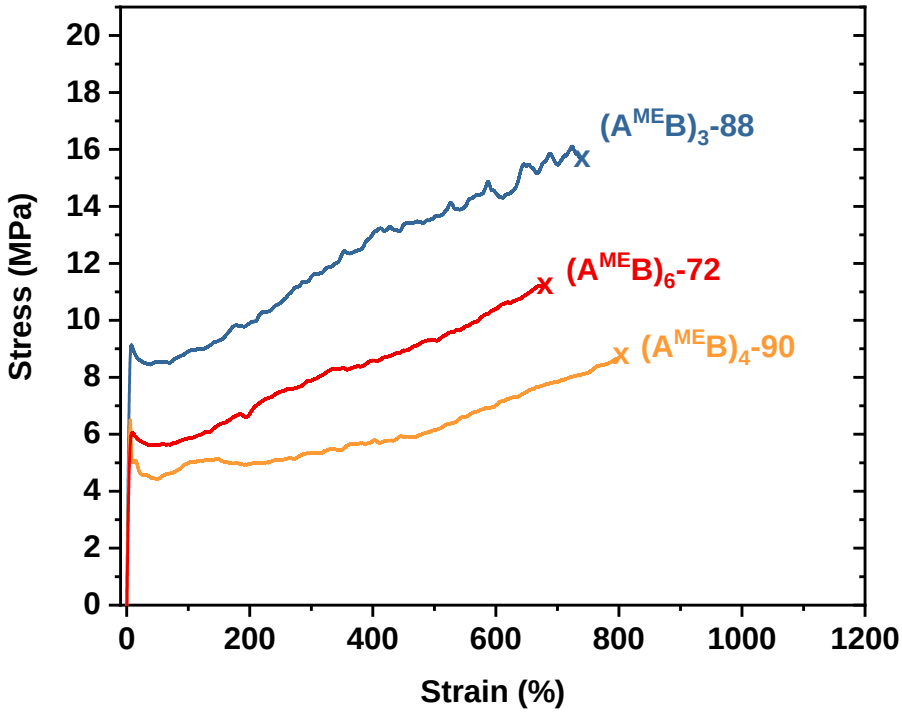


Figure 4.17. Stress-strain curves for modified star block polymer samples, $(A^{ME}B)_n$, with n = 3, 4, and 6 arms. Failure points marked with an "X".

Small-angle X-ray scattering (SAXS) experiments were conducted on non-modified, $(AB)_n$, and modified, $(A^{ME}B)_n$, thin film samples to determine the phase morphology of the star block polymers and probe the effect of post-polymerisation modification on the microstructure. 1D SAXS patterns were plotted as scattering intensity ($I(q)$) against scattering vector (q) and higher order peak positions were indexed relative to the principal scattering peak (q^*) (**Table 4.6**).

Table 4.6. Small-Angle X-ray Scattering (SAXS) Data of $(A^{[ME]}B)_n$ Star Block Polymers

Entry	Polymer	Observed q/q^*[a]	q^*[b] (nm^{-1})	d^*[c] (nm)	Morphology[d]
		Non-modified			
1	$(AB)_2$-63	1	0.332	18.9	*n.d.*
2	$(AB)_3$-52	1	0.452	13.9	*n.d.*
3	$(AB)_3$-88	1	0.375	16.8	*n.d.*
4	$(AB)_4$-90	1	0.438	14.3	*n.d.*
		Modified			
5	$(A^{ME}B)_2$-63	1, 2, 3, (4)	0.206	30.5	LAM
6	$(A^{ME}B)_3$-52	1, 2, 3, 4, 5	0.314	20.0	LAM
7	$(A^{ME}B)_3$-88	1, 2, 3, (4)	0.238	26.4	LAM
8	$(A^{ME}B)_4$-90	1, (2), 3	0.293	21.4	LAM

[a]Observed Bragg reflections, brackets indicate broad and/or near-absent higher-order reflections. [b]Principal scattering peak. [c]Domain spacing, calculated from the principal scattering peak, $d^* = 2\pi/q^*$. [d]Phase morphology (domain microstructure) assigned according to SAXS data; LAM = lamellar, *n.d.* = no assignment possible due to absence of higher order scattering peaks, likely weakly ordered/disordered. See Appendix Figures S7.62 – 7.69 for 1D SAXS patterns.

Non-modified star block polymers displayed only the principal scattering peak, q^*, with varying degrees of broadness which indicated a weakly ordered or disordered system (**Table 4.6**, entries 1-4). The broadest and least intense q^* peak was observed for $(AB)_3$-52 suggesting that this material had the highest probability of being in a disordered state (Appendix Figure S7.64). This correlated with the idea of partial block miscibility identified by the broad, shifted T_g in the DSC, as well as the poor performance in mechanical testing.

In all non-modified samples, the absence of higher order scattering peaks prevented the determination of phase morphology, but the position of q^* allowed for the calculation of the principal domain spacing, d^*. The largest domain spacing of 18.9 nm was observed for the linear analogue ($(AB)_2$-63) while the low molar mass 3-arm star ($(AB)_3$-52) showed the smallest spacing at 13.9 nm, however it should be noted that this value is speculative given the broadness of q^* and the likelihood of a disordered system (**Figure 4.18**). Comparing the three higher molar mass samples, $(AB)_2$-63, $(AB)_3$-88, and $(AB)_4$-90, revealed an inverse relationship between domain spacing and arm number – d^* decreasing with increasing n

(**Table 4.6**, entries 1, 3, 4). A similar relationship was observed for (PDL-*b*-PLLA)$_{2\text{-}6}$ star polymers of equal overall molar mass and relative hard/soft block ratio.[3]

Modified star block polymers showed sharper principal scattering peaks compared to their non-modified counterparts, as well as higher-order scattering peaks at positions equivalent to integer values of q/q^* which indicated microstructures with long-range order (**Table 4.6**, entries 5-8). Indexing of the peak positions identified the morphology as lamellar (LAM), which is expected for symmetric star polymers with equal arm lengths at $f \sim 0.5$ (**Figure 4.18**).[10]

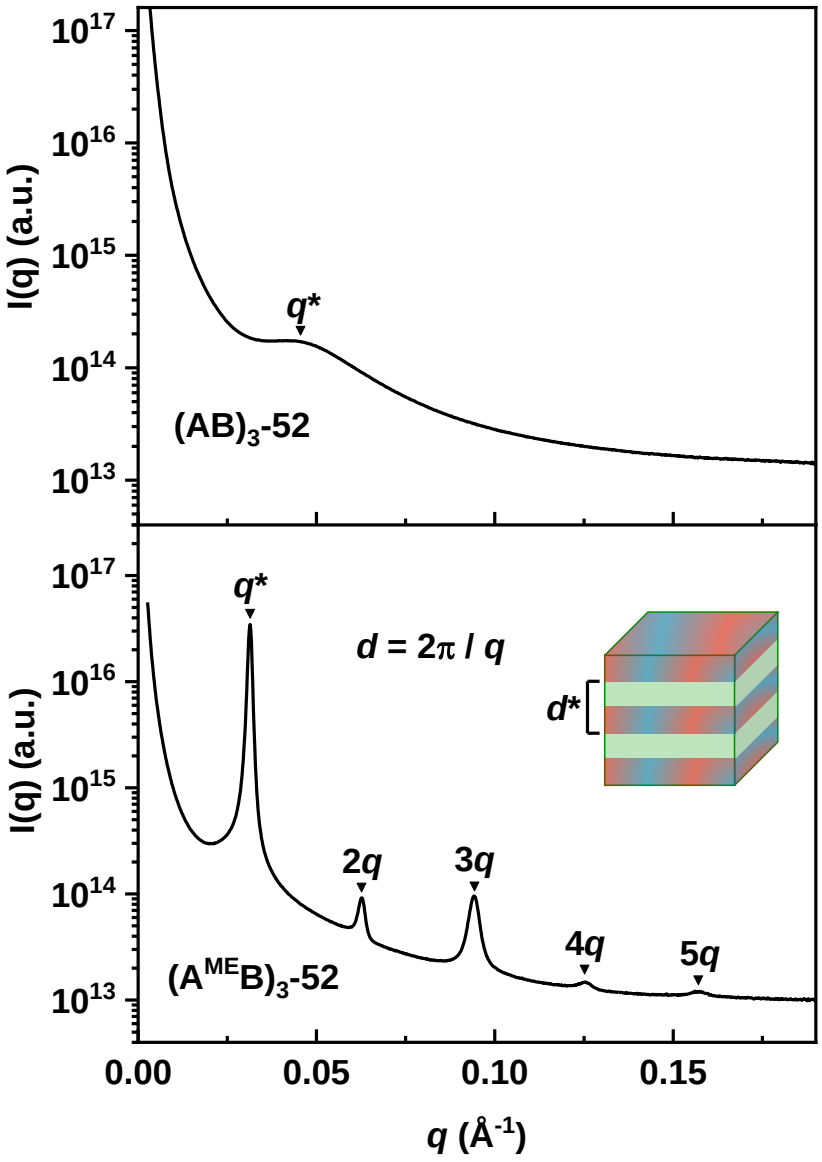


Figure 4.18. 1D SAXS profiles for non-modified ($(AB)_3$-52) and modified ($(A^{ME}B)_3$-52) star block polymers. $(A^{ME}B)_3$-52 indexed for lamellar morphology, *d** represents domain periodicity.

The principal domain spacing values calculated for the modified star polymers were larger and ranged from 20.0 – 30.5 nm. The same trend as with the non-modified specimens was observed across the samples, with the linear polymer $(A^{ME}B)_2$-63 showing the largest domain spacing and $(A^{ME}B)_3$-52, the smallest. The inverse relationship between *d** and *n* was again observed when comparing the series of higher molar mass samples: $(A^{ME}B)_2$-63,

$(A^{ME}B)_3$-88, and $(A^{ME}B)_4$-90 (**Table 4.6**, entries 5, 7, 8). Furthermore, a plot of d^* against $M_{n,arm}$ for both non-modified and modified samples highlights the overall shared trend of increased domain size with increasing arm molar mass (assumed to be proportional to arm size or length) (**Figure 4.19**).

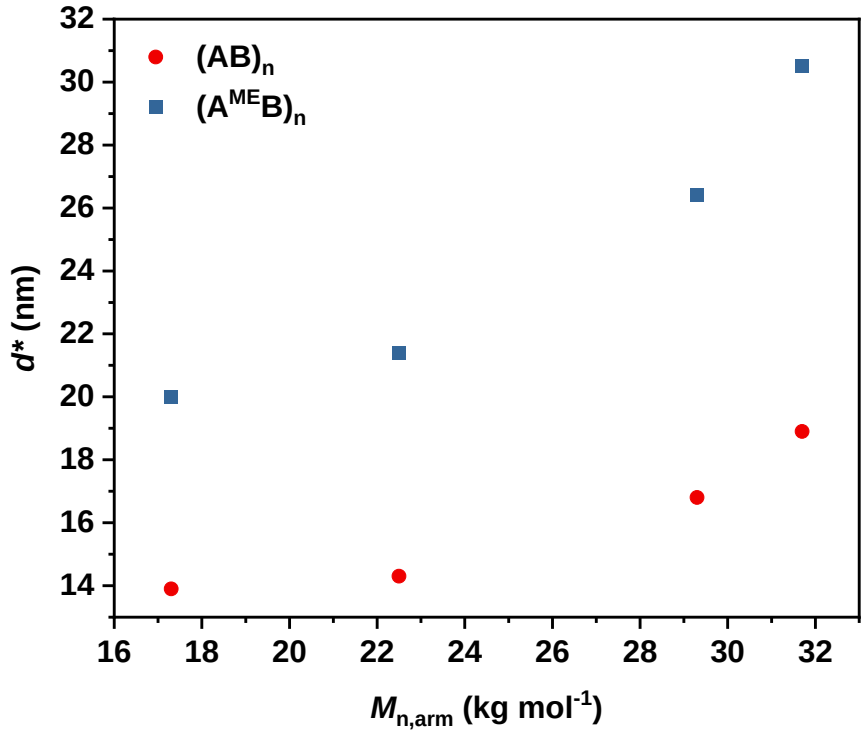


Figure 4.19. Plot of domain spacing (d^*) against arm molar mass ($M_{n,arm}$) for the series of non-modified ($(AB)_n$) and modified ($(A^{ME}B)_n$) star block polymers.

Interestingly, $(A^{ME}B)_3$-52 showed the largest number of scattering peaks (5), with sequentially fewer higher-order peaks observed for the polymer samples with increasing overall molar mass. In most samples, the higher order reflection corresponding to $2q$ showed diminished intensity compared to neighbouring q^* and $3q$ (Appendix Figures S7.63, 7.65, 7.67, 7.69). Reduced intensity, or in some cases near absence, of $2q$ scattering is consistent with a structure factor extinction for compositionally symmetric, two-domain lamellar samples.[11-12]

4.6. Summary and future work

A series of multi-arm (2-, 3-, 4-, 6-arm) star block polymers, each arm comprising a PDL-*b*-PvCHC diblock polymer, were prepared *via* a core-first approach utilising a switchable polymerisation catalysis technique and multifunctional alcohol initiators. Ring-opening polymerisation of ε-DL was followed by the ring-opening copolymerisation of vCHO and CO_2 to fashion polyester interior blocks and polycarbonate exterior blocks, respectively. The relative ratio between hard (PvCHC) and soft (PDL) blocks was fixed, according to starting monomer stoichiometry, at 50 wt % and the overall molar masses (M_n) ranged from 52 – 90 kg mol^{-1}. A thiol-ene post-polymerisation modification technique subsequently installed a pendent hydroxyl moiety in the repeat unit of the PvCHC blocks.

The thermal, mechanical, and morphological properties of the star block polymers were analysed using a combination of DSC, DMA, tensile testing, and SAXS which revealed properties characteristic of ductile plastics with, in the case of hydroxyl-modified samples, a clearly-defined lamellar morphology. Non-modified star polymers showed some evidence of block miscibility whereas modified analogues showed evidence for improved microphase separation. In the case of non-modified star polymers at similar overall molar mass, increasing the number of star arms resulted in inferior tensile strength and stiffness. A trend was identified which correlated increased strength and stiffness with increasing star arm molar mass, and accounted for variations in arm number and overall molar mass. In contrast to analogous linear materials, the star polymers were noted for their absence of stress-whitening under tensile load which pointed to a relationship between architecture and fracture mechanics for these polymers. The modified star polymers showed considerably less variation in mechanical performance across all samples which suggested that a limit had been reached, possibly due to them now possessing very similar phase-separated microstructures.

Aspects of the future research proposed for the linear ABA triblock polymer materials investigated in Chapter 3 are naturally also applicable to the star polymers, such changing the constituent hard/soft blocks. In addition to these, and given the results of changing the architecture, several other aspects of these polymers could be further explored including: (1) probing the limits of molar mass and material processing; (2) property modification through blend formulations and ionomer formation; (3) detailed studies into fracture mechanics.

Improving the control over polymer distributions should initially be sought, not least to better understand and ideally eliminate the multimodality currently present. Following this, higher molar stars with varying arm numbers should be targeted, mindful of obtaining equivalent arm molar mass across samples. There is strong potential to achieve stars that combine high molar mass with excellent mechanical properties (superior to what could be achieved with linear polymers) while still retaining processability due to the typically lower viscosities observed in stars compared to linear analogues. At the same time, it may be beneficial to also define the lower limit of $M_{n,arm}$ and hence the minimum molar mass required to process freestanding films, and probe how the limit translates across star arm numbers.

Secondly, these star polymers may be utilised effectively in blends with other polymers or alternative components, with the aim of either improving the thermomechanical properties of the other polymer or the star itself. Good candidates for this include brittle polycarbonates like PCHC and PLimC, where the star may function as an impact modifier or facilitate compatibility (i.e. miscibility) with additional polymer components. Star polymers are also frequently applied as viscosity modifiers, so lower molar mass variants of the materials reported here could be explored in this regard as more renewable alternatives.

Building on the post-polymerisation modification of the PvCHC blocks, an additional method of altering the properties would be to install pendent moieties with an affinity for binding various metal cations. Formation of ionomers should introduce dynamic cross-linking to the PvCHC domains with the possibility of providing additional strength and/or responsive functionality depending on the choice of metal ion.

Thirdly, the observations from tensile testing such as strain-hardening and presence/absence of stress whitening prompt a more in-depth study into the fracture dynamics of these materials. Only visual, macroscopic, differences have been observed so far so it could be interesting to probe these materials' microstructures during or after they are subjected to stress to better understand the effects of changing the architecture. Combining SAXS and tensile measurements may reveal morphological changes during the period of strain-hardening as polymer chains are aligned, while optical and/or electron microscopy of the selected surfaces of a tensile specimen (e.g. gauge length width, fracture cross-section) could highlight features of crazing and fracture propagation.

4.7. References

1. Ren, J. M.; McKenzie, T. G.; Fu, Q.; Wong, E. H. H.; Xu, J.; An, Z.; Shanmugam, S.; Davis, T. P.; Boyer, C.; Qiao, G. G., Star Polymers. *Chem. Rev.* **2016,** *116* (12), 6743-6836.
2. Shim, J. S.; Asthana, S.; Omura, N.; Kennedy, J. P., Novel thermoplastic elastomers. I. Synthesis and characterization of star-block copolymers of PSt-b-PIB arms emanating from cyclosiloxane cores. *J. Polym. Sci., Part A: Polym. Chem.* **1998,** *36* (17), 2997-3012.
3. Lee, S.; Lee, K.; Jang, J.; Choung, J. S.; Choi, W. J.; Kim, G.-J.; Kim, Y.-W.; Shin, J., Sustainable poly(ε-decalactone)–poly(l-lactide) multiarm star copolymer architectures for thermoplastic elastomers with fixed molar mass and block ratio. *Polymer* **2017,** *112*, 306-317.
4. Hilf, J.; Schulze, P.; Seiwert, J.; Frey, H., Controlled Synthesis of Multi-Arm Star Polyether–Polycarbonate Polyols Based on Propylene Oxide and CO2. *Macromol. Rapid Commun.* **2014,** *35* (2), 198-203.
5. Stößer, T.; Sulley, G. S.; Gregory, G. L.; Williams, C. K., Easy access to oxygenated block polymers via switchable catalysis. *Nat. Commun.* **2019,** *10* (1), 2668.
6. Deacy, A. C.; Gregory, G. L.; Sulley, G. S.; Chen, T. T. D.; Williams, C. K., Sequence Control from Mixtures: Switchable Polymerization Catalysis and Future Materials Applications. *J. Am. Chem. Soc.* **2021,** *143* (27), 10021-10040.
7. Shim, J. S.; Kennedy, J. P., Novel thermoplastic elastomers. II. Properties of star-block copolymers of PSt-b-PIB arms emanating from cyclosiloxane cores. *J. Polym. Sci., Part A: Polym. Chem.* **1999,** *37* (6), 815-824.
8. Kwee, T.; Taylor, S. J.; Mauritz, K. A.; Storey, R. F., Morphology and mechanical and dynamic mechanical properties of linear and star poly(styrene-b-isobutylene-b-styrene) block copolymers. *Polymer* **2005,** *46* (12), 4480-4491.
9. Burns, A. B.; Register, R. A., Mechanical Properties of Star Block Polymer Thermoplastic Elastomers with Glassy and Crystalline End Blocks. *Macromolecules* **2016,** *49* (24), 9521-9530.
10. Matsen, M. W.; Schick, M., Microphase Separation in Starblock Copolymer Melts. *Macromolecules* **1994,** *27* (23), 6761-6767.
11. Epps, T. H.; Cochran, E. W.; Bailey, T. S.; Waletzko, R. S.; Hardy, C. M.; Bates, F. S., Ordered Network Phases in Linear Poly(isoprene-b-styrene-b-ethylene oxide) Triblock Copolymers. *Macromolecules* **2004,** *37* (22), 8325-8341.
12. Pitet, L. M.; van Loon, A. H. M.; Kramer, E. J.; Hawker, C. J.; Meijer, E. W., Nanostructured Supramolecular Block Copolymers Based on Polydimethylsiloxane and Polylactide. *ACS Macro Lett.* **2013,** *2* (11), 1006-1010.

CHAPTER 5

Outlook

5.1. Challenges and opportunities

The developments and innovations made in recent years in both switchable polymerisation catalysis and in the utilisation of CO_2 in polymers have already provided various promising oxygenated (block) polymers, and have highlighted the importance of both themes in the drive towards a more sustainable future for plastics.[1-2] Naturally, challenges have been recognised and remain to be dealt with, yet from these emerge further opportunities for advancement.

Areas where future research has the potential to address certain challenges and further explore the work on switch catalysis and CO_2-derived block polymers presented in this thesis are: (1) catalyst design and optimisation; (2) block accessibility; (3) high value materials; (4) structure property-relationship (**Figure 5.1**).

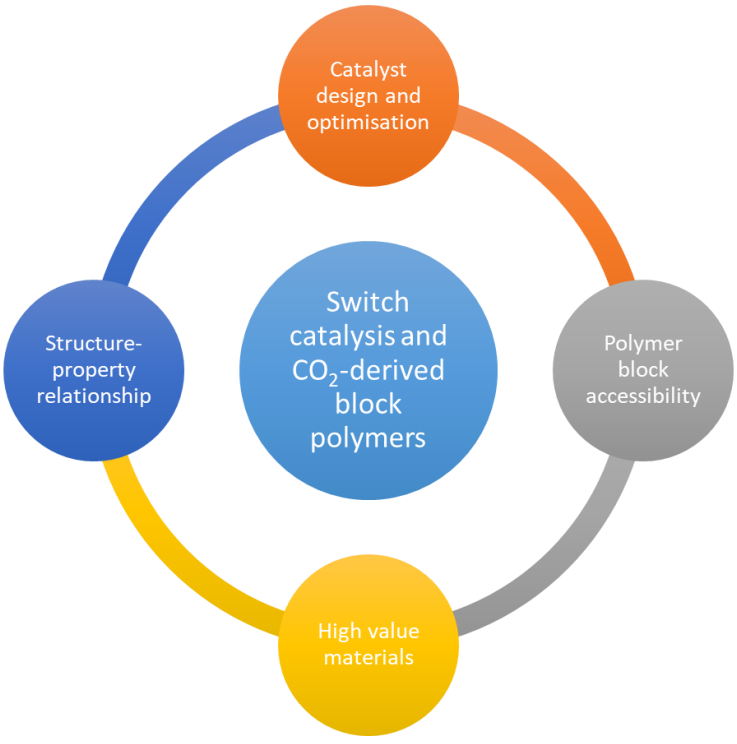


Figure 5.1. Future challenges and opportunities for switchable polymerisation catalysis and CO_2-derived polymers.

5.2. Switchable polymerisation catalysis

Switch catalysis techniques have shown their capability in delivering oxygenated block polymers, particularly with combinations of ether, ester, and carbonate linkages. Given the technique is still in a relatively early stage of development, there are plenty of opportunities still to be capitalised on in order to advance the catalysis and promote comprehensive utility.

Effective application of switchable catalysis mandates good catalytic activity across two or more distinct polymerisation cycles, but in order to prepare the desired block polymers without contamination then excellent end-group control must also be a feature. These two characteristics continue to be optimised for the various catalyst classes known to be active for "switch" or constituent polymerisation mechanisms.[3-8] For bimetallic catalysts, the current data reported separately for heterodinuclear cooperativity[9] and coligand optimisations[8, 10] suggest a promising catalyst could be a Mg(II)/Co(II) organometallic complex; combining the excellent catalytic activity from the optimised metal centre combination with the high end-group control provided by non-initiating coligands (**Figure 5.2**).

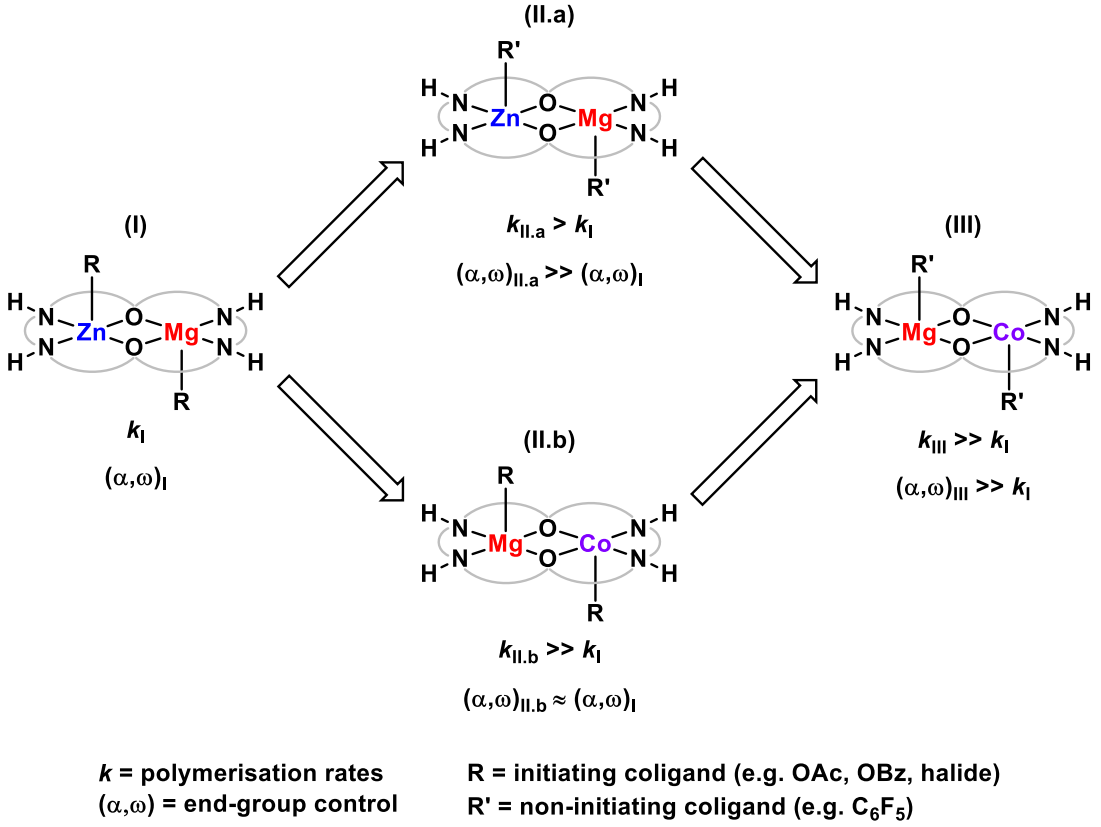


Figure 5.2. Heterodinuclear catalyst development to optimise polymerisation rates and end-group control.

Additional aspects of catalyst design and optimisation are developing their ability to access other polymerisation cycles (e.g. controlled radical) as well as improving their capability to incorporate a wider pool of monomers, particularly those derived from renewables. Addressing these challenges has the result of then further expanding the accessibility to different polymer blocks.

Examples of catalysts able to facilitate cycles involving metal-carbon chain-end intermediates as well as the metal-oxygen intermediate in ROP or ROCOP are rare, but such species could enable the preparation of copolymers with both oxygenated and acrylate/olefin blocks. To some degree this has been showcased using a Co(II) salen type catalyst to synthesise poly(vinyl acetate)-*b*-polycarbonate, but the process required intermediary purification of the poly(vinyl acetate) after an oxidative switch to facilitate the subsequent

epoxide/CO_2 ROCOP.[11] Taking inspiration from this, the immediate goal would be to avoid intermediary purification, instead having the catalyst facilitate the switch *in-situ* to prepare the block copolymer in a one-pot fashion.

Another aspect of the switch that warrants further exploration is the extent to which catalysts can fashion higher order or more complex block polymers while maintaining sequence control. Employing multiple sequential switches, for example by cycling back-and-forth between N_2 and CO_2 atmospheres with a mixture of lactone and epoxide monomers and a diol initiator, should result in the controlled enchainment of additional blocks, ultimately building oxygenated multiblock polymers (**Figure 5.3**). This strategy would depend heavily on the catalyst's tolerance to low loadings, multiple additions of monomer (e.g. if using anhydrides) and the potential impurities introduced *via* the gas streams with each successive switch, but similar considerations are applicable to most catalyses and features such as monomer purity are under constant scrutiny.

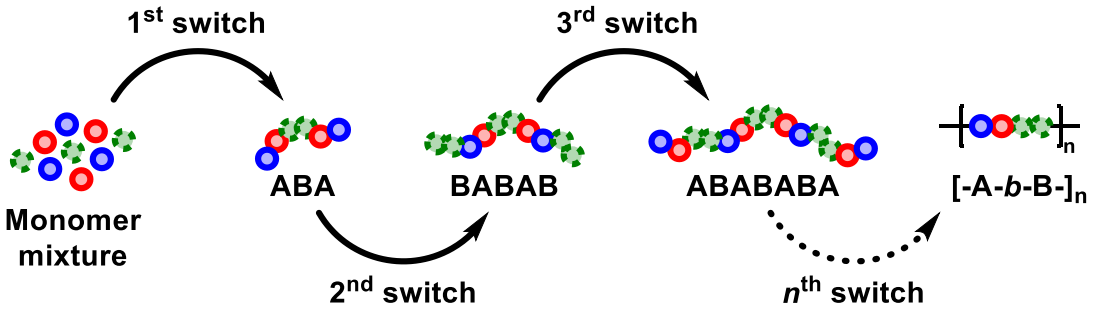


Figure 5.3. Multiple sequential switches to build [A-*b*-B]$_n$ multiblock polymers from a single starting monomer mixture.

5.3. High performance materials

As the field of switchable polymerisation catalysis is still in its early stages, the property profiles of many oxygenated multiblock polymers are not well examined, and high value applications for CO_2-derived polymers in particular are also underexplored. However, there is increasing incentive to target oxygenated polymers for various high profile applications, for example solid electrolytes[12-13] or tissue scaffolds[14], and switch catalysis is expected to play a major role in delivering diverse sequence controlled polymers with tuneable properties.

In addition to their potential as standalone materials, a future direction for select CO_2-derived block polymers may be their utilisation in blend formulations. It's possible they could act as compatibilisers or impact modifiers, adding value and increasing toughness of otherwise brittle materials like bulk CO_2-polycarbonates. By virtue of their degradability, they may also allay concerns surrounding the leaching and environmental pervasiveness of additives or plasticisers.

One interesting route to improve the properties of the current CO_2-derived block polymers is to explore the formation of dynamic networks, particularly within the microphase separated domains, using strategies that introduce reversible cross-linking (**Figure 5.4**). Several reports have detailed the preparation of ionomers or dynamically cross-linked networks based around polyesters, -ethers, and –carbonates which show enhanced strength and toughness, and in some cases self-healing capabilities.[15-17]

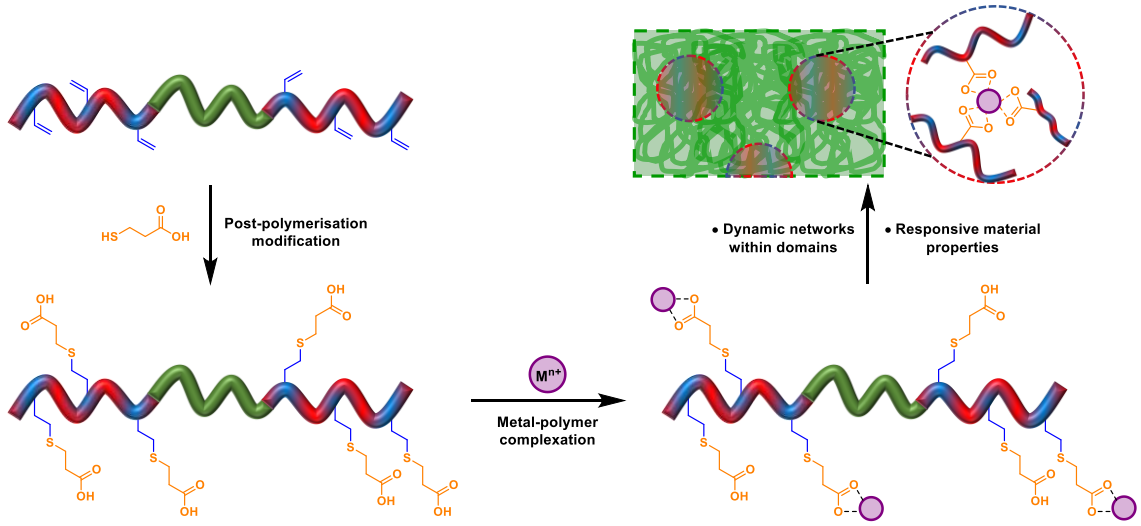


Figure 5.4. Formation of ionomers to promote dynamic cross-linking in block polymer domains and target enhanced properties or responsive behaviour.

Research is currently being carried out on the CO_2-derived poly(ester-*b*-carbonate) triblock and star block polymers to explore the formation of ionomers through metal-polymer complexation. It is anticipated that the mechanical performance of these polymers could be enhanced by establishing dynamic cross-links, with the potential that characteristics are responsive or tuneable based on the binding moiety and/or metal cation used.

5.4. Architectural control

An immediate aim for the work on architectural control in switch catalysis is to improve and optimise the multiarm star block poly(ester-*b*-carbonate)s. The preparation of an expanded series of samples that encompasses a larger variation in molar mass as well as equivalent arm molar masses across multiple arm numbers would encourage better comparisons of characteristics with respect to arm molar mass and number of star arms.[18-19] Moreover, varying the relative block ratio to target other material property profiles like TPEs could give a better overall understanding of the structure-property relationship for these CO_2-derived polymers.

Access to alternative non-linear architectures for CO_2-derived oxygenated polymers, such as core-shell or graft, should also be a future aim in the application of switch catalysis (**Figure 5.5**). Various reports describe the syntheses of these architectures (which incorporate polycarbonates, polyethers, and/or polyesters) but utilise conventional methods involving isolation and modification in order to facilitate grafting or growth of the core or shell segment.[20-23]

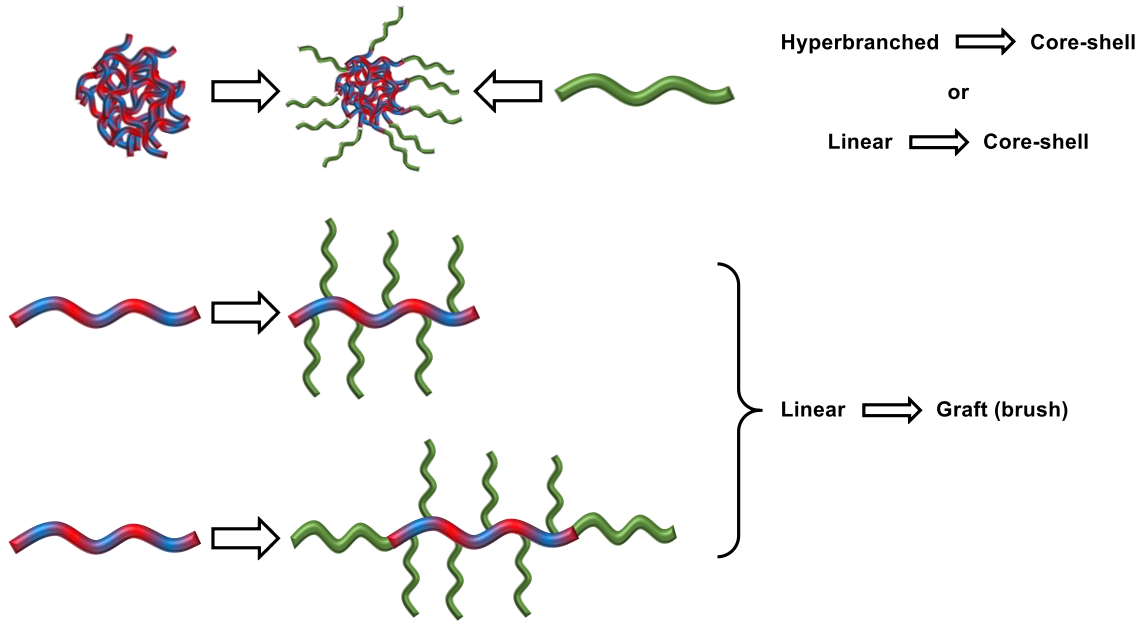


Figure 5.5. Additional non-linear architectures, possibly achievable by utilising switchable polymerisation catalysis.

Switchable catalysis techniques could be applied here to provide an elegant route to these non-linear architectures, avoiding intermediate steps, expediting the synthesis, and broadening access to block chemistry combinations in the resulting materials. Fashioning controlled core-shell type structures could feasibly be achieved by applying a switch catalysis to a judicious choice of monomers in one-pot. As an example, the first polymerisation cycle could either form a hyperbranched core from epoxide/CO_2 ROCOP or a linear block from lactone ROP, with the switch to the second cycle then forming the linear "shell" blocks or hyperbranched core, respectively.

Further design and optimisation of the catalysis may be necessary in order to access other architectures. The metal-alkoxide chain-end intermediate that is shared between ROP and ROCOP mechanisms in switch may create difficulties in obtaining controlled graft polymers from a mixture of monomers, but one solution to this may be the development of catalysts able to incorporate other polymerisation cycles into a switch.[11, 24]

5.5. References

1. Grignard, B.; Gennen, S.; Jérôme, C.; Kleij, A. W.; Detrembleur, C., Advances in the use of CO2 as a renewable feedstock for the synthesis of polymers. *Chem. Soc. Rev.* **2019,** *48* (16), 4466-4514.
2. Williams, C. K.; Plajer, A., Heterocycle/Heteroallene Ring Opening Copolymerisation: Selective Catalysis Delivering Alternating Copolymers. *Angew. Chem. Int. Ed.* **2021**.
3. Klaus, S.; Lehenmeier, M. W.; Anderson, C. E.; Rieger, B., Recent advances in CO2/epoxide copolymerization—New strategies and cooperative mechanisms. *Coord. Chem. Rev.* **2011,** *255* (13), 1460-1479.
4. Trott, G.; Saini, P. K.; Williams, C. K., Catalysts for CO2/epoxide ring-opening copolymerization. *Phil. Trans. R. Soc. A* **2016,** *374* (2061), 20150085.
5. Deacy, A. C.; Moreby, E.; Phanopoulos, A.; Williams, C. K., Co(III)/Alkali-Metal(I) Heterodinuclear Catalysts for the Ring-Opening Copolymerization of CO2 and Propylene Oxide. *J. Am. Chem. Soc.* **2020,** *142* (45), 19150-19160.
6. Trott, G.; Garden, J. A.; Williams, C. K., Heterodinuclear zinc and magnesium catalysts for epoxide/CO2 ring opening copolymerizations. *Chem. Sci.* **2019,** *10* (17), 4618-4627.
7. Garden, J. A.; Saini, P. K.; Williams, C. K., Greater than the Sum of Its Parts: A Heterodinuclear Polymerization Catalyst. *J. Am. Chem. Soc.* **2015,** *137* (48), 15078-15081.
8. Romain, C.; Garden, J. A.; Trott, G.; Buchard, A.; White, A. J. P.; Williams, C. K., Di-Zinc–Aryl Complexes: CO2 Insertions and Applications in Polymerisation Catalysis. *Chem. Eur. J.* **2017,** *23* (30), 7367-7376.
9. Deacy, A. C.; Kilpatrick, A. F. R.; Regoutz, A.; Williams, C. K., Understanding metal synergy in heterodinuclear catalysts for the copolymerization of CO2 and epoxides. *Nat. Chem.* **2020,** *12* (4), 372-380.
10. Sulley, G. S.; Gregory, G. L.; Chen, T. T. D.; Peña Carrodeguas, L.; Trott, G.; Santmarti, A.; Lee, K.-Y.; Terrill, N. J.; Williams, C. K., Switchable Catalysis Improves the Properties of CO2-Derived Polymers: Poly(cyclohexene carbonate-b-ε-decalactone-b-cyclohexene carbonate) Adhesives, Elastomers, and Toughened Plastics. *J. Am. Chem. Soc.* **2020,** *142* (9), 4367-4378.
11. Zhao, Y.; Wang, Y.; Zhou, X.; Xue, Z.; Wang, X.; Xie, X.; Poli, R., Oxygen-Triggered Switchable Polymerization for the One-Pot Synthesis of CO2-Based Block Copolymers from Monomer Mixtures. *Angew. Chem. Int. Ed.* **2019,** *58* (40), 14311-14318.
12. Pesko, D. M.; Jung, Y.; Hasan, A. L.; Webb, M. A.; Coates, G. W.; Miller, T. F.; Balsara, N. P., Effect of monomer structure on ionic conductivity in a systematic set of polyester electrolytes. *Solid State Ionics* **2016,** *289*, 118-124.
13. Zhao, Y.; Bai, Y.; Li, W.; An, M.; Bai, Y.; Chen, G., Design Strategies for Polymer Electrolytes with Ether and Carbonate Groups for Solid-State Lithium Metal Batteries. *Chem. Mater.* **2020,** *32* (16), 6811-6830.
14. Petersen, S. R.; Wilson, J. A.; Becker, M. L., Versatile Ring-Opening Copolymerization and Postprinting Functionalization of Lactone and Poly(propylene fumarate) Block Copolymers: Resorbable Building Blocks for Additive Manufacturing. *Macromolecules* **2018,** *51* (16), 6202-6208.
15. Filippidi, E.; Cristiani Thomas, R.; Eisenbach Claus, D.; Waite, J. H.; Israelachvili Jacob, N.; Ahn, B. K.; Valentine Megan, T., Toughening elastomers using mussel-inspired iron-catechol complexes. *Science* **2017,** *358* (6362), 502-505.
16. Ro, A. J.; Huang, S. J.; Weiss, R. A., Synthesis and thermal properties of telechelic poly(lactic acid) ionomers. *Polymer* **2008,** *49* (2), 422-431.

17. Yang, G.-W.; Wu, G.-P., High-Efficiency Construction of CO2-Based Healable Thermoplastic Elastomers via a Tandem Synthetic Strategy. *ACS Sustainable Chem. Eng.* **2019,** *7* (1), 1372-1380.
18. Shim, J. S.; Kennedy, J. P., Novel thermoplastic elastomers. II. Properties of star-block copolymers of PSt-b-PIB arms emanating from cyclosiloxane cores. *J. Polym. Sci., Part A: Polym. Chem.* **1999,** *37* (6), 815-824.
19. Kwee, T.; Taylor, S. J.; Mauritz, K. A.; Storey, R. F., Morphology and mechanical and dynamic mechanical properties of linear and star poly(styrene-b-isobutylene-b-styrene) block copolymers. *Polymer* **2005,** *46* (12), 4480-4491.
20. Alagi, P.; Zapsas, G.; Hadjichristidis, N.; Hong, S. C.; Gnanou, Y.; Feng, X., All-Polycarbonate Graft Copolymers with Tunable Morphologies by Metal-Free Copolymerization of CO2 with Epoxides. *Macromolecules* **2021,** *54* (13), 6144-6152.
21. Geschwind, J.; Wurm, F.; Frey, H., From CO2-Based Multifunctional Polycarbonates With a Controlled Number of Functional Groups to Graft Polymers. *Macromol. Chem. Phys.* **2013,** *214* (8), 892-901.
22. Li, Y.; Zhang, Y.-Y.; Hu, L.-F.; Zhang, X.-H.; Du, B.-Y.; Xu, J.-T., Carbon dioxide-based copolymers with various architectures. *Prog. Polym. Sci.* **2018,** *82*, 120-157.
23. Zhang, J.-F.; Ren, W.-M.; Sun, X.-K.; Meng, Y.; Du, B.-Y.; Zhang, X.-H., Fully Degradable and Well-Defined Brush Copolymers from Combination of Living CO2/Epoxide Copolymerization, Thiol–Ene Click Reaction and ROP of ε-caprolactone. *Macromolecules* **2011,** *44* (24), 9882-9886.
24. Higuchi, M.; Kanazawa, A.; Aoshima, S., Design of Graft Architectures via Simultaneous Kinetic Control of Cationic Vinyl-Addition Polymerization of Vinyl Ethers, Coordination Ring-Opening Polymerization of Cyclic Esters, and Merging at the Propagating Chain End. *Macromolecules* **2020,** *53* (10), 3822-3831.

CHAPTER 6

Experimental Section

6.1. General

Unless otherwise stated, all solvents and reagents were purchased from commercial sources (Merck/Sigma Aldrich) and used as received. Solvents used for synthesis and polymerisation (toluene, tetrahydrofuran, hexanes) were collected from a solvent purification system (SPS), degassed with three freeze-pump-thaw cycles, and stored over 4 Å molecular sieves under an inert atmosphere. Monomer purification and subsequent polymerisation were carried out under inert conditions using a nitrogen-filled glovebox or standard Schlenk line techniques.

Magnesium bis(hexamethyldisilazide) (97%, Sigma-Aldrich) ($Mg(HMDS)_2$) and bis(pentafluorophenyl)zinc (97%, Sigma-Aldrich) ($Zn(C_6F_5)_2$) were used as received. Cyclohexene oxide (98%, Acros Organics) (CHO) was dried by stirring over CaH_2 followed by fractional distillation at 130 °C and stored under a nitrogen atmosphere. 4-Vinyl-1-cyclohexene-1,2-epoxide (98%, Sigma-Aldrich) (vCHO) was dried by stirring over CaH_2 followed by fractional distillation at 75 °C under reduced pressure (7 mbar) and stored at -30 °C under a nitrogen atmosphere. ε-Decalactone (≥ 99%, Sigma-Aldrich) (ε-DL) was dried by stirring over CaH_2 followed by fractional distillation at 70 °C under reduced pressure (10^{-2} mbar) and stored under a nitrogen atmosphere. *trans*-1,2-Cyclohexanediol (98%, Sigma-Aldrich) (CHD) was recrystallized from ethyl acetate, dried *in vacuo*, and stored under a nitrogen atmosphere. 1,1,1-Tris(hydroxymethyl)propane (97%, Sigma-Aldrich) (TMP) was recrystallized from acetone:diethyl ether (50:50), dried *in vacuo*, and stored under a nitrogen atmosphere. Pentaerythritol (99%, Sigma-Aldrich) (PER) was recrystallized from methanol, dried *in vacuo* at 90 °C, and stored under a nitrogen atmosphere. Research-grade carbon dioxide (BOC) was dried through a Drierite column and two additional drying columns (Micro Torr, Model number: MC1-804FV) in series before use.

6.2. Analytical techniques

Nuclear Magnetic Resonance (NMR) Spectroscopy. ^{1}H, COSY, HSQC, HMBC, ^{31}P{^{1}H}, ^{19}F{^{1}H} NMR spectra were obtained using a Bruker AVIII HD 400 NMR spectrometer. ^{13}C{^{1}H} NMR spectra were obtained using a Bruker AVII 500 NMR spectrometer. Chemical shifts reported from low to high field in units of ppm. Abbreviations for commonly observed signal splitting: singlet = s, doublet = d, triplet = t, quartet = q, doublet doublet = dd, multiplet = m, broad = br. Values for coupling (*J*) reported in Hertz (Hz).

Size Exclusion Chromatography (SEC). SEC analysis was carried out on a Shimadzu LC-20AD instrument, equipped with a PSS SDV 5 µm precolumn and two PSS SDV 5 µm linear M columns in series and a refractive index (RI) detector. HPLC grade THF (inhibitor-free) was used as the eluent at 1.0 mL min^{-1} at 30 °C. Samples were dissolved in THF (5-10 mg mL^{-1}) and passed through 0.2 µm PTFE syringe filters (VWR International) prior to analysis. Monodisperse polystyrene standards were used for calibration (Agilent EasiVials, PS Medium 2 mL).

Matrix-Assisted Laser Desorption/Ionization – Time of Flight Mass Spectrometry (MALDI-ToF MS). MALDI-ToF MS was carried out on a Waters MALDI Micro MX or a Bruker Autoflex, set to positive ion reflectron mode. Samples were dissolved in THF at 10 mg mL^{-1}. Dithranol (10 mg mL^{-1} in THF) or *trans*-2-[3-(4-*tert*-butylphenyl)-2-methyl-2-propenylidene] malononitrile (DCTB) (10 mg mL^{-1} in THF) were used as the matrix. Potassium trifluoroacetate (KTFA) (10 mg mL^{-1} in THF) was used as a salt. The components were mixed in the ratio 1:1:1 (vol.) (polymer:KTFA:matrix), spotted onto a stainless steel MALDI plate repeatedly (2-3 times) and allowed to dry completely before analysis.

Electrospray Ionisation Mass Spectrometry (ESI MS). ESI MS was carried out using an Agilent 6120 bench-top single quadrupole instrument in direct infusion (loop injection,

methanol/formic acid) mode. Samples were dissolved in methanol (HPLC grade, 1 mg mL^{-1}), diluted 10-fold and passed through 0.2 μm PTFE syringe filters (VWR International).

Elemental Analysis (EA). EA was provided by Mr Stephen Boyer at London Metropolitan University, North Campus, Holland Road, London, N7.

Attenuated Total Reflectance – Infrared Spectroscopy (ATR-IR). *In-situ* IR reaction monitoring was performed using a Mettler-Toledo ReactIR 4000 spectrometer equipped with a MCT detector and a silver halide DiComp probe. Data were recorded and processed using the Mettler-Toledo icIR 7 software package, exported to csv, and replotted using Origin graphing software.

Differential Scanning Calorimetry (DSC). Thermal properties of polymers were measure using a DSC3+ (Mettler-Toledo Ltd) calibrated using zinc and indium standards. A sealed, empty crucible was used as a reference. Samples were heated from 25 °C to 120-150 °C, at a rate of 10 °C min^{-1}, under N_2 flow (100 mL min^{-1}), followed by a 5 minute isotherm, at 120-150 °C, to erase thermal history. Samples were subsequently cooled to -90 °C, as a rate of 10 °C min^{-1}, and kept at -90 °C for a further 5 minutes, followed by a heating-cooling cycle procedure from -90 °C to 120-150 °C, at a rate of 10 °C min^{-1}. Each sample was analysed over two full heating-cooling cycles. Glass transition temperatures (T_g) are reported as the midpoint of the transition taken from the second heating cycle.

Thermogravimetric Analysis (TGA). Thermal decomposition of polymer samples was measured using a TGA/DSC 1 system (Mettler-Toledo Ltd). Samples were heated in an open, ceramic, crucible from 25 °C to 500 °C, at a rate of 5 °C min^{-1}, under N_2 flow (100 cm^3 min^{-1}).

Dynamic Mechanical [Thermal] Analysis (DM[T]A). Viscoelastic properties of free-stranding polymer films were analysed using a RSA-G2 Solids Analyser (TA Instruments).

Specimens of uniform width were cut from a solvent cast film using a Zwick ZCP020 cutting press. Samples were heated from -70 °C to 40 °C and 35 °C to 80-130 °C at a rate of 5 °C min^{-1} for low and high temperature sweeps, respectively. The frequency was set to 1 Hz, the strain amplitude to 0.1%, and a 0.1 N pre-load was applied. Glass transition temperatures (T_g) are reported, where possible, as the peak maxima in tan(δ). Oscillatory rheology of softer specimens was performed on an Anton Paar Physica MCR301 rheometer equipped with 25 mm parallel plate (PP25) geometries. Frequency sweep analysis was conducted at 25 °C with γ = 0.5%, and a logarithmic frequency ramp between 0.01 and 30 Hz. The following parameters were used in other testing methods: γ = 0.5%, ω = 1 Hz.

Tensile Mechanical Analysis. Polymer specimens were analysed using an EZ-LX Universal Testing Instrument (Shimadzu). Dumbbell-shaped specimens were cut using a Zwick ZCP020 cutting press equipped with a cutting die for ISO 527-2 type 5B. Uniaxial extension experiments (10 mm min^{-1} cross-head speed) were run according to ISO 527. Cyclical hysteresis experiments (10 mm min^{-1} cross-head speed) were conducted from 0-200% strain over 10 cycles. Values for mechanical characteristics (e.g., Young's modulus, stress at break etc.) were averaged over at least 5 specimens.

Adhesion Testing. Polymer sample was dissolved in methylene chloride (DCM) to make a 30 wt % solution. The solution was then coated using a wound wire rod (K bar) onto either 5 μm thick PETE film (Mylar®) or PSTC-grade polished stainless steel, depending on the testing procedure. The coating was allowed to dry under ambient conditions overnight before further drying *in vacuo* at 40 °C.

180° Peel Test: A strip of polymer-coated Mylar® film (1.27 cm in width) was adhered to a stainless steel plate using a 500 g roller. The sample was tested using a Shimadzu EZ-LX

Universal Testing Instrument as a peel rate of 305 mm min^{-1}. The peel force was reported from the maximum measured force and averaged over four samples.

Loop Tack Test: A strip of polymer-coated Mylar® film (1.27 cm in width) was formed into a teardrop shape and clamped in the upper grip of the tensile testing instrument. The loop was lowered onto a stainless steel plate clamped in the lower grip until a contact area of 1.27 cm x 2.54 cm was established, at which point the upper grip was raised at a rate of 305 mm min^{-1}. The tack force was reported as the maximum force measured and averaged over at least three samples.

Crosshatch Test: Polymer-coated stainless steel was used. A cross-cut pattern was formed onto the polymer coating using a six-parallel cut testing rig. A piece a Scotch® tape was adhered to the coating to cover the cross-cut pattern, and subsequently peeled off quickly. The extent of coating removal/damage was assessed according to the ISO classification system (0-5 scale).

Small-Angle X-ray Scattering (SAXS). Synchrotron SAXS analysis of block polymer films was carried out at beamline I22, located at Diamond Light Source, Harwell, United Kingdom. Samples were mounted either between two pieces of Kapton®, Scotch tape, or free in a solids sample grid. A monochromatic X-ray radiation (λ = 0.1 nm) and 2D SAXS detector (Pilatus P3-2M, DECTRIS Ltd) were used for experiments. 2D scattering patterns were reduced to 1D using Dawn software developed at the Diamond Light Source.[1-2]

6.3. Experimental procedures

6.3.1. Synthesis of macrocyclic ancillary ligand (H_2L)

Previously reported synthetic routes were followed.[3-4]

Synthesis of 4-tert-Butyl-2,6-diformylphenol (i)

4-*tert*-Butylphenol (25.0 g, 0.17 mol), hexamethylene tetramine (HMTA) (37.4 g, 0.27 mol), and trifluoroacetic acid (130 mL, 1.73 mol) were added to a round-bottomed flask and stirred at 125 °C under reflux for 16 hours. A Dean-Stark apparatus was connected and the solution heated at 150 °C for 4 hours. The solution was then cooled to 100 °C and HCl (3 M, 250 mL) was slowly added. The solution was heated to reflux at 100 °C for 40 minutes, cooled to room temperature, and placed in a freezer overnight. The precipitate was filtered, washed twice with cold (-78 °C) methanol, and dried *in vacuo* to afford yellow crystals (15.3 g, 44%).

^{1}H NMR (400 MHz, $CDCl_3$, 298 K) δ(ppm): 11.47 (s, 2H, C***H***O), 10.24 (s, 1H, Ar-O***H***), 7.98 (s, 2H, Ar-***H***), 1.35 (s, 9H, C***H***$_3$). MS (ESI): *m*/*z* = 207.0 ([M+H]$^+$)

Synthesis of $[H_4L](ClO_4)_2$ (ii)

4-*tert*-Butyl-2,6-diformylphenol (6.0 g, 29 mmol), $NaClO_4$ (14.2 g, 116 mmol), and acetic acid (3.3 mL, 58 mmol) were added to a round-bottomed flask, dissolved in methanol (450 mL) and stirred at 70 °C. As the solution began to reflux, a second solution of 2,2-dimethyl-1,3-propanediamine (3.0 g, 29 mmol) in methanol (150 mL) was added dropwise. The solution was then cooled to room temperature and left stirring for 24 hours. The precipitate was filtered, washed twice with cold (-78 °C) methanol, and air-dried to afford an orange crystalline solid (9.2 g, 85%).

^{1}H NMR (400 MHz, DMSO-d_6, 298 K) δ(ppm): 13.60 (br d, 4H, *J* = 12, -O***H***N-), 8.69 (d, 4H, *J* = 12, imine C***H***), 7.65 (s, 4H, Ar-***H***), 3.87 (d, 8H, *J* = 8, =NC***H***$_2$-), 1.28 (s, 12H, C(C***H***$_3$)$_2$), 1.14 (s, 18H, C(C***H***$_3$)$_3$). MS (ESI): *m*/*z* = 545.3 ([M-H]$^+$, $C_{34}H_{49}N_4O_2$ requires 545.4), 273.2 (M^{2+}).

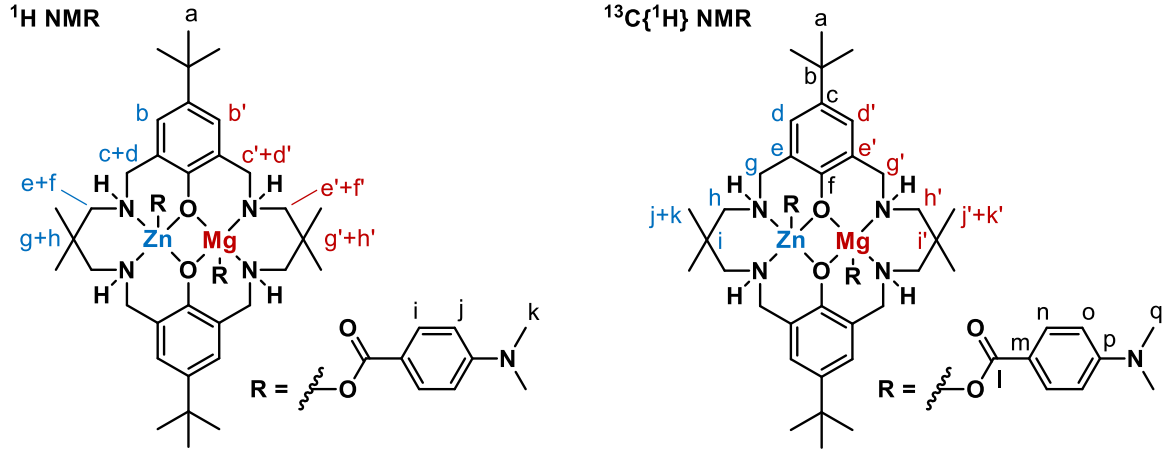
Synthesis of H_2L (iii)

$[H_4L](ClO_4)_2$ (6.0 g, 8.0 mmol) was suspended in methanol (600 mL) and cooled to 0 °C. $NaBH_4$ (7.9 g, 208 mmol) was slowly added with stirring. On addition of all $NaBH_4$, the solution was warmed to warm temperature and stirred for 1 hour, after which water was added until a cloudy precipitate started to form. The mixture was then left to stand overnight and the precipitate was subsequently filtered, washed twice with deionized water, and dried *in vacuo* to afford a white powder (3.8 g, 86%)

^{1}H NMR (400 MHz, $CDCl_3$, 298 K) δ(ppm): 6.90 (s, 4H, Ar-***H***), 3.74 (s, 8H, -CHCC***H***$_2$N-), 2.51 (s, 8H, CH_3CC***H***$_2$N-), 1.25 (s, 18H, -C(C***H***$_3$)$_3$), 1.05 (s, 12H, C(C***H***$_3$)$_2$). Anal. Calc. for $C_{34}H_{56}N_4O_2$ (%): C 73.87, H 10.21, N 10.12. Found: C 73.79, H 10.22, N 10.26. MS (ESI): *m*/*z* = 553.4 ($[M+H]^+$), 277.1 ($[M+2H]^{2+}$).

6.3.2. Synthesis of heterodinuclear catalyst [LZnMg(OBz^{NMe2})$_2$] (1)

Under inert conditions, a flame-dried Schlenk flask was charged with macrocyclic diphenol tetraamine-based pro-ligand (H_2L) (500 mg, 0.91 mmol) and anhydrous THF (5 mL). A solution of $ZnEt_2$ (112 mg, 0.91 mmol) in THF (5 mL) was then added to the Schlenk flask and the reaction mixture stirred for 16 hours, at 25 °C, before addition of further THF (5 mL). The solution was cooled to -78 °C whilst stirring, and a solution of $MgBr_2$ (167 mg, 0.91 mmol) in THF (10 mL) was added, dropwise, over a period of 15 minutes. The reaction was stirred at -78 °C for a further 15 min and then allowed to warm to room temperature for 30 min. The solvent was removed *in vacuo* to yield the intermediate complex, [$LZnMgBr_2$]. To the Schlenk flask with the intermediate complex was added THF (10 mL) and potassium *para*-(dimethlyamino)benzoate ($KOBz^{NMe2}$) (369 mg, 1.82 mmol) and the mixture stirred for 16 hours at room temperature. The resulting precipitate (KBr) was removed by filtration and the solution concentrated. The product was washed with pentane (3 x 5 mL) and dried *in vacuo* to afford a white powder (0.7 g, 79% yield).

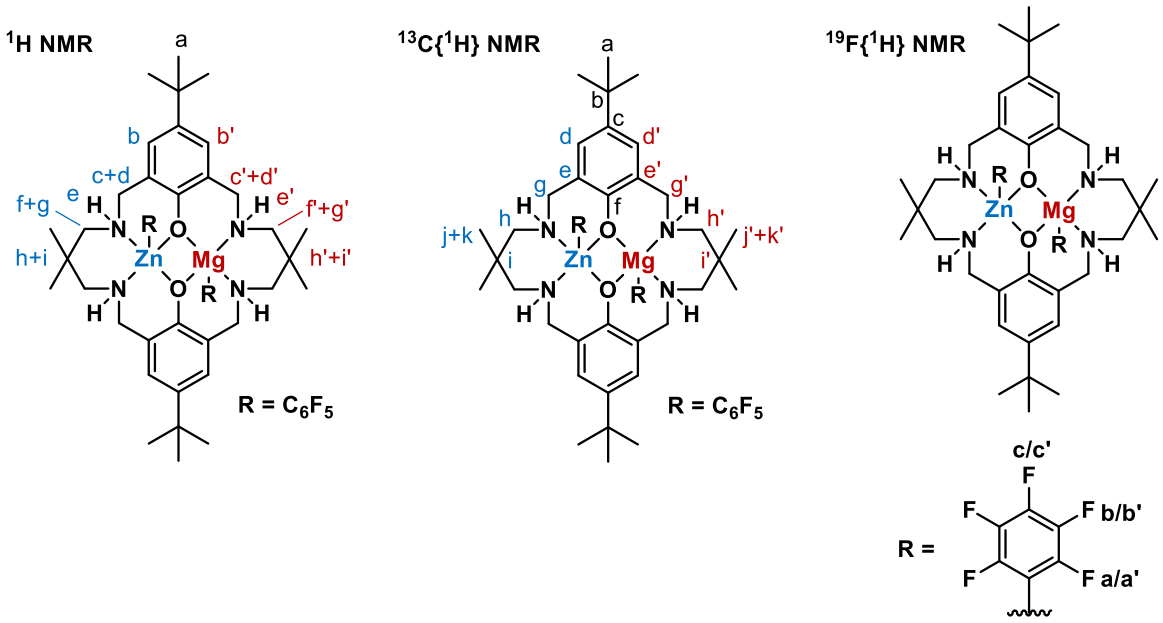


Characterisation data were in accordance with those previously reported.[5]

^{1}H NMR (400 MHz, methanol-d_4, 298 K) δ(ppm): 7.81 (br s, 4H, i), 6.96 (s, 4H, b+b'), 6.63 (br s, 4H, j), 4.22 (d, 2H, J = 12, c), 4.04 (m, 2H, c'), 3.29-3.23 (br m, 4H, d+d'), 2.95 (s, 6H, k), 2.89 (br d, 2H, e), 2.85-2.75 (m, 4H, f+e'), 2.71 (br d, 2H, f'), 1.43 (m, 6H, g+g'), 1.17 (m, 18H, a), 1.05 (m, 6H, h+h'). ^{13}C{^{1}H} NMR (125 MHz, methanol-d_4, 298 K) δ(ppm): 162.8 (f), 162.6 (l), 153.8 (p), 138.2 (c), 132.0 (n), 129.3 (d'), 129.3 (m), 129.0 (d), 125.3 (e'), 124.7 (e), 111.9 (o), 64.4 (h), 63.4 (h'), 56.9 (g), 56.3 (g'), 40.5 (q), 35.4 (i'), 34.8 (i), 34.3 (b), 32.0 (a), 28.9 (j'), 28.8 (j), 21.8 (k'), 21.3 (k). Anal. Calc. for $C_{52}H_{74}MgN_6O_6Zn$ (%): C 64.46, H 7.70, N 8.67. Found: C 64.58, H 7.81, N 8.84.

6.3.3. Synthesis of heterodinuclear catalyst [LZnMg(C$_6$F$_5$)$_2$] (2)

Under inert conditions, macrocyclic diphenol tetraamine-based pro-ligand (H_2L) (0.5 g, 0.90 mmol) and [Mg{N[Si(CH$_3$)$_3$]$_2$}$_2$] (0.31 g, 0.90 mmol) were stirred in anhydrous THF (10 mL) at 25 °C for 1 hour. A solution of Zn(C$_6$F$_5$)$_2$ (0.36 g, 0.90 mmol), in anhydrous THF (5 mL), was then added dropwise to the reaction solution which afforded an orange solution which was stirred overnight at 25 °C. The solvent was removed *in vacuo* to yield a pale orange solid. The product was isolated by washing with cold (-30 °C) THF (5 mL) and pentane (2 x 5 mL) followed by centrifugation. The off-white powder was dried *in vacuo* overnight at 25 °C (0.62 g, 70% yield).



^{1}H NMR (400 MHz, $CDCl_3$, 298 K) δ(ppm): 6.81 (d, 2H, *J* = 3, b'), 6.76 (d, 2H, *J* = 3, b), 4.37 (m, 2H, c'), 4.30 (m, 2H, c), 3.40 (d, 2H, *J* = 14, d), 3.26 (d, 2H, *J* = 13, d'), 3.08 (m, 2H, f'), 3.01 (m, 2H, f), 2.78-2.63 (m, 6H, g+g'+e), 2.12-2.02 (m, 2H, e'), 1.27 (s, 3H, h), 1.20 (s, 18H, a), 1.17 (s, 3H, h'), 1.06-1.02 (m, 6H, i+i'). ^{13}C{^{1}H} (125 MHz, $CDCl_3$, 298 K) δ(ppm): 159.2 (f), 137.2 (c), 126.3 (d or d'), 126.3 (d' or d), 124.5 (e'), 122.3 (e), 62.6 (h), 61.7 (h'), 57.8 (g), 55.9 (g'), 34.2 (i or i'), 33.9 (i or i'), 33.5 (b), 31.5 (a), 28.3 (j+j' or k+k'), 28.3 (j+j' or k+k'), 20.3 (j+j' or k+k'), 20.1 (j+j' or k+k'). ^{19}F{^{1}H} (376 MHz, $CDCl_3$, 298 K) δ(ppm): -111.2 (m, 2F, *o*-C_6F_5), -116.2 (br, 2F, *o*-C_6F_5), -157.8 (m, 1F, *p*-C_6F_5), -159.5 (m, 1F, *p*-C_6F_5), -161.2 (m, 2F, *m*-C_6F_5), -161.8 (m, 2F, *m*-C_6F_5). Anal. Calc. for $C_{46}H_{54}F_{10}MgN_4O_2Zn$ (%): C 56.69, H 5.58, N 5.75. Found: C 56.55, H 5.61, N 5.68. MS (ESI): *m*/*z* (rel. %) = 683.4 (100), 685.4 (84), 687.4 (62) ([LZnMg+HCOO]$^+$); 643.4 (31), 644.4 (21), 645.4 (16) ([LMg$_2$+HCOO]$^+$); 727.2 (26), 725.3 (27), 723.2 (24) ([LZn$_2$+HCOO]$^+$).

N.B. Assignment of signals as being on the zinc or magnesium "side" of the macrocycle and co-ligands was achieved using 2D NMR spectroscopic techniques (^{1}H and ^{19}F{^{1}H} COSY, ^{1}H-^{13}C HSQC and HMBC), and by comparison to spectra of a previously synthesised homodinuclear zinc complex.[6]

6.3.4. Representative Ring-Opening Polymerisation (ROP) of ε-Decalactone

Under anaerobic conditions, **2** (10 mg, 0.01 mmol), CHD (4.8 mg, 0.04 mmol), ε-DL (0.7 mL, 4 mmol) and toluene (1.6 mL) were added to a flame-dried vial and stirred at 80 °C for 1 hour. The viscous polymerisation solution was quenched by exposure to air. A crude sample was analysed by ^{1}H NMR spectroscopy. SEC analysis (THF, 1 mL min^{-1}, 30 °C) of a crude sample was performed on removal of residual polymerisation solvent. The polymer was purified by precipitation from a solution of DCM or THF (< 1 g mL^{-1}) into cold methanol (-78 °C, 100-200 mL) and subsequently dried *in vacuo* to a constant weight.

^{1}H NMR (400 MHz, $CDCl_3$, 298 K) δ(ppm): 4.85 (m, *n*H, C***H*** methine repeat unit), 3.58 (m, 2H, C***H*** methine end-group), 2.26 (m, 2*n*H, repeat unit α-C***H***$_2$ group), 1.72-1.14 (m, 12*n*H, repeat unit backbone & side-chain methylene C***H***$_2$ groups), 0.88 (m, 3*n*H, repeat unit side-chain C***H***$_3$). SEC (THF, PS calib.): M_n = 33.1 kg mol^{-1}, $Đ_M$ = 1.10.

6.3.5. Representative Ring-Opening Copolymerisation (ROCOP) of epoxide and CO_2

Under anaerobic conditions, **2** (20 mg, 0.02 mmol), CHD (9.5 mg, 0.08 mmol), and the chosen epoxide were added to a Schlenk tube in the molar ratio [**2**]:[CHD]:[epoxide] = 1:4:1000. The Schlenk tube was filled with CO_2 (P = 1 bar) through three vacuum/CO_2 cycles and then stirred at 80 °C for 5 hours. The reaction was quenched by exposure to air, and a crude sample taken for analysis by ^{1}H NMR spectroscopy. SEC analysis (THF, 1 mL min^{-1}, 30 °C) was performed after removing excess epoxide under reduced pressure. The polymer was purified by precipitation of a solution in DCM or THF (< 1 g mL^{-1}) into methanol (100-200 mL), and dried *in vacuo* to a constant weight.

^{1}H NMR (400 MHz, $CDCl_3$, 298 K) δ(ppm): 4.63 (m, 2*n*H, C***H*** methines repeat unit), 4.40 (m, 2H, C***H*** methine end-groups), 3.56 (m, 2H, C***H*** methine end-groups), 2.23-1.54 (m,

8*n*H, cyclohexyl ring methylene C***H***$_2$ groups). SEC (THF, PS calib.): M_n = 12.8 kg mol^{-1}, $Đ_M$ = 1.24.

6.3.6. Representative Switch Polymerisation of ε-Decalactone, Cyclohexene Oxide and CO_2 for ABA Triblock Polymer Synthesis

Low Pressure CO_2 (1 bar)

Under anaerobic conditions, **2** (30 mg, 0.03 mmol), CHD (14 mg, 0.12 mmol), ε-DL (2.1 mL, 12 mmol), and CHO (3 mL, 30 mmol) were added to Schlenk tube. The Schlenk was stirred at 80 °C under a N_2 atmosphere for 10 minutes. Subsequently the Schlenk was refilled with CO_2 through five vacuum/CO_2 cycles and then stirred at 80 °C for a further 5 hours. The polymerisation was quenched by exposure to air, and a crude sample was taken for analysis by ^{1}H NMR spectroscopy. SEC analysis (THF, 1 mL min^{-1}, 30 °C) was performed on a crude sample after removal of residual solvent and monomer. The polymer was isolated by precipitation from a solution of THF (< 1 g mL^{-1}) into methanol (200 mL), and dried *in vacuo* to a constant weight.

^{1}H NMR (400 MHz, $CDCl_3$, 298 K) δ(ppm): 4.85 (m, *n*H, PDL backbone C***H*** methine), 4.66 (m, 2*m*H, PCHC backbone C***H*** methines), 2.26 (m, 2*n*H, PDL backbone α-C***H***$_2$), 2.24-1.10 (m, (12*n*+8*m*)H, PDL+PCHC backbone & side-chain methylenes), 0.87 (m, 3*n*H, PDL side-chain C***H***$_3$). SEC (THF, PS calib.): M_n = 20.2 kg mol^{-1}, $Đ_M$ = 1.07.

High pressure CO_2 (20 bar)

Under anaerobic conditions, **2** (20 mg, 0.02 mmol), CHD (9.5 mg, 0.08 mmol), CHO (0.78 mL, 7.8 mmol), ε-DL (3.1 mL, 17.7 mmol), and toluene (2.14 mL) were added to a 25 mL stainless steel Parr pressure vessel. The vessel was heated to 80 °C under a N_2 atmosphere for 20 minutes. Subsequently, the vessel was pressurised with CO_2 at 20 bar and heated at 80 °C for a further 20 hours, before being cooled to 35 °C and the remaining CO_2 pressure vented. A sample of the crude polymer was removed for analysis by ^{1}H NMR spectroscopy. SEC

analysis (THF, 1 mL min^{-1}, 30 °C) was performed on the crude sample after removal of residual polymerisation solvent. The resulting block polymer was isolated by precipitation twice from a solution of THF (< 1 g mL^{-1}) into methanol (200 mL), and dried *in vacuo* to a constant weight.

^{1}H NMR (400 MHz, $CDCl_3$, 298 K) δ(ppm): 4.85 (m, *n*H, PDL backbone C***H*** methine), 4.66 (m, 2*m*H, PCHC backbone C***H*** methines), 2.26 (m, 2*n*H, PDL backbone α-C$\boldsymbol{H}_2$), 2.24-1.10 (m, (12*n*+8*m*)H, PDL+PCHC backbone & side-chain methylenes), 0.87 (m, 3*n*H, PDL side-chain C$\boldsymbol{H}_3$). SEC (THF, PS calib.): M_n = 59.8 kg mol^{-1}, $Đ_M$ = 1.10.

6.3.7. Representative Switch Polymerisation of ε-Decalactone, 4-Vinyl-1-cyclohexene-1,2-epoxide, and CO_2 for $(AB)_n$ Star Block Polymer Synthesis

Under anaerobic conditions, **2** (20 mg, 0.02 mmol), the chosen chain-transfer agent (TMP, PER) (0.08 mmol), ε-DL (3.3 mL, 18.8 mmol), and toluene (7.8 mL) were added to a flame-dried vial. The vial was stirred at 80 °C for 1 hour, after which it was cooled and an aliquot was taken to determine conversion of ε-DL to PDL by ^{1}H NMR spectroscopy. To the remaining solution in the vial was added vCHO (2.5 mL, 19.0 mmol), and the entire contents transferred to a stainless steel Parr pressure vessel. The vessel was then pressurised with CO_2 to 20 bar and stirred at 80 °C for 20 hours, before being cooled to 35 °C and the remaining CO_2 pressure vented. A sample of the crude polymer was removed for analysis by ^{1}H NMR spectroscopy. SEC analysis was performed on a crude sample after removal of residual solvent. The resulting polymer was isolated by precipitation twice from a solution of THF (< 1 g mL^{-1}) into methanol (200 mL), and dried *in vacuo* to a constant weight.

Characterisation representative for 3-arm star block polymer (x = DP_{PvCHC}, y = DP_{PDL}):
^{1}H NMR (400 MHz, $CDCl_3$, 298 K) δ(ppm): 5.77 (m, *x*H, PvCHC vinyl C***H***), 5.17-4.93 (m, 2*x*H, PvCHC vinyl C$\boldsymbol{H}_2$), 4.85 (m, (*x*+*y*)H, PvCHC -OC***H***CHO- & PDL backbone C***H*** methine), 4.77

(m, *x*H, PvCHC backbone -OCHC***H***O- methine), 4.09-3.94 (m, 6H, TMP CC***H***$_2$O), 2.42 (m, *x*H, PvCHC CH$_2$=CHC***H***-), 2.27 (m, 2*y*H, PDL backbone α-C***H***$_2$), 2.05-1.09 (m, (6*x*+12*y*)H, PvCHC & PDL backbone & side-chain methylenes), 0.88 (m, 3*y*H, PDL side-chain C***H***$_3$). SEC (THF, PS calib.): $M_{n,overall}$ = 75.1 kg mol^{-1}, $Đ_M$ = 1.18.

6.3.8. $^{31}P\{^1H\}$ NMR Spectroscopy for Polymer End-group Titration

A reported procedure for the analysis of hydroxyl end-groups was followed.[7] The polymer sample (20 mg) and stock solution (40 μL), in $CDCl_3$ (0.5 mL), were mixed in an NMR tube. Excess 2-chloro-4,4,5,5-tetramethyldioxaphospholane (40 μL) was then added to the NMR tube and shaken to combine. The mixture was allowed to react for 6 h before analysis by $^{31}P\{^1H\}$ NMR experiment. The contents of the stock solution were bisphenol A (400 mg), $Cr(acac)_3$ (5.5 mg), and pyridine (10 mL).

6.3.9. Representative Thiol-ene Post-polymerization Functionalization

To a flame-dried vial, under anaerobic conditions, was added the sample of polymer (1.0 g, 2.97 mmol of PvCHC repeat unit) in THF (5 mL). Once fully dissolved, 2,2-dimethoxyphenylacetophenone (DMPA) (305 mg, 1.20 mmol) and 2-mercaptoethanol (ME) (0.83 mL, 11.9 mmol) were added to the solution. The vial was sealed securely and stirred under UV irradiation (λ = 365 nm) for 2 hours, at which point the reaction was quenched by exposure to air. The crude material was isolated by precipitation twice from a solution of THF into diethyl ether (200 mL), filtered and washed with further diethyl ether (2 x 10 mL), and then dried *in vacuo* to a constant weight.

6.4. References

1. Filik, J.; Ashton, A. W.; Chang, P. C. Y.; Chater, P. A.; Day, S. J.; Drakopoulos, M.; Gerring, M. W.; Hart, M. L.; Magdysyuk, O. V.; Michalik, S.; Smith, A.; Tang, C. C.; Terrill, N. J.; Wharmby, M. T.; Wilhelm, H., Processing two-dimensional X-ray diffraction and small-angle scattering data in DAWN 2. *J. Appl. Crystallogr.* **2017,** *50* (3), 959-966.
2. Pauw, B. R.; Smith, A. J.; Snow, T.; Terrill, N. J.; Thunemann, A. F., The modular small-angle X-ray scattering data correction sequence. *J. Appl. Crystallogr.* **2017,** *50* (6), 1800-1811.
3. Dutta, B.; Bag, P.; Adhikary, B.; Flörke, U.; Nag, K., Efficient Proton-Templated Synthesis of 18- to 38-Membered Tetraimino(amino)diphenol Macrocyclic Ligands: Structural Features and Spectroscopic Properties. *J. Org. Chem.* **2004,** *69* (16), 5419-5427.
4. Kember, M. R.; Knight, P. D.; Reung, P. T. R.; Williams, C. K., Highly Active Dizinc Catalyst for the Copolymerization of Carbon Dioxide and Cyclohexene Oxide at One Atmosphere Pressure. *Angew. Chem. Int. Ed.* **2009,** *48* (5), 931-933.
5. Trott, G.; Garden, J. A.; Williams, C. K., Heterodinuclear zinc and magnesium catalysts for epoxide/CO2 ring opening copolymerizations. *Chem. Sci.* **2019,** *10* (17), 4618-4627.
6. Romain, C.; Garden, J. A.; Trott, G.; Buchard, A.; White, A. J. P.; Williams, C. K., Di-Zinc-Aryl Complexes: CO2 Insertions and Applications in Polymerisation Catalysis. *Chem. Eur. J.* **2017,** *23*, 7367-7376.
7. Spyros, A.; Argyropoulos, D. S.; Marchessault, R. H., A Study of Poly(hydroxyalkanoate)s by Quantitative 31P NMR Spectroscopy: Molecular Weight and Chain Cleavage. *Macromolecules* **1997,** *30*, 327-329.

CHAPTER 7

Appendices

7.1. Chapter 2

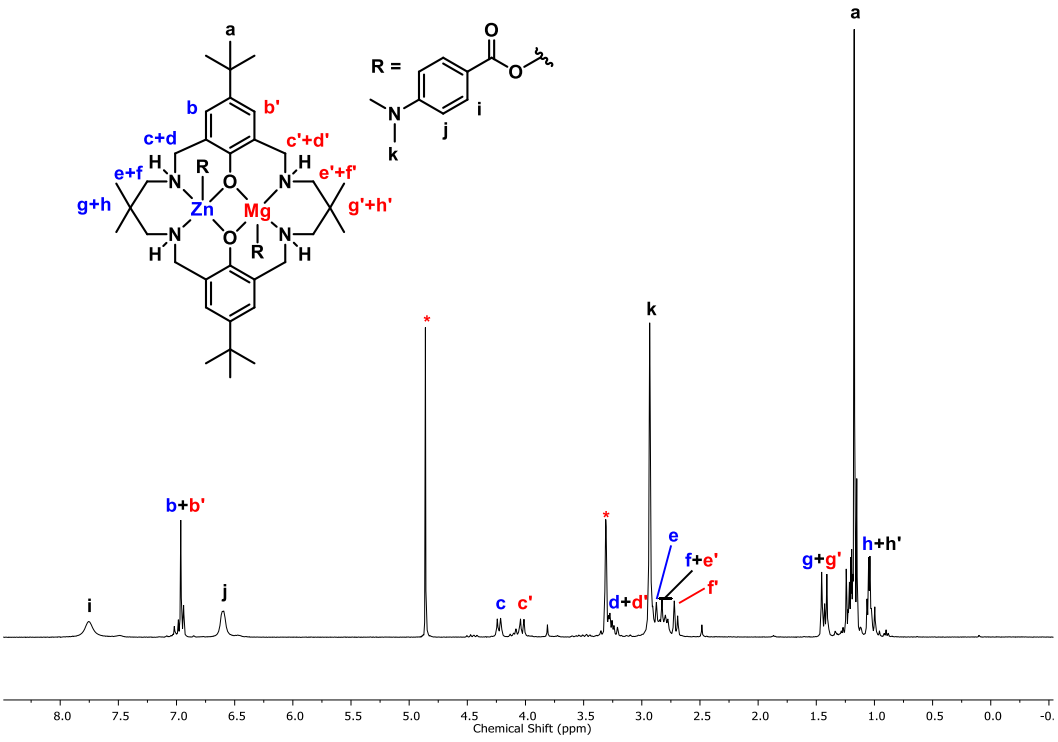


Figure S7.1. ^{1}H NMR spectrum of heterodinuclear catalyst [LZnMg(OBz^{NMe2})$_2$] (**1**). [400 MHz, CD_3OD].

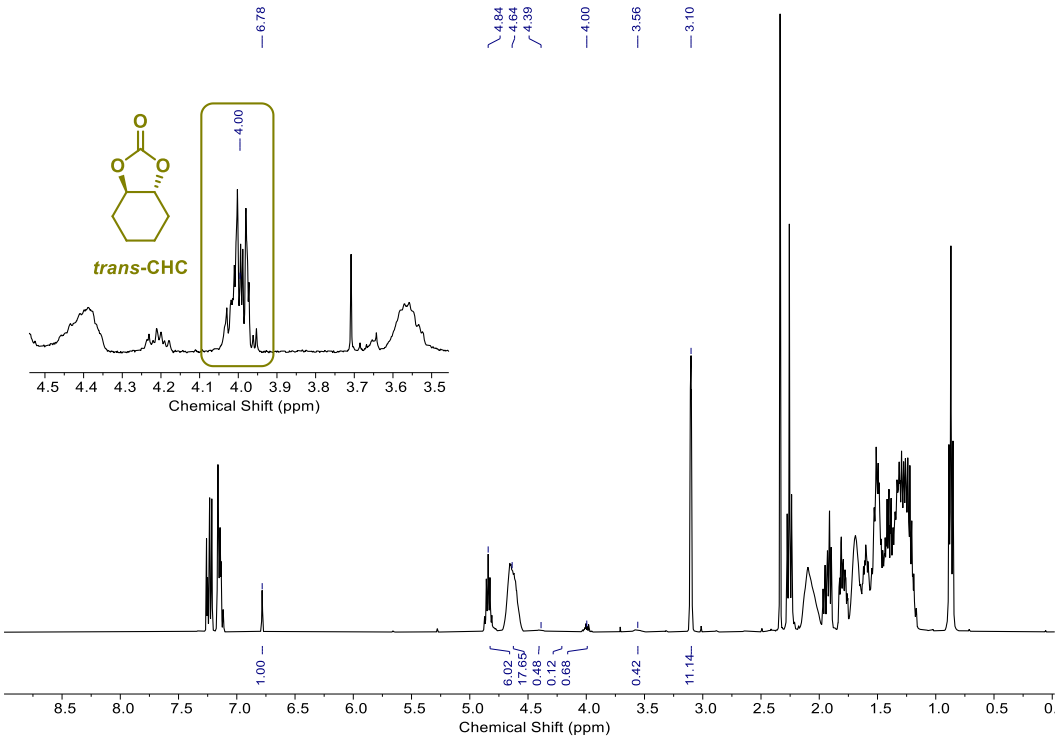


Figure S7.2. ^{1}H NMR spectrum of crude PCHC-*b*-PDL-*b*-PCHC highlighting formation of trans-cyclohexene carbonate by-product.

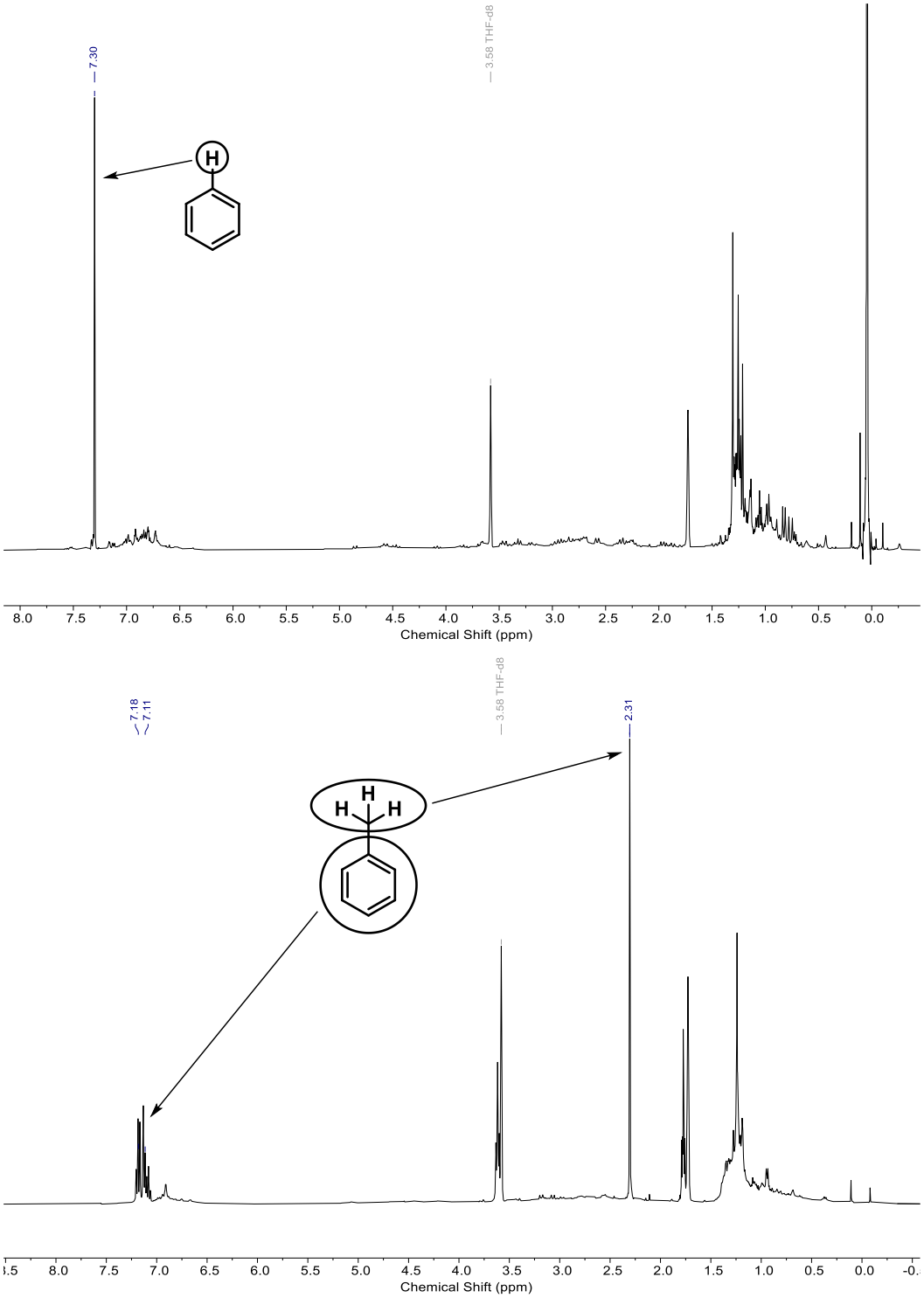


Figure S7.3. ^{1}H NMR spectra of unsuccessful attempts to synthesise heterodinuclear Zn(II)/Mg(II) catalysts with phenyl (top) and benzyl (bottom) coligands.

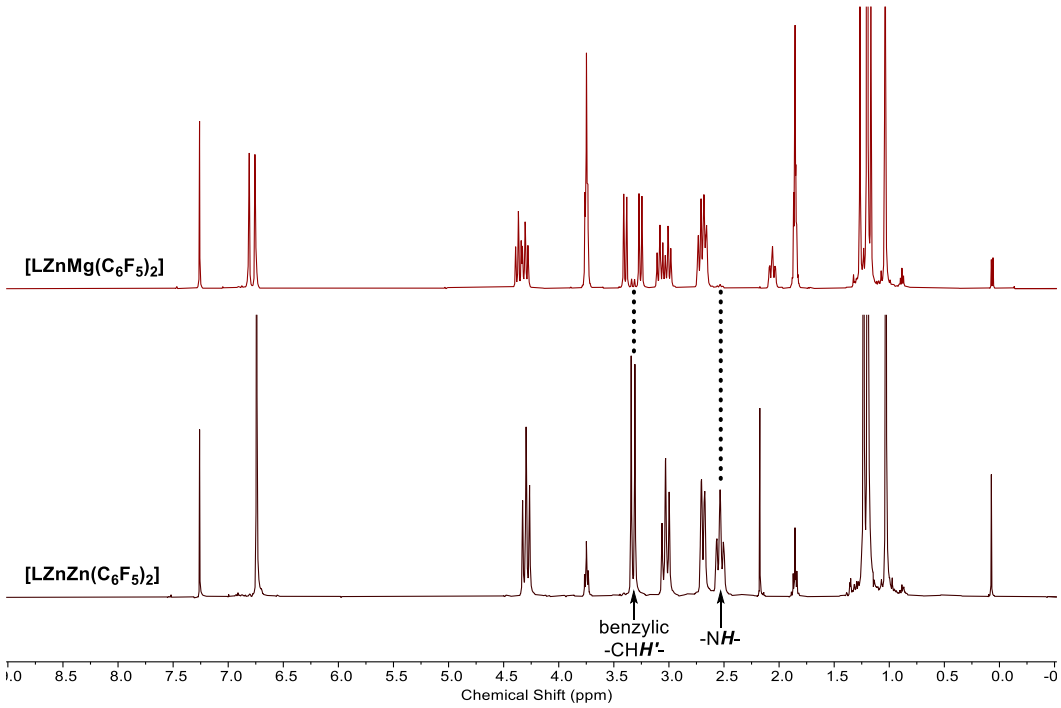


Figure S7.4. Comparison of ^{1}H NMR spectra for [LZnMg(C_6F_5)$_2$] and [LZn$_2$(C_6F_5)$_2$] complexes. [400 MHz, $CDCl_3$].

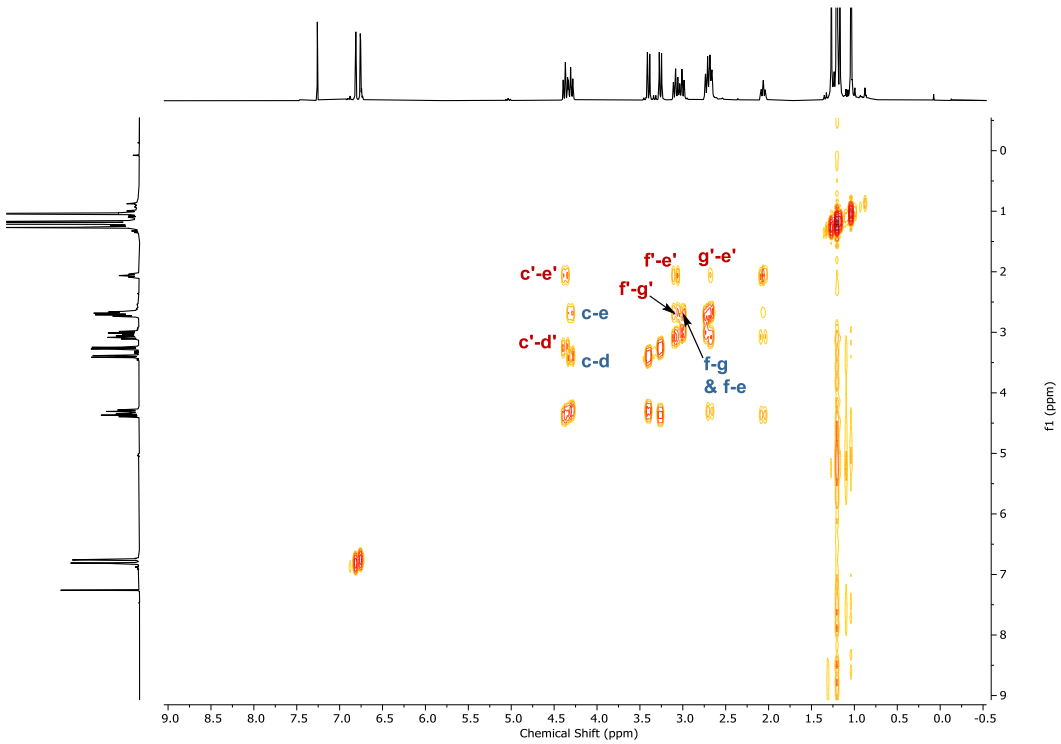


Figure S7.5. ^{1}H COSY spectrum of [LZnMg(C_6F_5)$_2$] catalyst with annotated couplings. [400 MHz, $CDCl_3$].

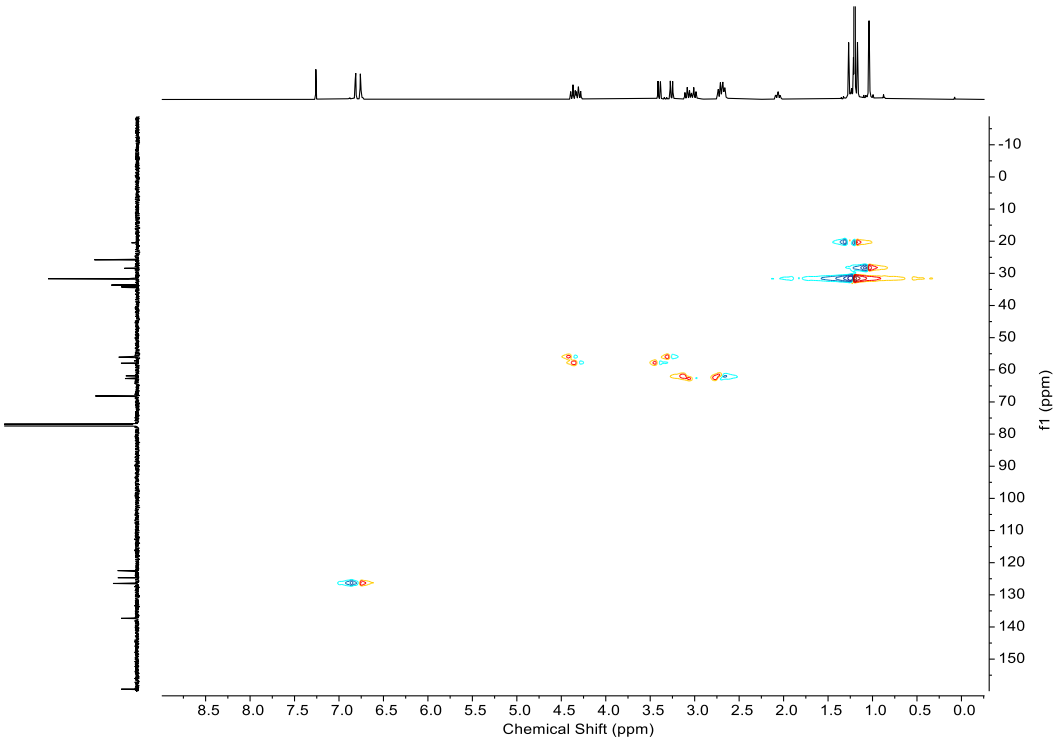


Figure S7.6. ^{1}H-^{13}C HSQC spectrum of [$LZnMg(C_6F_5)_2$] catalyst.

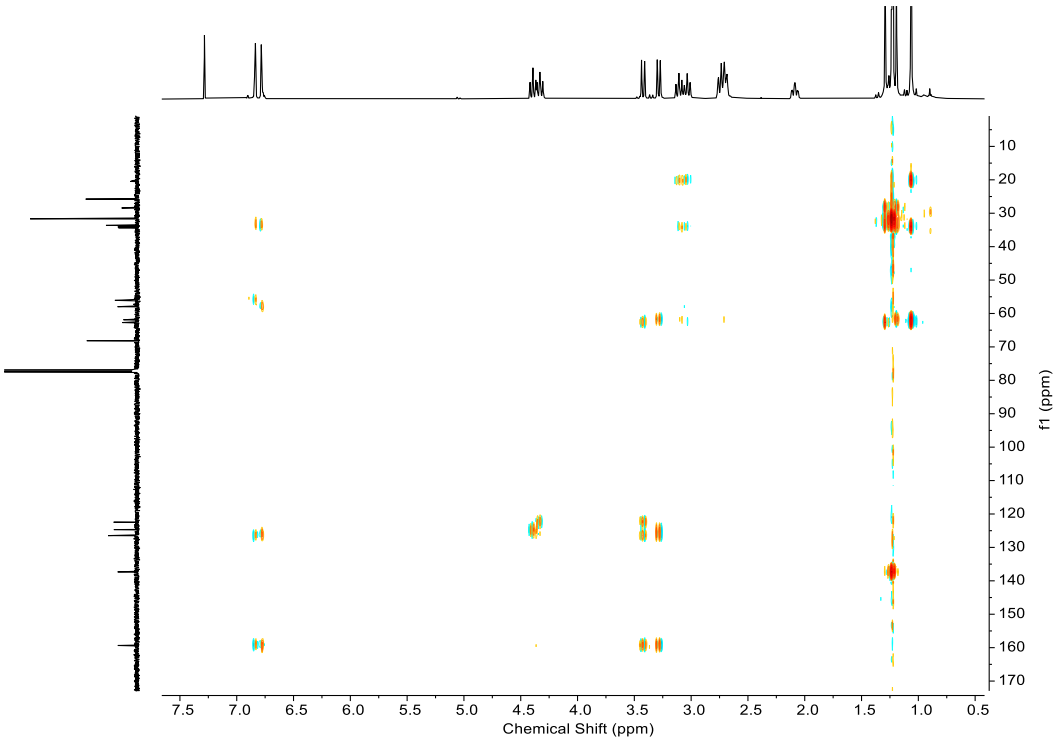


Figure S7.7. ^{1}H-^{13}C HMBC spectrum of [$LZnMg(C_6F_5)_2$] catalyst.

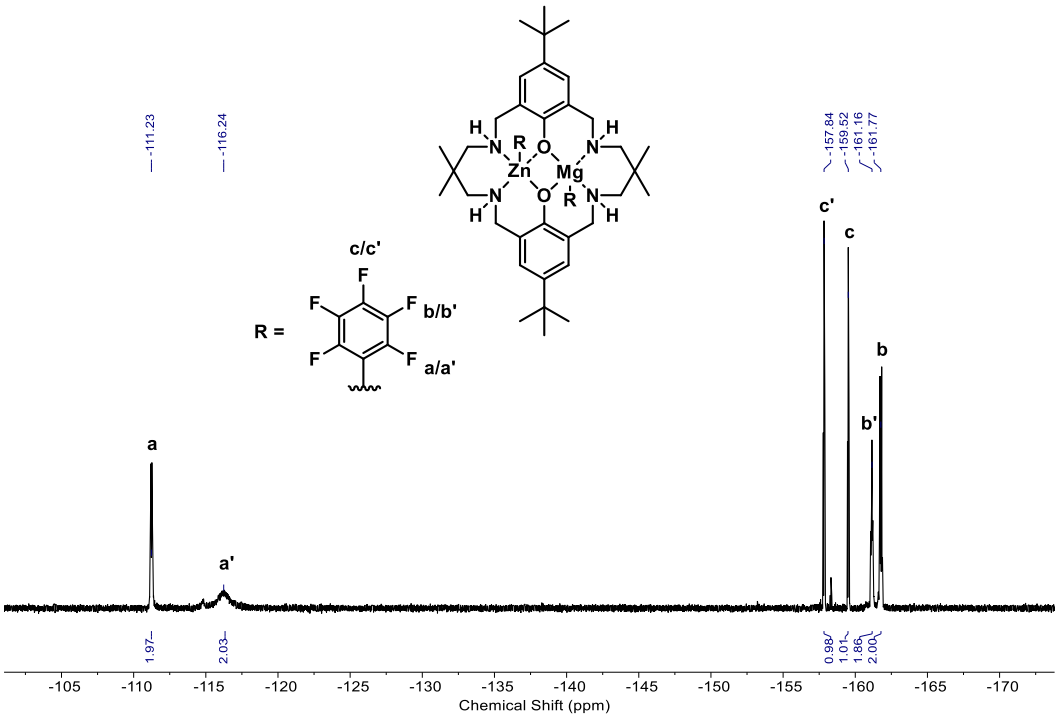


Figure S7.8. $^{19}F\{^{1}H\}$ NMR spectrum of $[LZnMg(C_6F_5)_2]$ catalyst. [376 MHz, $CDCl_3$].

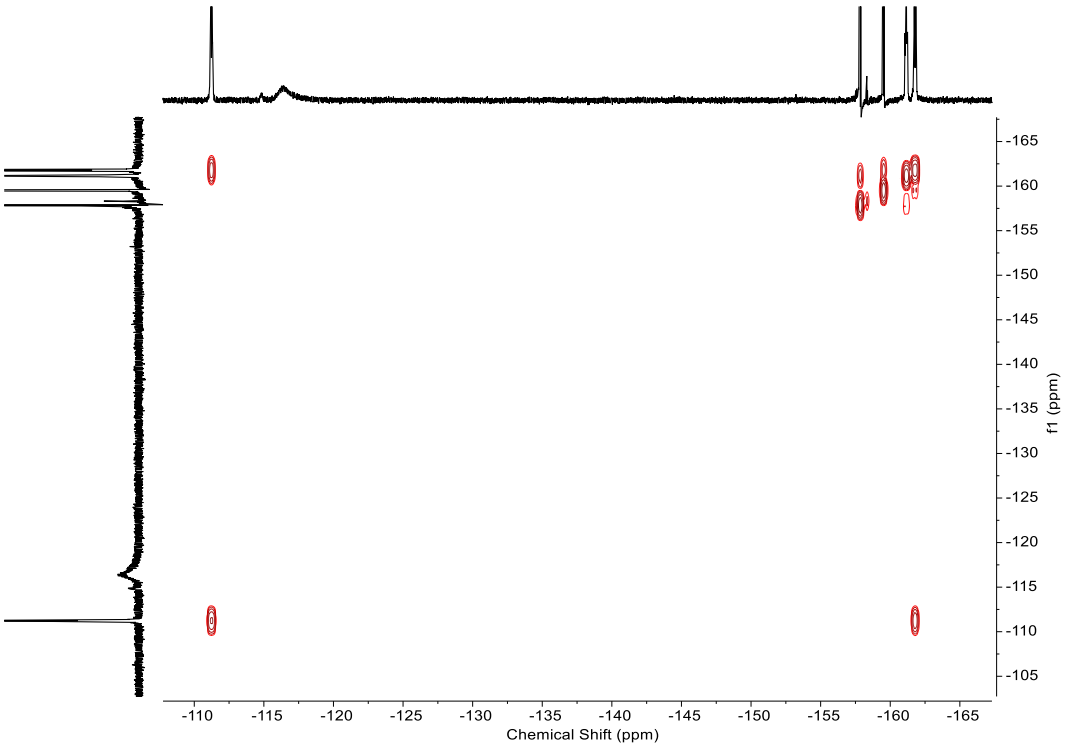


Figure S7.9. ^{19}F COSY NMR spectrum of $[LZnMg(C_6F_5)_2]$ catalyst. [376 MHz, $CDCl_3$].

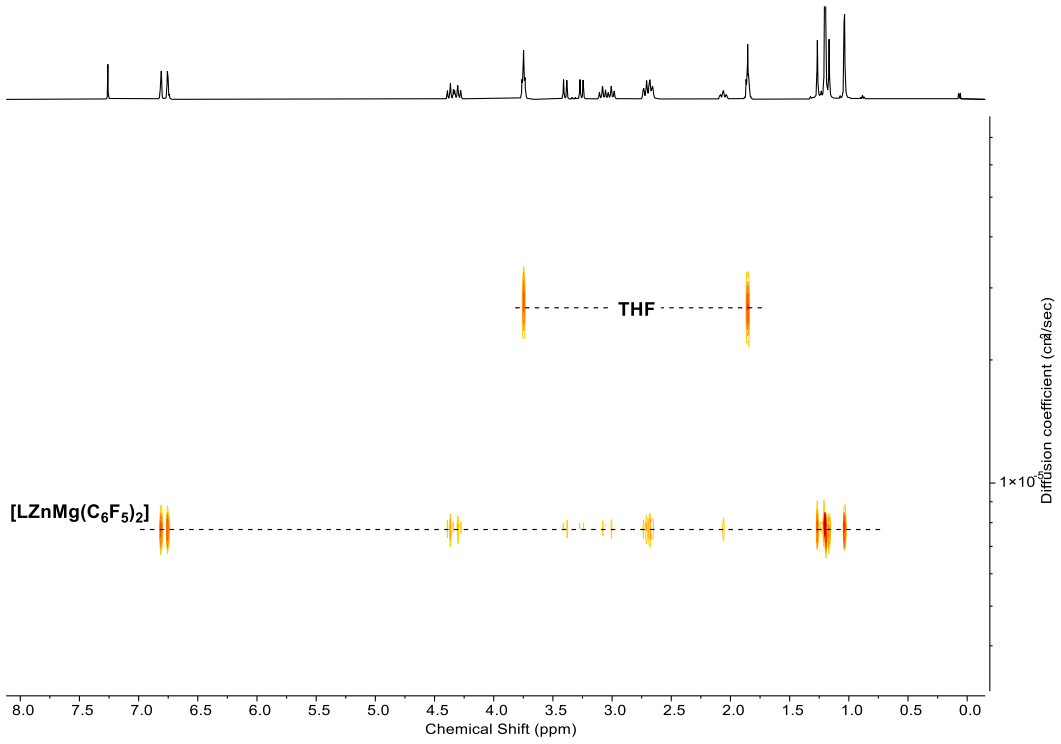


Figure S7.10. DOSY NMR spectrum of [LZnMg(C_6F_5)$_2$] catalyst. [400 MHz, $CDCl_3$].

7.2. Chapter 3

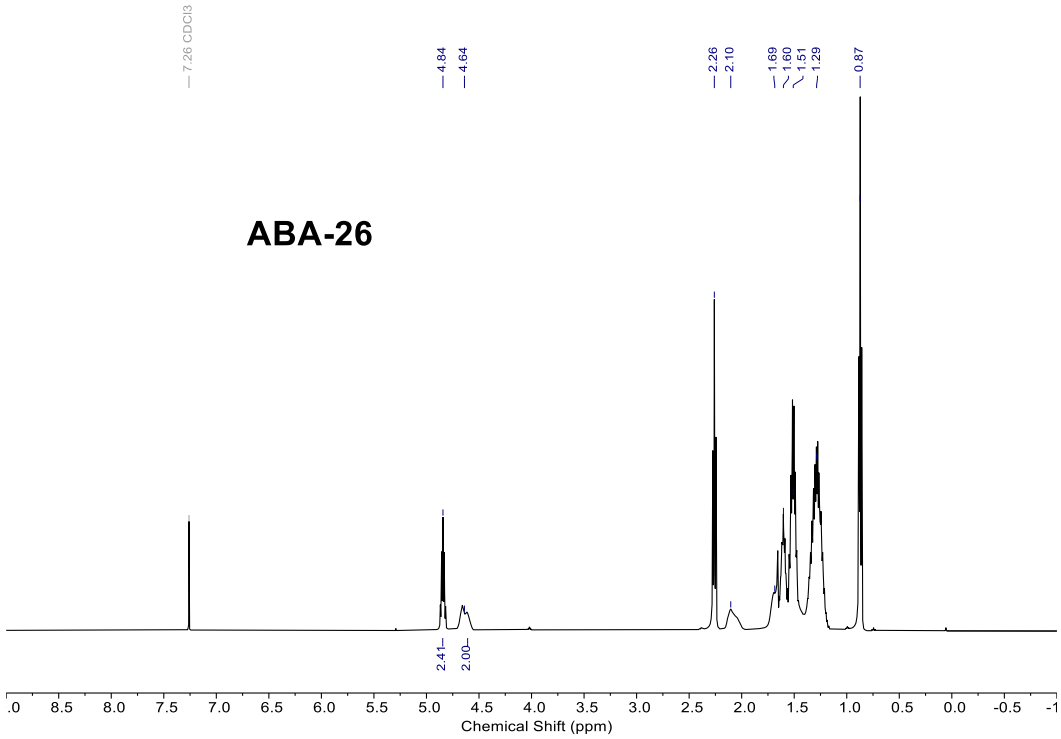


Figure S7.11. ^{1}H NMR spectrum of purified triblock polymer ABA-26.

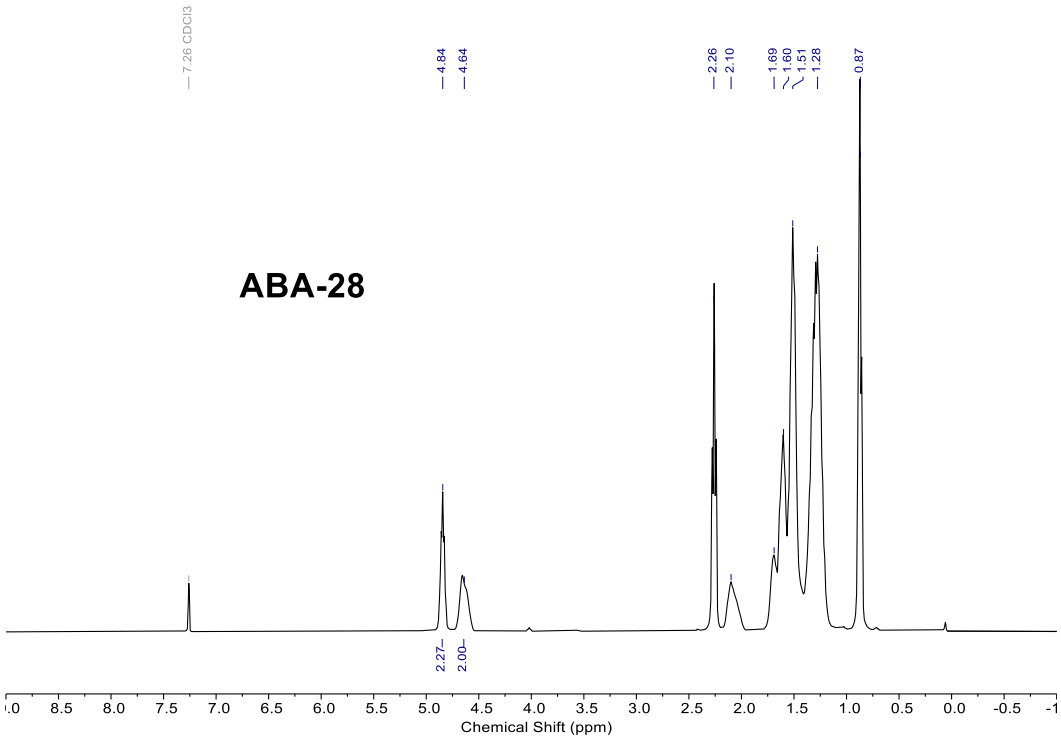


Figure S7.12. ^{1}H NMR spectrum of purified triblock polymer ABA-28.

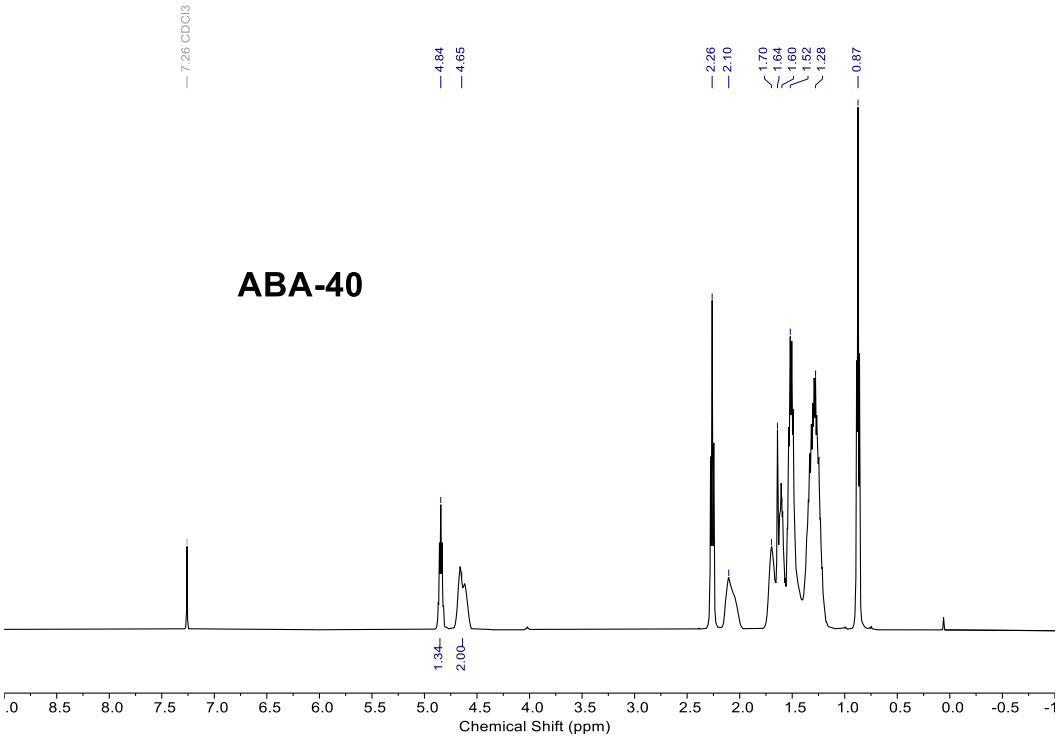


Figure S7.13. ^{1}H NMR spectrum of purified triblock polymer ABA-40.

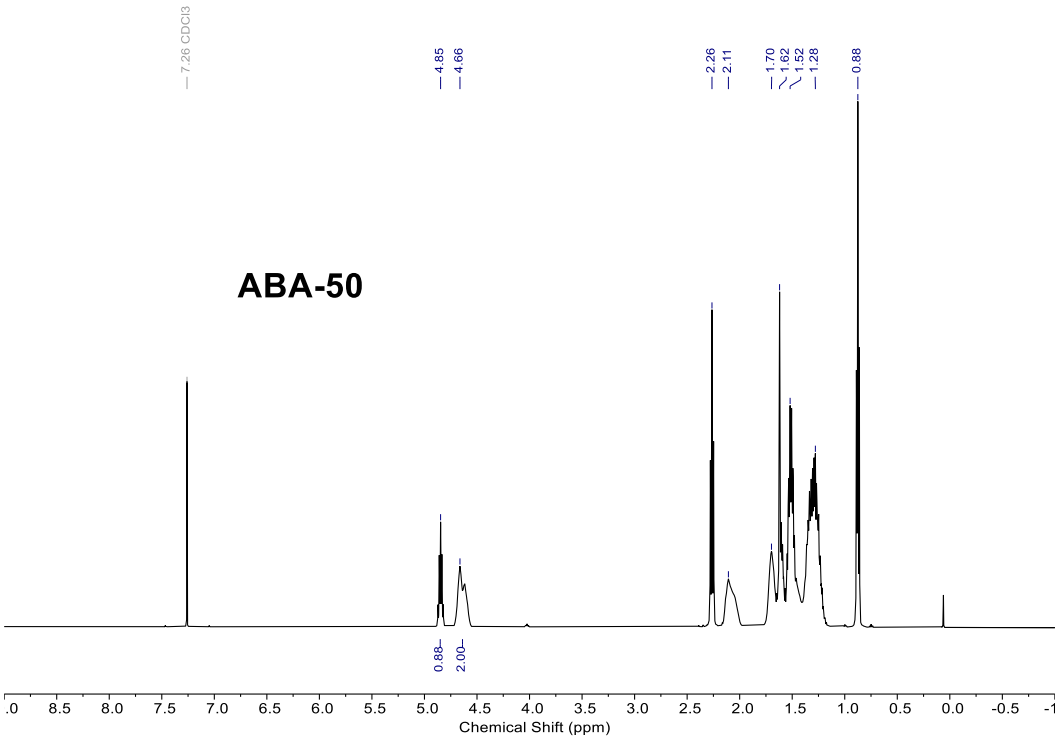


Figure S7.14. ^{1}H NMR spectrum of purified triblock polymer ABA-50.

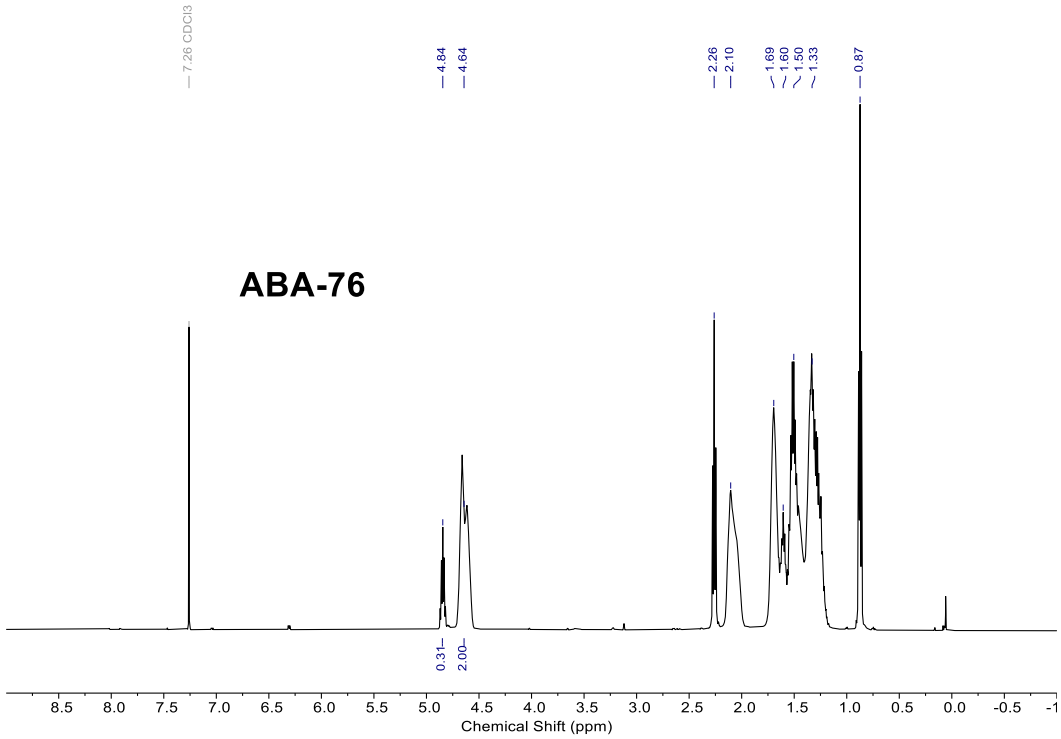


Figure S7.15. ^{1}H NMR spectrum of purified triblock polymer ABA-76.

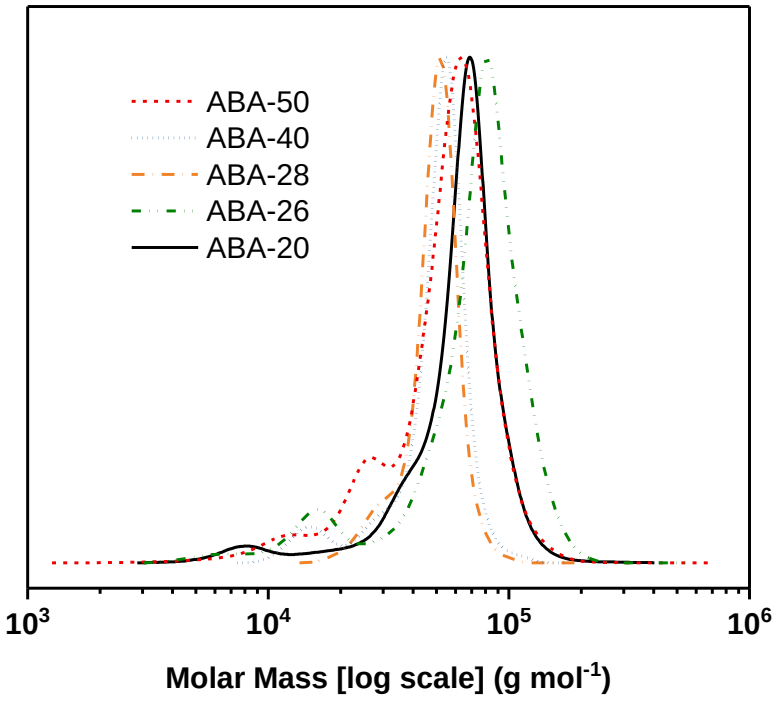


Figure S7.16. SEC chromatographs for ABA triblock polymer samples.

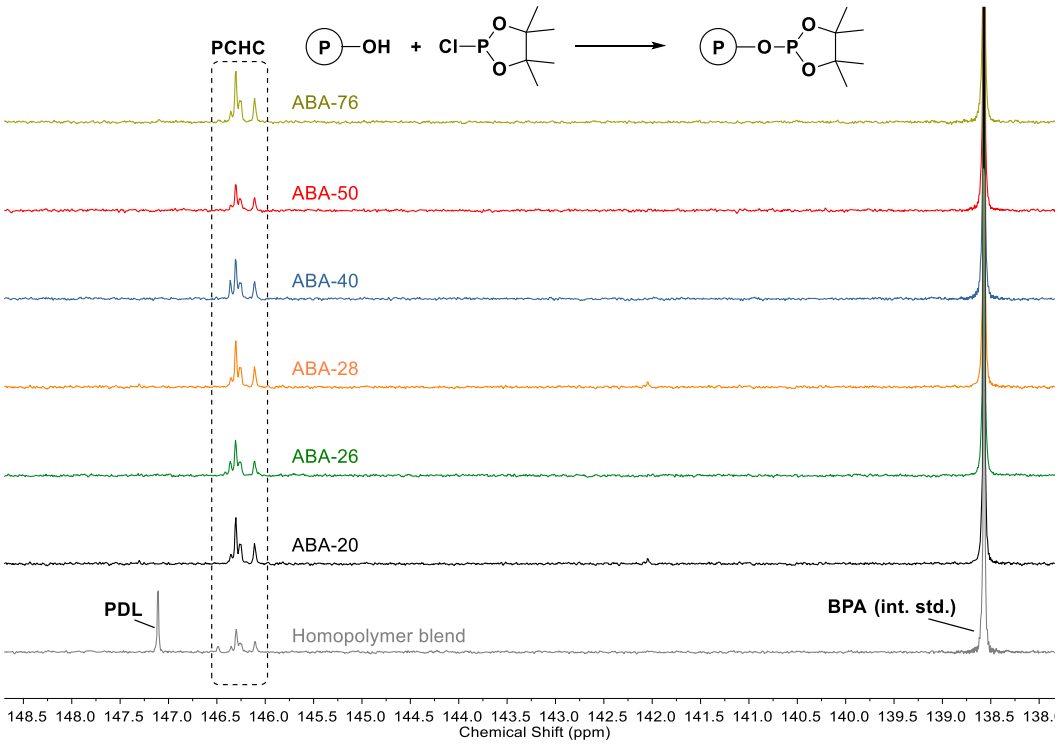


Figure S7.17. $^{31}P\{^{1}H\}$ NMR end-group analysis of ABA triblock polymer samples. [162 MHz, $CDCl_3$].



Figure S7.18. Digital photographs of ABA triblock polymer films after solvent casting.

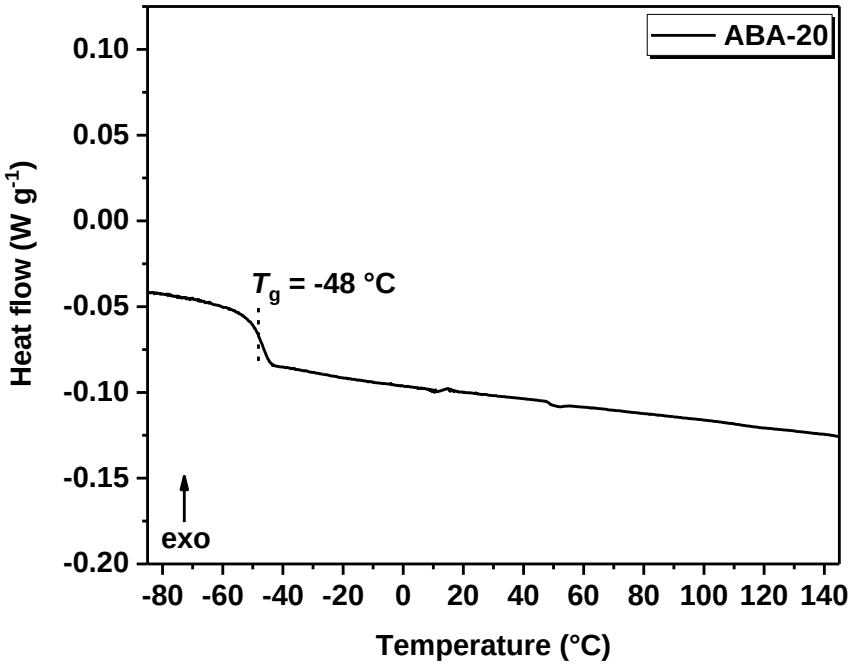


Figure S7.19. DSC thermogram of ABA-20.

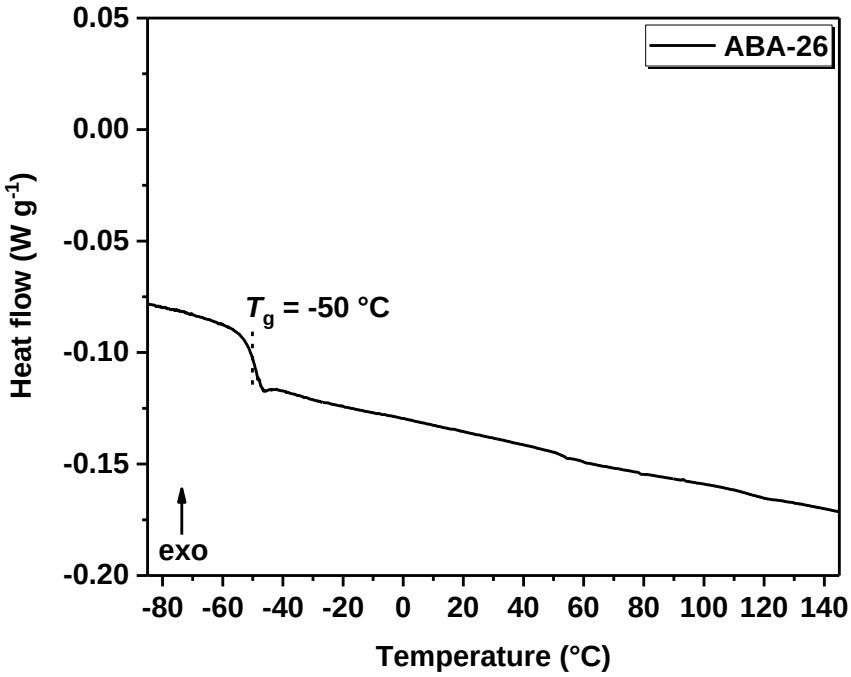


Figure S7.20. DSC thermogram of ABA-26.

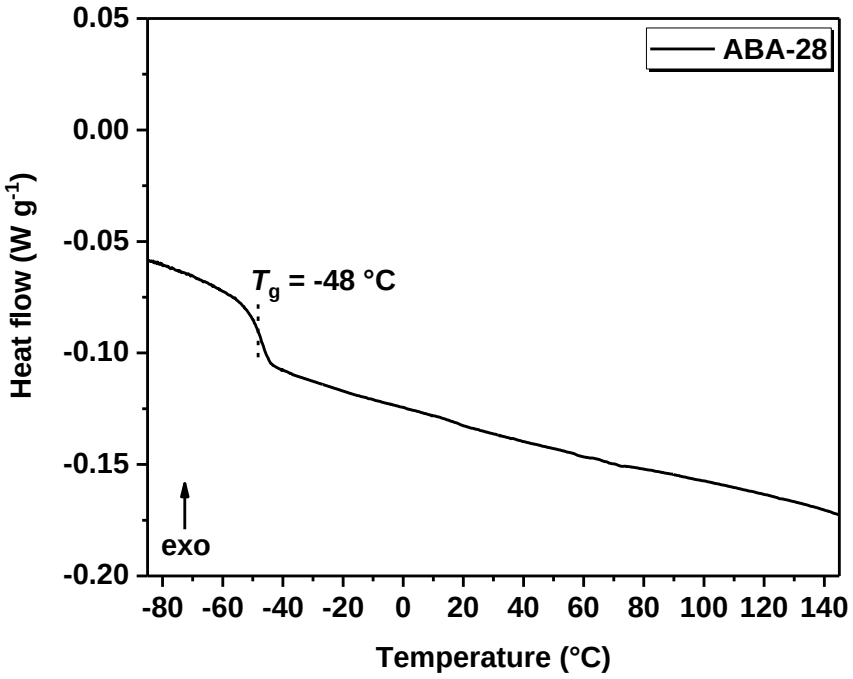


Figure S7.21. DSC thermogram of ABA-28.

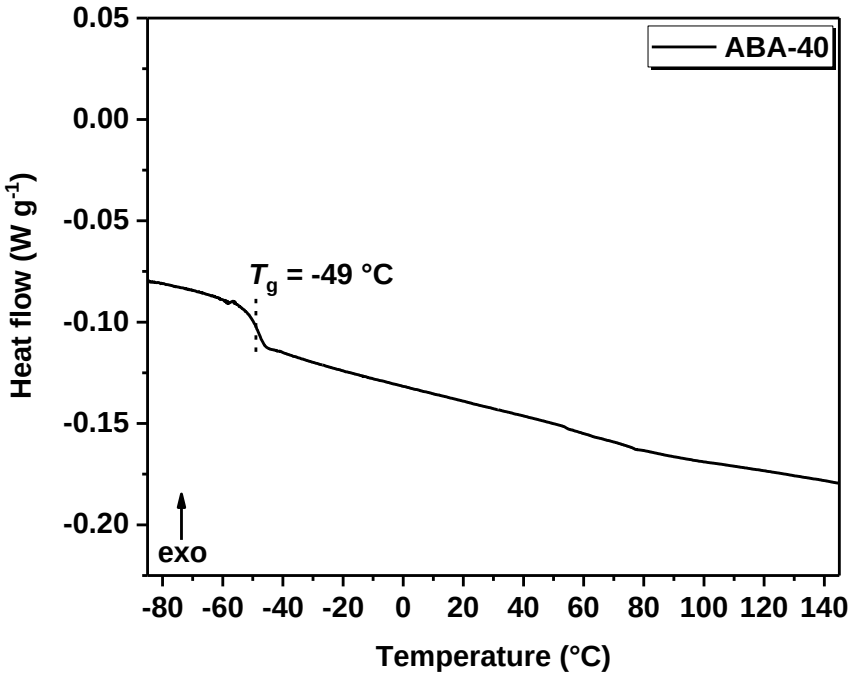


Figure S7.22. DSC thermogram of ABA-40.

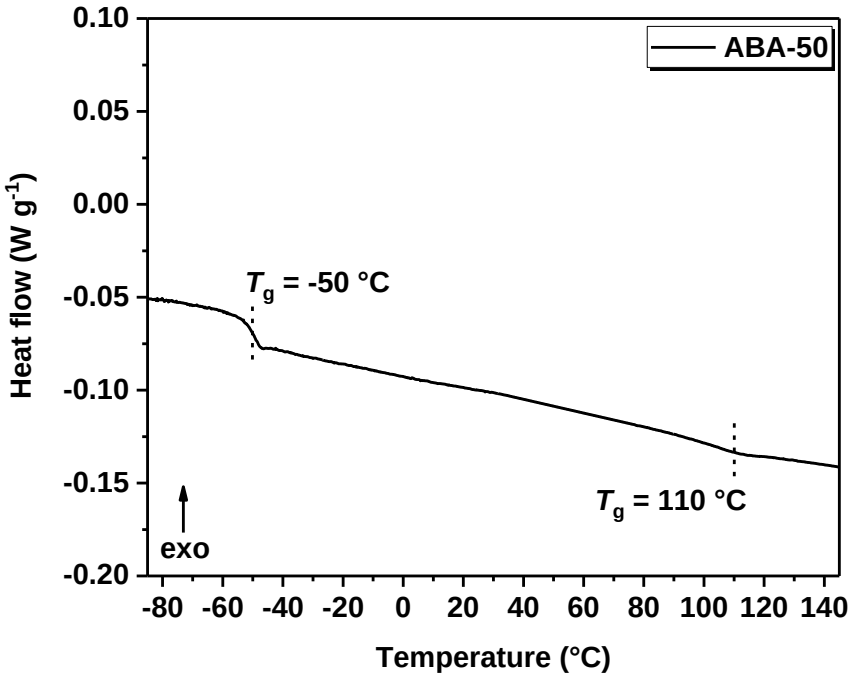


Figure S7.23. DSC thermogram of ABA-50.

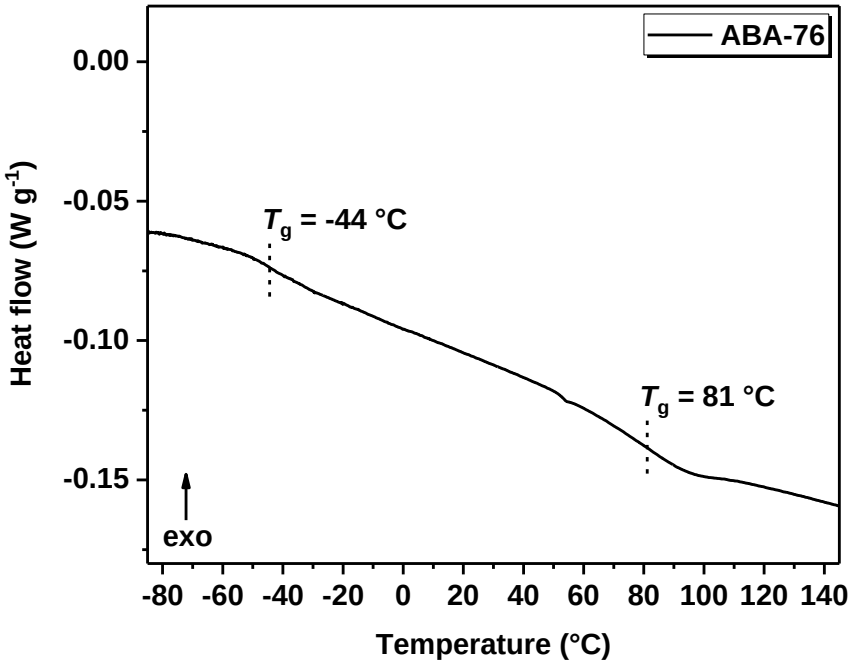


Figure S7.24. DSC thermogram of ABA-76.

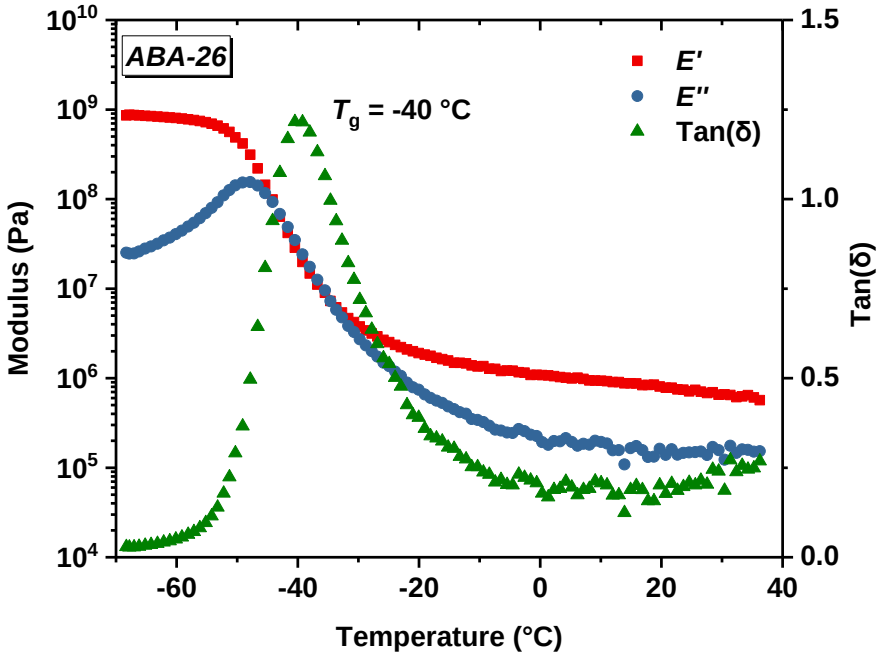


Figure S7.25. DMTA low temperature sweep profile (-70 – 40 °C) for ABA-26. ω = 1 Hz, γ = 0.1 %, heating rate = 5 °C min^{-1}.

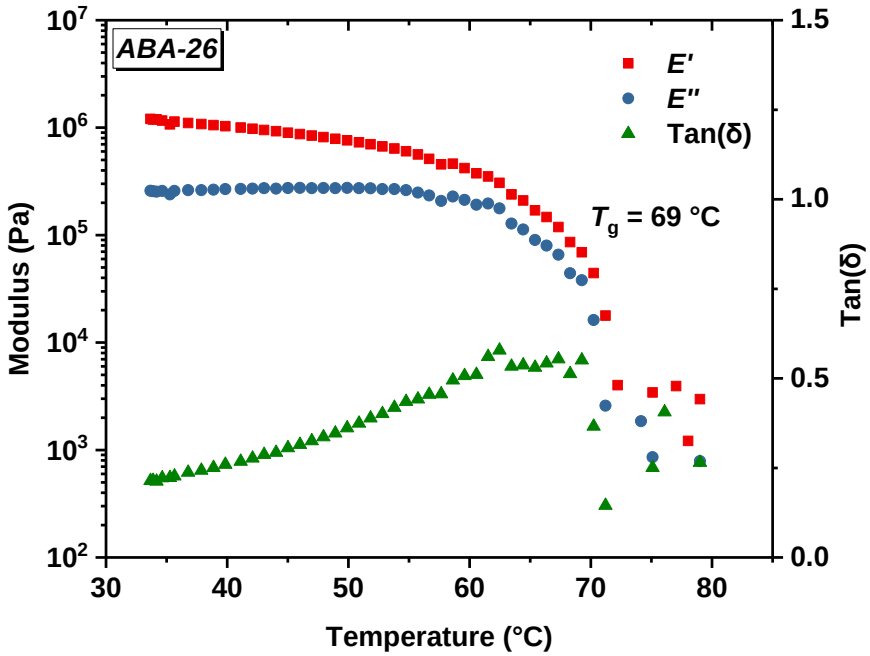


Figure S7.26. DMTA high temperature sweep profile (35 – 80 °C) for ABA-26. ω = 1 Hz, γ = 0.1 %, heating rate = 5 °C min^{-1}.

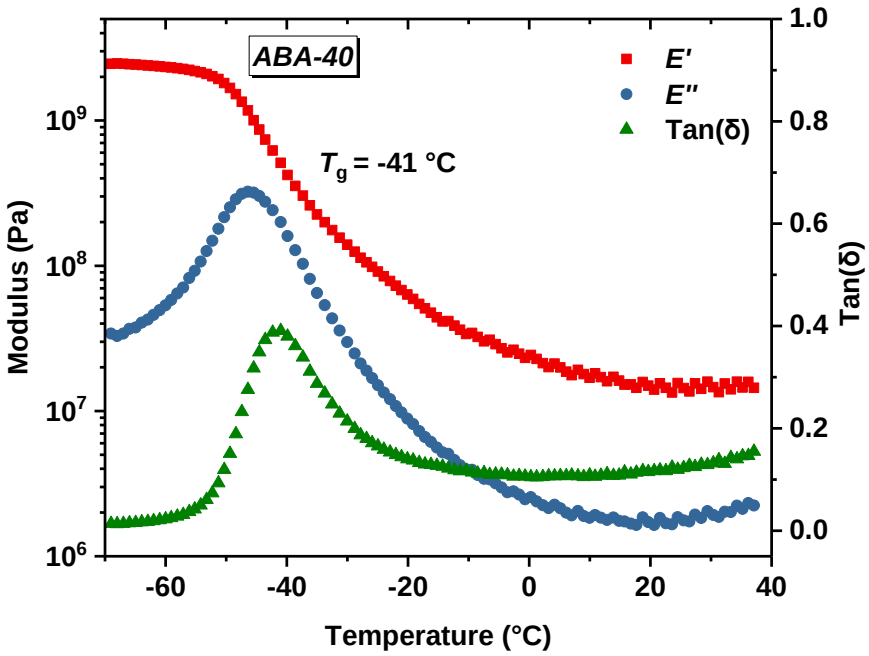


Figure S7.27. DMTA low temperature sweep profile (-70 – 40 °C) for ABA-40. ω = 1 Hz, γ = 0.1 %, heating rate = 5 °C min^{-1}.

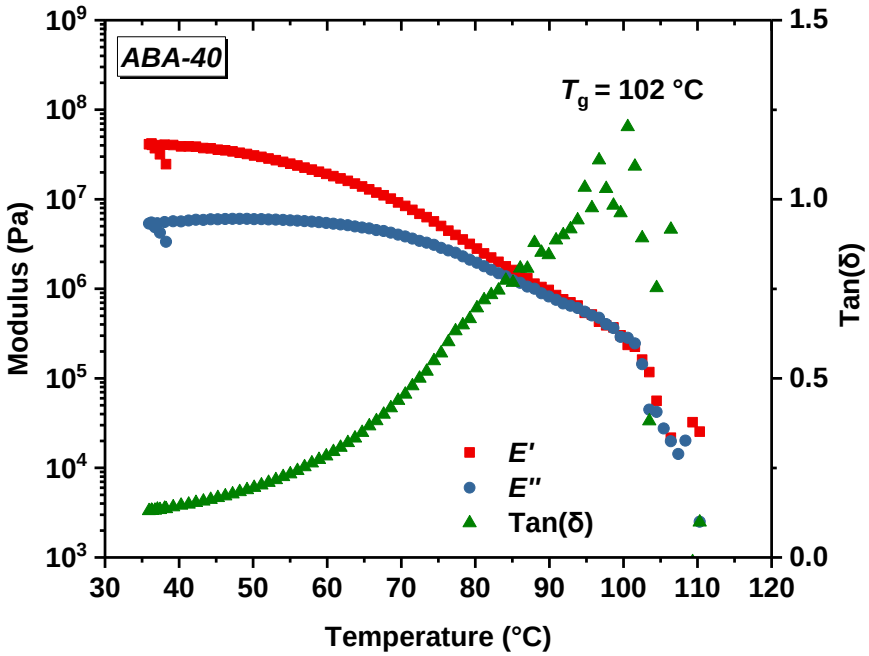


Figure S7.28. DMTA high temperature sweep profile (35 – 110 °C) for ABA-40. ω = 1 Hz, γ = 0.1 %, heating rate = 5 °C min^{-1}.

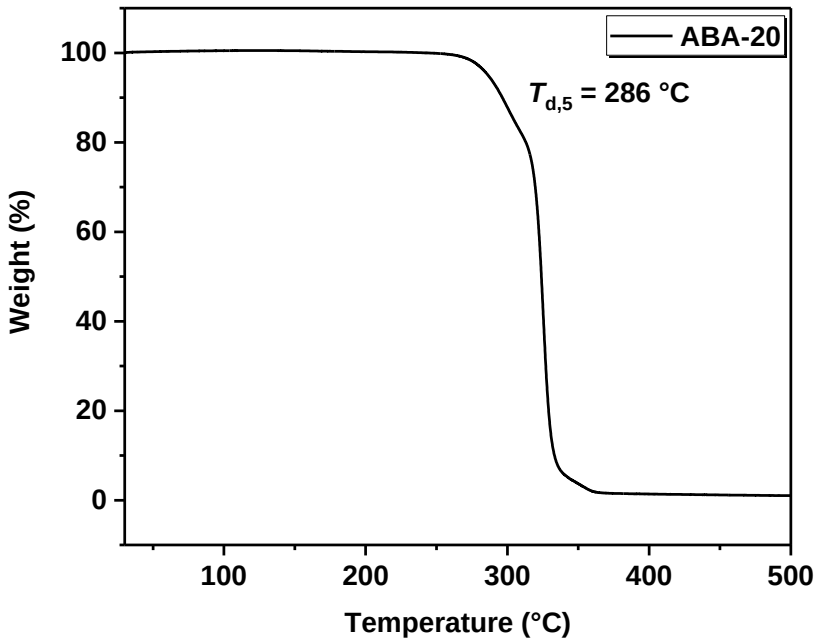


Figure S7.29. TGA profile of triblock polymer ABA-20.

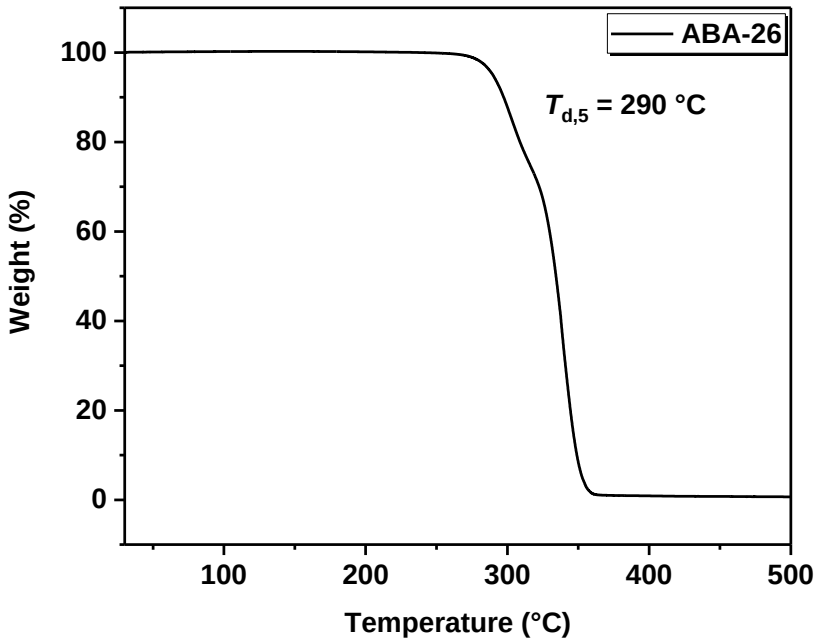


Figure S7.30. TGA profile of triblock polymer ABA-26.

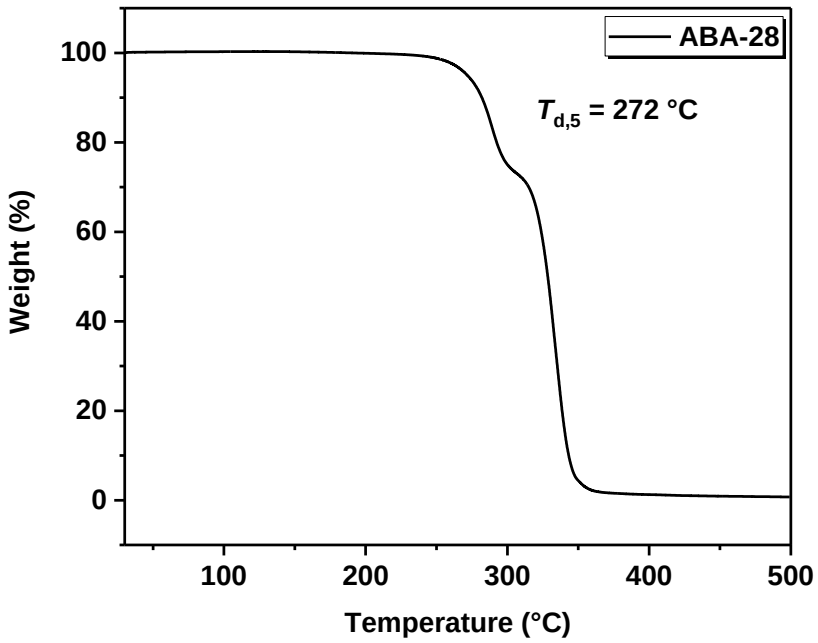


Figure S7.31. TGA profile of triblock polymer ABA-28.

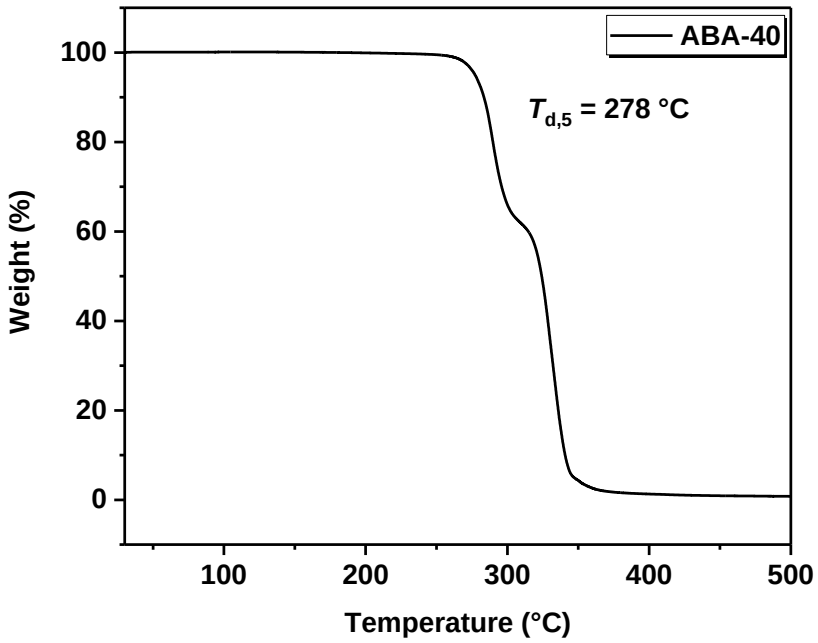


Figure S7.32. TGA profile of triblock polymer ABA-40.

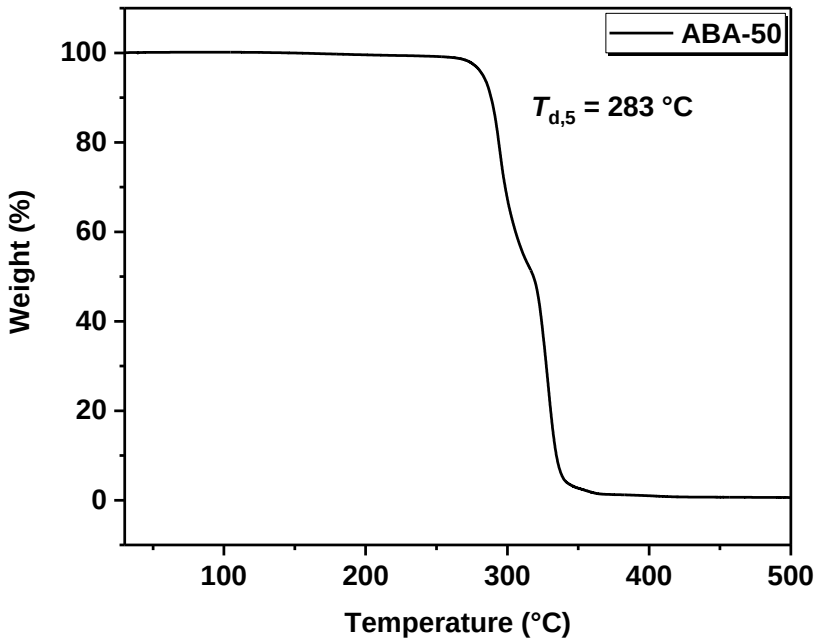


Figure S7.33. TGA profile of triblock polymer ABA-50.

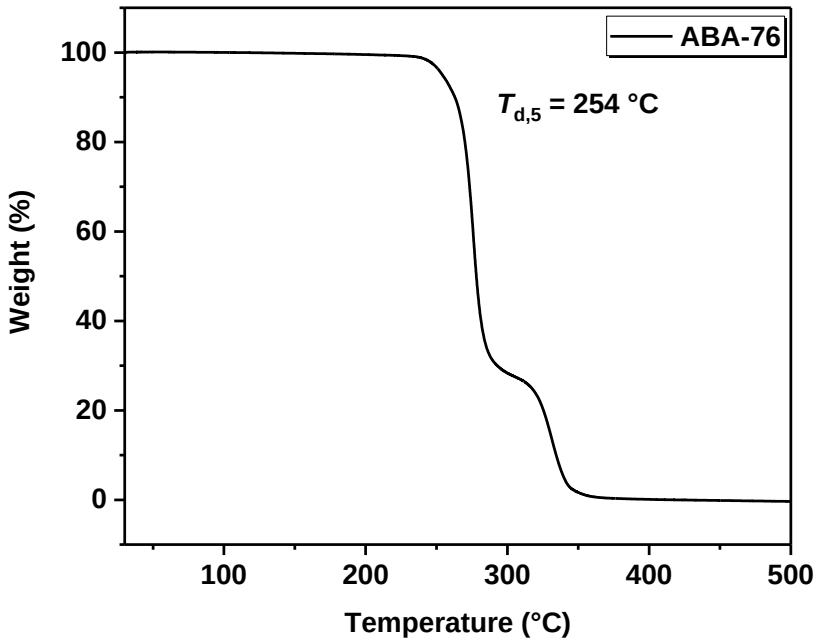


Figure S7.34. TGA profile of triblock polymer ABA-76.

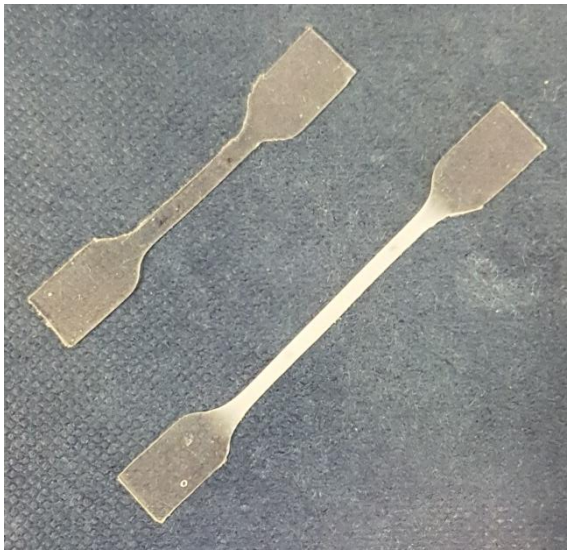


Figure S7.35. Digital photograph of ABA-50 tensile specimens (pristine and post-uniaxial extension) with visual identification of stress-whitening.

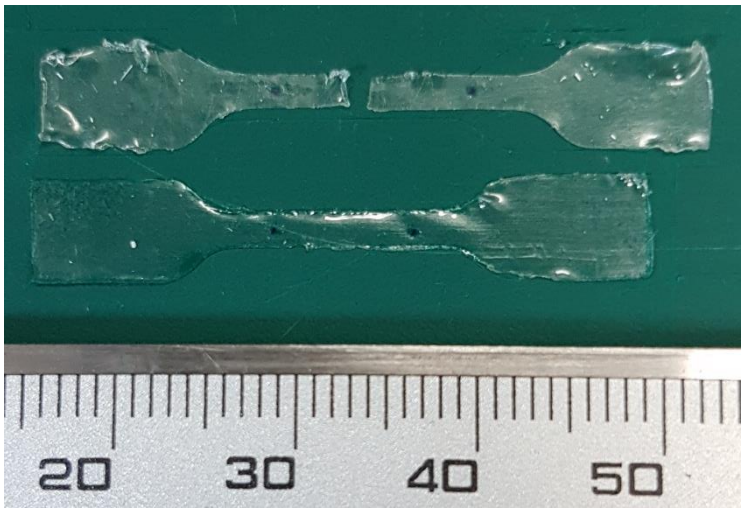


Figure S7.36. Digital photograph of ABA-28 tensile specimens (pristine and post-fracture).

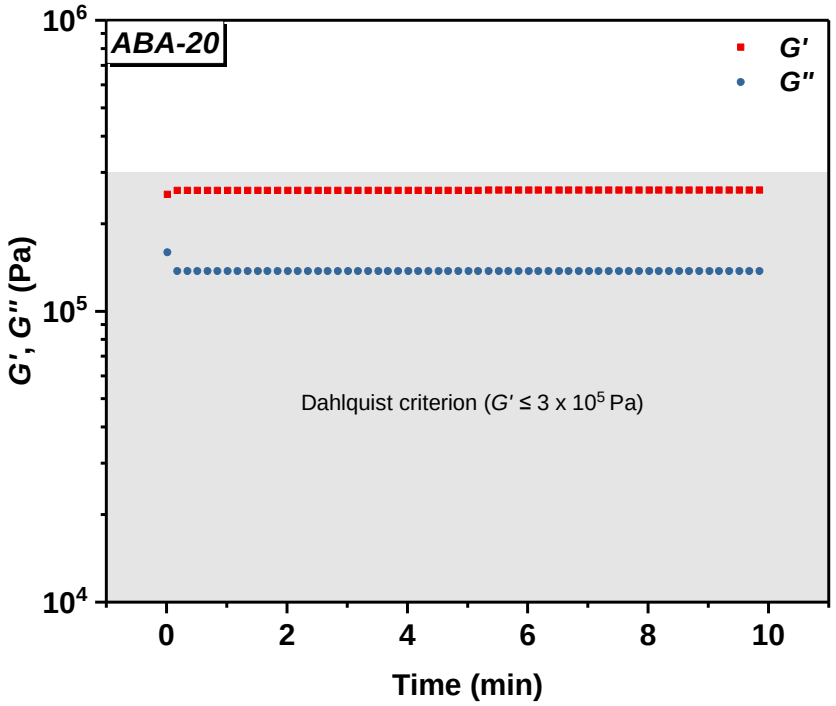


Figure S7.37. Fixed-strain oscillation *vs.* time for sample ABA-20, showing storage (*G'*) and loss (*G"*) modulus over a 10 minute period at ambient temperature (25 °C). Grey area represents *G'* values below the Dahlquist criterion. ω = 1 Hz, γ = 0.5%.



Figure S7.38. Digital photograph of ABA-20 after 180° Peel Test showing residue following cohesive failure.

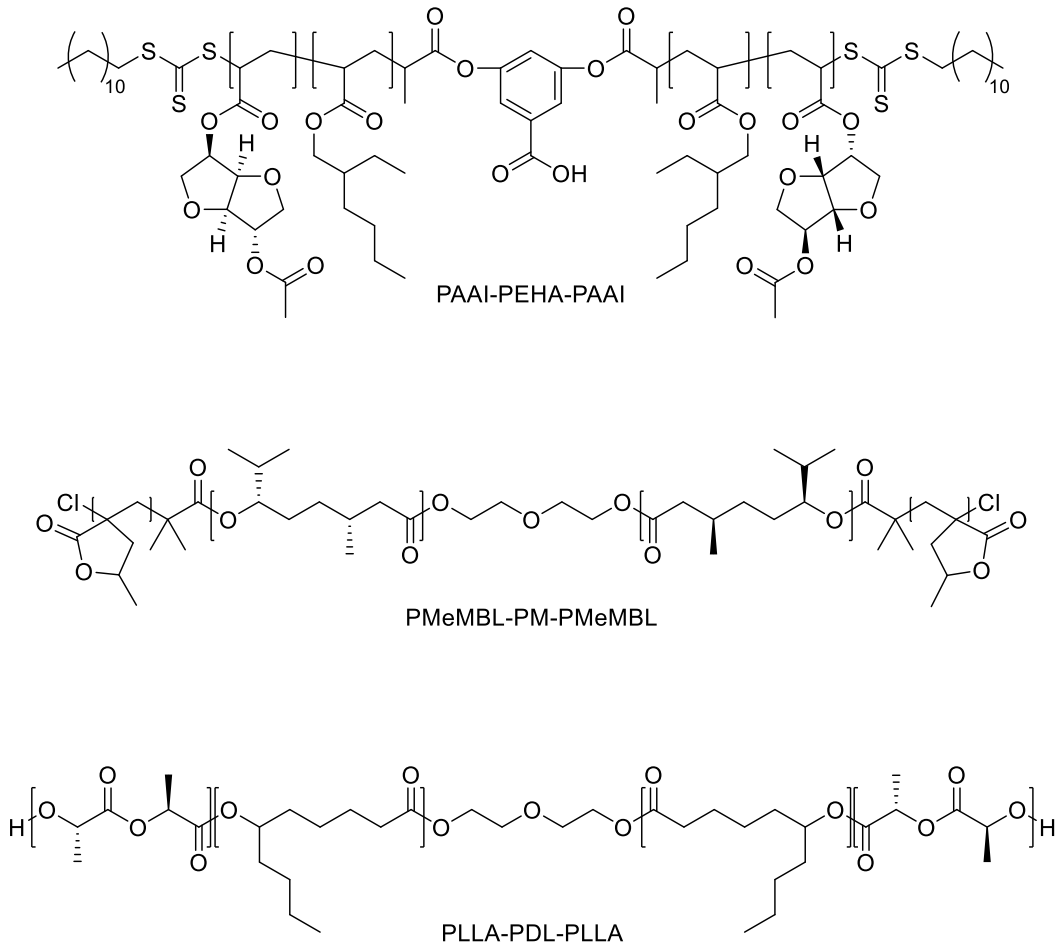


Figure S7.39. Chemical structures of triblock polymer pressure-sensitive adhesives selected from the literature. PAAI-PEHA-PAAI = acrylic PSA[1]; PMeMBL-PM-PMeMBL = acrylic/ester PSA[2]; PLLA-PDL-PLLA = ester PSA[3].

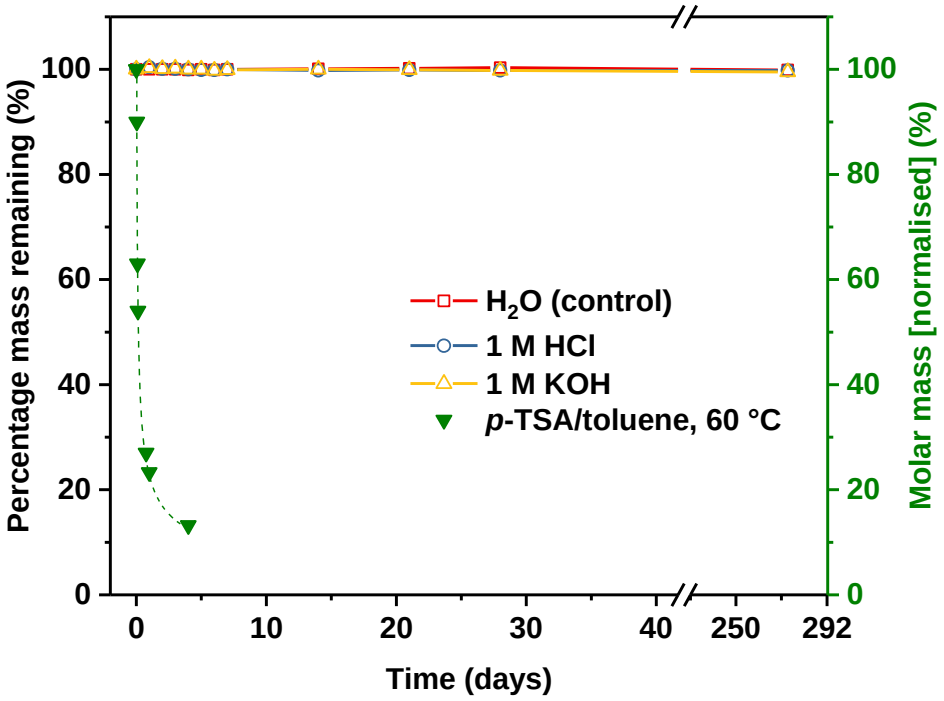


Figure S7.40. Stability tests on ABA-50 film submerged at 25 °C in distilled water (□), 1 M HCl (○), and 1 M KOH (△) (left y-axis); and accelerated degradation of ABA-50 sample dissolved in toluene at 60 °C with [*p*-TsOH.H_2O] = 5 mM (▼) (right y-axis).

7.3. Chapter 4

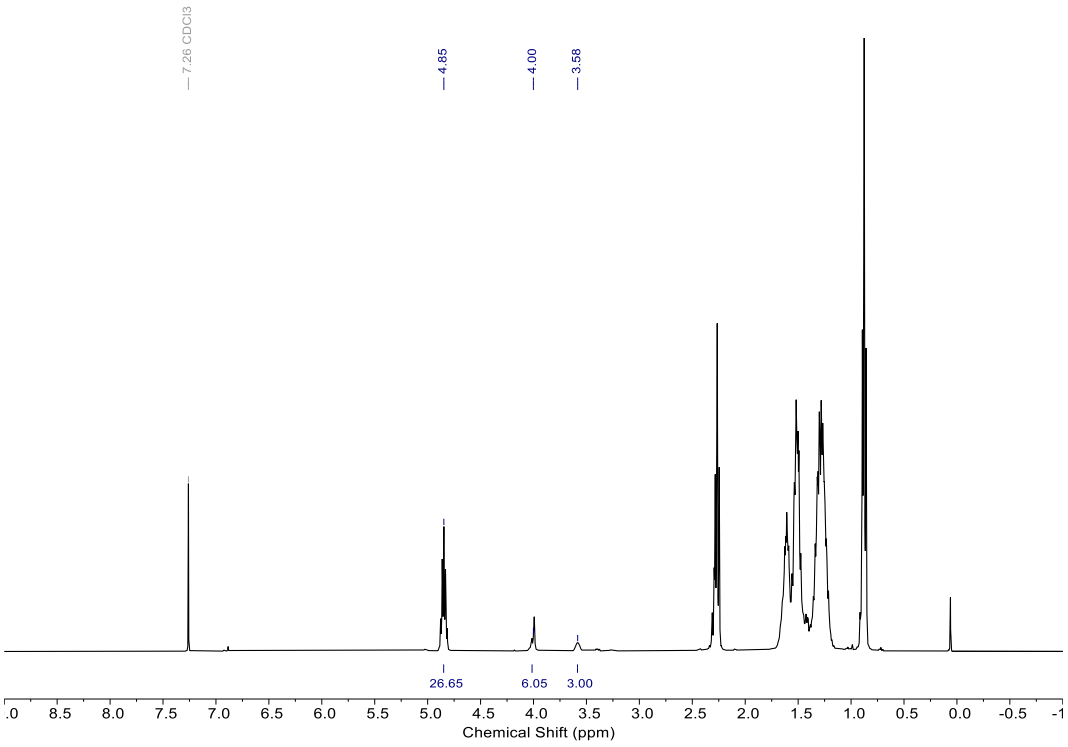


Figure S7.41. ^{1}H NMR spectrum of purified 3-arm star poly(ε-decalactone) $(PDL)_3$. [400 MHz, $CDCl_3$].

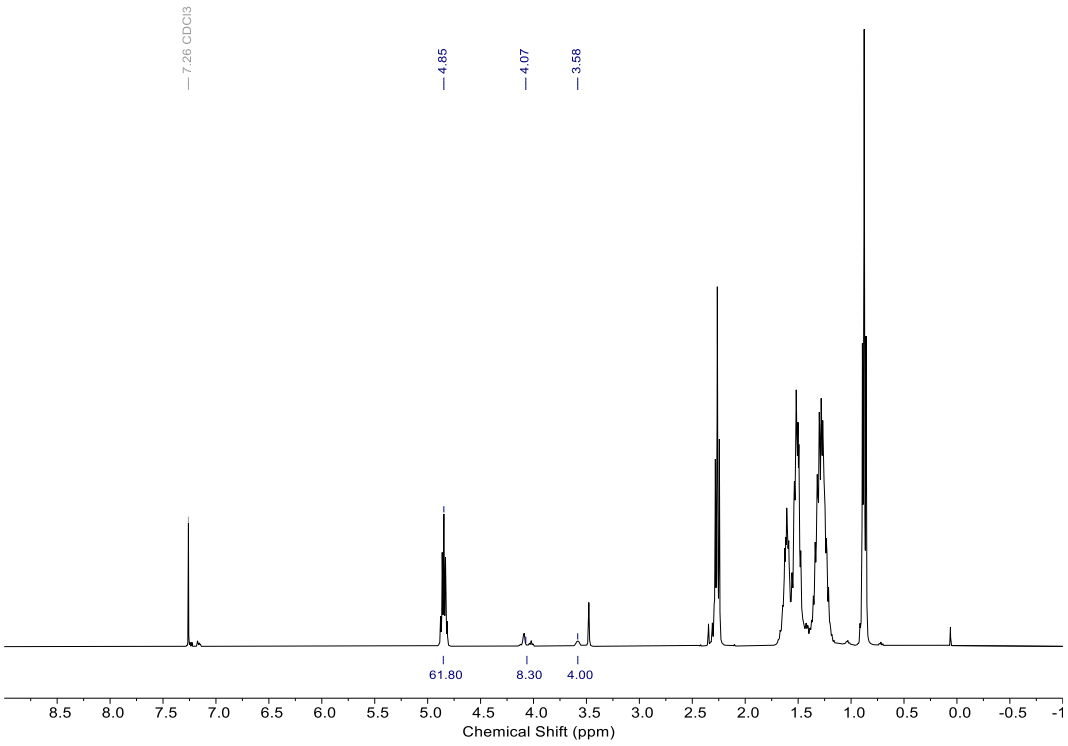


Figure S7.42. ^{1}H NMR spectrum of purified 4-arm star poly(ε-decalactone) $(PDL)_4$. [400 MHz, $CDCl_3$].

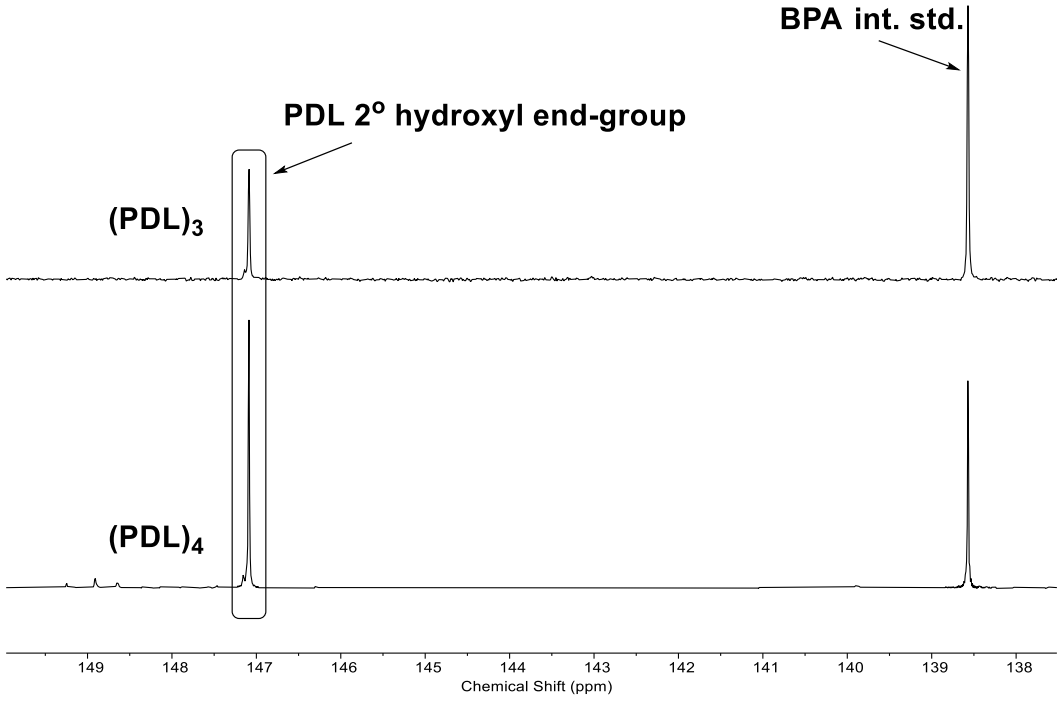


Figure S7.43. $^{31}P\{^{1}H\}$ NMR end-group analysis of $(PDL)_n$ star polymers.

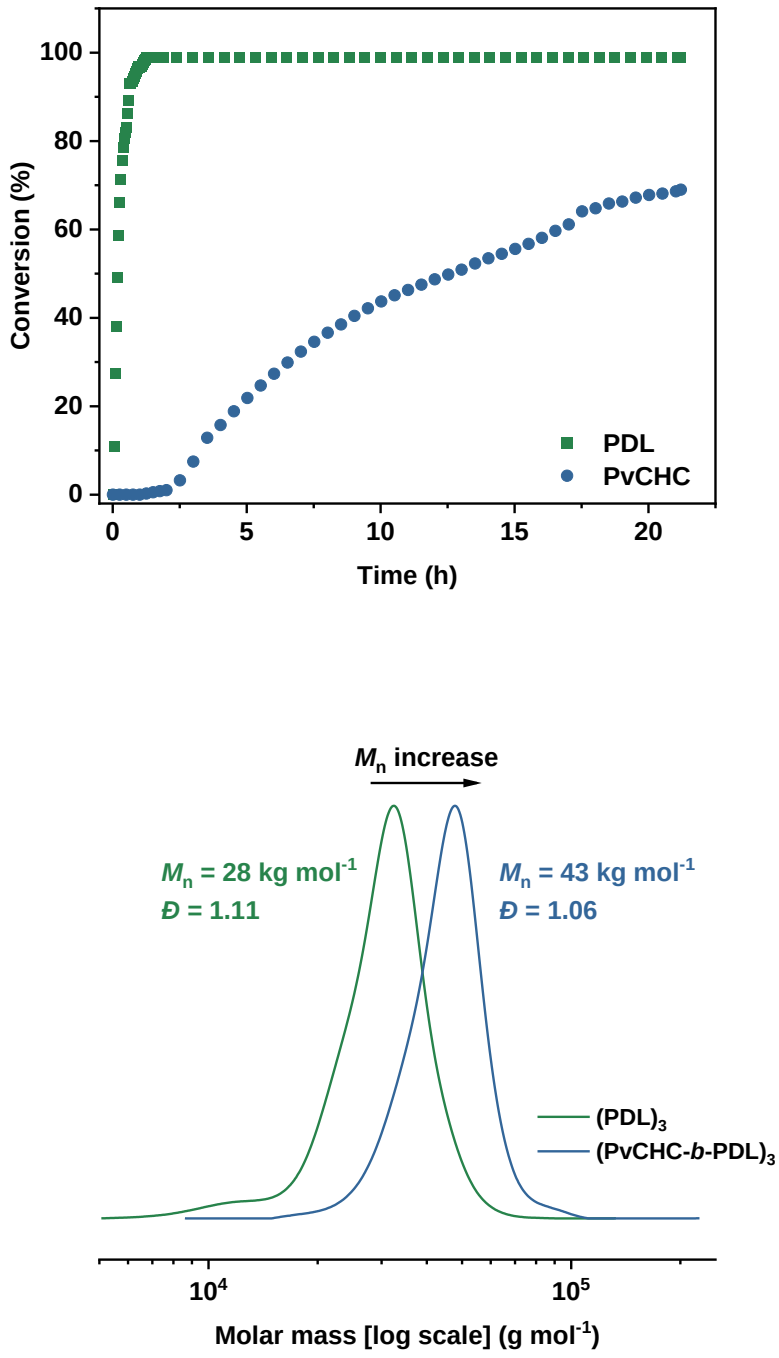


Figure S7.44. Reaction monitoring for synthesis of (PvCHC-*b*-PDL)$_3$ star block polymer. Top: *In-situ* ATR-IR spectroscopy. Bottom: SEC aliquots taken under N_2 (green) and CO_2 (blue) atmosphere reaction stages.

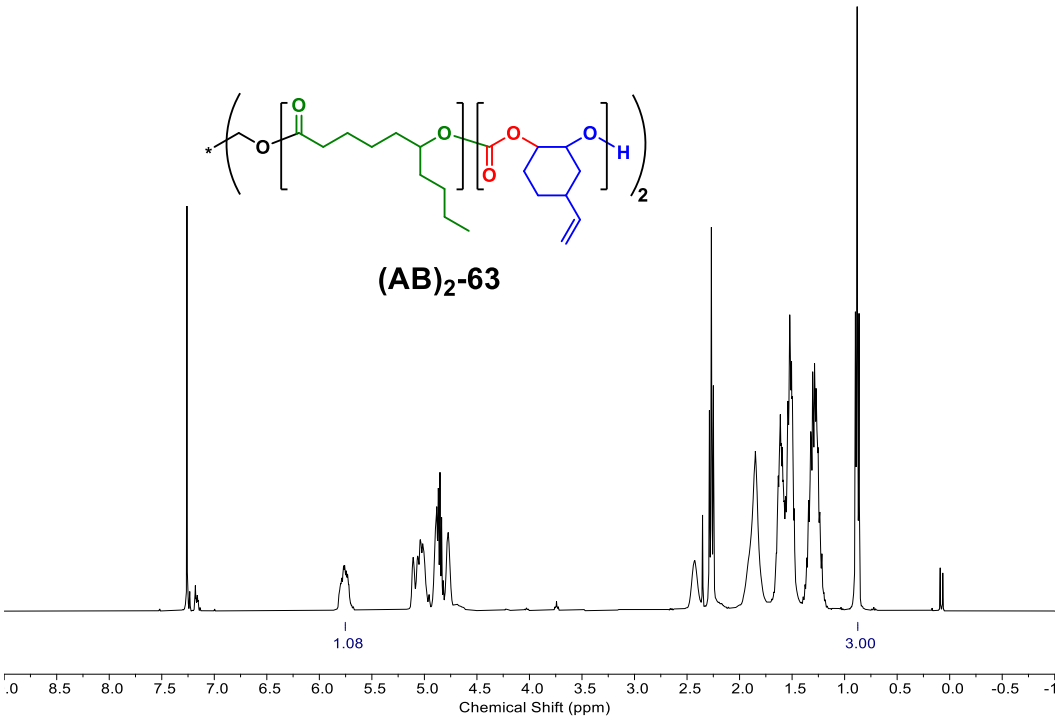


Figure S7.45. ^{1}H NMR spectrum of purified 2-arm star block polymer $(AB)_2$-63. [400 MHz, $CDCl_3$].

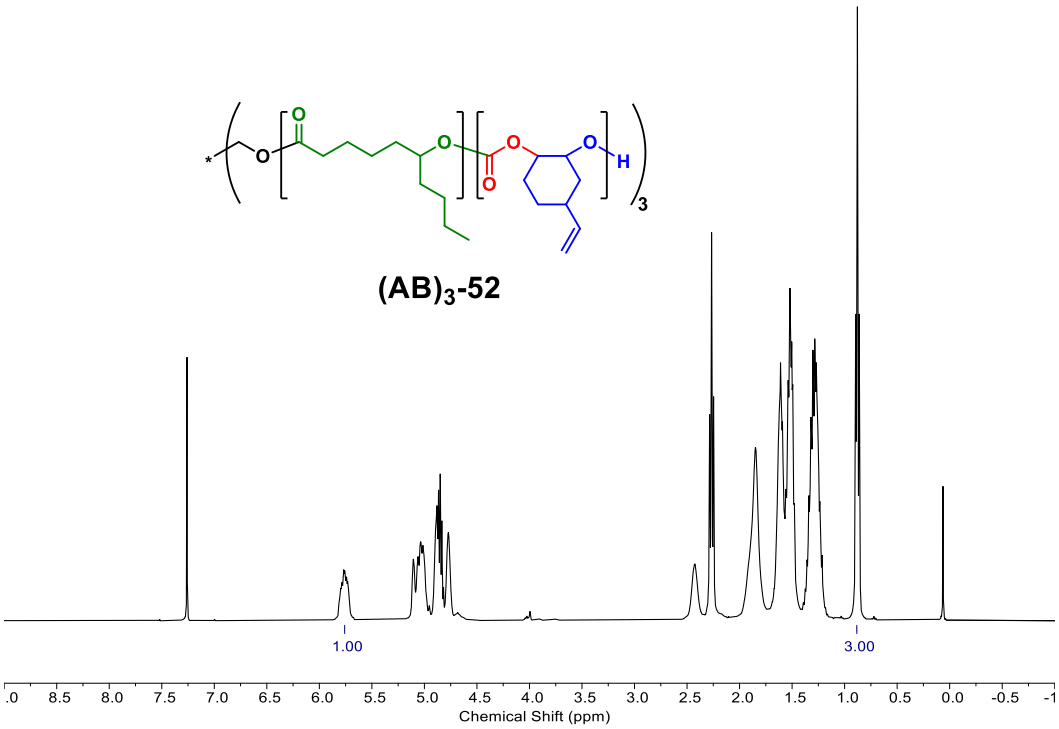


Figure S7.46. ^{1}H NMR spectrum of purified 3-arm star block polymer $(AB)_3$-52. [400 MHz, $CDCl_3$].

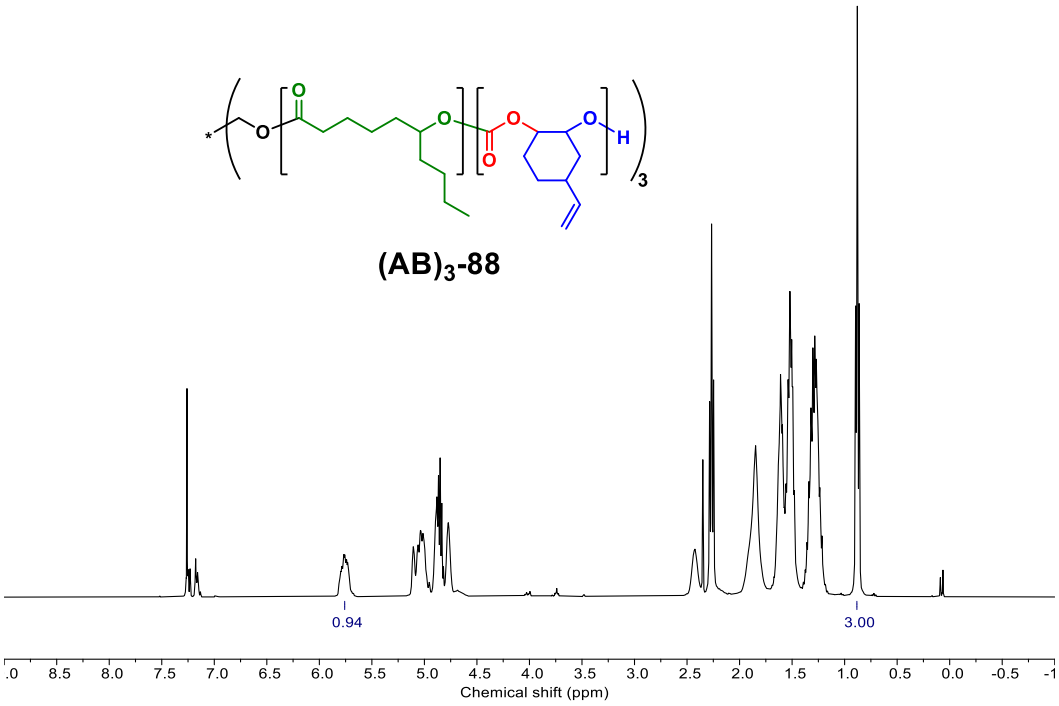


Figure S7.47. ^{1}H NMR spectrum of purified 3-arm star block polymer $(AB)_3$-88. [400 MHz, $CDCl_3$].

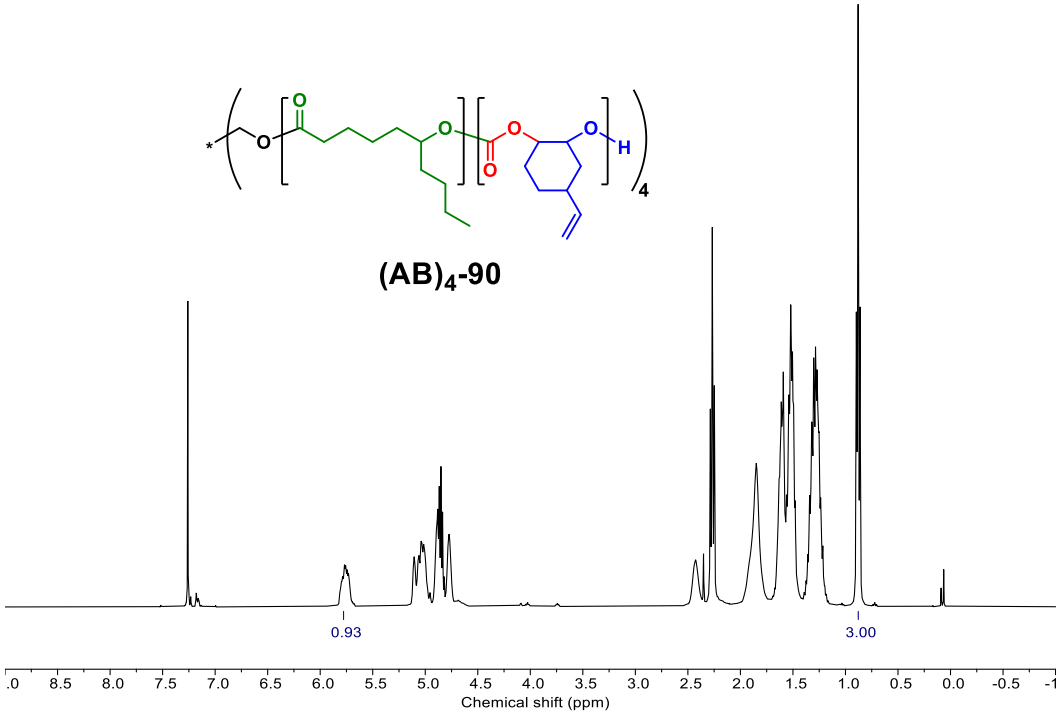


Figure S7.48. ^{1}H NMR spectrum of purified 4-arm star block polymer $(AB)_4$-90. [400 MHz, $CDCl_3$].

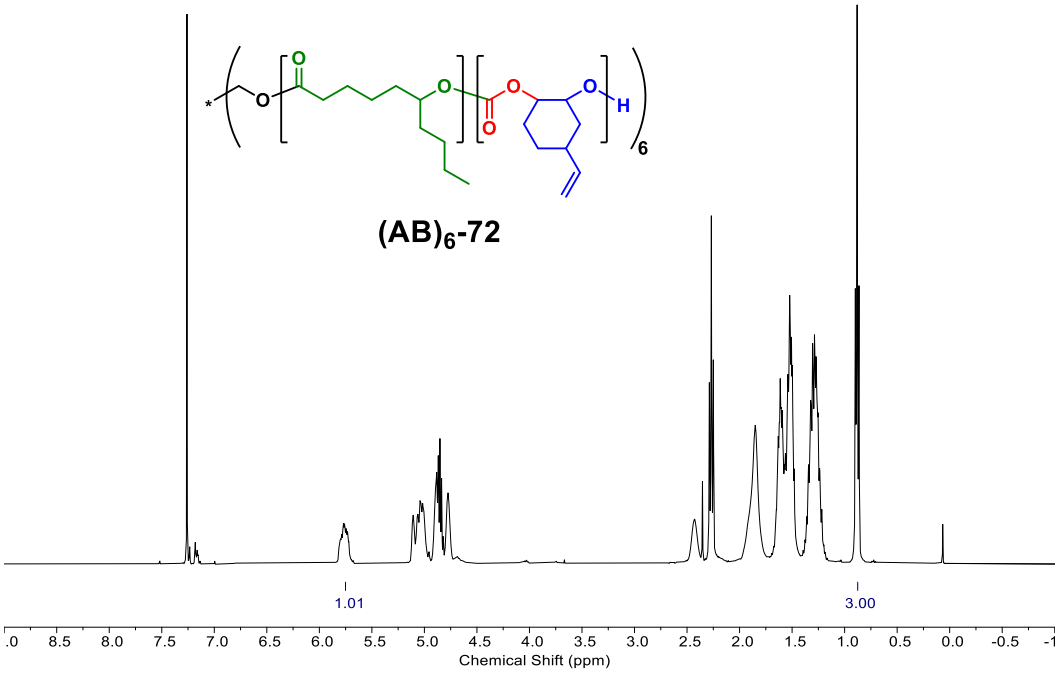


Figure S7.49. ^{1}H NMR spectrum of purified 6-arm star block polymer $(AB)_6$-72. [400 MHz, $CDCl_3$].

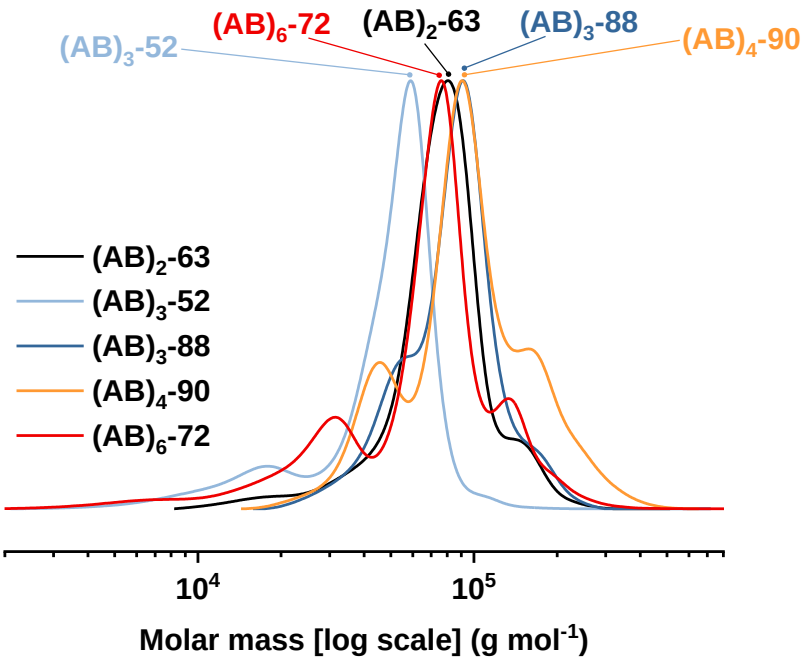


Figure S7.50. SEC chromatographs of $(AB)_n$ star block polymers.

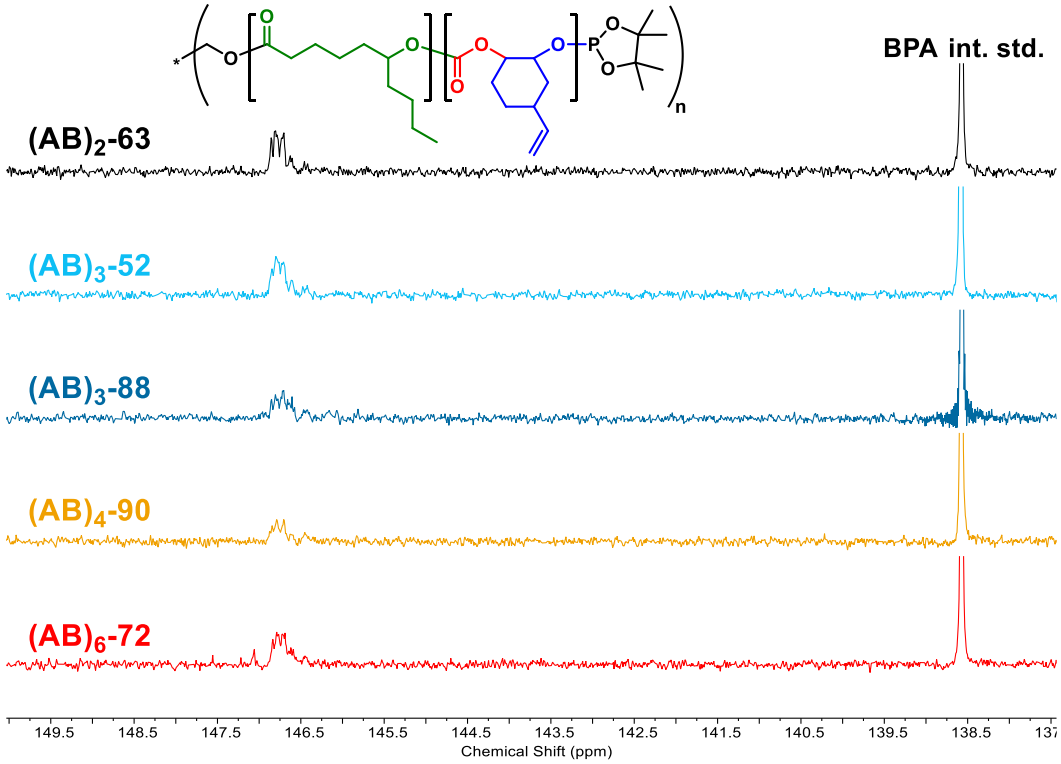


Figure S7.51. $^{31}P\{^{1}H\}$ NMR end-group analysis of $(AB)_n$-# star block polymers.

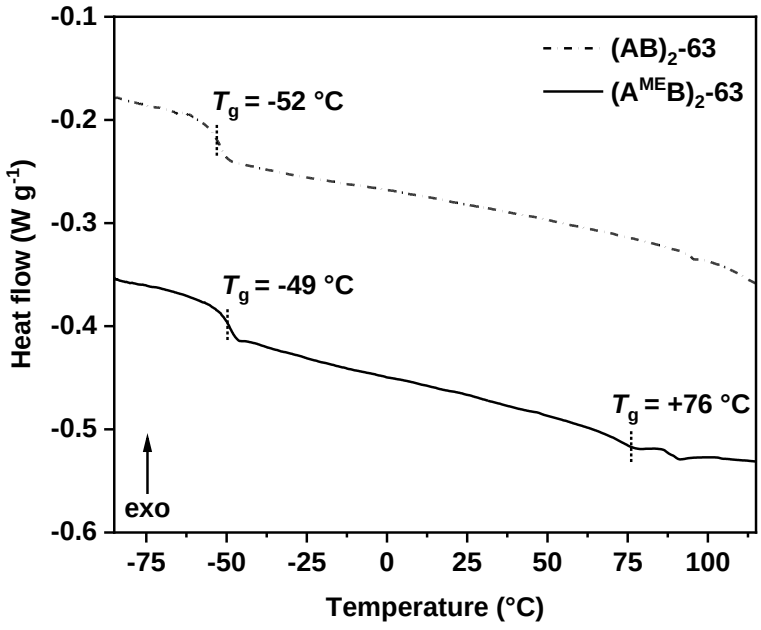


Figure S7.52. DSC thermograms for 2-arm star block polymer samples $(AB)_2$-63 (non-modified) and $(A^{ME}B)_2$-63 (modified).

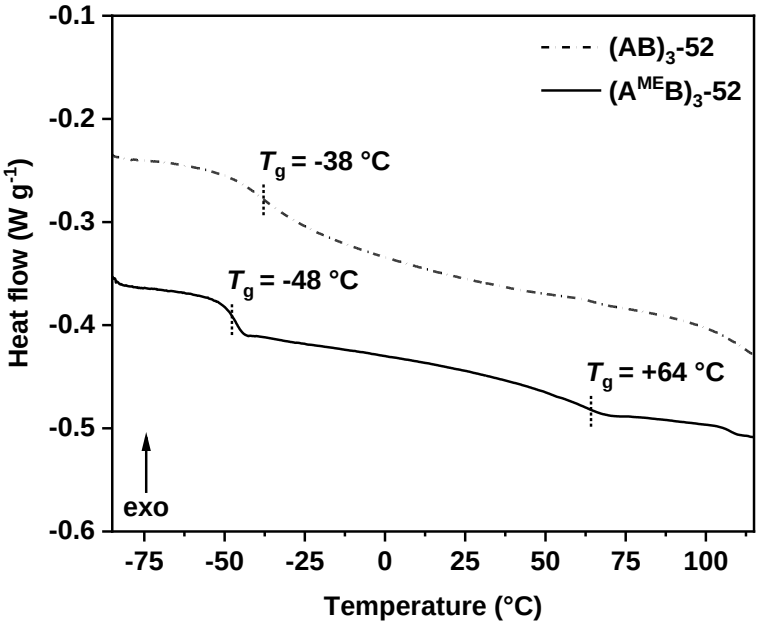


Figure S7.53. DSC thermograms for 3-arm star block polymer samples $(AB)_3$-52 (non-modified) and $(A^{ME}B)_3$-52 (modified).

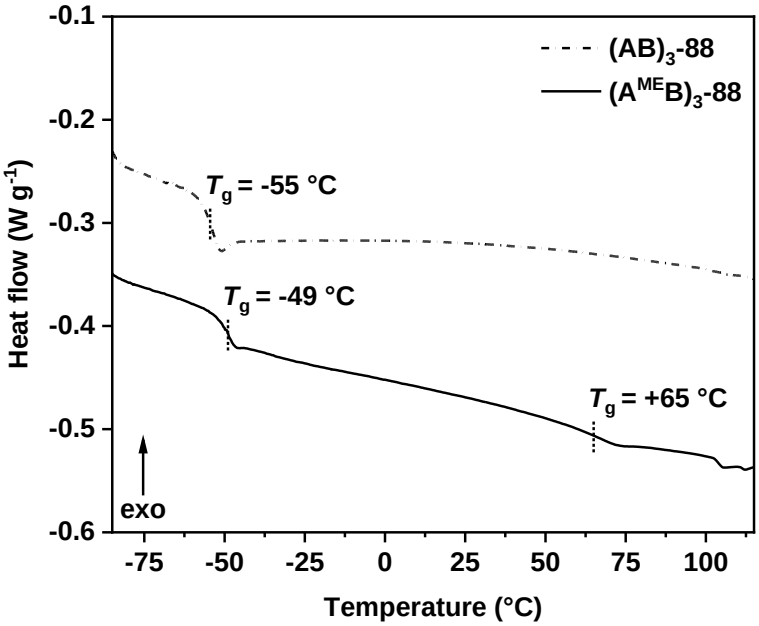


Figure S7.54. DSC thermograms for 3-arm star block polymer samples $(AB)_3$-88 (non-modified) and $(A^{ME}B)_3$-88 (modified).

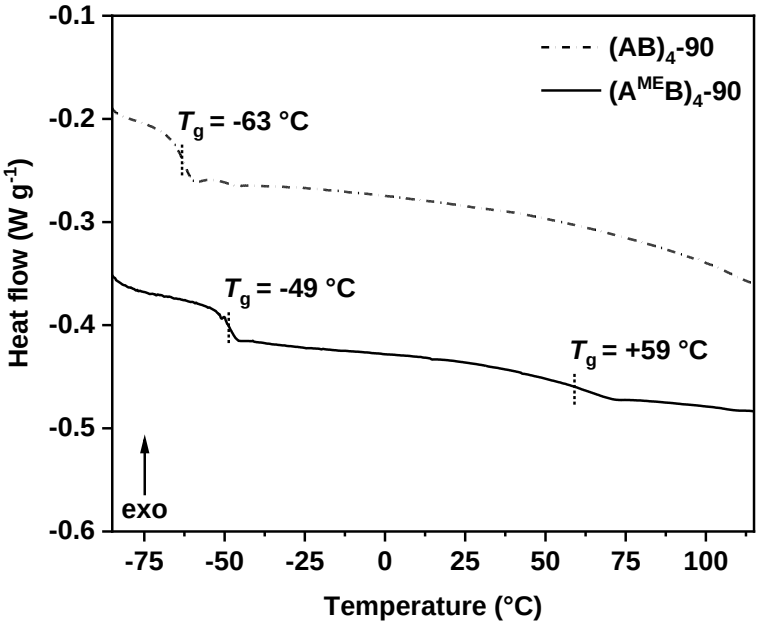


Figure S7.55. DSC thermograms for 4-arm star block polymer samples $(AB)_4$-90 (non-modified) and $(A^{ME}B)_4$-90 (modified).

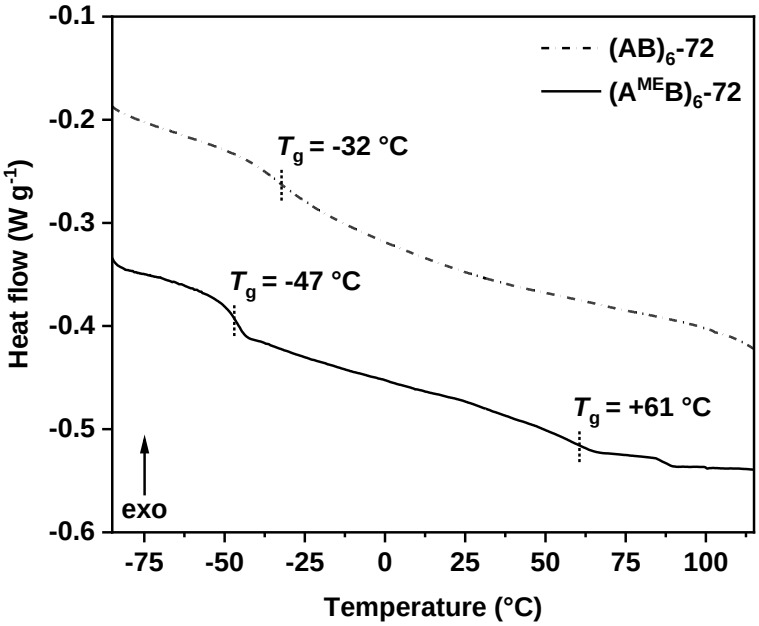


Figure S7.56. DSC thermograms for 6-arm star block polymer samples $(AB)_6$-72 (non-modified) and $(A^{ME}B)_6$-72 (modified).

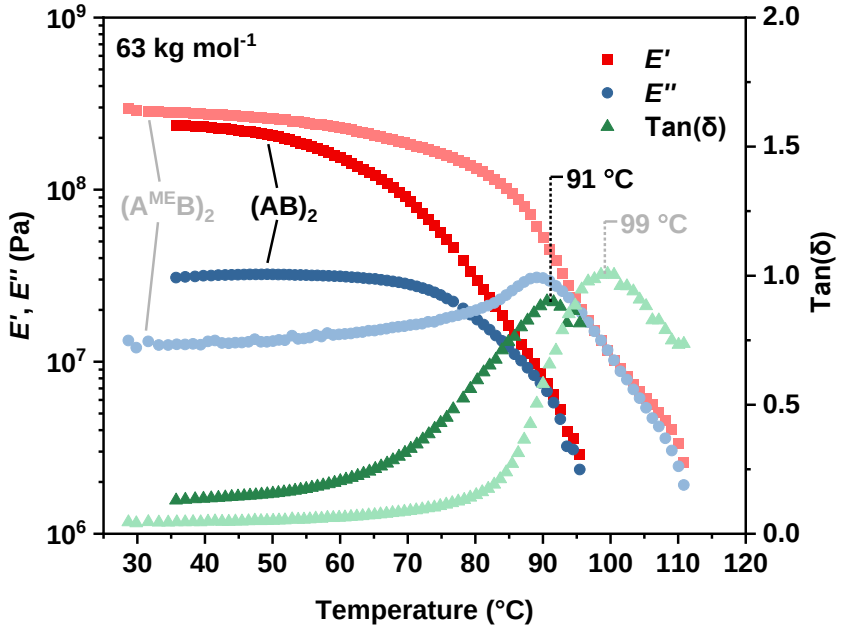


Figure S7.57. DMA temperature sweep profiles for star block polymer samples $(AB)_2$-63 (non-modified) and $(A^{ME}B)_2$-63 (modified).

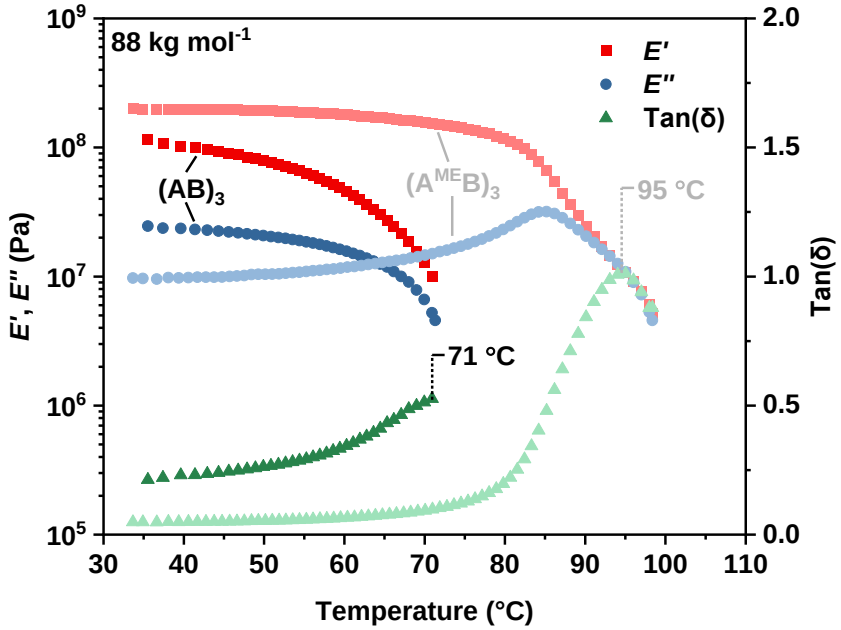


Figure S7.58. DMA temperature sweep profiles for star block polymer samples $(AB)_3$-88 (non-modified) and $(A^{ME}B)_3$-88 (modified).

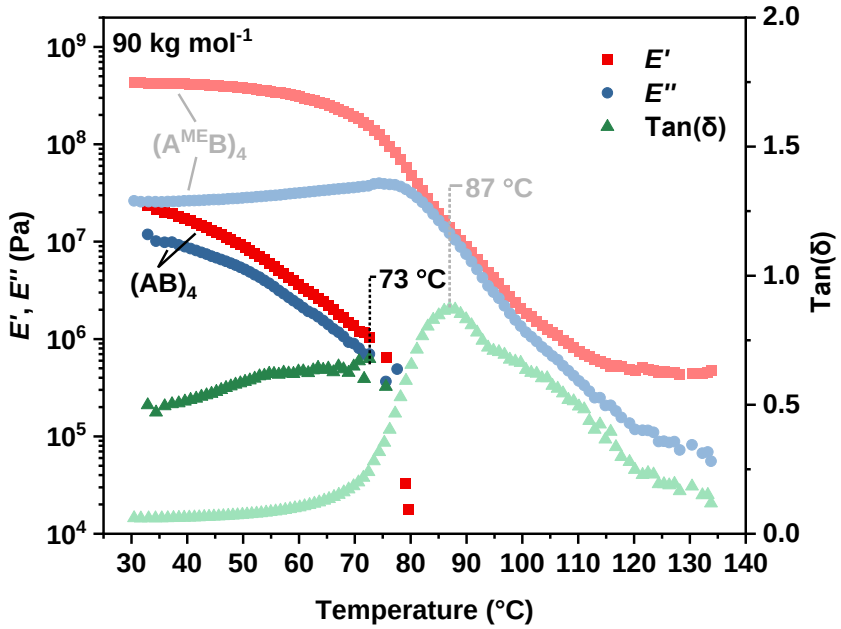


Figure S7.59. DMA temperature sweep profiles for star block polymer samples $(AB)_4$-90 (non-modified) and $(A^{ME}B)_4$-90 (modified).

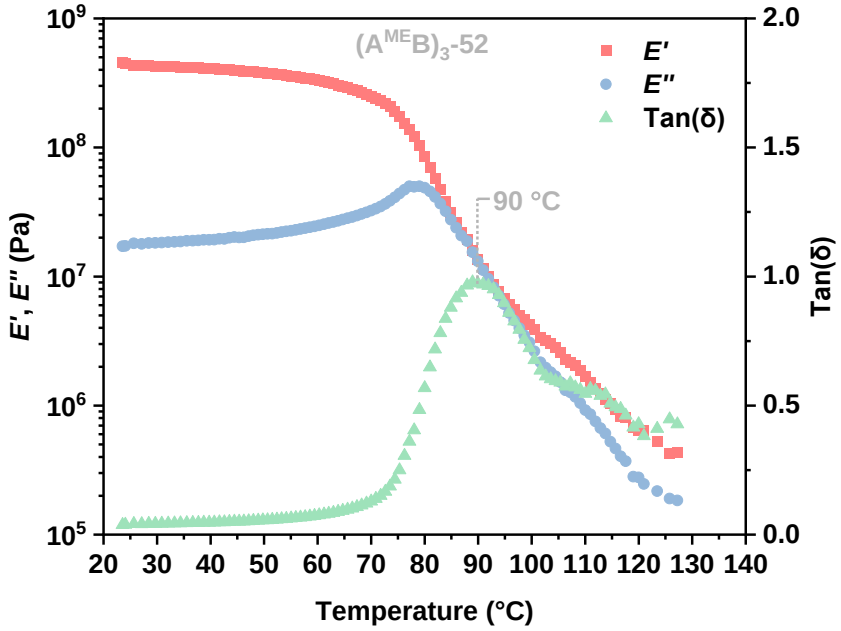


Figure S7.60. DMA temperature sweep profiles for star block polymer sample $(A^{ME}B)_3$-52 (modified).

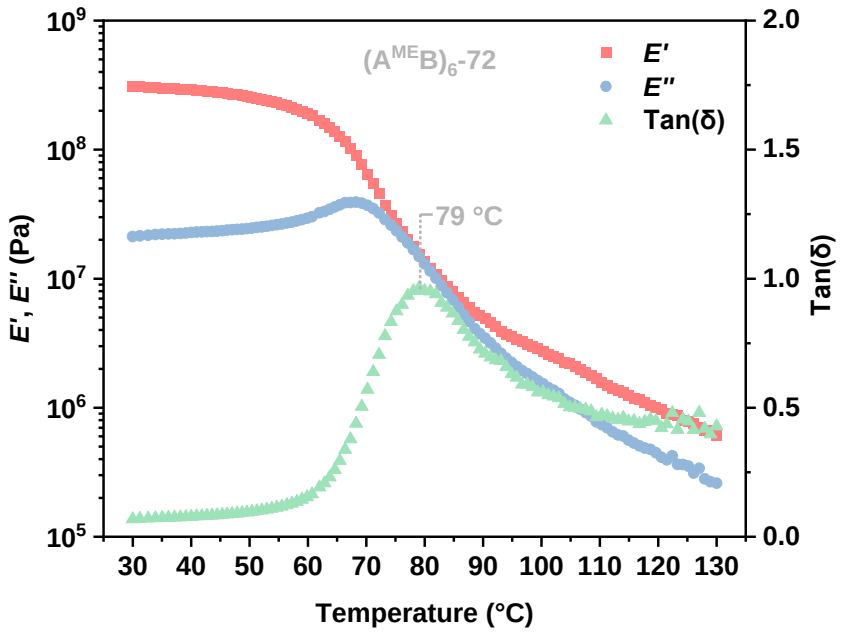


Figure S7.61. DMA temperature sweep profiles for star block polymer sample $(A^{ME}B)_6$-72 (modified).

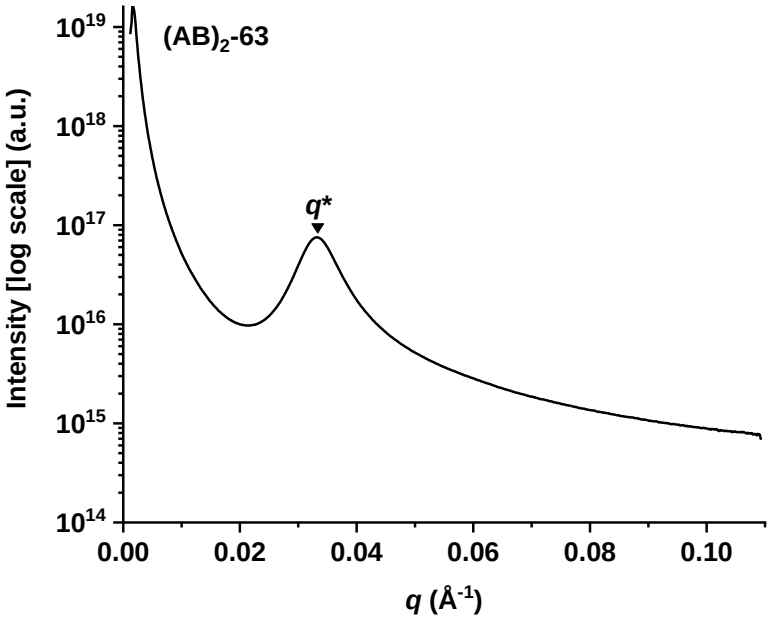


Figure S7.62. 1D SAXS profile for 2-arm star block polymer sample $(AB)_2$-63.

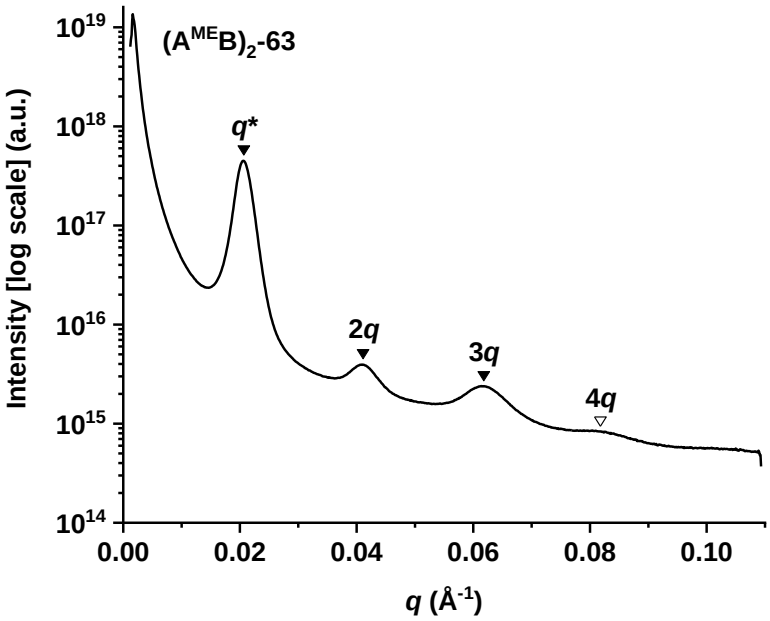


Figure S7.63. 1D SAXS profile for hydroxyl-modified 2-arm star block polymer sample $(A^{ME}B)_2$-63.

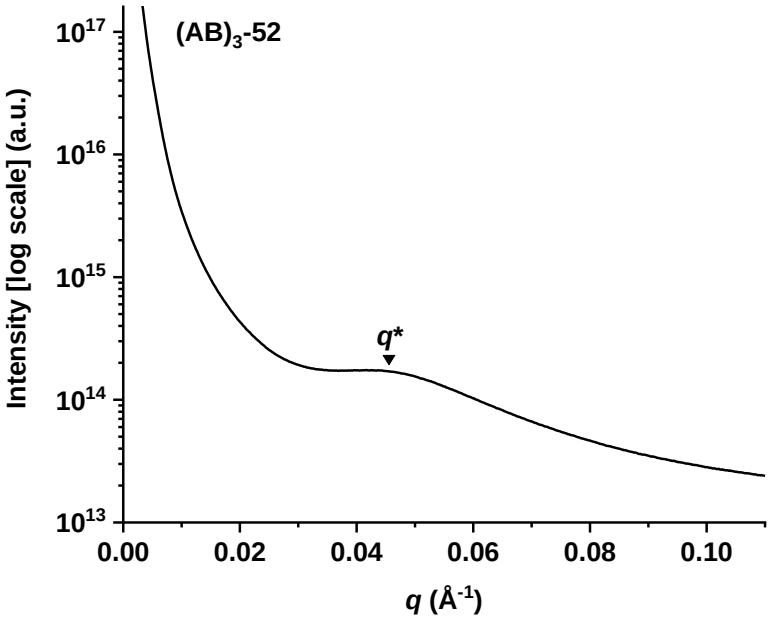


Figure S7.64. 1D SAXS profile for 3-arm star block polymer sample $(AB)_3$-52.

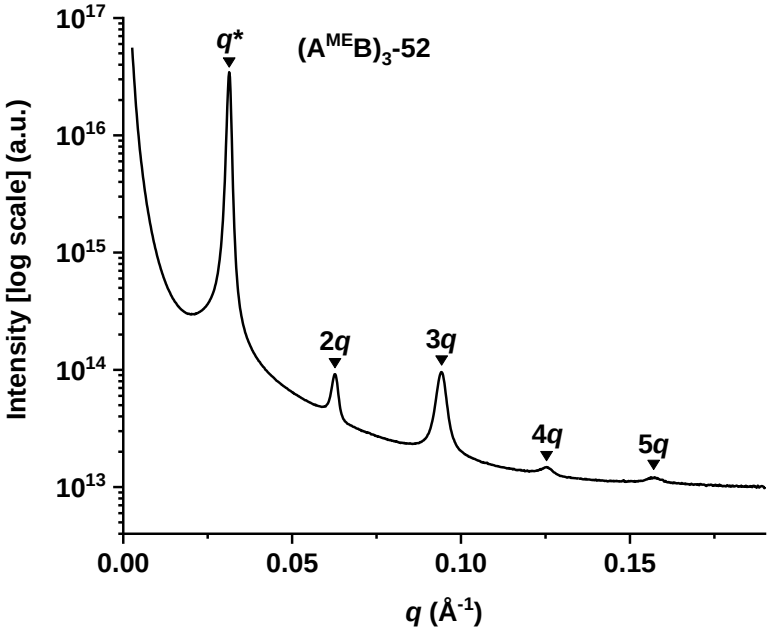


Figure S7.65. 1D SAXS profile for hydroxyl-modified 3-arm star block polymer sample $(A^{ME}B)_3$-52.

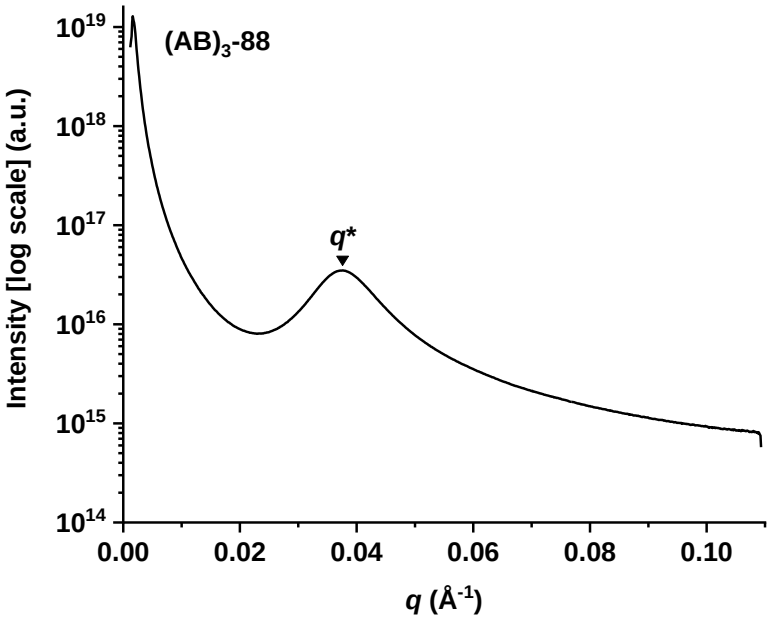


Figure S7.66. 1D SAXS profile for 3-arm star block polymer sample $(AB)_3$-88.

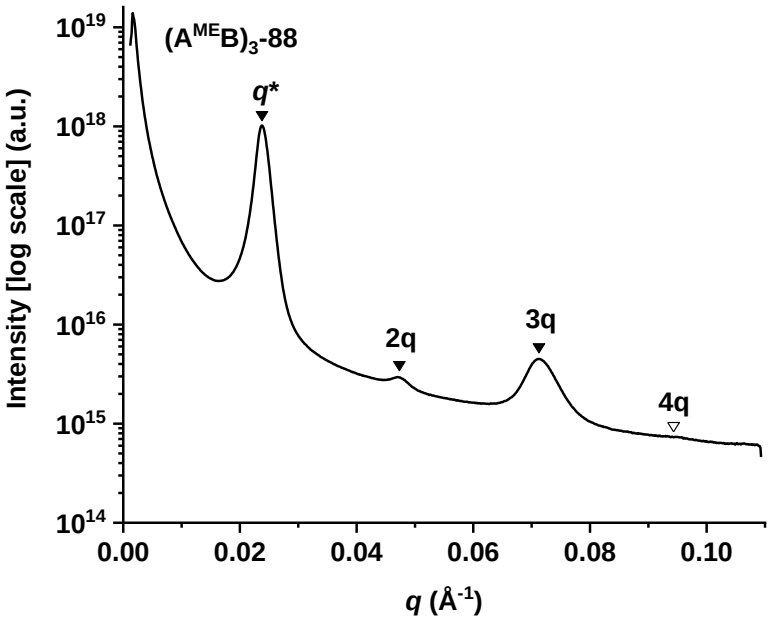


Figure S7.67. 1D SAXS profile for hydroxyl-modified 3-arm star block polymer sample $(A^{ME}B)_3$-88.

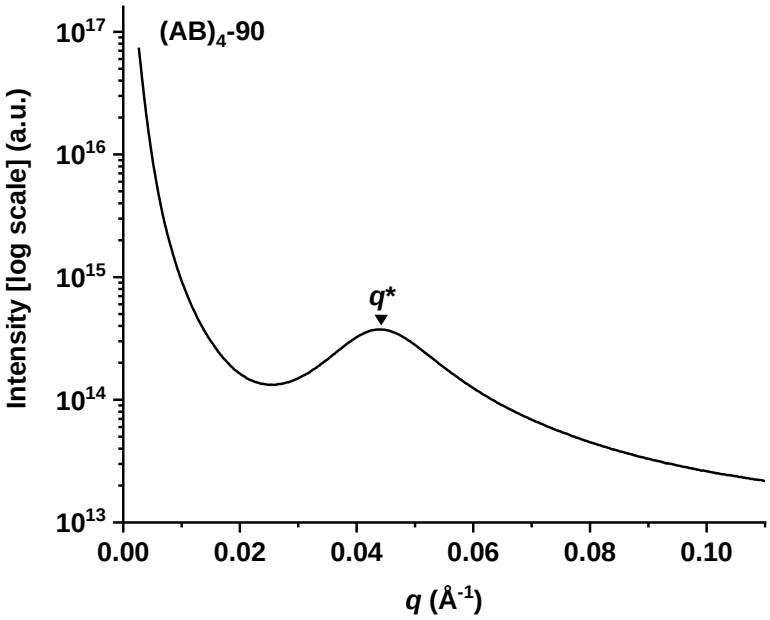


Figure S7.68. 1D SAXS profile for 4-arm star block polymer sample $(AB)_4$-90.

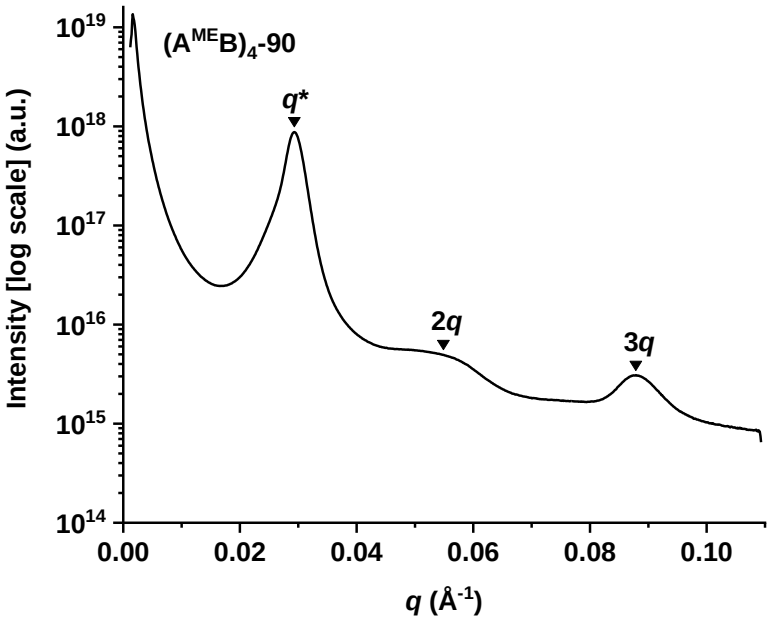


Figure S7.69. 1D SAXS profile for hydroxyl-modified 4-arm star block polymer sample $(A^{ME}B)_4$-90.

7.4. Permissions

3/15/2021 RightsLink Printable License
https://s100.copyright.com/AppDispatchServlet 1/6
SPRINGER NATURE LICENSE
TERMS AND CONDITIONS
Mar 15, 2021
This Agreement between Mr. Gregory Sulley ("You") and Springer Nature ("Springer Nature") consists of your license details and the terms and conditions provided by Springer Nature and Copyright Clearance Center.
License Number 5030200610200
License date Mar 15, 2021
Licensed Content Publisher Springer Nature
Licensed Content
Publication Nature
Licensed Content Title The technological and economic prospects for CO2 utilization and removal
Licensed Content Author Cameron Hepburn et al
Licensed Content Date Nov 6, 2019
Type of Use Thesis/Dissertation
Requestor type academic/university or research institute
Format print and electronic
Portion figures/tables/illustrations
Number of
figures/tables/illustrations 1
3/15/2021 RightsLink Printable License
https://s100.copyright.com/AppDispatchServlet 2/6
High-res required no
Will you be translating? no
Circulation/distribution 1 - 29
Author of this Springer
Nature content no
Title CO2 Utilisation in Block Polymers: Catalysis and Functional
Materials Development
Institution name University of Oxford
Expected presentation date May 2021
Portions Figure 2 only.
Requestor Location
Mr. Gregory Sulley
7 Olympus House
Fire Fly Avenue
Swindon, SN2 2FW
United Kingdom
Attn: Mr. Gregory Sulley
Total 0.00 GBP
Terms and Conditions
Springer Nature Customer Service Centre GmbH
Terms and Conditions
This agreement sets out the terms and conditions of the licence (the **Licence**) between you and **Springer Nature Customer Service Centre GmbH** (the **Licensor**). By clicking 'accept' and completing the transaction for the material (**Licensed Material**), you also

confirm your acceptance of these terms and conditions.

1. Grant of License

1. 1. The Licensor grants you a personal, non-exclusive, non-transferable, world-wide licence to reproduce the Licensed Material for the purpose specified in your order only. Licences are granted for the specific use requested in the order and for no other

3/15/2021 RightsLink Printable License
https://s100.copyright.com/AppDispatchServlet 3/6

use, subject to the conditions below.

1. 2. The Licensor warrants that it has, to the best of its knowledge, the rights to license reuse of the Licensed Material. However, you should ensure that the material you are requesting is original to the Licensor and does not carry the copyright of another entity (as credited in the published version).

1. 3. If the credit line on any part of the material you have requested indicates that it was reprinted or adapted with permission from another source, then you should also seek permission from that source to reuse the material.

2. Scope of Licence

2. 1. You may only use the Licensed Content in the manner and to the extent permitted by these Ts&Cs and any applicable laws.

2. 2. A separate licence may be required for any additional use of the Licensed Material, e.g. where a licence has been purchased for print only use, separate permission must be obtained for electronic re-use. Similarly, a licence is only valid in the language selected and does not apply for editions in other languages unless additional translation rights have been granted separately in the licence. Any content owned by third parties are expressly excluded from the licence.

2. 3. Similarly, rights for additional components such as custom editions and derivatives require additional permission and may be subject to an additional fee. Please apply to Journalpermissions@springernature.com/bookpermissions@springernature.com for these rights.

2. 4. Where permission has been granted **free of charge** for material in print, permission may also be granted for any electronic version of that work, provided that the material is incidental to your work as a whole and that the electronic version is essentially equivalent to, or substitutes for, the print version.

2. 5. An alternative scope of licence may apply to signatories of the STM Permissions Guidelines, as amended from time to time.

3. Duration of Licence

3. 1. A licence for is valid from the date of purchase ('Licence Date') at the end of the relevant period in the below table:

Scope of Licence	Duration of Licence
Post on a website	12 months
Presentations	12 months
Books and journals	Lifetime of the edition in the language purchased

4. Acknowledgement

3/15/2021 RightsLink Printable License
https://s100.copyright.com/AppDispatchServlet 4/6

4. 1. The Licensor's permission must be acknowledged next to the Licenced Material in print. In electronic form, this acknowledgement must be visible at the same time as the figures/tables/illustrations or abstract, and must be hyperlinked to the journal/book's homepage. Our required acknowledgement format is in the Appendix below.

5. Restrictions on use

5. 1. Use of the Licensed Material may be permitted for incidental promotional use and

minor editing privileges e.g. minor adaptations of single figures, changes of format, colour and/or style where the adaptation is credited as set out in Appendix 1 below. Any other changes including but not limited to, cropping, adapting, omitting material that affect the meaning, intention or moral rights of the author are strictly prohibited.
5. 2. You must not use any Licensed Material as part of any design or trademark.
5. 3. Licensed Material may be used in Open Access Publications (OAP) before publication by Springer Nature, but any Licensed Material must be removed from OAP sites prior to final publication.
6. Ownership of Rights
6. 1. Licensed Material remains the property of either Licensor or the relevant third party and any rights not explicitly granted herein are expressly reserved.
7. Warranty
IN NO EVENT SHALL LICENSOR BE LIABLE TO YOU OR ANY OTHER PARTY OR
ANY OTHER PERSON OR FOR ANY SPECIAL, CONSEQUENTIAL, INCIDENTAL OR INDIRECT DAMAGES, HOWEVER CAUSED, ARISING OUT OF OR IN CONNECTION WITH THE DOWNLOADING, VIEWING OR USE OF THE MATERIALS REGARDLESS OF THE FORM OF ACTION, WHETHER FOR BREACH
OF CONTRACT, BREACH OF WARRANTY, TORT, NEGLIGENCE, INFRINGEMENT
OR OTHERWISE (INCLUDING, WITHOUT LIMITATION, DAMAGES BASED ON LOSS OF PROFITS, DATA, FILES, USE, BUSINESS OPPORTUNITY OR CLAIMS OF
THIRD PARTIES), AND
WHETHER OR NOT THE PARTY HAS BEEN ADVISED OF THE POSSIBILITY OF SUCH DAMAGES. THIS LIMITATION SHALL APPLY NOTWITHSTANDING ANY FAILURE OF ESSENTIAL PURPOSE OF ANY LIMITED REMEDY PROVIDED HEREIN.
8. Limitations
8. 1. ***BOOKS ONLY:***Where **'reuse in a dissertation/thesis'** has been selected the following terms apply: Print rights of the final author's accepted manuscript (for clarity, NOT the published version) for up to 100 copies, electronic rights for use only on a personal website or institutional repository as defined by the Sherpa guideline

(www.sherpa.ac.uk/romeo/).
8. 2. For content reuse requests that qualify for permission under the STM Permissions Guidelines, which may be updated from time to time, the STM Permissions Guidelines supersede the terms and conditions contained in this licence.
9. Termination and Cancellation
9. 1. Licences will expire after the period shown in Clause 3 (above).
9. 2. Licensee reserves the right to terminate the Licence in the event that payment is not received in full or if there has been a breach of this agreement by you.
Appendix 1 — Acknowledgements:
For Journal Content:
Reprinted by permission from [**the Licensor**]: [**Journal Publisher** (e.g. Nature/Springer/Palgrave)] [**JOURNAL NAME**] [**REFERENCE CITATION** (Article name, Author(s) Name), [**COPYRIGHT**] (year of publication)
For **Advance Online Publication papers:**

Reprinted by permission from [**the Licensor**]: [**Journal Publisher** (e.g. Nature/Springer/Palgrave)] [**JOURNAL NAME**] [**REFERENCE CITATION** (Article name, Author(s) Name), [**COPYRIGHT**] (year of publication), advance online publication, day month year (doi: 10.1038/sj.[JOURNAL ACRONYM].)
For Adaptations/Translations:
Adapted/Translated by permission from [**the Licensor**]: [**Journal Publisher** (e.g. Nature/Springer/Palgrave)] [**JOURNAL NAME**] [**REFERENCE CITATION** (Article name, Author(s) Name), [**COPYRIGHT**] (year of publication)
Note: For any republication from the British Journal of Cancer, the following credit line style applies:
Reprinted/adapted/translated by permission from [**the Licensor**]: on behalf of Cancer Research UK: : [**Journal Publisher** (e.g. Nature/Springer/Palgrave)] [**JOURNAL NAME**] [**REFERENCE CITATION** (Article name, Author(s) Name), [**COPYRIGHT]** (year of publication)
For **Advance Online Publication** papers:
Reprinted by permission from The [**the Licensor**]: on behalf of Cancer Research UK: [**Journal Publisher** (e.g. Nature/Springer/Palgrave)] [**JOURNAL NAME**] [**REFERENCE CITATION** (Article name, Author(s) Name), [**COPYRIGHT**] (year of publication), advance online publication, day month year (doi: 10.1038/sj.[JOURNAL ACRONYM])
For Book content:
Reprinted/adapted by permission from [**the Licensor**]: [**Book Publisher** (e.g. Palgrave Macmillan, Springer etc) [**Book Title**] by [**Book author**(s)] [**COPYRIGHT**] (year of publication)
3/15/2021 RightsLink Printable License
https://s100.copyright.com/AppDispatchServlet 6/6
Other Conditions:
Version 1.3
Questions? customercare@copyright.com or +1-855-239-3415 (toll free in the US) or +1-978-646-2777.

7.5. References

1. Gallagher, J. J.; Hillmyer, M. A.; Reineke, T. M., Acrylic Triblock Copolymers Incorporating Isosorbide for Pressure Sensitive Adhesives. *ACS Sustainable Chem. Eng.* **2016,** *4* (6), 3379-3387.
2. Ding, K.; John, A.; Shin, J.; Lee, Y.; Quinn, T.; Tolman, W. B.; Hillmyer, M. A., High-Performance Pressure-Sensitive Adhesives from Renewable Triblock Copolymers. *Biomacromolecules* **2015,** *16* (8), 2537-2539.
3. Lee, S.; Lee, K.; Kim, Y.-W.; Shin, J., Preparation and Characterization of a Renewable Pressure-Sensitive Adhesive System Derived from ε-Decalactone, l-Lactide, Epoxidized Soybean Oil, and Rosin Ester. *ACS Sustainable Chem. Eng.* **2015,** *3* (9), 2309-2320.